

ornl

ORNL/TM-12672

RECEIVED
FEB 27 1996
OSTI

**OAK RIDGE
NATIONAL
LABORATORY**

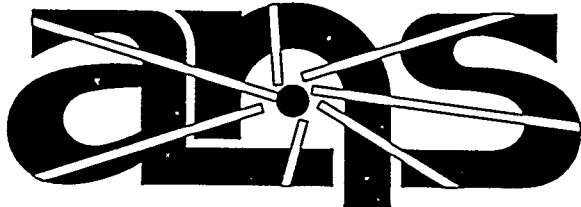
MARTIN MARIETTA

**Initial Global 2-D Shielding
Analysis for the ANS Core
and Reflector**

J. A. Bucholz

August 1995

MASTER



MANAGED BY
MARTIN MARIETTA ENERGY SYSTEMS, INC.
FOR THE UNITED STATES
DEPARTMENT OF ENERGY

DISTRIBUTION OF THIS DOCUMENT IS UNLIMITED
Advanced Neutron Source

This report has been reproduced directly from the best available copy.

Available to DOE and DOE contractors from the Office of Scientific and Technical Information, P.O. Box 62, Oak Ridge, TN 37831; prices available from (615) 576-8401, FTS 626-8401.

Available to the public from the National Technical Information Service, U.S. Department of Commerce, 5285 Port Royal Rd., Springfield, VA 22161.

This report was prepared as an account of work sponsored by an agency of the United States Government. Neither the United States Government nor any agency thereof, nor any of their employees, makes any warranty, express or implied, or assumes any legal liability or responsibility for the accuracy, completeness, or usefulness of any information, apparatus, product, or process disclosed, or represents that its use would not infringe privately owned rights. Reference herein to any specific commercial product, process, or service by trade name, trademark, manufacturer, or otherwise, does not necessarily constitute or imply its endorsement, recommendation, or favoring by the United States Government or any agency thereof. The views and opinions of authors expressed herein do not necessarily state or reflect those of the United States Government or any agency thereof.

Computational Physics and Engineering Division

**INITIAL GLOBAL 2-D SHIELDING ANALYSIS
FOR THE ADVANCED NEUTRON SOURCE CORE AND REFLECTOR**

Date Prepared: January 1994
Date Published: August 1995

J. A. Bucholz

Prepared by the
OAK RIDGE NATIONAL LABORATORY
Oak Ridge, Tennessee 37831
managed by
LOCKHEED MARTIN ENERGY SYSTEMS, INC.
for the
U.S. DEPARTMENT OF ENERGY
Under Contract No. DE-AC05-84OR21400

DISTRIBUTION OF THIS DOCUMENT IS UNLIMITED

PL



CONTENTS

LIST OF FIGURES	v
LIST OF TABLES	ix
ACRONYMS	xv
ABSTRACT	xvii
1.0 INTRODUCTION	1
2.0 GEOMETRIC AND NUMERICAL MODELS	3
3.0 MULTIGROUP SOURCE TERMS	25
4.0 CROSS-SECTION DATA USED IN THE GLOBAL ANALYSES	31
4.1 The Original DORT-Ready Cross Sections	31
4.2 Initial Adjustments to Obtain Error Mode Acceleration	34
4.3 Further Adjustments to Account for Photoneutron Production	35
5.0 OTHER MISCELLANEOUS DATA	45
6.0 THE PROGRESSION AND VERIFICATION OF THE DORT CALCULATIONS: LESSONS LEARNED	55
6.1 Overview	55
6.2 Early Problems With Slow Convergence (DORT Runs 1 and 2)	55
6.3 Error Mode Acceleration of DORT Run 3 Using SMURF Data	55
6.4 QA Check of DORT Run 3; Problem With Mesh	58
6.5 Modifications to Include Delayed Fission Gammas (New AJAX data for DORT Run 4)	65
6.6 Treatment of Photoneutrons (PHOTOX/SPARK Data in DORT Runs 4a and 5)	74
6.7 Correction of a Minor Data Error Prior to DORT Run 5	77
6.8 Discussion of the Final Solution (DORT Run 5: Strategy and Qualitative Results)	79

7.0 FINAL RESULTS	91
8.0 SUMMARY	95
REFERENCES	99
APPENDIX A: Listing of the PHOTOX program for generating a (g)group-to-(n)group scattering matrix that represents the microscopic photoneutron production cross section for deuterium	A-1
APPENDIX B: Listing of the SPARK program used to augment a premixed DORT-ready cross section library (previously produced by GIP or JIPSY) by expanding the scattering matrix and "adding in" the (g)group-to-(n)group upscatter terms that represent the photoneutron production cross sections for deuterium in the various mixtures as needed	B-1
APPENDIX C: Listing of the ANSIDOSE program for calculating neutron and gamma flux-to-dose-rate conversion factors as prescribed in ANSI Std. ANS-6.1.1-1977	C-1
APPENDIX D: Neutron and gamma kerma factors in aluminum and iron for the ANSL-V 39n/44g and 99n/44g energy group structures	D-1
APPENDIX E: Tabulated numerical results at particular points of interest	E-1
APPENDIX F: A simple solid angle procedure for estimating fluxes and dose rates several meters down the horizontal beam tubes	F-1

LIST OF FIGURES

1a.	Geometric model used to represent the ANS core and reflector in the global 2-D RZ shielding analyses	4
1b.	Enhanced view of the materials immediately surrounding the core in the global 2-D RZ shielding analysis of the ANS core and reflector	5
2a.	Map of materials used in each mesh interval of the global 2-D RZ analysis of the ANS core and reflector vessel in DORT Run 3	9
2b.	Map of materials used in each mesh interval of the global 2-D RZ analysis of the ANS core and reflector vessel in DORT Run 3	10
2c.	Map of materials used in each mesh interval of the global 2-D RZ analysis of the ANS core and reflector vessel in DORT Run 3	11
2d.	Map of materials used in each mesh interval of the global 2-D RZ analysis of the ANS core and reflector vessel in DORT Run 3	12
2e.	Map of materials used in each mesh interval of the global 2-D RZ analysis of the ANS core and reflector vessel in DORT Run 3	13
2f.	Map of materials used in each mesh interval of the global 2-D RZ analysis of the ANS core and reflector vessel in DORT Run 3	14
3a.	Map of materials used in each mesh interval of the global 2-D RZ analysis of the ANS core and reflector vessel in DORT Runs 4 and 5	17
3b.	Map of materials used in each mesh interval of the global 2-D RZ analysis of the ANS core and reflector vessel in DORT Runs 4 and 5	18
3c.	Map of materials used in each mesh interval of the global 2-D RZ analysis of the ANS core and reflector vessel in DORT Runs 4 and 5	19
3d.	Map of materials used in each mesh interval of the global 2-D RZ analysis of the ANS core and reflector vessel in DORT Runs 4 and 5	20
3e.	Map of materials used in each mesh interval of the global 2-D RZ analysis of the ANS core and reflector vessel in DORT Runs 4 and 5	21
3f.	Map of materials used in each mesh interval of the global 2-D RZ analysis of the ANS core and reflector vessel in DORT Runs 4 and 5	22
4.	Relative location of the 30 source zones used in the global 2-D shielding analysis	26

5.	Photoneutron production cross section for deuterium (in millibarns) as a function of photon energy	37
6.	Evolution of the global 2-D shielding calculations for the ANS core and reflector vessel	56
7a.	Contours showing the 2-D spatial distribution of the thermal neutron flux below 0.625 eV as given by DORT Run 3 after 10 outer iterations over all groups for which thermal upscattering is possible	59
7b.	Contours showing the 2-D spatial distribution of the thermal neutron flux below 0.625 eV as given by DORT Run 3 after 71 outer iterations over all groups for which thermal upscattering is possible	60
7c.	Contours showing the 2-D spatial distribution of the thermal neutron flux below 0.625 eV as given by DORT Run 3 after 130 outer iterations over all groups for which thermal upscattering is possible	61
8.	Illustration showing the unnatural advancement of the flux via artificial numerical diffusion in the direction of elongation when numerous long thin mesh intervals are used	64
9a.	Contours showing the 2-D spatial distribution of the fast neutron flux in the ANS core and reflector ($E \geq 0.1$ MeV), as given by DORT Run 4, which did not account for photoneutrons	66
9b.	Contours showing the 2-D spatial distribution of the intermediate-energy neutron flux in the ANS core and reflector (100 eV $\leq E \leq 0.1$ MeV), as given by DORT Run 4, which did not account for photoneutrons	67
9c.	Contours showing the 2-D spatial distribution of the epithermal neutron flux in the ANS core and reflector (0.625 eV $\leq E \leq 100$ eV), as given by DORT Run 4, which did not account for photoneutrons	68
9d.	Contours showing the 2-D spatial distribution of the thermal neutron flux in the ANS core and reflector ($E \leq 0.625$ eV), as given by DORT Run 4, which did not account for photoneutrons	69
9e.	Contours showing the 2-D spatial distribution of the high-energy gamma flux above 2.15 MeV in the ANS core and reflector, as given by DORT Run 4, which did not account for photoneutrons	70
9f.	Contours showing the 2-D spatial distribution of the total gamma flux in the ANS core and reflector (summed over all gamma energy groups), as given by DORT Run 4, which did not account for photoneutrons	71
9g.	Contours showing the 2-D spatial distribution of the neutron dose rate (mrem/h) in the ANS core and reflector, as given by DORT Run 4, which did not account for photoneutrons	72

9h.	Contours showing the 2-D spatial distribution of the gamma dose rate (mrem/h) in the ANS core and reflector, as given by DORT Run 4, which did not account for photoneutrons	73
10a.	Contours showing the 2-D spatial distribution of the fast neutron flux in the ANS core and reflector ($E \geq 0.1$ MeV), as given by DORT Run 5, which did account for photoneutrons and is considered the final reference solution	82
10b.	Contours showing the 2-D spatial distribution of the intermediate-energy neutron flux in the ANS core and reflector (100 eV $\leq E \leq 0.1$ MeV), as given by DORT Run 5, which did account for photoneutrons and is considered the final reference solution	83
10c.	Contours showing the 2-D spatial distribution of the epithermal neutron flux in the ANS core and reflector (0.625 eV $\leq E \leq 100$ eV), as given by DORT Run 5, which did account for photoneutrons and is considered the final reference solution	84
10d.	Contours showing the 2-D spatial distribution of the thermal neutron flux in the ANS core and reflector ($E \leq 0.625$ eV), as given by DORT Run 5, which did account for photoneutrons and is considered the final reference solution	85
10e.	Contours showing the 2-D spatial distribution of the high-energy gamma flux above 2.15 MeV in the ANS core and reflector, as given by DORT Run 5, which did account for photoneutrons and is considered the final reference solution	86
10f.	Contours showing the 2-D spatial distribution of the total gamma flux in the ANS core and reflector (summed over all gamma energy groups), as given by DORT Run 5, which did account for photoneutrons and is considered the final reference solution	87
10g.	Contours showing the 2-D spatial distribution of the neutron dose rate (mrem/h) in the ANS core and reflector, as given by DORT Run 5, which did account for photoneutrons and is considered the final reference solution	88
10h.	Contours showing the 2-D spatial distribution of the gamma dose rate (mrem/h) in the ANS core and reflector, as given by DORT Run 5, which did account for photoneutrons and is considered the final reference solution	89
11.	Relative location of the 9 zones in the reflector vessel and 7 zones in the inner and outer core boundary pressure tubes for which the volume-averaged neutron and gamma heating rates are reported in Table 23	93
E.1a.	Points of particular interest in the global 2-D RZ analysis of the ANS core and reflector vessel in DORT Run 5	E-6
E.1b.	Points of particular interest in the global 2-D RZ analysis of the ANS core and reflector vessel in DORT Run 5	E-7
E.1c.	Points of particular interest in the global 2-D RZ analysis of the ANS core and reflector vessel in DORT Run 5	E-8

E.1d. Points of particular interest in the global 2-D RZ analysis of the ANS core and reflector vessel in DORT Run 5	E-9
E.1e. Points of particular interest in the global 2-D RZ analysis of the ANS core and reflector vessel in DORT Run 5	E-10
E.1f. Points of particular interest in the global 2-D RZ analysis of the ANS core and reflector vessel in DORT Run 5	E-11
F.1. Location of a horizontal tangential beam tube relative to the system centerline and a point of interest, (P), several meters down the beam tube	F-4
F.2. Sketch used to calculate the fractional solid angle subtended by an incremental length of the beam tube wall as seen from a point, (P), several meters down the beam tube	F-4

LIST OF TABLES

1.	Description of the geometric model used in all of the global 2-D RZ analyses described in this report	6
2.	CSASI and JIPSY input describing the ten material mixtures used in the global 2-D RZ analysis of the ANS core and reflector tank.	7
3a.	Radial mesh boundaries (mm) used in the numerical model for DORT Run 3	15
3b.	Axial mesh boundaries (mm) used in the numerical model for DORT Run 3	16
4a.	Radial mesh boundaries (mm) used in the numerical model for DORT Runs 4 and 5	23
4b.	Axial mesh boundaries (mm) used in the numerical model for DORT Runs 4 and 5	24
5.	Average power densities in the upper and lower sections of the ANS reactor core as a function of time	27
6a.	Volume-averaged power densities in various portions of the ANS core as a function of time ..	28
6b.	Volume-averaged neutron sources in various portions of the ANS core as a function of time ..	29
7a.	Neutron and gamma energy group structures for the ANSL-V 39n/44g cross section library ..	32
7b.	Neutron energy group structure for the ANSL-V 99n/44g cross section library, where the 44 gamma groups have the same energy group structure as in the 39n/44g library	33
8.	Complete listing of the SMURF program that was used to read the DORT-ready macroscopic cross sections for each material and set the value of $v\Sigma_F$ equal to a negligibly small value (1.0E-10/cm) in each material so that the DORT code could take advantage of Vondy's "error mode acceleration" scheme	36
9.	Total photoneutron production cross section (barns) as a function of photon energy (eV)	38
10.	Gamma spectrum deep in the D ₂ O reflector, at R=1650 mm (just 100 mm short of the reflector vessel starting at R=1750 mm), across from the top section of the core, based on a 1-D ANISN analysis using the original 39n/44g coupled library	40
11.	Group-to-group photoneutron production cross sections for deuterium in the ANSL-V 39n/44g library energy group structure as calculated by the PHOTOX program in Appendix A	41
12.	Fully symmetric, standard S ₈ quadrature with 48 discrete directions, as used in all of the global 2-D RZ DORT shielding analyses for the ANS core and reflector vessel	46

13.	Neutron and gamma flux-to-dose-rate conversion factors for the energy groups in the ANSL-V 39n/44g and 99n/44g cross section libraries, as calculated in accordance with ANSI/ANS-6.1.1-1977	47
14a.	Total kerma factors (prompt plus total decay heat) in aluminum and natural iron, for the 39 neutron and 44 gamma energy groups in the ANSL-V 39n/44g cross section library shown in Table 7a	48
14b.	Total kerma factors (prompt plus total decay heat) in aluminum and natural iron, for the 99 neutron energy groups in the ANSL-V 99n/44g cross section library shown in Table 7b	49
15.	ASTM DPA (displacements per atom) cross section (in barns) for iron, collapsed to the 39-neutron-group and 99-neutron-group ANSL-V cross section energy group structures using (1) the recommended ASTM fission-1/E weighting function and (2) a potentially more realistic fission-1/E-Maxwellian weighting function	52
16.	Comparison of integrated DPA values at several locations of interest using the two different collapsed response functions and the multigroup neutron fluxes from DORT Run 5	53
17.	Calculational strategy for converging the upscatter source terms for the thermal neutron groups (15-39) in DORT Run 3	57
18.	Comparison of the neutron fluxes ($s^{-1}m^{-2}$) for DORT Run 3 and Run 4 at 10.4 mm past the outside of the reflector vessel (halfway up the top section of the core), against the corresponding 1-D radial GB-ANISN results using 1, 3, and 9 times as many radial mesh intervals as in the DORT Run 3 analysis	63
19.	Partial listing of the ratios of the group-banded ANISN neutron fluxes with/without the photoneutrons generated in the D_2O as a function of energy and position, as determined by using a standard cross section library and a series of manual iterations as described in the text .	76
20.	Erroneous and correct material specifications for material 10, which represents the 10-mm-thick homogenized poison plates at the top and bottom of the upper and lower fuel elements in the core	78
21a.	Description of the calculational steps for DORT Run 4a with photoneutrons, where each step used the flux moment file generated by the previous step as the initial flux guess, and Step A1 was run from scratch	80
21b.	Description of the calculational steps for DORT Run 5 with photoneutrons, where each step used the flux moment file generated by the previous step as the initial flux guess, except for Step A1 which used Step F1 of DORT Run 4a as its initial flux guess	80
22.	Calculational strategy for converging the fast photoneutrons in Step D1 of DORT Run 4a and DORT Run 5	81

23.	Volume-averaged neutron and gamma heating rates, and the total volume-integrated heating rate, in 9 different regions of the reflector vessel and 14 different regions of the core boundary pressure tube	92
-----	---	----

Miscellaneous

A.1.	Listing of the PHOTOX program for generating a (gamma)group-to-(neutron)group scattering matrix that represents the microscopic photoneutron production cross section for deuterium (in barns)	A-3
A.2.	Group-to-group photoneutron production cross sections for deuterium in the ANSL-V 39n/44g library energy group structure as calculated by the PHOTOX program in Table A.1	A-10
B.1.	Listing of the SPARK program used to augment a premixed DORT-ready cross section library (previously produced by GIP or JIPSY) by expanding the scattering matrix and "adding in" the (g)group-to-(n)group upscatter terms that represent the photoneutron production cross sections for deuterium in the various mixtures as needed	B-3
C.1.	Listing of the ANSIDOSE program for calculating neutron and gamma flux-to-dose-rate conversion factors as prescribed in ANSI Std. ANSI-6.1.1-1977	C-3

Kerma Factors

D.1.	Recommended "prompt" kerma factors (alone) for Al-27 as given by the KAOS-V data library, extracted using the KAOS/RETRIEVE program, and expressed here in units of eV·barns for each of the 99 neutron energy groups in Table 7b	D-3
D.2.	Recommended prompt kerma factors for Al-27 plus the "charged particle" decay heat associated with its activation products (i.e., the beta decay of Al-28 produced from activation of the Al-27) as given by the KAOS-V data library, extracted using the KAOS/RETRIEVE program, and expressed here in units of eV·barns for each of the 99 neutron energy groups in Table 7b	D-3
D.3.	Recommended prompt kerma factors for Al-27 plus the "total decay heat" associated with its activation products (i.e., the beta and gamma decay of Al-28 produced from activation of the Al-27) as given by the KAOS-V data library, extracted using the KAOS/RETRIEVE program, and expressed here in units of eV·barns for each of the 99 neutron energy groups in Table 7b	D-4
D.4.	Recommended "prompt" kerma factors (alone) for Al-27 as given by the KAOS-V data library, extracted using the KAOS/RETRIEVE program, and expressed here in units of eV·barns for each of the 39 neutron energy groups in Table 7a	D-4

- D.5. Recommended prompt kerma factors for Al-27 plus the "charged particle" decay heat associated with its activation products (i.e., the beta decay of Al-28 produced from activation of the Al-27) as given by the KAOS-V data library, extracted using the KAOS/RETRIEVE program, and expressed here in units of eV· barns for each of the 39 neutron energy groups in Table 7a D-4
- D.6. Recommended prompt kerma factors for Al-27 plus the "total decay heat" associated with its activation products (i.e., the beta and gamma decay of Al-28 produced from activation of the Al-27) as given by the KAOS-V data library, extracted using the KAOS/RETRIEVE program, and expressed here in units of eV· barns for each of the 39 neutron energy groups in Table 7a D-5
- D.7. Kerma factors for gammas interacting with Al-27 as calculated by the SMUG module of the AMPX cross section processing code system, stored in the ANSL-V 39n/44g cross section library (as nuclide 13027, MT-process 1527), subsequently extracted using the PAL module of the AMPX code system, and expressed here in units of eV· barns for each of the 44 gamma energy groups in Table 7a D-5
- D.8. Recommended "prompt" kerma factors (alone) for natural iron as given by the KAOS-V data library, extracted using the KAOS/RETRIEVE program, and expressed here in units of eV· barns for each of the 99 neutron energy groups in Table 7b D-6
- D.9. Recommended prompt kerma factors for natural iron plus the "charged particle" decay heat associated with its activation products as given by the KAOS-V data library, extracted using the KAOS/RETRIEVE program, and expressed here in units of eV· barns for each of the 99 neutron energy groups in Table 7b D-6
- D.10. Recommended prompt kerma factors for natural iron plus the "total decay heat" associated with either charged particle or gamma decay (of all isotopes produced by neutron activation) as given by the KAOS-V data library, extracted using the KAOS/RETRIEVE program, and expressed here in units of eV· barns for each of the 99 neutron energy groups in Table 7b ... D-7
- D.11. Recommended "prompt" kerma factors (alone) for natural iron as given by the KAOS-V data library, extracted using the KAOS/RETRIEVE program, and expressed here in units of eV· barns for each of the 39 neutron energy groups in Table 7a D-7
- D.12. Recommended prompt kerma factors for natural iron plus the "charged particle" decay heat associated with its activation products as given by the KAOS-V data library, extracted using the KAOS/RETRIEVE program, and expressed here in units of eV· barns for each of the 39 neutron energy groups in Table 7a D-8
- D.13. Recommended prompt kerma factors for natural iron plus the "total decay heat" associated with either charged particle or gamma decay (of all isotopes produced by neutron activation) as given by the KAOS-V data library, extracted using the KAOS/RETRIEVE program, and expressed here in units of eV· barns for each of the 39 neutron energy groups in Table 7a ... D-8

- D.14. Kerma factors for gammas interacting with natural iron as calculated by the SMUG module of the AMPX cross section processing code system, stored in the ANSL-V 39n/44g cross section library (as nuclide 26000, MT-process 1527), subsequently extracted using the PAL module of the AMPX code system, and expressed here in units of eV· barns for each of the 44 gamma energy groups in Table 7a D-8

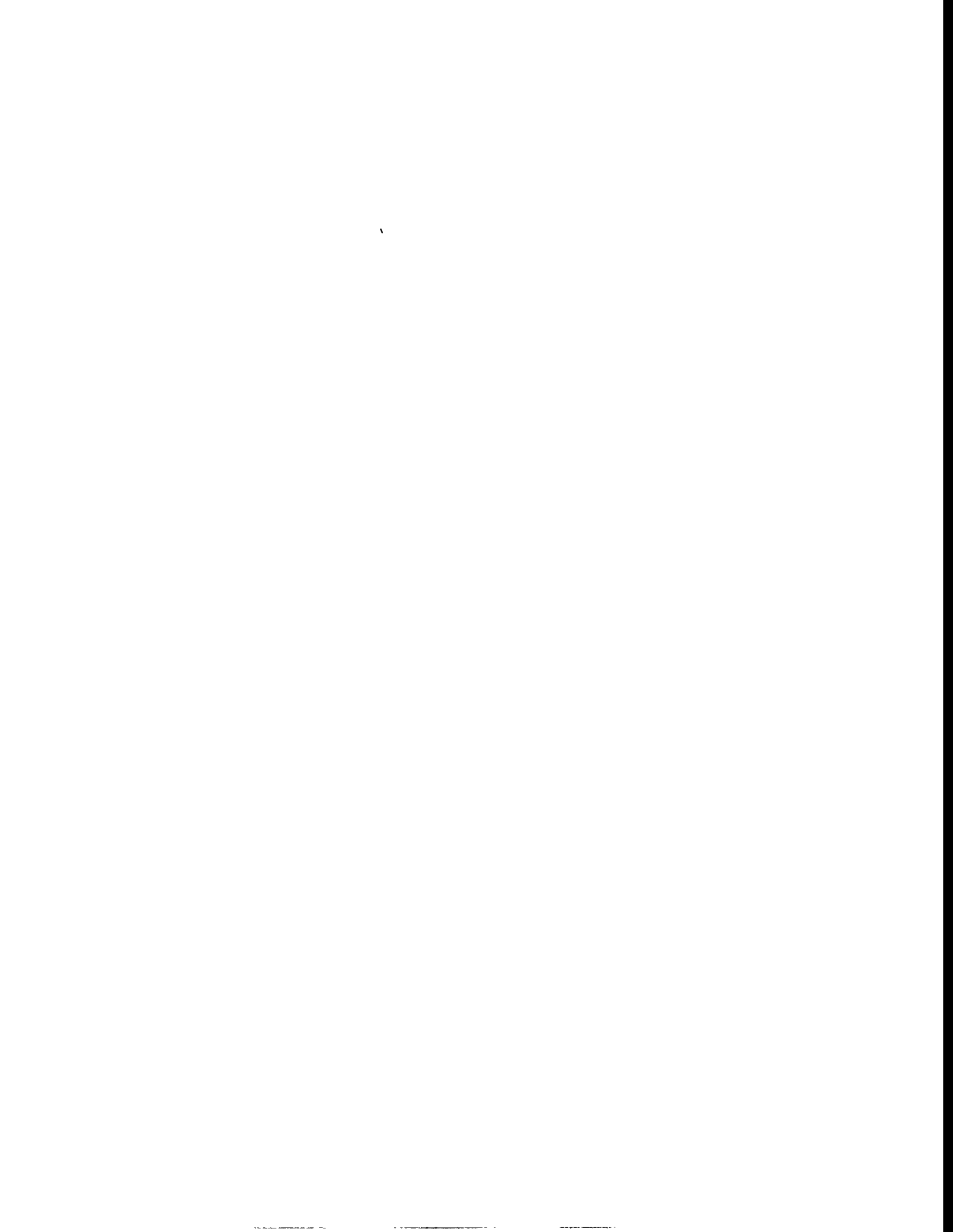
Final Results

- E.1. Radial trace along top of reflector vessel (at mid-thickness) E-12
- E.2. Radial trace about 1.20 m above the midplane E-13
- E.3. Radial trace about 0.30 m above the midplane, roughly halfway up the upper fuel element .. E-14
- E.4. Radial trace exactly at the axial midplane (by HB-1,2,3,4 and HB-6,7,8,9) E-16
- E.5. Radial trace about 0.30 m below the midplane, by the horizontal through-tube (HB-5/HB-10), roughly halfway up bottom fuel element E-18
- E.6. Radial trace about 1.20 m below the midplane E-20
- E.7. Radial trace along bottom of reflector vessel (at mid-thickness) E-21
- E.8. Partial axial trace along system centerline E-22
- E.9. Partial axial trace near inner surface of lower fuel element E-23
- E.10. Full axial trace at radial midpoint of lower (inner) fuel element E-24
- E.11. Partial axial trace near outer surface of lower fuel element E-25
- E.12. Partial axial trace near inner surface of upper fuel element E-26
- E.13. Full axial trace at radial midpoint of upper (outer) fuel element E-27
- E.14. Partial axial trace near outer surface of upper fuel element E-28
- E.15. Partial axial trace corresponding to radial location for lower portion of HT-2 E-29
- E.16. Partial axial trace corresponding to radial location for lower portion of SH-1 and SH-2 E-30
- E.17. Partial axial trace corresponding to radial location for lower portion of HT-4 E-31
- E.18. Full axial trace at radial location corresponding to HT-1 and HT-3 E-32
- E.19. Axial trace up through VT-1,2,3,4 E-33

E.20.	Axial trace up through PT-1	E-34
E.21.	Axial trace through side of reflector vessel (at mid-thickness)	E-35
E.22.	Partial axial trace corresponding to radial location for lower portion of PF-1	E-36
E.23.	Partial axial trace corresponding to radial location for lower portion of PF-2	E-36
E.24.	Trace along axis of the long slanted beam tube (LSBT)	E-37
E.25.	Trace along axis of PT-2 and PT-5	E-37
E.26.	Trace along axis of PT-3 and PT-4	E-38

ACRONYMS

1-D	one-dimensional
2-D	two-dimensional
3-D	three-dimensional
ANS	Advanced Neutron Source
ANSI	American National Standards Institute
ASTM	American Society for Testing and Materials
CPBT	core pressure boundary tube
CPU	central processing unit
DORT	discrete ordinates transport code
dpa	displacements per atom
HB	horizontal beam tube (HB-1 through HB-10)
HT	hydraulic tube (HT-1 through HT-4)
INEL	Idaho National Engineering Laboratory
LSBT	long slant beam tube
MHTGR	modular high-temperature gas-cooled reactor
ORNL	Oak Ridge National Laboratory
PF	pneumatic facility (PF-1 and PF-2)
PT	pneumatic tube (PT-1 through PT-5)
SH	slant hole facility (SH-1 and SH-2)
VT	vertical tube (VT-1 through VT-4)



ABSTRACT

This document describes the initial global 2-D shielding analyses for the Advanced Neutron Source (ANS) reactor, the D₂O reflector, the reflector vessel, and the first 200 mm of light water beyond the reflector vessel. Flux files generated here will later serve as source terms in subsequent shielding analyses. In addition to reporting fluxes and other data at key points of interest, a major objective of this report was to document how these analyses were performed, the phenomena that were included, and checks that were made to verify that these phenomena were properly modeled.

In these shielding analyses, the fixed neutron source distribution in the core was based on the "lifetime-averaged" spatial power distribution. Secondary gamma production cross sections in the fuel were modified so as to account intrinsically for delayed fission gammas in the fuel as well as prompt fission gammas. In and near the fuel, this increased the low-energy gamma fluxes by 50 to 250%, but out near the reflector vessel, these same fluxes changed by only a few percent. Sensitivity studies with respect to mesh size were performed, and a new 2-D mesh distribution developed after some problems were discovered with respect to the use of numerous elongated mesh cells in the reflector.

All of the shielding analyses were performed using the ANSL-V 39n/44g coupled library with 25 thermal neutron groups in order to obtain a rigorous representation of the thermal neutron spectrum throughout the reflector. Because of upscatter in the heavy water, convergence was very slow. Ultimately, the fission cross section in the various materials had to be artificially modified in order to solve this fixed source problem as an eigenvalue problem and invoke the Vondy error-mode extrapolation technique which greatly accelerated convergence in the large 2-D RZ DORT analyses. While this was quite effective, 150 outer iterations (over energy) were still required.

Accounting for photoneutron production in the heavy water was found to have a profound effect on the calculated fast flux levels deep in the reflector where those flux levels would otherwise be fairly depressed. Deep in the heavy water reflector, for example, the fast flux was found to be over 3300 times higher than when photoneutrons were not included. As noted in the report, however, the significance of that is strongly dependent on the particular situation one is analyzing; in many cases it makes no real difference, while in other cases it may be quite important. Two new programs, PHOTOX and SPARK, were therefore written to generate the necessary group-to-group photoneutron production cross sections and insert that data into the DORT-ready working cross section library as an enlarged scattering matrix. That data, and the iterative procedures for automatically converging the photoneutron sources, were first verified using a series of rapidly converging 1-D calculations.

The final reference solution was very tightly converged, included delayed fission gammas, employed the revised spatial mesh, and properly accounted for photoneutron production. The report includes 2-D plots showing the fast, intermediate, epithermal, and thermal neutron flux contours, as well as other plots for the gamma flux, and the neutron and gamma dose rates. Tabulated results for these parameters are also reported at 761 particular points of interest throughout the system. Tabulated results also show the total neutron plus gamma heating rates that would exist in any aluminum that might be present at these locations, as well as the displacements per atom (per year) that could be produced in small ferritic test specimens that might eventually be placed at many of these locations. Volume-integrated total heating rates for the reflector vessel and the inner and outer portions of the core pressure boundary tube were found to be 1.36, 1.18, and 1.71 megawatts, respectively. Lastly, the report describes a simple solid angle procedure for estimating the fluxes and dose rates several meters down the horizontal beam tubes.



1.0 INTRODUCTION

Shielding calculations for all parts of the Advanced Neutron Source (ANS) reactor and its various subsystems must ultimately be related back to the distribution of neutrons and gammas in the core and main reflector. This document therefore describes the large global shielding analyses for the core, the D₂O reflector, the reflector vessel, and the first 200 mm of light water out beyond the reflector vessel. These results will then serve as the basis for many of the source terms to be used in subsequent analyses involving other portions of the plant or the various subsystems.

While the global 2-D RZ shielding calculations described here include the same components and materials as in earlier reactor physics analyses, it should be realized that the final objectives of the physics and shielding studies, and hence the numerical approximations used in those respective models, are frequently quite different:

1. In reactor physics analyses, for example, one is usually preoccupied with the characteristics of the system at a particular point in time (beginning of cycle, end of cycle, etc.), whereas in shielding studies, one is generally concerned with lifetime-averaged fluxes or dose rates.
2. In a physics model, one typically has many fine mesh intervals in and immediately around the core, with a relatively coarse mesh deep in the reflector where the behavior of the flux is of much less concern. In the shielding analyses, by contrast, one is far less concerned with local peaking effects in the core and more concerned with the flux deeper in the reflector. A shielding analysis may therefore use a coarser mesh representation in the core but require a finer mesh representation in the reflector.
3. In physics calculations where one is concerned with burnup and reactivity effects, the resonance self-shielding of the fuel and fission products will be of paramount importance, whereas for shielding analyses, these effects (while still important) can be treated in a much more approximate fashion.
4. In the physics analysis of the core, where the fast and thermal fluxes are extremely high, the effect of photoneutron production may be negligible (except, of course, in reactor kinetic studies), while deep in the reflector, where the fast flux would otherwise be quite small, the shielding analyst must be concerned with photoneutrons which may dominate the fast flux in these regions.

Moreover, other differences in the type of details that must be represented in reactor physics and reactor shielding calculations will be noted throughout this report. Not surprisingly, the results of reactor physics calculations will typically be more accurate and more applicable in certain regions, while the results of the shielding calculations reported here will be more accurate and applicable in other regions of interest.

This report contains (1) a brief description of the geometry model and materials used; (2) a description of the cross section processing (resonance self-shielding) methods used; (3) a description of how the (g,n) photoneutron production cross sections were later added into the original cross section dataset and how the calculational methods were modified to account for this effect; (4) a description of the source terms used in the core for this analysis; (5) a description of three sets of analyses performed, including calculations using the original reactor physics mesh model and no photoneutrons (Run 3), a revised 2-D mesh model for reactor shielding but no photoneutrons (Run 4), and the revised 2-D mesh, with photoneutrons included in the analysis (Run 5). Limited results for the first two models will be presented,

while 2-D flux contours (and detailed tabulated listings of the results) for the final reference solution (Run 5) will be presented and contrasted with earlier results. Lastly, the role of several 1-D calculations used to verify the global 2-D calculations will be discussed briefly.

2.0 GEOMETRIC AND NUMERICAL MODELS

The geometric model used to represent the ANS core and reflector in the global 2-D RZ shielding analysis is illustrated in Figs. 1a and 1b and detailed more precisely in Table 1, which shows the exact location of each material in the model. Table 2 describes the atomic composition of each of the ten materials used in this model. Except for the fact that this geometric model uses homogenized "beginning of cycle" number densities for the fuel in the upper and lower sections of the core (cf. materials 8 and 9), this simplified 19-zone model is geometrically and materially identical to the more sophisticated 638-zone (double-walled CPBT) model used by the physics task in Dec. 1992. [Moreover, one of the initial objectives of the shielding task was to simplify the geometric model, the resonance self-shielding models, and the source representation and to perform an independent global analysis to verify that one would obtain ostensibly the same results in the regions of interest here as were previously obtained by the more sophisticated physics model.]

The geometric model shown in Fig. 1a and Table 1 was common to all of the global 2-D RZ DORT¹ analyses performed to date, although the number of radial and axial mesh intervals used to represent each zone was different in the various DORT models.

To interpret correctly the geometric description given in Table 1, it is important to realize that each zone overlays the earlier ones so that the material assigned to zone 2 may redefine the material used in some portions of zone 1, while the material assigned to zone 3 may redefine the materials used in some portions of zones 1 and 2, etc. To visually see the whole picture, it is frequently helpful to look at a colorized copy of the material mesh map showing the final location of each material. Figs. 2a-2f symbolically show the materials (1,2,3,...,8,9,A) used in each mesh interval in the global 2-D RZ model designated here as DORT Run 3, while Tables 3a and 3b list the corresponding radial and axial mesh boundaries. Note that these mesh specifications (originally developed by the physics task for detailed core analyses) used a relatively fine radial and axial mesh spacing in the upper and lower portions of the core (cf. materials 8 and 9, respectively, in Figs. 2b through 2e), and a relatively coarse mesh out in the reflector region. As noted in Sect. 6.4, this created many long but axially flat intervals in the side reflector which, in turn, tended to overestimate the flux deep in the reflector. Thus, for shielding analyses, a new radial and axial mesh was developed to avoid this problem by keeping the mesh cell aspect ratios as close to 1:1 as possible (i.e., generally below 1:2 or 2:1) throughout the bulk of the problem. The new scheme, shown in Figs. 3a-3f and described in Tables 4a and 4b, uses fewer radial and axial mesh intervals in the fuel (materials 8 and 9) where one has a fixed source (cf. Sect. 3) but uses more radial mesh intervals in the side reflector and more axial mesh intervals in the top and bottom axial reflector regions. Moreover, comparisons with 1-D radial calculations (cf. Sect. 6.4) show that the new mesh scheme now gives credible results deep in the side reflector, whereas the original scheme (which is better for reactor physics calculations) did not. Thus, this latter mesh scheme was used in DORT Runs 4 and 5. [Note that limitations on the overall CPU time prevented us from simply using more mesh intervals everywhere.]

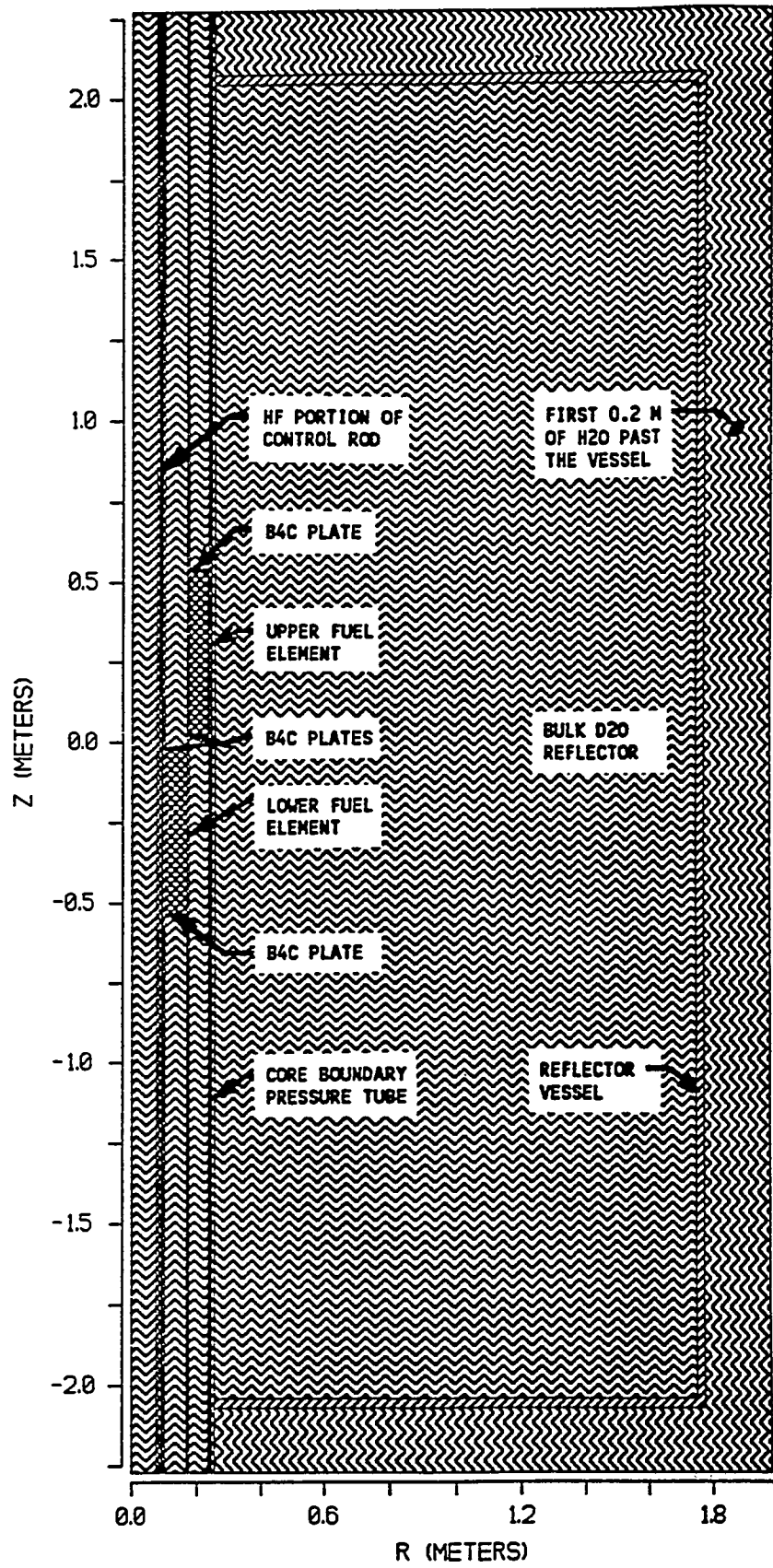


Fig. 1a. Geometric model used to represent the ANS core and reflector in the global 2-D RZ shielding analyses. See Table 1 for a more detailed description and/or Fig. 1b for a closer view of the core and surrounding materials.

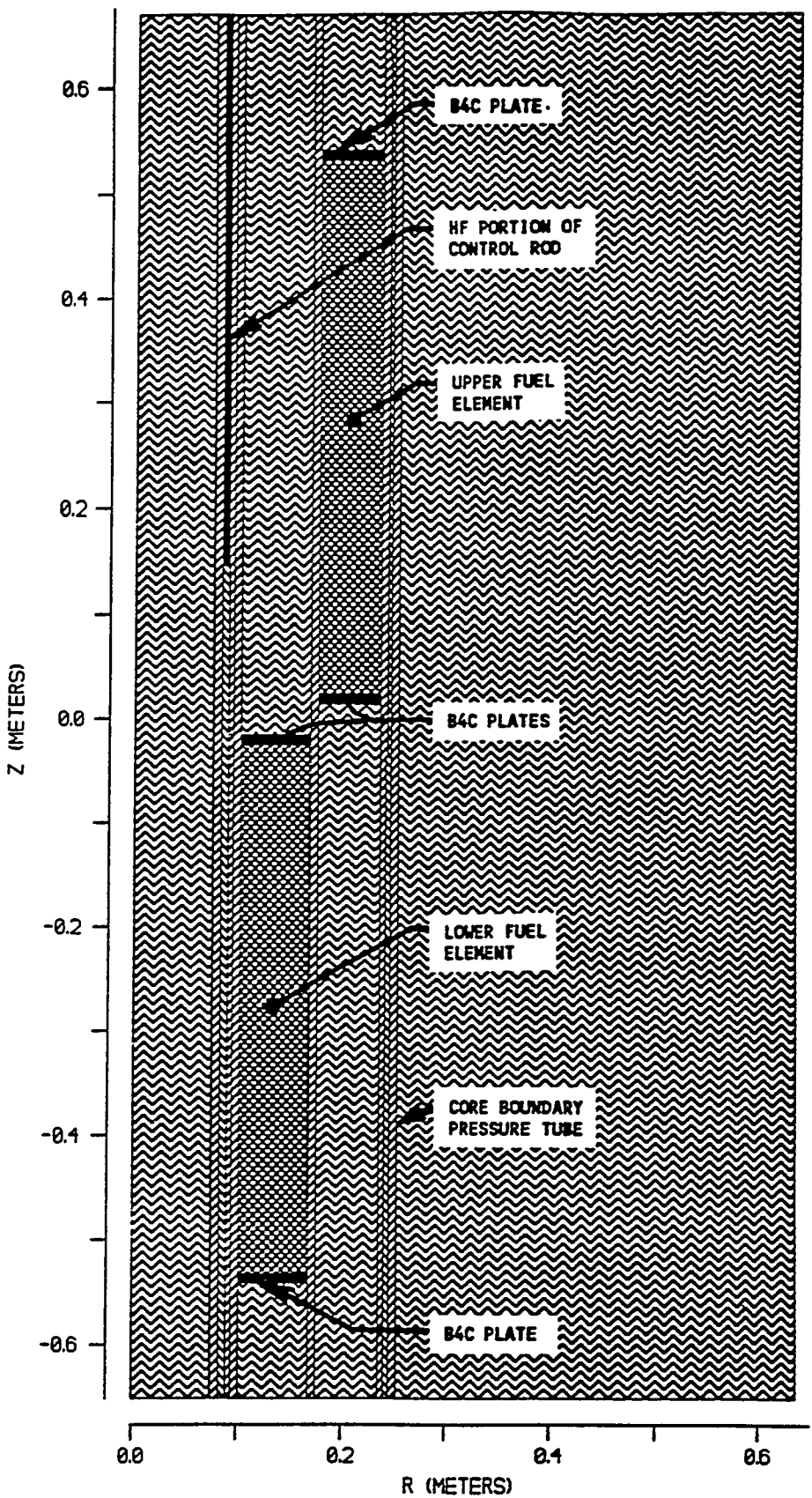


Fig. 1b. Enhanced view of the materials immediately surrounding the core in the global 2-D RZ shielding analysis of the ANS core and reflector. See Fig. 1a for a global view of the entire 2-D model.

Table 1. Description of the geometric model used in all of the global 2-D RZ analyses described in this report.

ZONE	RMIN mm	RMAX mm	ZMIN mm	ZMAX mm	MATL ID	DESCRIPTION
1	0.0	1983.0	-2272.0	2272.0	2	D2O everywhere (except as noted below)
2	253.0	1983.0	-2272.0	2272.0	3	H2O outer reflector/shield (less zones 3 & 4)
3	253.0	1775.0	-2072.0	2072.0	5	AL reflector tank (less zone 4)
4	253.0	1750.0	-2042.0	2042.0	2	D2O inside reflector tank
5	245.0	253.0	-2272.0	2272.0	5	AL for outer core bndry pressure tube (CBPT)
6	235.0	240.0	-2272.0	2272.0	5	AL for inner portion of CBPT
7	240.0	242.0	-35.0	632.0	5	AL sleeve on inner portion of CBPT
8	175.0	235.0	15.0	542.0	10	B4C plates on upper fuel elem (less zone 9)
9	175.0	235.0	25.0	532.0	8	Fuel in upper (outer) fuel element
10	168.0	175.0	-2272.0	2272.0	5	AL pipe between inner & outer elements
11	102.0	168.0	-542.0	-15.0	10	B4C plates on bottom fuel elem (less zone 12)
12	102.0	168.0	-532.0	-25.0	9	Fuel in bottom (inner) fuel element
13	95.0	102.0	-2272.0	2272.0	6	AL outer housing for control rods
14	90.0	95.0	-15.0	2272.0	1	D2O in CR housing by Hafnium control rod
15	83.0	90.0	-2272.0	2272.0	4	Zr trailer on control rod (less zone 16)
16	83.0	90.0	146.75	1416.0	7	Hf portion of control rod
17	76.1	83.0	-2272.0	2272.0	6	AL for inner housing for control rods
18	74.9	76.1	-2272.0	2272.0	4	Zr liner on inner housing for cntl rods
19	0.0	74.9	-2272.0	2272.0	1	D2O inside control rod housing

- 1) Rmin, Rmax, Zmin, and Zmax are all given here in mm, with Z=0.0 corresponding to the core midplane as shown in Fig. 1a. In the actual DORT input, these parameters (described by the 32, 33, 34, and 35** input arrays) were necessarily specified in cm, with Z=227.2 cm corresponding to the core midplane.
- 2) Table 2 gives the atomic number density of each nuclide comprising materials 1 to 10, above. Since the cross-section data for the P0, P1, P2, and P3 scattering moments for each of these is treated as a separate pseudo material in DORT, the corresponding ID numbers in the DORT 9\$\$ input array are given by N=4*M-3, for M=1 to 10.
- 3) The final geometry model used by the DORT code, illustrated in Figs. 1a and 1b, is constructed by overlaying the materials in each successive zone. Thus, the material in zone 2 may redefine the material used in some portions of zone 1, while the material in zone 3 may redefine the materials used in some portions of zones 1 and 2, etc.

Table 2. CSASI and JIPSY input describing the ten material mixtures used in the global 2-D RZ analysis of the ANS core and reflector tank. Shown here are the number densities [atoms/(barn*cm)] for each nuclide and the assumed bulk mean temperature (deg.K) for Doppler broadening and/or the selection of the thermal scattering matrices to be used.

```

=csasi
dummy run to get anisn x-sects for jpr model of ans
39n-44couple infhommedium
' place above (or any) ampx master library on ft70f001
' if name is not recognized, code will read ft70f001
'
' mix 1 = heavy water in central region
d    1      0.0    5.956e-02      322.2  end
o    1      0.0    2.978e-02      322.2  end
'
' mix 2 = heavy water (bulk):
d    2      0.0    5.947e-02      322.2  end
o    2      0.0    2.973e-02      322.2  end
'
' mix 3 = reg water (h20) in refl outside d2o tank:
h    3      0.0    6.611e-02      322.2  end
o    3      0.0    3.306e-02      322.2  end
'
' mix 4 = zircalloy (6.44 g/cc)
zr   4      0.0    4.251e-02      322.2  end
'
' mix 5 = aluminum 6061
mg   5      0.0    6.687e-04      339.2  end
al   5      0.0    5.822e-02      339.2  end
si   5      0.0    3.472e-04      339.2  end
ti   5      0.0    5.092e-05      339.2  end
cr   5      0.0    6.252e-05      339.2  end
mn   5      0.0    4.438e-05      339.2  end
fe   5      0.0    2.037e-04      339.2  end
cu   5      0.0    7.607e-05      339.2  end
cu   5      0.0    6.215e-05      339.2  end
'
' mix 6 = aluminum 6061:
mg   6      0.0    6.687e-04      322.2  end
al   6      0.0    5.822e-02      322.2  end
si   6      0.0    3.472e-04      322.2  end
ti   6      0.0    5.092e-05      322.2  end
cr   6      0.0    6.252e-05      322.2  end
mn   6      0.0    4.438e-05      322.2  end
fe   6      0.0    2.037e-04      322.2  end
cu   6      0.0    7.607e-05      322.2  end
cu   6      0.0    6.215e-05      322.2  end
'

```

Table 2 (cont)

```

'mix 7 = natural hafnium for control rod (13.31 g/cc)
hf    7      0.0     4.477e-02      322.2   end

'mix 8 = homogenized fuel zone (upper element):
homogenized densities due to fuel itself:
u-233  8      0.0     1.000e-15      505.4   end
u-234  8      0.0     7.100e-06      505.4   end
u-235  8      0.0     6.256e-04      505.4   end
u-236  8      0.0     2.866e-06      505.4   end
u-238  8      0.0     3.525e-05      505.4   end
si     8      0.0     4.472e-04      505.4   end

homogenized densities due to cladding:
mg    8      0.0     1.337e-04      505.4   end
al    8      0.0     2.791e-02      505.4   end
si    8      0.0     1.406e-04      505.4   end
ti    8      0.0     1.018e-05      505.4   end
cr    8      0.0     1.250e-05      505.4   end
mn    8      0.0     1.292e-05      505.4   end
fe    8      0.0     8.051e-05      505.4   end
cu    8      0.0     2.214e-05      505.4   end
cu    8      0.0     1.922e-05      505.4   end

homogenized densities due to heavy water:
d     8      0.0     2.949e-02      339.2   end
o     8      0.0     1.474e-02      339.2   end

'mix 9 = homogenized fuel zone (lower element):
homogenized densities due to fuel itself:
u-233  9      0.0     1.000e-15      505.4   end
u-234  9      0.0     5.921e-06      505.4   end
u-235  9      0.0     5.218e-04      505.4   end
u-236  9      0.0     2.390e-06      505.4   end
u-238  9      0.0     2.940e-05      505.4   end
si    9      0.0     3.730e-04      505.4   end

homogenized densities due to cladding:
mg    9      0.0     1.337e-04      505.4   end
al    9      0.0     2.814e-02      505.4   end
si    9      0.0     1.416e-04      505.4   end
ti    9      0.0     1.018e-05      505.4   end
cr    9      0.0     1.250e-05      505.4   end
mn    9      0.0     1.298e-05      505.4   end
fe    9      0.0     8.108e-05      505.4   end
cu    9      0.0     2.224e-05      505.4   end
cu    9      0.0     1.932e-05      505.4   end

homogenized densities due to heavy water:
d     9      0.0     2.949e-02      339.2   end
o     9      0.0     1.474e-02      339.2   end

'mix 10 = homogenized poison plates at ends of fuel:
```

Table 2 (cont)

```
' homogenized densities due to boron itself:  
b-10 10 0.0 2.980e-04 339.2 end  
b-11 10 0.0 1.199e-03 339.2 end  
' homogenized densities due to cladding:  
mg 10 0.0 1.337e-04 339.2 end  
al 10 0.0 2.868e-02 339.2 end  
si 10 0.0 1.440e-04 339.2 end  
ti 10 0.0 1.018e-05 339.2 end  
cr 10 0.0 1.250e-05 339.2 end  
mn 10 0.0 1.311e-05 339.2 end  
fe 10 0.0 8.241e-05 339.2 end  
cu 10 0.0 2.247e-05 339.2 end  
cu 10 0.0 1.955e-05 339.2 end  
' homogenized densities due to heavy water:  
d 10 0.0 3.265e-02 339.2 end  
o 10 0.0 1.632e-02 339.2 end  
'  
end comp  
end  
=jipsy  
' 1$$ igm iht ihs ihm ms mcr mtp mtm ith isct iprt iout idot nbuf e t  
1$$ 83 3 28 110 0 0 40 40 0 0 0 0 2 60 e t  
13$$ f1 t  
nomore  
end
```

Fig. 2a. Map of materials used in each mesh interval of the global 2-D RZ analysis of the ANS core and reflector vessel in DORT Run 3 ($Ir=1$ to 133, $Jz=1$ to 236). For a description of each material and the coordinates at each point, see Tables 2 and 3, respectively.

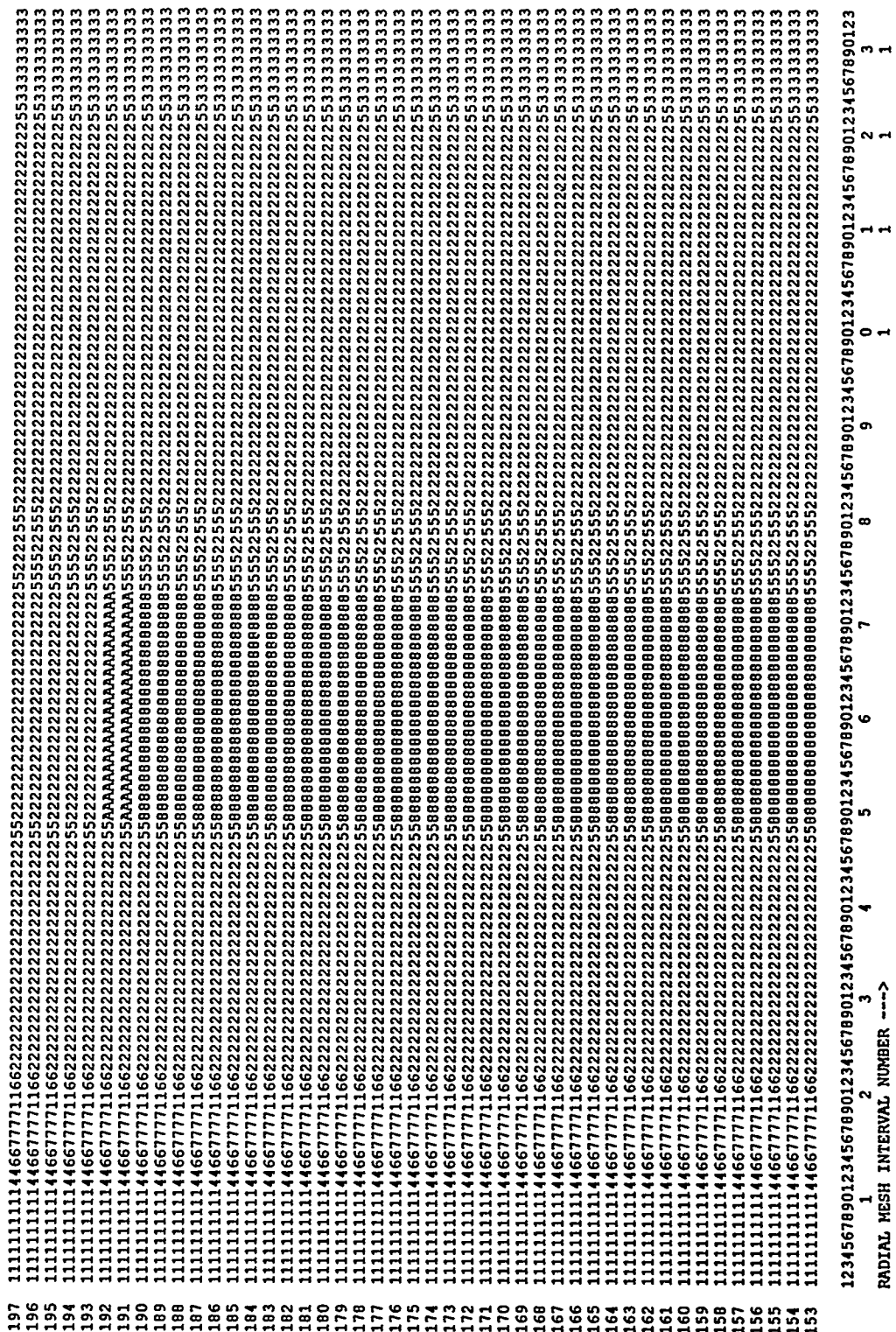


Fig. 2b. Map of materials used in each mesh interval of the ANS core and reflector vessel in DORT Run 3 ($Ir=1$ to 133, $Jz=1$ to 236). For a description of each material and the coordinates at each point, see Tables 2 and 3, respectively.

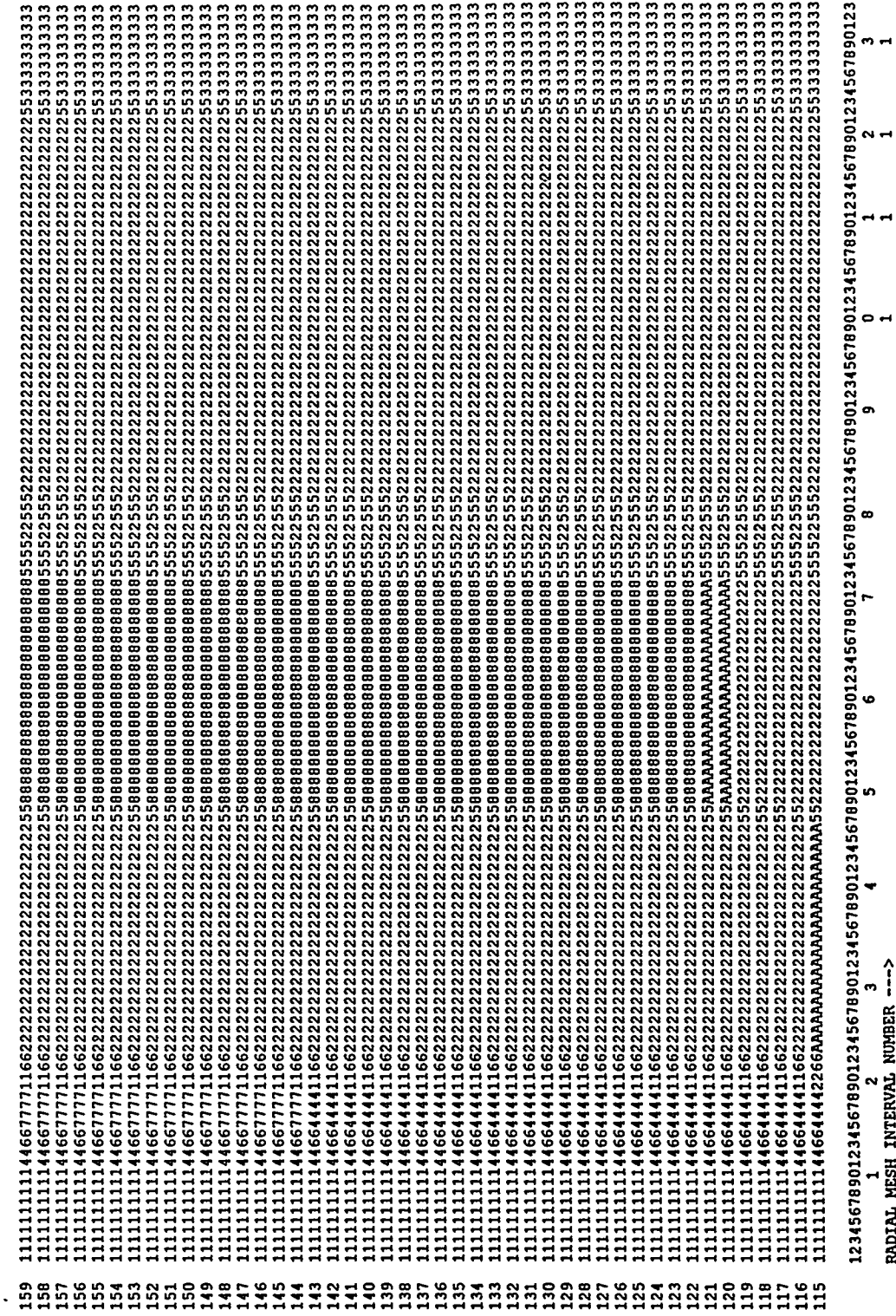


Fig. 2c. Map of materials used in each mesh interval of the ANS core and reflector vessel in DORT Run 3 ($\mathbf{Ir} = 1$ to 133, $Jz = 1$ to 236). For a description of each material and the coordinates at each point, see Tables 2 and 3, respectively.

Fig. 2d. Map of materials used in each mesh interval of the global 2-D RZ analysis of the ANS core and reflector vessel in DORT Run 3 ($Ir=1$ to 133, $Jz=1$ to 236). For a description of each material and the coordinates at each point, see Tables 2 and 3, respectively.

Fig. 2e. Map of materials used in each mesh interval of the global 2-D RZ analysis of the ANS core and reflector vessel in DORT Run 3 ($\text{Ir}=1$ to 133, $\text{Jz}=1$ to 236). For a description of each material and the coordinates at each point, see Tables 2 and 3, respectively.

Fig. 2f. Map of materials used in each mesh interval of the ANS core and reflector vessel in DORT Run 3 ($Ir=1$ to 133, $Jz=1$ to 236). For a description of each material and the coordinates at each point, see Tables 2 and 3, respectively.

Table 3a. Radial mesh boundaries (mm) used in the numerical model for DORT Run 3.

Ir	Rmin	Rmax	Ir	Rmin	Rmax	Ir	Rmin	Rmax
1	0.0000	8.3333	46	165.938	168.000	91	433.000	453.000
2	8.3333	16.6667	47	168.000	171.500	92	453.000	473.000
3	16.6667	25.0000	48	171.500	175.000	93	473.000	493.000
4	25.0000	33.3333	49	175.000	176.875	94	493.000	513.000
5	33.3333	41.6667	50	176.875	178.750	95	513.000	533.000
6	41.6667	50.0000	51	178.750	180.625	96	533.000	553.000
7	50.0000	56.2250	52	180.625	182.500	97	553.000	573.000
8	56.2250	62.4500	53	182.500	184.375	98	573.000	593.000
9	62.4500	68.6750	54	184.375	186.250	99	593.000	613.000
10	68.6750	74.9000	55	186.250	190.000	100	613.000	633.000
11	74.9000	75.5000	56	190.000	192.500	101	633.000	653.000
12	75.5000	76.1000	57	192.500	195.000	102	653.000	707.850
13	76.1000	79.5500	58	195.000	197.500	103	707.850	762.700
14	79.5500	83.0000	59	197.500	201.250	104	762.700	817.550
15	83.0000	84.7500	60	201.250	205.000	105	817.550	872.400
16	84.7500	86.5000	61	205.000	208.750	106	872.400	927.250
17	86.5000	88.2500	62	208.750	212.500	107	927.250	982.100
18	88.2500	90.0000	63	212.500	216.250	108	982.100	1036.95
19	90.0000	92.5000	64	216.250	220.000	109	1036.95	1091.80
20	92.5000	95.0000	65	220.000	221.875	110	1091.80	1146.65
21	95.0000	98.5000	66	221.875	223.750	111	1146.65	1201.50
22	98.5000	102.000	67	223.750	225.625	112	1201.50	1256.35
23	102.000	104.062	68	225.625	227.500	113	1256.35	1311.20
24	104.062	106.125	69	227.500	229.375	114	1311.20	1366.05
25	106.125	108.188	70	229.375	231.250	115	1366.05	1420.90
26	108.188	110.250	71	231.250	233.125	116	1420.90	1475.75
27	110.250	112.312	72	233.125	235.000	117	1475.75	1530.60
28	112.312	114.375	73	235.000	237.500	118	1530.60	1585.45
29	114.375	118.500	74	237.500	240.000	119	1585.45	1640.30
30	118.500	121.250	75	240.000	241.000	120	1640.30	1695.15
31	121.250	124.000	76	241.000	242.000	121	1695.15	1750.00
32	124.000	126.750	77	242.000	243.500	122	1750.00	1762.50
33	126.750	130.875	78	243.500	245.000	123	1762.50	1775.00
34	130.875	135.000	79	245.000	247.667	124	1775.00	1795.80
35	135.000	139.125	80	247.667	250.333	125	1795.80	1816.60
36	139.125	143.250	81	250.333	253.000	126	1816.60	1837.40
37	143.250	147.375	82	253.000	273.000	127	1837.40	1858.20
38	147.375	151.500	83	273.000	293.000	128	1858.20	1879.00
39	151.500	153.562	84	293.000	313.000	129	1879.00	1899.80
40	153.562	155.625	85	313.000	333.000	130	1899.80	1920.60
41	155.625	157.688	86	333.000	353.000	131	1920.60	1941.40
42	157.688	159.750	87	353.000	373.000	132	1941.40	1962.20
43	159.750	161.813	88	373.000	393.000	133	1962.20	1983.00
44	161.813	163.875	89	393.000	413.000			
45	163.875	165.938	90	413.000	433.000			

Note: In the actual DORT model, dimensions are entered in cm (not mm).

Table 3b. Axial mesh boundaries (mm) used in the numerical model for DORT Run 3 (see note).

Jz	Zmin	Zmax	Jz	Zmin	Zmax	Jz	Zmin	Zmax	Jz	Zmin	Zmax
1	-2272.00	-2252.00	60	-468.67	-462.00	119	7.50	15.00	178	482.00	488.67
2	-2252.00	-2232.00	61	-462.00	-455.33	120	15.00	20.00	179	488.67	495.33
3	-2232.00	-2212.00	62	-455.33	-448.67	121	20.00	25.00	180	495.33	502.00
4	-2212.00	-2192.00	63	-448.67	-442.00	122	25.00	27.50	181	502.00	505.33
5	-2192.00	-2172.00	64	-442.00	-431.42	123	27.50	30.00	182	505.33	508.67
6	-2172.00	-2152.00	65	-431.42	-420.83	124	30.00	32.50	183	508.67	512.00
7	-2152.00	-2132.00	66	-420.83	-410.25	125	32.50	35.00	184	512.00	515.33
8	-2132.00	-2112.00	67	-410.25	-399.67	126	35.00	37.50	185	515.33	518.67
9	-2112.00	-2092.00	68	-399.67	-389.08	127	37.50	40.00	186	518.67	522.00
10	-2092.00	-2072.00	69	-389.08	-378.50	128	40.00	42.50	187	522.00	524.50
11	-2072.00	-2062.00	70	-378.50	-368.50	129	42.50	45.00	188	524.50	527.00
12	-2062.00	-2052.00	71	-368.50	-358.50	130	45.00	50.00	189	527.00	529.50
13	-2052.00	-2042.00	72	-358.50	-348.50	131	50.00	55.00	190	529.50	532.00
14	-2042.00	-1977.00	73	-348.50	-338.50	132	55.00	60.00	191	532.00	537.00
15	-1977.00	-1912.00	74	-338.50	-328.50	133	60.00	65.00	192	537.00	542.00
16	-1912.00	-1847.00	75	-328.50	-318.50	134	65.00	75.00	193	542.00	564.50
17	-1847.00	-1782.00	76	-318.50	-308.50	135	75.00	81.67	194	564.50	587.00
18	-1782.00	-1717.00	77	-308.50	-298.50	136	81.67	88.33	195	587.00	609.50
19	-1717.00	-1652.00	78	-298.50	-288.50	137	88.33	95.00	196	609.50	632.00
20	-1652.00	-1587.00	79	-288.50	-278.50	138	95.00	101.67	197	632.00	647.00
21	-1587.00	-1522.00	80	-278.50	-268.50	139	101.67	108.33	198	647.00	662.00
22	-1522.00	-1457.00	81	-268.50	-258.50	140	108.33	115.00	199	662.00	682.00
23	-1457.00	-1392.00	82	-258.50	-248.50	141	115.00	125.58	200	682.00	702.00
24	-1392.00	-1327.00	83	-248.50	-238.50	142	125.58	136.17	201	702.00	722.00
25	-1327.00	-1262.00	84	-238.50	-228.50	143	136.17	146.75	202	722.00	742.00
26	-1262.00	-1197.00	85	-228.50	-218.50	144	146.75	152.00	203	742.00	803.27
27	-1197.00	-1132.00	86	-218.50	-208.50	145	152.00	165.25	204	803.27	864.55
28	-1132.00	-1067.00	87	-208.50	-198.50	146	165.25	178.50	205	864.55	925.82
29	-1067.00	-1002.00	88	-198.50	-188.50	147	178.50	188.50	206	925.82	987.09
30	-1002.00	-937.00	89	-188.50	-178.50	148	188.50	198.50	207	987.09	1048.36
31	-937.00	-872.00	90	-178.50	-165.80	149	198.50	208.50	208	1048.36	1109.64
32	-872.00	807.00	91	-165.80	-153.10	150	208.50	218.50	209	1109.64	1170.91
33	-807.00	-742.00	92	-153.10	-140.40	151	218.50	228.50	210	1170.91	1232.18
34	-742.00	-720.00	93	-140.40	-127.70	152	228.50	238.50	211	1232.18	1293.45
35	-720.00	-698.00	94	-127.70	-115.00	153	238.50	248.50	212	1293.45	1354.73
36	-698.00	-676.00	95	-115.00	-108.33	154	248.50	258.50	213	1354.73	1416.00
37	-676.00	-654.00	96	-108.33	-101.67	155	258.50	269.60	214	1416.00	1462.67
38	-654.00	-632.00	97	-101.67	-95.00	156	269.67	280.83	215	1462.67	1509.33
39	-632.00	-609.50	98	-95.00	-88.33	157	280.83	292.00	216	1509.33	1556.00
40	-609.50	-587.00	99	-88.33	-81.67	158	292.00	298.50	217	1556.00	1618.50
41	-587.00	-564.50	100	-81.67	-75.00	159	298.50	308.50	218	1618.50	1681.00
42	-564.50	-542.00	101	-75.00	-68.33	160	308.50	318.50	219	1681.00	1743.50
43	-542.00	-537.00	102	-68.33	-61.67	161	318.50	328.50	220	1743.50	1806.00
44	-537.00	-532.00	103	-61.67	-55.00	162	328.50	338.50	221	1806.00	1884.67
45	-532.00	-529.50	104	-55.00	-51.67	163	338.50	348.50	222	1884.67	1963.33
46	-529.50	-527.00	105	-51.67	-48.33	164	348.50	358.50	223	1963.33	2042.00
47	-527.00	-524.50	106	-48.33	-45.00	165	358.50	368.50	224	2042.00	2052.00
48	-524.50	-522.00	107	-45.00	-41.67	166	368.50	378.50	225	2052.00	2062.00
49	-522.00	-519.50	108	-41.67	-38.33	167	378.50	391.20	226	2062.00	2072.00
50	-519.50	-517.00	109	-38.33	-35.00	168	391.20	403.90	227	2072.00	2092.00
51	-517.00	-514.50	110	-35.00	-32.50	169	403.90	416.60	228	2092.00	2112.00
52	-514.50	-512.00	111	-32.50	-30.00	170	416.60	429.30	229	2112.00	2132.00
53	-512.00	-507.00	112	-30.00	-27.50	171	429.30	442.00	230	2132.00	2152.00
54	-507.00	-502.00	113	-27.50	-25.00	172	442.00	448.67	231	2152.00	2172.00
55	-502.00	-497.00	114	-25.00	-20.00	173	448.67	455.33	232	2172.00	2192.00
56	-497.00	-492.00	115	-20.00	-15.00	174	455.33	462.00	233	2192.00	2212.00
57	-492.00	-482.00	116	-15.00	-7.50	175	462.00	468.67	234	2212.00	2232.00
58	-482.00	-475.33	117	-7.50	0.00	176	468.67	475.33	235	2232.00	2252.00
59	-475.33	-468.67	118	0.00	7.50	177	475.33	482.00	236	2252.00	2272.00

Note: Here the core midplane is located at Z=0.0 mm; in the actual DORT model, dimensions are entered in cm, and Z=227.2 cm was the core midplane.

Fig. 3a. Map of materials used in each mesh interval of the global 2-D RZ analysis of the ANS core and reflector vessel in DORT Runs 4 and 5 ($Ir=1$ to 138, $Jz=1$ to 266). For a description of each material and the coordinates at each point, see Tables 2 and 4, respectively.

Fig. 3b. Map of materials used in each mesh interval of the ANS core and reflector vessel in DORT Runs 4 and 5 ($Ir=1$ to 138, $Jz=1$ to 266). For a description of each material and the coordinates at each point, see Tables 2 and 4, respectively.

Fig. 3c. Map of materials used in each mesh interval of the global 2-D RZ analysis of the ANS core and reflector vessel in DORT Runs 4 and 5 ($Ir=1$ to 138, $Jz=1$ to 266). For a description of each material and the coordinates at each point, see Tables 2 and 4, respectively.

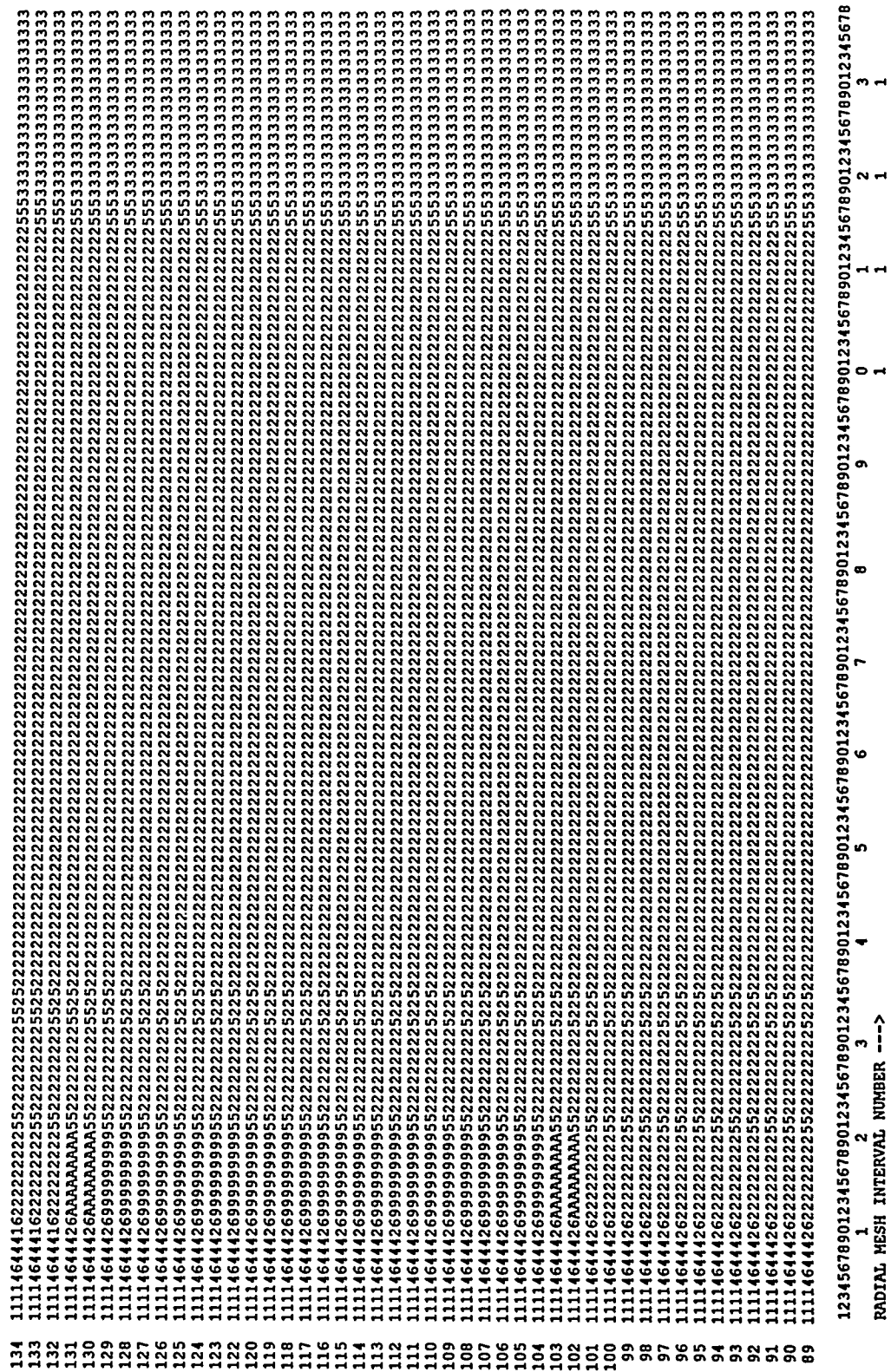


Fig. 3d. Map of materials used in each mesh interval of the ANS core and reflector vessel in DORT Runs 4 and 5 ($\text{Ir} = 1$ to 138, $\text{Jz} = 1$ to 266). For a description of each material and the coordinates at each point, see Tables 2 and 4, respectively.

Fig. 3e. Map of materials used in each mesh interval of the global 2-D RZ analysis of the ANS core and reflector vessel in DORT Runs 4 and 5 ($Ir = 1$ to 138, $Jz = 1$ to 266). For a description of each material and the coordinates at each point, see Tables 2 and 4, respectively.

Fig. 3f. Map of materials used in each mesh interval of the ANS core and reflector vessel in DORT Runs 4 and 5 ($Ir=1$ to 138, $Jz=1$ to 266). For a description of each material and the coordinates at each point, see Tables 2 and 4, respectively.

Table 4a. Radial mesh boundaries (mm) used in the numerical model for DORT Runs 4 and 5.

Ir	Rmin	Rmax	Ir	Rmin	Rmax	Ir	Rmin	Rmax
1	0.0000	18.7250	47	422.743	442.700	93	1340.77	1360.73
2	18.7250	37.4500	48	442.700	462.657	94	1360.73	1380.69
3	37.4500	56.1750	49	462.657	482.614	95	1380.69	1400.64
4	56.1750	74.9000	50	482.614	502.571	96	1400.64	1420.60
5	74.9000	76.1000	51	502.571	522.529	97	1420.60	1440.56
6	76.1000	83.0000	52	522.529	542.486	98	1440.56	1460.51
7	83.0000	85.3333	53	542.486	562.443	99	1460.51	1480.47
8	85.3333	87.6667	54	562.443	582.400	100	1480.47	1500.43
9	87.6667	90.0000	55	582.400	602.357	101	1500.43	1520.39
10	90.0000	95.0000	56	602.357	622.314	102	1520.39	1540.34
11	95.0000	102.000	57	622.314	642.271	103	1540.34	1560.30
12	102.000	108.188	58	642.271	662.229	104	1560.30	1580.26
13	108.188	114.375	59	662.229	682.186	105	1580.26	1600.21
14	114.375	122.625	60	682.186	702.143	106	1600.21	1620.17
15	122.625	130.875	61	702.143	722.100	107	1620.17	1640.13
16	130.875	139.125	62	722.100	742.057	108	1640.13	1660.09
17	139.125	147.375	63	742.057	762.014	109	1660.09	1680.04
18	147.375	155.625	64	762.014	781.971	110	1680.04	1700.00
19	155.625	161.812	65	781.971	801.929	111	1700.00	1710.00
20	161.812	168.000	66	801.929	821.886	112	1710.00	1720.00
21	168.000	171.500	67	821.886	841.843	113	1720.00	1730.00
22	171.500	175.000	68	841.843	861.800	114	1730.00	1740.00
23	175.000	180.625	69	861.800	881.757	115	1740.00	1750.00
24	180.625	186.250	70	881.757	901.714	116	1750.00	1758.33
25	186.250	193.750	71	901.714	921.671	117	1758.33	1766.67
26	193.750	201.250	72	921.671	941.629	118	1766.67	1775.00
27	201.250	208.750	73	941.629	961.586	119	1775.00	1785.40
28	208.750	216.250	74	961.586	981.543	120	1785.40	1795.80
29	216.250	223.750	75	981.543	1001.50	121	1795.80	1806.20
30	223.750	229.375	76	1001.50	1021.46	122	1806.20	1816.60
31	229.375	235.000	77	1021.46	1041.41	123	1816.60	1827.00
32	235.000	240.000	78	1041.41	1061.37	124	1827.00	1837.40
33	240.000	242.000	79	1061.37	1081.33	125	1837.40	1847.80
34	242.000	245.000	80	1081.33	1101.29	126	1847.80	1858.20
35	245.000	253.000	81	1101.29	1121.24	127	1858.20	1868.60
36	253.000	263.000	82	1121.24	1141.20	128	1868.60	1879.00
37	263.000	273.000	83	1141.20	1161.16	129	1879.00	1889.40
38	273.000	283.000	84	1161.16	1181.11	130	1889.40	1899.80
39	283.000	293.000	85	1181.11	1201.07	131	1899.80	1910.20
40	293.000	303.000	86	1201.07	1221.03	132	1910.20	1920.60
41	303.000	322.957	87	1221.03	1240.99	133	1920.60	1931.00
42	322.957	342.914	88	1240.99	1260.94	134	1931.00	1941.40
43	342.914	362.871	89	1260.94	1280.90	135	1941.40	1951.80
44	362.871	382.829	90	1280.90	1300.86	136	1951.80	1962.20
45	382.829	402.786	91	1300.86	1320.81	137	1962.20	1972.60
46	402.786	422.743	92	1320.81	1340.77	138	1972.60	1983.00

Note: In the actual DORT models, dimensions are entered in cm (not mm).

**Table 4b. Axial mesh boundaries (mm) used in the numerical model for DORT Runs 4 and 5
(see note).**

Jz	Zmin	Zmax	Jz	Zmin	Zmax	Jz	Zmin	Zmax	Jz	Zmin	Zmax
1	-2272.00	-2262.00	68	-1189.06	-1168.47	135	15.00	20.00	202	1230.32	1250.95
2	-2262.00	-2252.00	69	-1168.47	-1147.88	136	20.00	25.00	203	1250.95	1271.58
3	-2252.00	-2242.00	70	-1147.88	-1127.29	137	25.00	41.67	204	1271.58	1292.21
4	-2242.00	-2232.00	71	-1127.29	-1106.71	138	41.67	58.33	205	1292.21	1312.84
5	-2232.00	-2222.00	72	-1106.71	-1086.12	139	58.33	75.00	206	1312.84	1333.47
6	-2222.00	-2212.00	73	-1086.12	-1065.53	140	75.00	92.94	207	1333.47	1354.11
7	-2212.00	-2202.00	74	-1065.53	-1044.94	141	92.94	110.88	208	1354.11	1374.74
8	-2202.00	-2192.00	75	-1044.94	-1024.35	142	110.88	128.8	209	1374.74	1395.37
9	-2192.00	-2182.00	76	-1024.35	-1003.76	143	128.81	146.75	210	1395.37	1416.00
10	-2182.00	-2172.00	77	-1003.76	-983.18	144	146.75	164.69	211	1416.00	1436.57
11	-2172.00	-2162.00	78	-983.18	-962.59	145	164.69	182.62	212	1436.57	1457.14
12	-2162.00	-2152.00	79	-962.59	-942.00	146	182.62	200.56	213	1457.14	1477.71
13	-2152.00	-2142.00	80	-942.00	-921.41	147	200.56	218.50	214	1477.71	1498.29
14	-2142.00	-2132.00	81	-921.41	-900.82	148	218.50	238.50	215	1498.29	1518.86
15	-2132.00	-2122.00	82	-900.82	-880.24	149	238.50	258.50	216	1518.86	1539.43
16	-2122.00	-2112.00	83	-880.24	-859.65	150	258.50	278.50	217	1539.43	1560.00
17	-2112.00	-2102.00	84	-859.65	-839.06	151	278.50	298.50	218	1560.00	1580.57
18	-2102.00	-2092.00	85	-839.06	-818.47	152	298.50	318.50	219	1580.57	1601.14
19	-2092.00	-2082.00	86	-818.47	-797.88	153	318.50	338.50	220	1601.14	1621.71
20	-2082.00	-2072.00	87	-797.88	-777.29	154	338.50	359.00	221	1621.71	1642.29
21	-2072.00	-2062.00	88	-777.29	-756.71	155	359.00	379.50	222	1642.29	1662.86
22	-2062.00	-2052.00	89	-756.71	-736.12	156	379.50	400.00	223	1662.86	1683.43
23	-2052.00	-2042.00	90	-736.12	-715.53	157	400.00	420.50	224	1683.43	1704.00
24	-2042.00	-2032.00	91	-715.53	-694.94	158	420.50	441.00	225	1704.00	1724.57
25	-2032.00	-2022.00	92	-694.94	-674.35	159	441.00	461.50	226	1724.57	1745.14
26	-2022.00	-2012.00	93	-674.35	-653.76	160	461.50	482.00	227	1745.14	1765.71
27	-2012.00	-2002.00	94	-653.76	-633.18	161	482.00	498.67	228	1765.71	1786.29
28	-2002.00	-1992.00	95	-633.18	-612.59	162	498.67	515.33	229	1786.29	1806.86
29	-1992.00	-1971.41	96	-612.59	-592.00	163	515.33	532.00	230	1806.86	1827.43
30	-1971.41	-1950.82	97	-592.00	-582.00	164	532.00	537.00	231	1827.43	1848.00
31	-1950.82	-1930.23	98	-582.00	-572.00	165	537.00	542.00	232	1848.00	1868.57
32	-1930.23	-1909.65	99	-572.00	-562.00	166	542.00	552.00	233	1868.57	1889.14
33	-1909.65	-1889.06	100	-562.00	-552.00	167	552.00	562.00	234	1889.14	1909.71
34	-1889.06	-1868.47	101	-552.00	-542.00	168	562.00	572.00	235	1909.71	1930.29
35	-1868.47	-1847.88	102	-542.00	-537.00	169	572.00	582.00	236	1930.29	1950.86
36	-1847.88	-1827.29	103	-537.00	-532.00	170	582.00	592.00	237	1950.86	1971.43
37	-1827.29	-1806.71	104	-532.00	-515.33	171	592.00	612.00	238	1971.43	1992.00
38	-1806.71	-1786.12	105	-515.33	-498.67	172	612.00	632.00	239	1992.00	2002.00
39	-1786.12	-1765.53	106	-498.67	-482.00	173	632.00	652.63	240	2002.00	2012.00
40	-1765.53	-1744.94	107	-482.00	-461.50	174	652.63	673.26	241	2012.00	2022.00
41	-1744.94	-1724.35	108	-461.50	-441.00	175	673.26	693.89	242	2022.00	2032.00
42	-1724.35	-1703.76	109	-441.00	-420.50	176	693.89	714.53	243	2032.00	2042.00
43	-1703.76	-1683.18	110	-420.50	-400.00	177	714.53	735.16	244	2042.00	2052.00
44	-1683.18	-1662.59	111	-400.00	-379.50	178	735.16	755.79	245	2052.00	2062.00
45	-1662.59	-1642.00	112	-379.50	-359.00	179	755.79	776.42	246	2062.00	2072.00
46	-1642.00	-1621.41	113	-359.00	-338.50	180	776.42	797.05	247	2072.00	2082.00
47	-1621.41	-1600.82	114	-338.50	-318.50	181	797.05	817.68	248	2082.00	2092.00
48	-1600.82	-1580.23	115	-318.50	-298.50	182	817.68	838.32	249	2092.00	2102.00
49	-1580.23	-1559.65	116	-298.50	-278.50	183	838.32	858.95	250	2102.00	2112.00
50	-1559.65	-1539.06	117	-278.50	-258.50	184	858.95	879.58	251	2112.00	2122.00
51	-1539.06	-1518.47	118	-258.50	-238.50	185	879.58	900.21	252	2122.00	2132.00
52	-1518.47	-1497.88	119	-238.50	-218.50	186	900.21	920.84	253	2132.00	2142.00
53	-1497.88	-1477.29	120	-218.50	-198.00	187	920.84	941.47	254	2142.00	2152.00
54	-1477.29	-1456.71	121	-198.00	-177.50	188	941.47	962.11	255	2152.00	2162.00
55	-1456.71	-1436.12	122	-177.50	-157.00	189	962.11	982.74	256	2162.00	2172.00
56	-1436.12	-1415.53	123	-157.00	-136.50	190	982.74	1003.37	257	2172.00	2182.00
57	-1415.53	-1394.94	124	-136.50	-116.00	191	1003.37	1024.00	258	2182.00	2192.00
58	-1394.94	-1374.35	125	-116.00	-95.50	192	1024.00	1044.63	259	2192.00	2202.00
59	-1374.35	-1353.76	126	-95.50	-75.00	193	1044.63	1065.26	260	2202.00	2212.00
60	-1353.76	-1333.18	127	-75.00	-55.00	194	1065.26	1085.89	261	2212.00	2222.00
61	-1333.18	-1312.59	128	-55.00	-35.00	195	1085.89	1106.53	262	2222.00	2232.00
62	-1312.59	-1292.00	129	-35.00	-25.00	196	1106.53	1127.16	263	2232.00	2242.00
63	-1292.00	-1271.41	130	-25.00	-20.00	197	1127.16	1147.79	264	2242.00	2252.00
64	-1271.41	-1250.82	131	-20.00	-15.00	198	1147.79	1168.42	265	2252.00	2262.00
65	-1250.82	-1230.24	132	-15.00	-5.00	199	1168.42	1189.05	266	2262.00	2272.00
66	-1230.24	-1209.65	133	-5.00	5.00	200	1189.05	1209.68	267	2272.00	2282.00
67	-1209.65	-1189.06	134	5.00	15.00	201	1209.68	1230.32	268	2282.00	2292.00

* Here core midplane is located at Z = 0.0 mm

Note: In the actual DORT models, dimensions are entered in cm, and Z=227.2 cm was the core midplane.

3.0 MULTIGROUP SOURCE TERMS

The multigroup neutron source distribution in the core is based on data presented in the *ANS Conceptual Safety Analysis Report*² of June 1992, with minor corrections as noted below. Pages 4.3-41 to 4.3-50 of that report show the relative (and absolute) power densities in each of 13 radial and 23 axial mesh intervals in the upper section of the core, as well as in 13 radial and 23 axial mesh intervals in the lower section of the core, at each of 5 times [$t=0.0$ days (beginning of cycle), $t=4.25$ days, $t=8.5$ days, $t=12.75$ days, and $t=17.0$ days (end of cycle)] based on detailed physics analyses involving 3-D burnup studies and control rod motion studies over the lifetime of the core. Such fine detail, with 598 separate source regions, however, is typically not necessary for global shielding analyses, as long as reasonable care is taken to model the shape of the source near the outer edges of the core. Also, in shielding analyses, one is generally more concerned with the average dose rates and fluences over the lifetime of the system rather than the details at any particular time during the burnup cycle. To simplify the description of the source, the upper and lower fuel elements were each divided into 15 source zones (30 altogether) as illustrated in Fig. 4 and described more precisely in Table 6a. A simple utility routine was then written to read the absolute and relative power densities in each of the 598 fine mesh fuel zones reported by the Physics Task and to determine the volumetrically averaged power densities in each of our 30 source zones at each time step shown in Table 5. The program tabulates the peak power in each zone over the lifetime of the core, as well as the lifetime-averaged power densities in each of these 30 source zones (cf. Table 6a). The lifetime-averaged power densities in each of these 30 source zones then served as the basis for computing the lifetime-averaged neutron source terms in each zone (cf. Table 6b) used in the global 2-D shielding analyses. These neutron source terms were computed assuming an energy yield of 3.11E10 fissions per second per watt, and an average neutron yield of 2.43 neutrons per fission in U-235. The multigroup form of the neutron source was obtained by folding the local neutron yields with the 39-group U-235 fission yield spectrum (χ^g).

As is standard procedure in fixed source shielding calculations, the prompt fission gammas in the core were not entered explicitly as external source terms but were accounted for intrinsically as secondary gammas during the course of the 2-D DORT analysis. Prompt fission gammas normally include only the gammas generated in the first 50 to 100 nanoseconds after fission. While lower energy delayed fission gammas typically include everything out to 1.0E13 seconds, the bulk of these are generated in the first 1 to 10 seconds, and indeed in the first few hundredths of a second after fission. As such, they should also be included in any steady-state reactor shielding analysis. To accomplish this, the delayed fission gamma yield spectra for U-235 and U-238 were combined with the prompt fission gamma yield spectra for these isotopes as described in Sects. 4.1 and 6.5 so that both types of fission gammas would be intrinsically represented as secondary gammas in the subsequent shielding analyses.

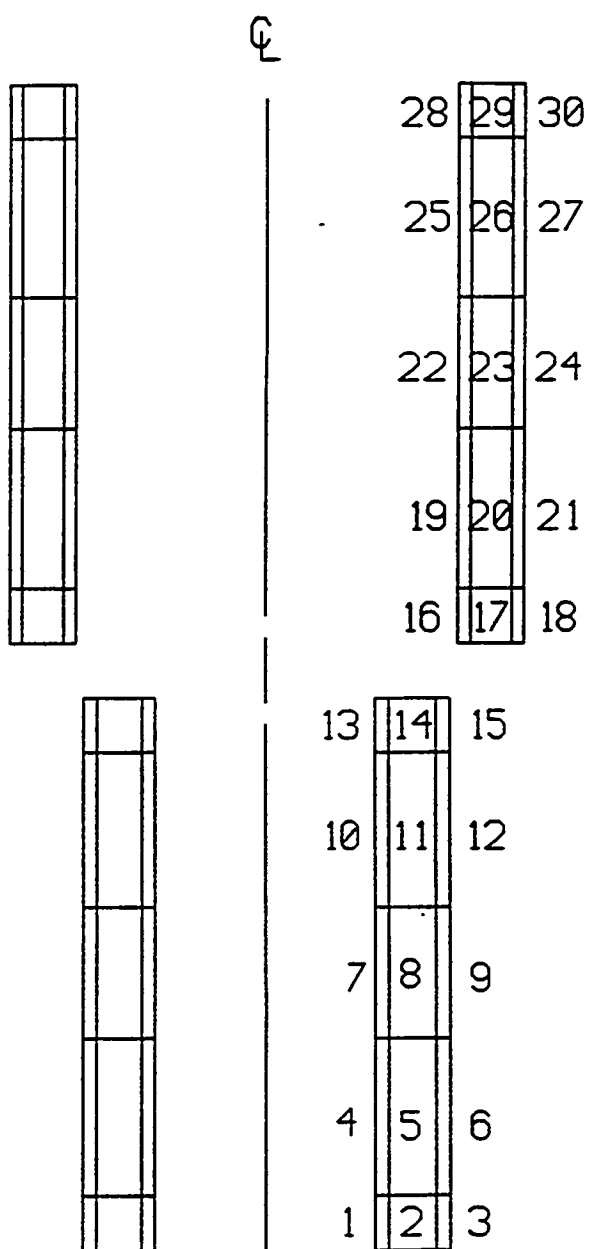


Fig. 4. Relative location of the 30 source zones used in the global 2-D shielding analysis. See Tables 6a and 6b for additional details.

**Table 5. Average power densities in the upper and lower sections
of the ANS reactor core as a function of time.**

Burnup (Time)	Top Fuel Element	Bottom Fuel Element
t= 0.00 days	4.336 MW/L	6.109 MW/L
t= 4.25 days	4.496 MW/L	5.903 MW/L
t= 8.50 days	4.772 MW/L	5.553 MW/L
t=12.75 days (a)	6.212 MW/L	3.488 MW/L
(b)	5.396 MW/L	4.716 MW/L
t=17.00 days (a)	4.984 MW/L	5.242 MW/L
(b)	6.212 MW/L	3.488 MW/L

(a) Published values taken from Ref. 2 (1992).

(b) Revised values supplied by the Physics Task on March 15,
1993 and used in all of the shielding studies reported here.

Table 6a. Volume-averaged power densities in various portions of the ANS core as a function of time (cf Fig.4).

Zone	Rmin(i) mm	Rmax(i) mm	Zmin(i) mm	Zmax(i) mm	N(i)	Power Density (megawatts/liter)						
						0 DAYS	4.25 D	8.50 D	12.75 D	17.0 D	Avg	Max
1	102.000	114.375	-532.000	-482.000	120	7.0955	8.0649	7.7848	6.0946	4.2063	6.8988	8.0649
2	114.375	155.625	-532.000	-482.000	280	5.5675	6.9206	7.1865	5.9216	4.2576	6.2353	7.1865
3	155.625	168.000	-532.000	-482.000	120	10.0704	10.1274	8.6464	6.1766	3.9365	7.9884	10.1274
4	102.000	114.375	-482.000	-338.500	75	6.5446	6.3467	5.9250	5.0115	3.8079	5.6149	6.5446
5	114.375	155.625	-482.000	-338.500	175	5.7668	5.7074	5.5171	4.8395	3.7747	5.2087	5.7668
6	155.625	168.000	-482.000	-338.500	75	9.9926	8.8628	7.2862	5.4505	3.6601	7.1064	9.9926
7	102.000	114.375	-338.500	-218.500	45	7.0157	6.5128	6.0763	5.3514	4.1927	5.8862	7.0157
8	114.375	155.625	-338.500	-218.500	105	6.5176	6.2350	5.9358	5.2818	4.1728	5.6994	6.5176
9	155.625	168.000	-338.500	-218.500	45	8.8126	7.4009	5.9091	4.3708	2.8981	5.8840	8.8126
10	102.000	114.375	-218.500	-75.000	45	5.1017	4.8791	4.8394	4.3422	3.2368	4.5575	5.1017
11	114.375	155.625	-218.500	-75.000	105	4.9829	4.8347	4.7750	4.3246	3.2911	4.5178	4.9829
12	155.625	168.000	-218.500	-75.000	45	6.4349	5.4512	4.5155	3.4240	2.2182	4.4293	6.4349
13	102.000	114.375	-75.000	-25.000	60	3.2019	3.3587	3.8165	3.4585	2.3086	3.3472	3.8165
14	114.375	155.625	-75.000	-25.000	140	3.0043	3.2777	3.7899	3.5588	2.4907	3.3435	3.7899
15	155.625	168.000	-75.000	-25.000	60	3.8951	3.8071	3.6720	2.9871	1.8863	3.3392	3.8951
16	175.000	186.250	25.000	75.000	120	6.1029	7.3073	8.6472	8.7995	7.1209	7.8415	8.7995
17	186.250	223.750	25.000	75.000	280	5.5301	6.8385	7.9334	8.0491	6.8320	7.2505	8.0491
18	223.750	235.000	25.000	75.000	120	9.3086	9.2897	8.5452	7.1349	5.1397	8.0485	9.3086
19	175.000	186.250	75.000	218.500	75	5.0116	5.2858	6.1479	7.6605	7.6459	6.3557	7.6605
20	186.250	223.750	75.000	218.500	175	4.6333	4.8763	5.4401	6.3419	6.5572	5.5634	6.5572
21	223.750	235.000	75.000	218.500	75	7.9392	7.5930	7.1299	6.7499	5.8358	7.0901	7.9392
22	175.000	186.250	218.500	338.500	45	3.6587	3.6791	4.0118	5.8998	8.1377	4.8722	8.1377
23	186.250	223.750	218.500	338.500	105	3.8254	3.8716	4.1169	5.0758	6.3495	4.5379	6.3495
24	223.750	235.000	218.500	338.500	45	6.1323	5.8026	5.4409	5.5194	5.5588	5.6521	6.1323
25	175.000	186.250	338.500	482.000	45	2.9048	2.9653	3.1829	4.0521	7.7078	3.8766	7.7078
26	186.250	223.750	338.500	482.000	105	3.1100	3.1887	3.3781	4.0248	5.9265	3.7775	5.9265
27	223.750	235.000	338.500	482.000	45	4.3407	4.1895	3.9894	4.1485	4.7605	4.2195	4.7605
28	175.000	186.250	482.000	532.000	60	2.1198	2.4112	2.7833	3.4207	5.8691	3.1524	5.8691
29	186.250	223.750	482.000	532.000	140	2.2406	2.5358	2.9044	3.4782	5.0994	3.1471	5.0994
30	223.750	235.000	482.000	532.000	60	2.8785	2.9414	2.9518	3.1169	3.7476	3.0808	3.7476

General notes:

- (a) These power densities are based on the relative power distributions shown on pages 4.3-41 to 4.3-50 of the ANS "Conceptual Safety Analysis Report" (Ref. 2), with minor corrections as noted in Table 5 above.
- (b) N(i) is the number of subintervals from reactor physics calculation that are included in source zone (i).
- (c) This corresponds to a volume-integrated lifetime-averaged total power of 344.615 MWth for the entire core.

Table 6b. Volume-averaged neutron sources in various portions of the ANS core as a function of time (cf Fig.4).

Zone	Rmin(i) mm	Rmax(i) mm	Zmin(i) mm	Zmax(i) mm	Neutron source (neutrons per second, per cubic centimeter)						
					0 DAYS	4.25 D	8.50 D	12.75 D	17.0 D	AVG	MAX
1	102.000	114.375	-532.00	-482.00	5.36E+14	6.09E+14	5.88E+14	4.61E+14	3.18E+14	5.21E+14	6.09E+14
2	114.375	155.625	-532.00	-482.00	4.21E+14	5.23E+14	5.43E+14	4.48E+14	3.22E+14	4.71E+14	5.43E+14
3	155.625	168.000	-532.00	-482.00	7.61E+14	7.65E+14	6.53E+14	4.67E+14	2.97E+14	6.04E+14	7.65E+14
4	102.000	114.375	-482.00	-338.50	4.95E+14	4.80E+14	4.48E+14	3.79E+14	2.88E+14	4.24E+14	4.95E+14
5	114.375	155.625	-482.00	-338.50	4.36E+14	4.31E+14	4.17E+14	3.66E+14	2.85E+14	3.94E+14	4.36E+14
6	155.625	168.000	-482.00	-338.50	7.55E+14	6.70E+14	5.51E+14	4.12E+14	2.77E+14	5.37E+14	7.55E+14
7	102.000	114.375	-338.50	-218.50	5.30E+14	4.92E+14	4.59E+14	4.04E+14	3.17E+14	4.45E+14	5.30E+14
8	114.375	155.625	-338.50	-218.50	4.93E+14	4.71E+14	4.49E+14	3.99E+14	3.15E+14	4.31E+14	4.93E+14
9	155.625	168.000	-338.50	-218.50	6.66E+14	5.59E+14	4.47E+14	3.30E+14	2.19E+14	4.45E+14	6.66E+14
10	102.000	114.375	-218.50	-75.00	3.86E+14	3.69E+14	3.66E+14	3.28E+14	2.45E+14	3.44E+14	3.86E+14
11	114.375	155.625	-218.50	-75.00	3.77E+14	3.65E+14	3.61E+14	3.27E+14	2.49E+14	3.41E+14	3.77E+14
12	155.625	168.000	-218.50	-75.00	4.86E+14	4.12E+14	3.41E+14	2.59E+14	1.68E+14	3.35E+14	4.86E+14
13	102.000	114.375	-75.00	-25.00	2.42E+14	2.54E+14	2.88E+14	2.61E+14	1.74E+14	2.53E+14	2.88E+14
14	114.375	155.625	-75.00	-25.00	2.27E+14	2.48E+14	2.86E+14	2.69E+14	1.88E+14	2.53E+14	2.86E+14
15	155.625	168.000	-75.00	-25.00	2.94E+14	2.98E+14	2.78E+14	2.26E+14	1.43E+14	2.52E+14	2.94E+14
16	175.000	186.250	25.00	75.00	4.61E+14	5.52E+14	6.53E+14	6.65E+14	5.38E+14	5.93E+14	6.65E+14
17	186.250	223.750	25.00	75.00	4.18E+14	5.17E+14	6.00E+14	6.08E+14	5.16E+14	5.48E+14	6.08E+14
18	223.750	235.000	25.00	75.00	7.03E+14	7.02E+14	6.46E+14	5.39E+14	3.88E+14	6.08E+14	7.03E+14
19	175.000	186.250	75.00	218.50	3.79E+14	3.99E+14	4.65E+14	5.79E+14	5.78E+14	4.80E+14	5.79E+14
20	186.250	223.750	75.00	218.50	3.50E+14	3.69E+14	4.11E+14	4.79E+14	4.96E+14	4.20E+14	4.96E+14
21	223.750	235.000	75.00	218.50	6.00E+14	5.74E+14	5.39E+14	5.10E+14	4.41E+14	5.36E+14	6.00E+14
22	175.000	186.250	218.50	338.50	2.76E+14	2.78E+14	3.03E+14	4.46E+14	6.15E+14	3.68E+14	6.15E+14
23	186.250	223.750	218.50	338.50	2.89E+14	2.93E+14	3.11E+14	3.84E+14	4.80E+14	3.43E+14	4.80E+14
24	223.750	235.000	218.50	338.50	4.63E+14	4.39E+14	4.11E+14	4.17E+14	4.20E+14	4.27E+14	4.63E+14
25	175.000	186.250	338.50	482.00	2.20E+14	2.24E+14	2.41E+14	3.06E+14	5.83E+14	2.93E+14	5.83E+14
26	186.250	223.750	338.50	482.00	2.35E+14	2.41E+14	2.55E+14	3.04E+14	4.48E+14	2.85E+14	4.48E+14
27	223.750	235.000	338.50	482.00	3.28E+14	3.17E+14	3.01E+14	3.14E+14	3.60E+14	3.19E+14	3.60E+14
28	175.000	186.250	482.00	532.00	1.60E+14	1.82E+14	2.10E+14	2.59E+14	4.44E+14	2.38E+14	4.44E+14
29	186.250	223.750	482.00	532.00	1.69E+14	1.92E+14	2.19E+14	2.63E+14	3.85E+14	2.38E+14	3.85E+14
30	223.750	235.000	482.00	532.00	2.18E+14	2.22E+14	2.23E+14	2.36E+14	2.83E+14	2.33E+14	2.83E+14

Note: These neutron sources are based on the relative power distributions shown on pages 4.3-41 to 4.3-50 of the ANS "Conceptual Safety Analysis Report" (Ref. 2), with minor corrections as noted in Table 5 above.

4.0 CROSS-SECTION DATA USED IN THE GLOBAL ANALYSES

4.1 The Original DORT-Ready Cross Sections

The 39n/44g ANSL-V AMPX cross section library described in Ref. 3 served as the starting point for all of the cross sections used in the global analysis of the ANS core and reflector vessel. (The neutron and gamma energy group structures for this and the 99n/44g ANSL-V library are shown in Tables 7a and 7b, respectively. While a 99n/44g fine-group coupled library was generated in the summer of 1993, that library was not available in the March to June 1993 time frame when the present set of global 2-D shielding analyses were performed.) Moreover, that original 39n/44g AMPX master library had been supplemented by J-P. Renier who (1) added the hafnium data in late 1992/early 1993, (2) processed the data through the PERFUME module⁴ of the AMPX system⁵ to make slight adjustments to the scattering moments [to assure that the same data could also be used in Monte Carlo analyses], and (3) downloaded the resulting AMPX master library to the IBM workstation cluster.

Initial processing of the U-235 and U-238 data through the NITAWL code⁶ gave a message saying "the neutron cross section cannot be found to convert the yield data for MT=181," which meant that the delayed fission gammas would not be included in the (n,g) production terms. [See discussion of MT=181 data in Sect. 4.6 of ref. 3.] In reality, these secondary gamma source terms should be included, and that particular yield data should be folded with the fission cross section (MT=18) to obtain the (n,g) production terms. To remedy this deficiency, the following small block of programming

```
DO 135 JAB=1,N2DY
IF (MTX(JAB).EQ.181) MTX(JAB)=18
135 CONTINUE
```

was inserted between the end of do-loop 130 and the beginning of do-loop 150 in Subroutine KOPY in a special (ANS) version of the AJAX module⁷ in the AMPX code system.⁵ This special ANS version of the AJAX program was then used to copy the entire master library from one dataset to another, while making this one small change for the U-235 and U-238 data. [This allows both the prompt and the delayed fission gammas to be folded with the fission cross section and allows both to be included in the secondary gamma production cross sections in the working library created by NITAWL.] This revised AMPX master library was then used in all subsequent shielding analyses.

From the microscopic AMPX master cross section library for the various nuclides, the macroscopic cross sections for the ten materials of interest (cf. Table 2) were initially created using the CSASI and JIPSY codes^{8,9} whose input data is also listed in Table 2. Both of these codes run under the SCALE driver.¹⁰ In this case, the CSASI control module processed the data for each nuclide through the BONAMI and NITAWL resonance self-shielding modules^{6,11} where each of the 10 materials was treated as an infinite homogeneous medium — an assumption that would be wholly inadequate for reactor physics work but which is generally completely adequate for reactor shielding calculations. The CSASI control module then (automatically) passes the resonance self-shielded microscopic cross section data to the ICE module¹² of the SCALE system,¹⁰ which creates the macroscopic cross section data for each mixture in an ANISN format. The JIPSY code, whose input is also shown in Table 2, then transforms the material-oriented ANISN library into a group-oriented (i.e., group-independent) library that is suitable for use with the 2-D DORT shielding code. The JIPSY code used here is essentially the same as the GIP code¹³ normally packaged with the DORT/TORT code system¹ but with a few minor exceptions in order to allow the code to run

Table 7a. Neutron and gamma energy group structures for the ANSL-V 39n/44g cross section library.

Neutron Group	Emax (eV)	Emin (eV)	Gamma Group	Emax (eV)	Emin (eV)
1	2.00E+07	--	6.43E+06	1	2.00E+07
2	6.43E+06	--	3.00E+06	2	1.40E+07
3	3.00E+06	--	1.85E+06	3	1.20E+07
4	1.85E+06	--	1.40E+06	4	1.00E+07
5	1.40E+06	--	9.00E+05	5	8.00E+06
6	9.00E+05	--	4.00E+05	6	7.50E+06
7	4.00E+05	--	1.00E+05	7	7.00E+06
8	1.00E+05	--	1.70E+04	8	6.50E+06
9	1.70E+04	--	3.00E+03	9	6.00E+06
10	3.00E+03	--	5.50E+02	10	5.50E+06
11	5.50E+02	--	1.00E+02	11	5.00E+06
12	1.00E+02	--	3.00E+01	12	4.50E+06
13	3.00E+01	--	1.00E+01	13	4.00E+06
14	1.00E+01	--	3.00E+00	14	3.50E+06
15	3.00E+00	--	1.77E+00	15	3.00E+06
16	1.77E+00	--	1.30E+00	16	2.50E+06
17	1.30E+00	--	1.00E+00	17	2.35E+06
18	1.00E+00	--	7.65E-01	18	2.15E+06
19	7.65E-01	--	6.25E-01	19	2.00E+06
20	6.25E-01	--	4.79E-01	20	1.80E+06
21	4.79E-01	--	3.97E-01	21	1.66E+06
22	3.97E-01	--	3.30E-01	22	1.57E+06
23	3.30E-01	--	2.70E-01	23	1.50E+06
24	2.70E-01	--	2.15E-01	24	1.44E+06
25	2.15E-01	--	1.62E-01	25	1.33E+06
26	1.62E-01	--	1.04E-01	26	1.20E+06
27	1.04E-01	--	5.00E-02	27	1.00E+06
28	5.00E-02	--	3.00E-02	28	8.00E+05
29	3.00E-02	--	1.00E-02	29	7.00E+05
30	1.00E-02	--	4.45E-03	30	6.00E+05
31	4.45E-03	--	3.25E-03	31	5.12E+05
32	3.25E-03	--	2.60E-03	32	5.10E+05
33	2.60E-03	--	2.15E-03	33	4.50E+05
34	2.15E-03	--	1.80E-03	34	4.00E+05
35	1.80E-03	--	1.45E-03	35	3.00E+05
36	1.45E-03	--	1.15E-03	36	2.00E+05
37	1.15E-03	--	8.50E-04	37	1.50E+05
38	8.50E-04	--	5.50E-04	38	1.00E+05
39	5.50E-04	--	1.00E-05	39	7.50E+04
			40	7.00E+04	--
			41	6.00E+04	--
			42	4.50E+04	--
			43	3.00E+04	--
			44	2.00E+04	--

Table 7b. Neutron energy group structure for the ANSL-V 99n/44g cross section library, where the 44 gamma groups have the same energy group structure as in the 39n/44g library.

Neutron Group	Emax (eV)	Emin (eV)	Neutron Group	Emax (eV)	Emin (eV)
1	2.0000E+07	-- 1.5941E+07	51	5.5000E+02	-- 3.9110E+02
2	1.5941E+07	-- 1.2706E+07	52	3.9110E+02	-- 2.7811E+02
3	1.2706E+07	-- 1.0127E+07	53	2.7811E+02	-- 1.9776E+02
4	1.0127E+07	-- 8.0722E+06	54	1.9776E+02	-- 1.4063E+02
5	8.0722E+06	-- 6.4340E+06	55	1.4063E+02	-- 1.0000E+02
6	6.4340E+06	-- 5.5234E+06	56	1.0000E+02	-- 7.8600E+01
7	5.5234E+06	-- 4.7417E+06	57	7.8600E+01	-- 6.1780E+01
8	4.7417E+06	-- 4.0707E+06	58	6.1780E+01	-- 4.8559E+01
9	4.0707E+06	-- 3.4946E+06	59	4.8559E+01	-- 3.8168E+01
10	3.4946E+06	-- 3.0000E+06	60	3.8168E+01	-- 3.0000E+01
11	3.0000E+06	-- 2.7235E+06	61	3.0000E+01	-- 2.4082E+01
12	2.7235E+06	-- 2.4725E+06	62	2.4082E+01	-- 1.9332E+01
13	2.4725E+06	-- 2.2447E+06	63	1.9332E+01	-- 1.5518E+01
14	2.2447E+06	-- 2.0378E+06	64	1.5518E+01	-- 1.2457E+01
15	2.0378E+06	-- 1.8500E+06	65	1.2457E+01	-- 1.0000E+01
16	1.8500E+06	-- 1.7497E+06	66	1.0000E+01	-- 7.8600E+00
17	1.7497E+06	-- 1.6548E+06	67	7.8600E+00	-- 6.1780E+00
18	1.6548E+06	-- 1.5651E+06	68	6.1780E+00	-- 4.8559E+00
19	1.5651E+06	-- 1.4803E+06	69	4.8559E+00	-- 3.8168E+00
20	1.4803E+06	-- 1.4000E+06	70	3.8168E+00	-- 3.0000E+00
21	1.4000E+06	-- 1.2816E+06	71	3.0000E+00	-- 2.6995E+00
22	1.2816E+06	-- 1.1732E+06	72	2.6995E+00	-- 2.4292E+00
23	1.1732E+06	-- 1.0740E+06	73	2.4292E+00	-- 2.1859E+00
24	1.0740E+06	-- 9.8315E+05	74	2.1859E+00	-- 1.9670E+00
25	9.8315E+05	-- 9.0000E+05	75	1.9670E+00	-- 1.7700E+00
26	9.0000E+05	-- 7.6525E+05	76	1.7700E+00	-- 1.3000E+00
27	7.6525E+05	-- 6.5068E+05	77	1.3000E+00	-- 1.0000E+00
28	6.5068E+05	-- 5.5326E+05	78	1.0000E+00	-- 7.6500E-01
29	5.5326E+05	-- 4.7043E+05	79	7.6500E-01	-- 6.2500E-01
30	4.7043E+05	-- 4.0000E+05	80	6.2500E-01	-- 4.7900E-01
31	4.0000E+05	-- 3.0314E+05	81	4.7900E-01	-- 3.9700E-01
32	3.0314E+05	-- 2.2974E+05	82	3.9700E-01	-- 3.3000E-01
33	2.2974E+05	-- 1.7411E+05	83	3.3000E-01	-- 2.7000E-01
34	1.7411E+05	-- 1.3195E+05	84	2.7000E-01	-- 2.1500E-01
35	1.3195E+05	-- 1.0000E+05	85	2.1500E-01	-- 1.6200E-01
36	1.0000E+05	-- 7.0160E+04	86	1.6200E-01	-- 1.0400E-01
37	7.0160E+04	-- 4.9224E+04	87	1.0400E-01	-- 5.0000E-02
38	4.9224E+04	-- 3.4536E+04	88	5.0000E-02	-- 3.0000E-02
39	3.4536E+04	-- 2.4230E+04	89	3.0000E-02	-- 1.0000E-02
40	2.4230E+04	-- 1.7000E+04	90	1.0000E-02	-- 4.4500E-03
41	1.7000E+04	-- 1.2017E+04	91	4.4500E-03	-- 3.2500E-03
42	1.2017E+04	-- 8.4941E+03	92	3.2500E-03	-- 2.6000E-03
43	8.4941E+03	-- 6.0042E+03	93	2.6000E-03	-- 2.1500E-03
44	6.0042E+03	-- 4.2441E+03	94	2.1500E-03	-- 1.8000E-03
45	4.2441E+03	-- 3.0000E+03	95	1.8000E-03	-- 1.4500E-03
46	3.0000E+03	-- 2.1368E+03	96	1.4500E-03	-- 1.1500E-03
47	2.1368E+03	-- 1.5220E+03	97	1.1500E-03	-- 8.5000E-04
48	1.5220E+03	-- 1.0841E+03	98	8.5000E-04	-- 5.5000E-04
49	1.0841E+03	-- 7.7217E+02	99	5.5000E-04	-- 1.0000E-05
50	7.7217E+02	-- 5.5000E+02			

under the SCALE driver and to allow the user to input just the bare minimum amount of input data, as shown in Table 2. These two factors made the (GIP/JIPSY) code much more convenient to use and greatly reduced the probability of accidental input errors. It should also be noted that while the ISCT input parameter is shown as zero in Table 2, the dataset really includes P_0 , P_1 , P_2 , and P_3 scattering data for all 10 of the original materials. Thus, since DORT treats each P_L component as a separate material, the MTP and MTM parameters were both set to 40 rather than 10.

4.2 INITIAL ADJUSTMENTS TO OBTAIN ERROR MODE ACCELERATION

Initial 2-D calculations for the core and reflector (DORT Runs 1 and 2) were performed with the DORT-ready macroscopic cross sections described above. These were fixed-source calculations with the internal fission source turned off, as is standard practice for such calculations. After 100 outer iterations and more than a week of CPU time on an IBM Model 530 workstation, the neutron fluxes in the thermal groups (i.e., groups 15-39) were still far from being converged. Moreover, this is a common problem for transport calculations where one has a large region of an almost nonabsorbing media such as graphite or heavy water. One scheme for accelerating this type of fixed-source problem is to turn it into an eigenvalue problem where one

1. sets $v\Sigma_F = 0$ (or some negligibly small value) in the fuel,
2. sets $v\Sigma_F$ equal to some negligibly small (but finite) value for every other material in the problem,
3. lets the DORT code calculate the (negligibly small) fission source distribution and eigenvalue during each outer iteration, but
4. throws away these fictitious fission neutrons by placing them all (via a fictitious χ^2 fission spectrum) into a group that is not included in the present set of outer iterations so they don't contribute to the actual internal source. [If one is performing outer iterations to converge the thermal neutron groups (15-39), for example, the chi spectrum could be used to place this negligibly small fictitious source in group 1 or in one of the gamma groups.]

This scheme was originally suggested by Dave Vondy and successfully demonstrated by Wayne Rhoades and Dick Lillie (all of ORNL). While more details of how the scheme was implemented here are discussed in Sect. 6.3, suffice it to say for now that the ratios of the eigenvalues (associated with the negligibly small fission distribution) between successive outer iterations are used by the code as a measure of how fast the thermal groups are converging and, periodically, can be used to "project" where the flux is going, and get there earlier by applying a multiplicative adjustment to all the fluxes of interest (i.e., extrapolating). Typically the problem will be allowed to converge slowly for 7 to 15 outer iterations before a large and significant adjustment is made. It will then be allowed to converge at its normal (slow) pace for another 7 to 15 outer iterations before another large and significant adjustment is made, etc. Proceeding in this fashion, highly diffusive problems that would have been virtually impossible to solve in any practical amount of CPU time can thus be made to converge, and problems that would have converged eventually will now converge more rapidly. The key thing to be careful of here is that the fictitious value of $v\Sigma_F$ introduced everywhere be completely negligible relative to the macroscopic absorption cross section in the least absorbing media. Here, the default value of $v\Sigma_F=1.0E-10/cm$ was chosen so as to be completely negligible relative to the macroscopic absorption cross section in D_2O where, for example, $\Sigma_A=6.01E-6/cm$ in group 18.

Within the context of the global 2-D DORT calculations, it was therefore decided (1) to converge the fast neutron groups (1-14) with one calculation using the original DORT-ready cross section library, (2) to use a second DORT calculation (or series of calculations) to perform a large number of outer iterations over the thermal neutron groups (15-39) using this modified DORT-ready cross section library, and (3) to use a final DORT calculation to converge the gamma groups (40-83) using the original DORT-ready cross section library. Table 8 shows a complete listing of the SMURF code used to create the modified DORT-ready cross section library necessary for Step 2. Note that it reads in the original DORT-ready cross section library, sets $\nu\Sigma_F=0$ in all materials and in all energy groups except the thermal neutron groups (15-39) where it sets $\nu\Sigma_F=1.0E-10/cm$ for all materials prior to writing out the modified DORT-ready cross section dataset needed for Step 2. This modified dataset was used in Step 2 of DORT Runs 3 and 4 using the original and revised spatial mesh descriptions of the basic geometry model. DORT Run 5, which accounts for the generation of photoneutrons, used a somewhat different modified cross section dataset, as described in Sect. 4.3.

4.3 FURTHER ADJUSTMENTS TO ACCOUNT FOR PHOTONEUTRON PRODUCTION

On page 24 of the section on Radiation Shielding in Vol III of the 1962 Reactor Handbook by E. P. Blizzard,¹⁴ former Director of the Neutron Physics Division at ORNL, it was noted that "With a shield which attenuates neutrons rapidly but is practically transparent to gamma rays, photoneutrons can provide most of the observed dose in the outer regions of the shield." Later 1-D calculations by J. A. Bucholz confirmed that this was the case for the ANS reactor where photoneutron production is compounded by the fact that low energy (n,g) reactions in the aluminum reflector vessel yield high-energy gammas which are capable of producing photoneutrons in the D_2O reflector. The remainder of this section focuses on how the multigroup photoneutron production cross sections necessary for sophisticated 2-D calculations were produced, while other sections later in this report will describe how these were verified and used.

Page 143 of the 1965 textbook on the "Physics of Nuclear Kinetics" by G. R. Keepin¹⁵ shows the experimentally measured cross section for photoneutron production in deuterium as a function of photon energy, as well as a "best fit" smooth curve representation of the cross section based on the experimental and theoretical data available at that time. For completeness, a photographic reproduction of that original plot is included here as Fig. 5, while Table 9 shows a digitized tabulation of the data [XSECT(plot)] at each of 29 energy points between 2.20 and 12.45 MeV. (Note that this is a threshold reaction whose cross section goes to zero below 2.225 MeV.) At higher energies (above 6 or 8 MeV), this reaction is represented very nicely by the theoretical formulae for the photomagnetic and photoelectric disintegration cross sections for the deuteron as given on pages 334-336 of the 1955 textbook on "The Atomic Nucleus" by R. D. Evans.¹⁶ For reference, these theoretical formulae are embedded in Subroutine XPND2O at the end of the PHOTOX program which is listed in Appendix A of this report. Moreover, theoretical values [XSECT(theory)] over the full energy range (up to 20 MeV) based on these formulae are also listed in Table 9 for comparison purposes.

The PHOTOX program listed in Appendix A was written to determine the (gamma)group-to-(neutron)group photoneutron production cross sections that would be needed in later shielding studies. At the heart of this is Subroutine XPND2O, which returns the total photoneutron production cross section as a function of photon energy. There, a linear-linear interpolation of the XSECT(plot) vs Energy data in Table 9 is used for energies below 11.44 MeV, while the theoretical formulae in the book by Evans¹⁶ are used for energies at and above 11.44 MeV. To determine the resulting neutron energy, it is assumed that

Table 8. Complete listing of the SMURF program that was used to read the DORT-ready macroscopic cross sections for each material and set the value of nu*sigf equal to a negligibly small value (1.0e-10/cm) in each material so that the DORT code could take advantage of Vondy's "error mode acceleration" scheme.

```

dimension d(100000)
limit=100000
c
c   read the following:
c   =====
      igm=83
      iht=3
      ihs=28
      ihm=110
      mtm=40
      isct=3
      idot=2
c   =====
c
      nus=ihs - iht - 1
      ihp=ihm
      if(idot.eq.2) idot = 0
      if(nus.gt.0 .and. idot.lt.2) ihp = ihm + 1
c
      open (8,status='old',form='unformatted')
      open (9,status='new',form='unformatted')
c
      need=ihp*mtm
      if (need.gt.limit) stop 9999
c
      do ig=1,igm
      call modify (d(l),ihp,iht,mtm,isct,ig)
      enddo
c
      stop
      end
      subroutine modify (xsect,ihp,iht,mtm,isct,ig)
c
      dimension xsect(ihp,mtm)
c
      read (8) ((xsect(ipos,imat),ipos=1,ihp),imat=1,mtm)
c
      isctpl=isct+1
      do imat=1,mtm
          xsect(iht-1,imat)=0.0           ! set nu*sigf=0.0
          if (isctpl*((imat-1)/isctpl).eq.(imat-1)) then
              if (ig.ge.15) xsect(iht-1,imat)=1.0e-10    ! if real matl (not PL component), then:
              ! set nu*sigf=1.0e-10 for thermal groups
          endif
          enddo
c
          write (9) ((xsect(ipos,imat),ipos=1,ihp),imat=1,mtm)
c
          if (ig.ne.18) return
          write (6,11) (imat,xsect(1,imat),xsect(2,imat),xsect(3,imat),
* xsect(4,imat),xsect(110,imat),xsect(111,imat),imat=1,40)
11         format (1x,i3,1p,6e16.5)
c
          return
          end

```

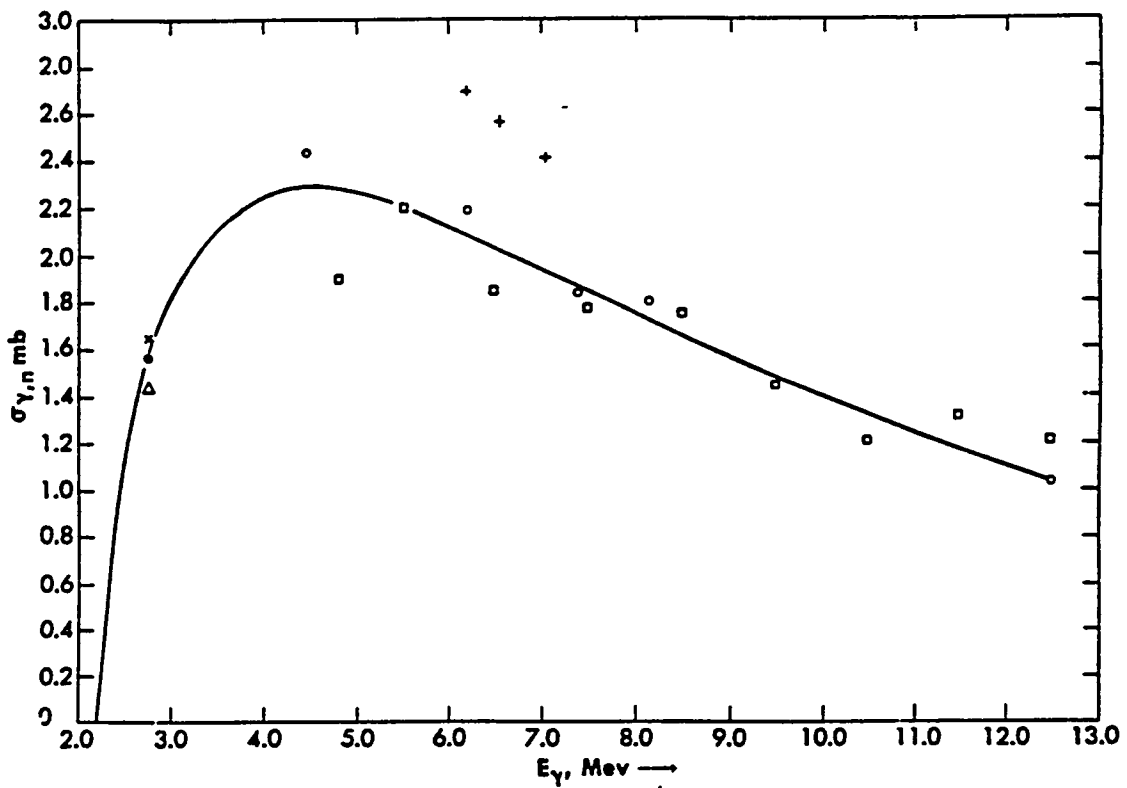


Fig. 5. Photoneutron production cross section for deuterium (in millibarns) as a function of photon energy. Taken from page 143 of ref. 15 by G. R. Keepin.

Table 9. Total photoneutron production cross section (barns) as a function of photon energy (eV).

N	x(*)	Energy (eV)	y(*)	XSECT(plot) barns	XSECT(theory) barns
1	0.300	2.20233E+06	0.000	0.00000E+00	0.00000E+00
2	0.350	2.23605E+06	1.000	2.62697E-04	3.86941E-04
3	0.400	2.26977E+06	2.000	5.25394E-04	5.90429E-04
4	0.500	2.33722E+06	3.000	7.88091E-04	7.12543E-04
5	0.610	2.41140E+06	4.000	1.05079E-03	8.29866E-04
6	0.800	2.53955E+06	5.000	1.31349E-03	1.06088E-03
7	1.000	2.67443E+06	5.800	1.52364E-03	1.30913E-03
8	1.500	3.01165E+06	7.070	1.85727E-03	1.82426E-03
9	2.000	3.34887E+06	7.850	2.06217E-03	2.15524E-03
10	2.500	3.68608E+06	8.300	2.18039E-03	2.34061E-03
11	3.000	4.02330E+06	8.600	2.25919E-03	2.42604E-03
12	3.500	4.36052E+06	8.700	2.28546E-03	2.44587E-03
13	4.000	4.69773E+06	8.650	2.27233E-03	2.42367E-03
14	4.500	5.03495E+06	8.600	2.25919E-03	2.37517E-03
15	5.000	5.37216E+06	8.400	2.20665E-03	2.31077E-03
16	5.500	5.70938E+06	8.200	2.15412E-03	2.23734E-03
17	6.000	6.04660E+06	8.000	2.10158E-03	2.15942E-03
18	6.500	6.38381E+06	7.770	2.04116E-03	2.07997E-03
19	7.000	6.72103E+06	7.550	1.98336E-03	2.00094E-03
20	7.500	7.05825E+06	7.310	1.92032E-03	1.92356E-03
21	8.000	7.39546E+06	7.070	1.85727E-03	1.84861E-03
22	9.000	8.06990E+06	6.600	1.73380E-03	1.70756E-03
23	10.000	8.74433E+06	6.100	1.60245E-03	1.57926E-03
24	11.000	9.41876E+06	5.660	1.48687E-03	1.46350E-03
25	12.000	1.00932E+07	5.250	1.37916E-03	1.35942E-03
26	13.000	1.07676E+07	4.880	1.28196E-03	1.26589E-03
27	14.000	1.14421E+07	4.470	1.17426E-03	1.18175E-03
28	15.000	1.21165E+07	4.120	1.08231E-03	1.10592E-03
29	15.500	1.24537E+07	3.960	1.04028E-03	1.07082E-03
30		1.30000E+07			1.01754E-03
31		1.35000E+07			9.72365E-04
32		1.40000E+07			9.30296E-04
33		1.45000E+07			8.91062E-04
34		1.50000E+07			8.54418E-04
35		1.55000E+07			8.20141E-04
36		1.60000E+07			7.88032E-04
37		1.65000E+07			7.57911E-04
38		1.70000E+07			7.29616E-04
39		1.75000E+07			7.03000E-04
40		1.80000E+07			6.77931E-04
41		1.85000E+07			6.54289E-04
42		1.90000E+07			6.31966E-04
43		1.95000E+07			6.10863E-04
44		2.00000E+07			5.90891E-04

* Here, x and y represent a unitless digitized representation of the original plotted data shown in Fig. 5 (taken from page 143 of Ref. 15 by G. R. Keepin), while XSECT(theory) shows the theoretical value based on equations from pp. 334-336 of Ref. 16 by R. D. Evans. Note that x and y, and the corresponding values of energy and XSECT(plot), are used with linear interpolation in the PHOTOX program to obtain values for energies below 11.44 MeV, while the theoretical formulae in Ref. 16 are used for all values above 11.44 MeV.

all of the incident photon energy above the threshold energy is divided equally between the neutron and the proton subsequent to the photodisintegration of the deuteron — i.e., it is assumed that

$$E_n = (E_\gamma - 2.225 \text{ MeV}) / 2 \quad \text{for} \quad E_\gamma > 2.225 \text{ MeV}, \quad (1)$$

where E_γ is the energy of the incident photon. Thus, in this simplistic model, gamma ray photons of one unique energy produce neutrons of one unique energy. Here we shall denote that cross section as $\Sigma(E_\gamma, E_n)$. Since a single gamma energy group may span a wide energy range (see Table 7a), the corresponding photoneutrons may also span a wide energy range which may lie within the confines of a single neutron group or span two or more neutron groups. To obtain the "group averaged" group-to-group photoneutron production cross sections, the PHOTOX program divides each gamma source group into one hundred increments and averages the photoneutron production cross section over the source group using an assumed gamma spectrum:

$$\sigma(g_i \rightarrow g_n) = \int \phi(E_\gamma) \sigma(E_\gamma, E_n) dE_\gamma / \int \phi(E_\gamma) dE_\gamma . \quad (2)$$

Initially, there was some debate over what assumed gamma spectrum should be used in this averaging process. While neither the AMPX or NJOY cross section processing code systems^{5,17} are designed to calculate photoneutron production cross sections, there are modules in each for producing other photon interaction cross sections. Historically, people have used a "flat" gamma spectrum in these cross section processing codes. More recently, R. Roussin of the ORNL Radiation Shielding Information Center has recommended a 1/E gamma weighting spectrum for some situations involving materials used for thick gamma shields. It was also noted that Appendix B.3 of the NJOY code system¹⁷ now provides for the use a 1/E gamma weighting spectrum with "rolloff" (i.e., lower than 1/E values at both high and low energies). To resolve this question, we examined the results of a 1-D ANISN¹⁸ analysis deep in the D₂O reflector, close to the reflector vessel, across from the upper portion of the ANS core. These results are shown in Table 10. While not exactly "flat," the gamma spectrum between 1.9 and 7.75 MeV at the point of interest was clearly not 1/E. Moreover, across much of this energy range, it was rather flat. Based on this information, it was decided to assume a flat weighting spectrum in the group averaging procedure described above. [In reality, we generated the group-to-group photoneutron production cross sections both ways and found that the gamma flux weighting spectrum used made no appreciable difference.] The final resulting group-to-group photoneutron production cross sections based on the flat gamma flux weighting spectrum are shown in Table 11. From this one can see that most photoneutrons are highly energetic and that gamma group 17 (which extends from 2.35 MeV down to 2.15 MeV) is the lowest gamma group that can produce photoneutrons — i.e., photons above 2.225 MeV can, while those below 2.225 MeV cannot. Had one used many more energy points per source group, the resulting cross section data for gamma group 17, would begin to show increasingly smaller and smaller numbers of photoneutrons being produced in neutron groups 11, 12, 13, etc. Nevertheless, the resolution provided in Table 11 is considered to be wholly adequate for the present purpose. Moreover, the total photoneutron production cross sections for each gamma group (as obtained by adding all the elements in a horizontal line of Table 11) have been compared to the average values one might obtain using Fig. 5 or Table 9 for the corresponding range of photon energies and were found to agree quite well.

Lastly, the SPARK program (listed in Appendix B) was used to take the original DORT-ready macroscopic cross section library prepared by JIPSY (see Sect. 4.1) and expand the DORT-ready cross section library so as to include the macroscopic photoneutron production cross sections for each material containing deuterium. Subsequent to expanding the scattering matrix and the size of the cross section dataset as described below, this program folds the microscopic (gamma)group-to-(neutron)group

Table 10. Gamma spectrum deep in the D2O reflector, at R=1650 mm (just 100 mm short of the reflector vessel starting at R=1750 mm), across from the top section of the core, based on a 1-D ANISN analysis using the original 39n/44g coupled library. While not exactly "flat", the spectrum in the energy range of interest (1.9 to 7.75 MeV) was clearly not 1/E.

Gamma group	Gamma energy(eV)	Gamma spectrum p/s/m2/eV
1	1.700E+07	1.05852E+04
2	1.300E+07	5.37005E+04
3	1.100E+07	5.44330E+05
4	9.000E+06	2.76273E+08
5	7.750E+06	4.44244E+10
6	7.250E+06	4.93338E+09
7	6.750E+06	4.68132E+09
8	6.250E+06	2.98316E+10
9	5.750E+06	7.63466E+09
10	5.250E+06	1.26262E+10
11	4.750E+06	2.53020E+10
12	4.250E+06	2.22588E+10
13	3.750E+06	2.16460E+10
14	3.250E+06	2.59334E+10
15	2.750E+06	2.87664E+10
16	2.425E+06	1.86029E+10
17	2.250E+06	1.95246E+11
18	2.075E+06	4.59251E+10
19	1.900E+06	4.24630E+10

Table 11. Group-to-group photoneutron production cross sections for deuterium in the ANSL-V 39n/44g library energy group structure (cf Table 7a), as calculated by the PHOTOX program in Appendix A.

FROM GAMMA GROUP	PHOTONEUTRON PRODUCTION XSECTS (IN BARNS) FOR DEUTERIUM IN THE ANSL-V 39N/44G LIBRARY (*)									
	TO NGRP 1	TO NGRP 2	TO NGRP 3	TO NGRP 4	TO NGRP 5	TO NGRP 6	TO NGRP 7	TO NGRP 8	TO NGRP 9	TO NGRP 10
1	5.79901E-4	1.59937E-4	0.0	0.0	0.0	0.0	0.0	0.0	0.0	0.0
2	0.0	1.01982E-3	0.0	0.0	0.0	0.0	0.0	0.0	0.0	0.0
3	0.0	1.24817E-3	0.0	0.0	0.0	0.0	0.0	0.0	0.0	0.0
4	0.0	1.37300E-3	1.89845E-4	0.0	0.0	0.0	0.0	0.0	0.0	0.0
5	0.0	0.0	1.79236E-3	0.0	0.0	0.0	0.0	0.0	0.0	0.0
6	0.0	0.0	1.88451E-3	0.0	0.0	0.0	0.0	0.0	0.0	0.0
7	0.0	0.0	1.97719E-3	0.0	0.0	0.0	0.0	0.0	0.0	0.0
8	0.0	0.0	2.06519E-3	0.0	0.0	0.0	0.0	0.0	0.0	0.0
9	0.0	0.0	3.17202E-4	1.83059E-3	0.0	0.0	0.0	0.0	0.0	0.0
10	0.0	0.0	0.0	2.11254E-3	1.13003E-4	0.0	0.0	0.0	0.0	0.0
11	0.0	0.0	0.0	0.0	2.27029E-3	0.0	0.0	0.0	0.0	0.0
12	0.0	0.0	0.0	0.0	2.16166E-3	1.12834E-4	0.0	0.0	0.0	0.0
13	0.0	0.0	0.0	0.0	0.0	2.19128E-3	0.0	0.0	0.0	0.0
14	0.0	0.0	0.0	0.0	0.0	1.90334E-3	9.28385E-5	0.0	0.0	0.0
15	0.0	0.0	0.0	0.0	0.0	0.0	1.58033E-3	0.0	0.0	0.0
16	0.0	0.0	0.0	0.0	0.0	0.0	5.77769E-4	4.82154E-4	0.0	0.0
17	0.0	0.0	0.0	0.0	0.0	0.0	0.0	2.97099E-4	4.32129E-5	3.99949E-6

(*) All other terms not shown are zero. Used 100 energy points to integrate across each gamma source group.

production cross sections in Table 11 with the deuterium number density [atoms/(barn· cm)] in each mixture in order to obtain the macroscopic photoneutron production cross sections for each mixture. By setting the input parameter IVON=1, the acroscopic value of $v\Sigma_F$ in each mixture was also set to 1.0E-15/cm for all energy groups and all materials so that, when used in a fixed-source DORT calculation, the Vondy error mode acceleration would be applied automatically as described in Sect. 4.2.

To understand the following discussion of how and why the scattering matrix and the size of the DORT-ready cross section dataset had to be expanded, one is referred to the cross section table layout diagram on page 21 of the AXMIX Code Package document,¹⁹ available from the Radiation Shielding Information Center. The original DORT-ready cross section dataset (described by the parameters IHT=3, IHS=28, IHM=110, and ITL=111) had:

- 3 positions at the top of the table for Σ_A , $v\Sigma_F$, and Σ_T
 - 24 positions to accommodate upscatter cross sections; for example:
 - group 39→group 15, 38→15, 37→15, ..., 17→15, 16→15
 - 1 position to describe within-group scattering (1→1, 2→2, ..., 83→83)
 - 82 positions to accommodate downscatter cross sections; for example:
 - group 82→group 83, 81→83, 80→83, ..., 2→83, 1→83
 - 1 position to represent the sum of all the upscattering cross sections
-

111 positions (total) for all groups, for all materials.

In this case, the number of positions needed to represent upscatter was dictated by the necessity of representing upscatter from all the thermal neutron energy groups into group 15. In the case where one wishes to represent the photoneutron production cross sections as group-to-group scattering cross sections in this matrix format (IHT=3, IHS=52, IHM=134, ITL=135), one has:

- 3 positions at the top of the table for Σ_A , $v\Sigma_F$, and Σ_T
 - 48 positions to accommodate upscatter cross sections; for example:
 - from group 56 (gamma group 17) to neutron group 8, 55→8, 54→8, ..., 9→8
 - 1 position to describe within-group scattering (as before)
 - 82 positions to accommodate downscatter cross sections (as before)
 - 1 position to represent the sum of all the upscattering cross sections
-

135 positions (total) for all groups, for all materials.

In this case, the number of positions needed to accommodate the photoneutron production cross section data (48) is determined by the number of possible photoneutron "transfers" into group 8 (i.e., 56→8, 55→8, 54→8, ..., 9→8, even though all but the first two terms will be zero) and by the number of such "transfers" that are possible into group 7 (i.e., 55→7, 54→7, 53→7, ..., 8→7, even though all but the first three terms will be zero). None of the other group-to-group photoneutron production terms (or "upscatter" cross sections) in Table 11 will require more than 48 terms in the upscatter portion of the cross section matrix. Transfers from group 40 (gamma group 1) to neutron group 1, for example, would only have required 39 positions: from group 40 to group 1, 39→1, 38→1, ..., 2→1, with only the first being nonzero. Thus, 48 positions to accommodate the photoneutron production ("upscatter") cross sections is both necessary and sufficient, while the overall length of the multigroup cross section table (ITL) had to be increased from 111 positions in the original DORT-ready cross section library to 135 positions in the final DORT-ready cross section table when the photoneutron production cross sections are represented as upscatter cross sections.

As shown in Appendix B, the SPARK program will read the original DORT-ready macroscopic cross section library prepared by JIPSY (without photoneutrons), automatically expand the matrix as outlined above, fold the deuterium number densities in each material (as specified by the user's input data) with the necessary microscopic cross section data, and output the final DORT-ready macroscopic cross section library (with photoneutron data) as well as a message showing what the new cross section parameters (IHT, IHS, IHM, ITL) should be when the newly produced final library is used with DORT. The typical input data shown on the first page of Appendix B corresponds to the actual SPARK input used for this particular case.



5.0 OTHER MISCELLANEOUS DATA

Other data needed in the shielding analysis or in the subsequent application or interpretation of those results would include: the directional quadrature set used, the neutron and gamma flux-to-dose-rate conversion factors, kerma factors for estimating heating rates in selected materials, and the dpa cross section data for estimating the displacements per atom produced in ferritic test specimens.

Table 12 shows the 48 discrete directions and quadrature weights for the fully symmetric standard S_8 quadrature set used in the global 2-D RZ shielding analyses for the core and reflector vessel. If one were to later use the VISTA and DTD codes^{20,21} to obtain a directional boundary source on the surface of some arbitrary horizontal or off-vertical cylinder, such as around one of the beam tubes (not modeled here), one would need this information.

Table 13 shows the neutron and gamma flux-to-dose-rate conversion factors for the energy groups in the ANSL-V 39n/44g and 99n/44g cross section libraries. While that data is not an integral part of the cross section libraries per se, it was generated for these groups structures (cf. Tables 7a and 7b) using the ANSIDOSE program listed in Appendix C. This program, originally written by Dr. John R. Knight, calculates the neutron and gamma flux-to-dose-rate conversion factors as prescribed in ANSI Standard ANSI/ANS-6.1.1-1977 (Ref. 22). While a newer standard (ANSI/ANS-6.1.1-1991)²³ has since been issued, there remains considerable debate in the technical community regarding the quality factor (Q) for neutrons that should be applied when using the newer standard.²⁴ For that reason, a conscious decision was made to use the old 1977 standard instead.

Table 14a shows the total multigroup kerma factors for both aluminum and iron in terms of the 39 neutron groups and 44 gamma groups in the ANSL-V 39n/44g cross section library, while Table 14b shows the corresponding total kerma factors for aluminum and iron in terms of the 99 neutron groups in the ANSL-V 99n/44g coupled library where the data for the 44 gamma groups is the same as that in the 39n/44g library. These data are necessary for calculating neutron and gamma heating rates in the reflector vessel, the core pressure boundary tube, and the beam tubes (not explicitly modeled here). In all cases, the kerma factors shown here are expressed in units of kW·s/m, which is equivalent to "watts per liter" per unit flux (where the flux is assumed to be in units of neutrons or photons per second, per square meter).

Aluminum and iron kerma factors for the 44 gamma groups were calculated directly by the SMUG module²⁵ of the AMPX cross section processing code system⁵ (using theoretical expressions) and are stored in the ANSL-V cross section libraries as MT-process 1527 for nuclides 13027 and 26000, respectively. These kerma factors, originally in units of eV· barns, were subsequently extracted from the ANSL-V 39n/44g cross section library using the PAL module²⁶ of the AMPX cross section processing system. These original kerma factors are also listed in Tables D.7 and D.14 of Appendix D. The units used in Tables 14a and 14b, however, are more convenient and more clearly understood.

Data for the various neutron groups are based on the KAOS-V kerma factor library²⁷ from Argonne, which is also available from the Radiation Shielding Information Center at ORNL as data library DLC-160. There, data is stored in a 174-group library structure corresponding to the VITAMIN-E cross section library.²⁸ Collapsing the data to the 39 and 99 neutron energy groups in the ANSL-V library structure (cf. Tables 7a and 7b) was accomplished using the RETRIEVE program supplied with the KAOS-V library. In the KAOS-V library, a multitude of kerma factors are available, including a

Table 12. Fully symmetric, standard S8 quadrature with 48 discrete directions, as used in all of the global 2-D RZ DORT shielding analyses for the ANS core and reflector vessel.

N	Weight 81**	mu 82**	eta 83**	N	Weight 81**	mu 82**	eta 83**
1	0.00000E+00	-3.08610E-01	-9.51190E-01	25	0.00000E+00	-3.08610E-01	9.51190E-01
2	3.02470E-02	-2.18220E-01	-9.51190E-01	26	3.02470E-02	-2.18220E-01	9.51190E-01
3	3.02470E-02	2.18220E-01	-9.51190E-01	27	3.02470E-02	2.18220E-01	9.51190E-01
4	0.00000E+00	-6.17210E-01	-7.86800E-01	28	0.00000E+00	-6.17210E-01	7.86800E-01
5	2.26850E-02	-5.77350E-01	-7.86800E-01	29	2.26850E-02	-5.77350E-01	7.86800E-01
6	2.26850E-02	-2.18220E-01	-7.86800E-01	30	2.26850E-02	-2.18220E-01	7.86800E-01
7	2.26850E-02	2.18220E-01	7.86800E-01	31	2.26850E-02	2.18220E-01	7.86800E-01
8	2.26850E-02	5.77350E-01	-7.86800E-01	32	2.26850E-02	5.77350E-01	7.86800E-01
9	0.00000E+00	-8.16500E-01	-5.77350E-01	33	0.00000E+00	-8.16500E-01	5.77350E-01
10	2.26850E-02	-7.86800E-01	-5.77350E-01	34	2.26850E-02	-7.86800E-01	5.77350E-01
11	2.31480E-02	-5.77350E-01	-5.77350E-01	35	2.31480E-02	-5.77350E-01	5.77350E-01
12	2.26850E-02	-2.18220E-01	-5.77350E-01	36	2.26850E-02	-2.18220E-01	5.77350E-01
13	2.26850E-02	2.18220E-01	-5.77350E-01	37	2.26850E-02	2.18220E-01	5.77350E-01
14	2.31480E-02	5.77350E-01	-5.77350E-01	38	2.31480E-02	5.77350E-01	5.77350E-01
15	2.26850E-02	7.86800E-01	-5.77350E-01	39	2.26850E-02	7.86800E-01	5.77350E-01
16	0.00000E+00	-9.75900E-01	-2.18220E-01	40	0.00000E+00	-9.75900E-01	2.18220E-01
17	3.02470E-02	-9.51190E-01	-2.18220E-01	41	3.02470E-02	-9.51190E-01	2.18220E-01
18	2.26850E-02	-7.86800E-01	-2.18220E-01	42	2.26850E-02	-7.86800E-01	2.18220E-01
19	2.26850E-02	-5.77350E-01	-2.18220E-01	43	2.26850E-02	-5.77350E-01	2.18220E-01
20	3.02470E-02	-2.18220E-01	-2.18220E-01	44	3.02470E-02	-2.18220E-01	2.18220E-01
21	3.02470E-02	2.18220E-01	-2.18220E-01	45	3.02470E-02	2.18220E-01	2.18220E-01
22	2.26850E-02	5.77350E-01	-2.18220E-01	46	2.26850E-02	5.77350E-01	2.18220E-01
23	2.26850E-02	7.86800E-01	-2.18220E-01	47	2.26850E-02	7.86800E-01	2.18220E-01
24	3.02470E-02	9.51190E-01	-2.18220E-01	48	3.02470E-02	9.51190E-01	2.18220E-01

Mu is the cosine of the discrete direction vector at a point with respect to the +R direction.

Eta is the cosine of the discrete direction vector at a point with respect to the +Z axis.

Table 13. Neutron and gamma flux-to-dose-rate conversion factors for the energy groups in the ANSL-V 39n/44g and 99n/44g cross section libraries (cf. Tables 7a and 7b), as calculated in accordance with ANSI/ANS-6.1.1-1977. Here, the flux-to-dose-rate conversion factors are given in terms of mrem/h per unit flux where the flux is assumed to be in units of neutrons or photons per second, per square meter. Note that the gamma group structure (and dose factors) are the same in both cases.

Neutron Group 39n/44g	Conversion factor for neutrons	Gamma Group	Conversion factor for photons	Neutron Group 99n/44g	Conversion factor for neutrons	Neutron Group 99n/44g	Conversion factor for neutrons
1	1.4916E-05	1	1.4880E-06	1	2.1867E-05	51	3.8856E-07
2	1.4464E-05	2	1.1776E-06	2	2.0157E-05	52	3.9485E-07
3	1.2701E-05	3	1.0264E-06	3	1.6305E-05	53	4.0137E-07
4	1.2811E-05	4	8.7716E-07	4	1.4708E-05	54	4.0802E-07
5	1.2977E-05	5	7.8468E-07	5	1.4761E-05	55	4.1470E-07
6	1.0281E-05	6	7.4783E-07	6	1.5153E-05	56	4.2036E-07
7	5.1183E-06	7	7.1104E-07	7	1.5490E-05	57	4.2495E-07
8	1.2319E-06	8	6.7426E-07	8	1.4972E-05	58	4.2942E-07
9	3.8365E-07	9	6.3749E-07	9	1.4259E-05	59	4.3373E-07
10	3.7247E-07	10	6.0069E-07	10	1.3578E-05	60	4.3783E-07
11	4.0150E-07	11	5.6001E-07	11	1.3049E-05	61	4.4151E-07
12	4.2926E-07	12	5.2272E-07	12	1.2653E-05	62	4.4477E-07
13	4.4744E-07	13	4.8324E-07	13	1.2542E-05	63	4.4775E-07
14	4.5677E-07	14	4.4117E-07	14	1.2610E-05	64	4.5042E-07
15	4.5576E-07	15	3.9596E-07	15	1.2678E-05	65	4.5273E-07
16	4.5185E-07	16	3.6472E-07	16	1.2732E-05	66	4.5473E-07
17	4.4779E-07	17	3.4703E-07	17	1.2772E-05	67	4.5632E-07
18	4.4299E-07	18	3.2876E-07	18	1.2812E-05	68	4.5736E-07
19	4.3793E-07	19	3.0979E-07	19	1.2852E-05	69	4.5781E-07
20	4.3207E-07	20	2.9067E-07	20	1.2892E-05	70	4.5761E-07
21	4.2569E-07	21	2.7730E-07	21	1.2944E-05	71	4.5708E-07
22	4.1988E-07	22	2.6775E-07	22	1.3008E-05	72	4.5656E-07
23	4.1336E-07	23	2.5985E-07	23	1.3073E-05	73	4.5590E-07
24	4.0551E-07	24	2.4928E-07	24	1.3125E-05	74	4.5511E-07
25	3.9534E-07	25	2.3392E-07	25	1.2719E-05	75	4.5417E-07
26	3.7835E-07	26	2.1180E-07	26	1.1868E-05	76	4.5185E-07
27	3.6750E-07	27	1.8326E-07	27	1.0837E-05	77	4.4779E-07
28	3.6748E-07	28	1.6038E-07	28	9.8957E-06	78	4.4299E-07
29	3.6748E-07	29	1.4417E-07	29	9.1274E-06	79	4.3793E-07
30	3.6748E-07	30	1.2815E-07	30	8.1738E-06	80	4.3207E-07
31	3.6748E-07	31	1.2019E-07	31	6.7503E-06	81	4.2569E-07
32	3.6748E-07	32	1.1281E-07	32	5.2610E-06	82	4.1988E-07
33	3.6748E-07	33	1.0321E-07	33	4.0999E-06	83	4.1336E-07
34	3.6748E-07	34	8.7594E-08	34	3.1948E-06	84	4.0551E-07
35	3.6748E-07	35	6.3060E-08	35	2.4894E-06	85	3.9534E-07
36	3.6748E-07	36	4.3908E-08	36	1.9203E-06	86	3.7835E-07
37	3.6748E-07	37	3.2767E-08	37	1.4380E-06	87	3.6750E-07
38	3.6748E-07	38	2.6816E-08	38	1.0885E-06	88	3.6748E-07
39	3.6748E-07	39	2.5783E-08	39	8.2436E-07	89	3.6748E-07
		40	2.6006E-08	40	6.2429E-07	90	3.6748E-07
		41	2.8439E-08	41	4.7411E-07	91	3.6748E-07
		42	4.1154E-08	42	3.7048E-07	92	3.6748E-07
		43	8.2669E-08	43	3.5579E-07	93	3.6748E-07
		44	2.1439E-07	44	3.5752E-07	94	3.6748E-07
				45	3.6010E-07	95	3.6748E-07
				46	3.6342E-07	96	3.6748E-07
				47	3.6738E-07	97	3.6748E-07
				48	3.7194E-07	98	3.6748E-07
				49	3.7704E-07	99	3.6748E-07
				50	3.8260E-07		

Table 14a. Total kerma factors (prompt plus total decay heat) in aluminum and natural iron, for the 39 neutron and 44 gamma energy groups in the ANSL-V 39n/44g cross section library shown in Table 7a. While based on Tables D.6, D.7, D.13, and D.14 in Appendix D, the values shown here are in units of kW*s/m. See note below.

Neutron Group	Aluminum (Al-27)	Natural Iron	Gamma Group	Aluminum (Al-27)	Natural Iron
1	5.25369e-15	2.49202e-15	1	1.33945E-14	5.87361e-14
2	3.92241E-16	4.66030E-16	2	9.96493E-15	4.15231E-14
3	2.78324E-16	2.47298E-16	3	8.37192E-15	3.36838E-14
4	2.16635E-16	1.59016E-16	4	6.84673E-15	2.63201E-14
5	1.63635E-16	1.10550E-16	5	5.91852E-15	2.19264E-14
6	1.32356E-16	7.91952E-17	6	5.55163E-15	2.02194E-14
7	6.32432E-17	3.64418E-17	7	5.19572E-15	1.85873E-14
8	3.24566E-17	1.64185E-17	8	4.84987E-15	1.70279E-14
9	2.65388E-17	2.44169E-18	9	4.50525E-15	1.54982E-14
10	7.02712E-18	6.20829E-19	10	4.16355E-15	1.40106E-14
11	8.35551E-18	1.52079E-19	11	3.82598E-15	1.25746E-14
12	1.47802E-17	6.52524E-20	12	3.49306E-15	1.11998E-14
13	2.63071E-17	7.19857E-20	13	3.16086E-15	9.87414E-15
14	4.67252E-17	1.14970E-19	14	2.83011E-15	8.61276E-15
15	7.13718E-17	1.72211E-19	15	2.49450E-15	7.39588E-15
16	8.80539E-17	2.11795E-19	16	2.27308E-15	6.63194E-15
17	1.01174E-16	2.43217E-19	17	2.15345E-15	6.24083E-15
18	1.15461E-16	2.77360E-19	18	2.03199E-15	5.85489E-15
19	1.29942E-16	3.11639E-19	19	1.90484E-15	5.45595E-15
20	1.46258E-16	3.50543E-19	20	1.77844E-15	5.07105E-15
21	3.01783E-16	7.12240E-19	21	1.69121E-15	4.81345E-15
22	3.01880E-16	7.12512E-19	22	1.62917E-15	4.63316E-15
23	3.01880E-16	7.12512E-19	23	1.57687E-15	4.47914E-15
24	3.01880E-16	7.12512E-19	24	1.50734E-15	4.27938E-15
25	3.01880E-16	7.12512E-19	25	1.40701E-15	3.99828E-15
26	3.01880E-16	7.12512E-19	26	1.26047E-15	3.58970E-15
27	6.23936E-16	1.47454E-18	27	1.06781E-15	3.05533E-15
28	6.24902E-16	1.47726E-18	28	9.11292E-16	2.62544E-15
29	6.24902E-16	1.47726E-18	29	7.99827E-16	2.32354E-15
30	6.24902E-16	1.47726E-18	30	6.89886E-16	2.03131E-15
31	6.24902E-16	1.47726E-18	31	6.35589E-16	1.88995E-15
32	6.24902E-16	1.47726E-18	32	5.97295E-16	1.79301E-15
33	6.24902E-16	1.47726E-18	33	5.28202E-16	1.62316E-15
34	6.24902E-16	1.47726E-18	34	4.31454E-16	1.40927E-15
35	6.24902E-16	1.47726E-18	35	3.01146E-16	1.22442E-15
36	6.24902E-16	1.47726E-18	36	2.09370E-16	1.34283E-15
37	6.24902E-16	1.47726E-18	37	1.68192E-16	2.01186E-15
38	6.24902E-16	1.47726E-18	38	1.78123E-16	3.64520E-15
39	6.24902E-16	1.47726E-18	39	2.12839E-16	5.12736E-15
			40	2.49879E-16	6.38782E-15
			41	3.67387E-16	9.90620E-15
			42	7.37027E-16	1.96161E-14
			43	1.72730E-15	4.26726E-14
			44	5.40094E-15	1.15030E-13

Note: the above data assumes that the aluminum has a density of 2.70 kg/L and that the iron has a density of 7.874 kg/L (which corresponds to pure iron). In reality, carbon steel has a density of 7.8212 kg/L, while SS304 has a density of 7.92 kg/L. One may multiply the above kerma factors by 10 to obtain the more familiar units of (watts/cc)/(neut/sec/cm²) for the neutron groups, or (watts/cc)/(photons/sec/cm²) for the gamma groups.

Table 14b. Total kerma factors (prompt plus total decay heat) in aluminum and natural iron, for the 99 neutron energy groups in the ANSL-V 99n/44g cross section library shown in Table 7b. While based on Tables D.3 and D.10 in Appendix D, the values shown here are in units of kW*s/m. See note below.

Neutron Group	Aluminum (Al-27)	Natural Iron	Neutron Group	Aluminum (Al-27)	Natural Iron
1	4.66673E-15	3.49046E-15	51	6.72206E-18	2.40224E-19
2	5.26721E-15	2.49746E-15	52	7.40073E-18	1.84997E-19
3	4.94959E-15	2.24445E-15	53	8.31110E-18	1.39156E-19
4	1.97134E-15	1.31117E-15	54	9.18672E-18	1.08019E-19
5	8.68761E-16	9.57225E-16	55	1.01753E-17	8.72344E-20
6	4.48427E-16	7.25843E-16	56	1.14013E-17	7.39581E-20
7	4.77485E-16	5.96208E-16	57	1.28881E-17	6.70207E-20
8	4.11742E-16	4.84938E-16	58	1.45678E-17	6.29127E-20
9	3.67913E-16	3.98969E-16	59	1.64504E-17	6.11443E-20
10	3.34896E-16	3.48774E-16	60	1.85646E-17	6.13348E-20
11	3.06320E-16	3.07286E-16	61	2.09202E-17	6.32664E-20
12	3.02266E-16	2.90963E-16	62	2.33626E-17	6.64358E-20
13	2.46080E-16	2.39952E-16	63	2.60561E-17	7.08431E-20
14	2.82572E-16	2.04585E-16	64	2.90198E-17	7.64338E-20
15	2.56892E-16	1.99824E-16	65	3.23022E-17	8.31400E-20
16	2.27254E-16	1.75747E-16	66	3.62796E-17	9.16009E-20
17	2.31213E-16	1.52079E-16	67	4.08846E-17	1.01613E-19
18	2.05533E-16	1.56704E-16	68	4.60687E-17	1.13216E-19
19	2.16442E-16	1.60784E-16	69	5.19094E-17	1.26574E-19
20	2.02733E-16	1.49902E-16	70	5.84838E-17	1.41877E-19
21	1.73578E-16	1.40788E-16	71	6.54539E-17	1.58200E-19
22	1.91631E-16	1.36300E-16	72	6.54539E-17	1.58200E-19
23	1.79564E-16	1.00715E-16	73	7.27813E-17	1.75475E-19
24	1.40272E-16	9.94225E-17	74	7.41425E-17	1.78740E-19
25	1.32742E-16	7.55360E-17	75	7.90178E-17	1.90302E-19
26	1.79371E-16	9.71780E-17	76	8.80539E-17	2.11795E-19
27	1.28108E-16	1.00497E-16	77	1.01174E-16	2.43217E-19
28	1.23088E-16	5.00717E-17	78	1.15461E-16	2.77360E-19
29	1.15944E-16	6.60957E-17	79	1.29942E-16	3.11639E-19
30	1.15172E-16	8.21606E-17	80	1.46258E-16	3.50543E-19
31	7.75697E-17	5.67507E-17	81	3.01783E-16	7.12240E-19
32	5.97967E-17	3.27690E-17	82	3.01880E-16	7.12512E-19
33	6.00091E-17	4.16652E-17	83	3.01880E-16	7.12512E-19
34	8.37675E-17	3.55712E-17	84	3.01880E-16	7.12512E-19
35	3.51211E-17	1.55071E-17	85	3.01880E-16	7.12512E-19
36	5.77887E-17	2.57228E-17	86	3.01880E-16	7.12512E-19
37	1.09862E-17	1.08632E-17	87	6.23936E-16	1.47454E-18
38	5.76439E-17	1.16780E-17	88	6.24902E-16	1.47726E-18
39	2.69828E-17	3.30003E-17	89	6.24902E-16	1.47726E-18
40	9.60280E-18	1.19636E-18	90	6.24902E-16	1.47726E-18
41	9.81809E-18	1.82277E-18	91	6.24902E-16	1.47726E-18
42	1.13048E-17	3.25650E-18	92	6.24902E-16	1.47726E-18
43	6.18626E-17	4.32839E-18	93	6.24902E-16	1.47726E-18
44	3.69844E-17	1.59832E-18	94	6.24902E-16	1.47726E-18
45	1.27529E-17	1.16725E-18	95	6.24902E-16	1.47726E-18
46	9.73120E-18	8.55749E-19	96	6.24902E-16	1.47726E-18
47	7.60250E-18	6.87483E-19	97	6.24902E-16	1.47726E-18
48	6.12351E-18	6.97141E-19	98	6.24902E-16	1.47726E-18
49	5.59254E-18	5.49415E-19	99	6.24902E-16	1.47726E-18
50	6.07138E-18	3.13815E-19			

Note: the above data assumes that the aluminum has a density of 2.70 kg/L and that the iron has a density of 7.874 kg/L (which corresponds to pure iron). In reality, carbon steel has a density of 7.8212 kg/L, while SS304 has a density of 7.92 kg/L. One may multiply the above kerma factors by 10 to obtain the more familiar units of (watts/cc)/(neut/sec/cm²) for neutrons.

recommended dataset (rec), one based on a direct energy balance (deb), and one based only on particle kinematics (kin). Here, only those from the recommended dataset were used. Within the recommended dataset, there are three types of response functions:

1. The basic prompt kerma factor.
2. The basic kerma factor plus charged particle decay heat. [For Al-27, for example, this would include the basic prompt kerma factor for neutron interactions with Al-27, as well as the energy associated with the beta decay of the Al-28 that resulted from neutron activation of the Al-27.]
3. The basic kerma factor plus the total decay heat. [For Al-27, for example, this would include the basic prompt kerma factor for neutrons interacting with Al-27, as well as the energy associated with both the beta and gamma decay of the Al-28 that resulted from neutron activation of the Al-27, even though this gamma energy may ultimately be deposited some distance away from the aluminum.]

For completeness, all three types of kerma factors are reported in Appendix D, in case one ever needs to differentiate between these three components at some later time. There, as in the original KAOS library, these parameters are reported in units of eV· barns. In Tables 14a and 14b, however, the multigroup kerma factors are listed in terms of kW· s/m and correspond to the third type of response function described above (i.e., the "basic prompt kerma factor plus total decay heat") since the Al-28 has a very short halflife of only 2.25 minutes. Moreover, while it is recognized that the energy associated with the gamma decay of any Al-28 produced by neutron activation of Al-27 may be deposited some distance from the aluminum, it was also recognized that its inclusion here was the only convenient way to account for this energy production term since these "decay gammas" (from the Al-28) are not included as part of the secondary gammas in a regular neutron/gamma shielding analysis.

Eventually, it will be necessary to estimate the dpa that can be produced per unit time in ferritic test specimens that may be placed in the various irradiation facilities. ASTM Std. E693-79 (Ref. 29) gives the dpa cross section for iron (in barns) at each of 641 energy points from 1.0E-4 eV to 20 MeV and uses a 1/v tail at low energies to account for damage due to knock-on gammas produced by low-energy (n,g) reactions in the iron. Here we take the liberty of extending that 1/v tail down to 1.0E-5 eV. To be useful, however, this ultra fine-group neutron irradiation data must first be collapsed to the 39 neutron energy groups and/or the 99 neutron energy groups in the ANSL-V cross section libraries (cf. Table 7a and 7b). ASTM Std. E693-79 recommends collapsing the pointwise data to a broad group structure using the following energy-dependent weighting function:

$$W_1(X) = C_1 X^{0.5} e^{-X/(1.4E6)} \quad \text{for } X \geq 0.82E6 \text{ eV} , \quad (3)$$

$$W_1(X) = C_2 / X \quad \text{for } X \leq 0.82E6 \text{ eV} . \quad (4)$$

Alternately, a more realistic "fission-1/E-Maxwellian" weighting function such as

$$W_2(X) = C_3 X^{0.5} e^{-X/(1.289E6)} \quad \text{for } X \geq 0.9E6 \text{ eV} , \quad (5)$$

$$W_2(X) = C_4 / X \quad \text{for } 0.225 \text{ eV} \leq X \leq 0.9E6 \text{ eV} , \quad (6)$$

$$W_2(X) = C_5 X e^{-X/(0.045)} \quad \text{for } X \leq 0.225 \text{ eV} . \quad (7)$$

might well represent the flux more accurately at very low energies and reduce the importance of the low-energy $1/v$ tail in the dpa cross section. Table 15 shows the resulting multigroup dpa cross sections (in barns) for both the 39 neutron group structure and the 99 neutron group structure using both sets of weighting functions. For light water reactors, the second set of multigroup cross sections (dpa2) may be more realistic (especially if one extends the $1/v$ tail down to 1.0E-5 eV), while for the ANS reactor with a higher low-energy flux, the most realistic cross sections are probably somewhere between the two sets of values shown in Table 15. [Note that the value of the dpa cross section in the lowest energy group using the standard weighting function is about 2.4 times higher than if one assumed a Maxwellian weighting function in this energy range.] To assess the importance of this, the integrated dpa values at two of the original locations of interest in the ANS system [i.e., (a) directly above the lower fuel element and (b) a short distance radially beyond the upper fuel element, near slant hole facility tubes SH-1 and SH-2] were evaluated using the actual multigroup fluxes and both sets of cross sections. These results, shown in Table 16, indicate that, at these locations at least, there was very little difference between the integrated dpa values calculated using these two sets of cross sections. For irradiation facilities further out in the reflector where the effect of the fast flux is less pronounced, it is expected that this difference would be more pronounced. Nevertheless, because the prescribed weighting function in ASTM Std. E693-79 [$W_1(X)$] is widely recognized while the second ad hoc weighting function [$W_2(X)$] is somewhat arbitrary, the first set of cross sections [dpa1] was used in Appendix E to calculate the integrated dpa values at all locations of interest, although the corresponding values based on dpa2 are still available upon request. In either case, it must be recognized that: (1) While the dpa response function accounts for displacements due to both neutrons and secondary knock-on gammas produced in the iron itself, it does not in any way account for displacements due to gammas coming directly from the core; this latter effect may become significant at locations deeper in the reflector where the fast neutron flux has been severely attenuated and the high energy gamma flux has not. (2) The displacements per atom in austenitic steels (as opposed to ferritic steels) will be somewhat different; this is not covered by ASTM Std. E693-79. (3) All of the dpa values cited in Appendix E are based on unperturbed fluxes at these various locations as calculated using the rather simplistic geometric model described earlier in this report (cf. Sect. 2). In reality, the very presence of a test specimen as well as any accompanying irradiation capsule will cause a local depression in both the flux and the associated dpa value which must be evaluated separately using a local perturbation analysis. The unperturbed values in Table 16 and Appendix E must therefore be regarded only as rough preliminary estimates.

Table 15. ASTM DPA (displacements per atom) cross section (in barns) for iron, collapsed to the 39-neutron-group and 99-neutron-group ANSL-V cross section energy group structures using (1) the recommended ASTM fission-1/E weighting function and (2) a potentially more realistic fission-1/E-Maxwellian weighting function. Based on ASTM Std. E693-79 (cf. Ref. 29).

GRP	DPA1 XSECT	DPA2 XSECT	GRP	DPA1 XSECT	DPA2 XSECT	GRP	DPA1 XSECT	DPA2 XSECT
1	2.099E+3	2.085E+3	1	3.010E+3	3.004E+3	51	8.083E-2	8.083E-2
2	1.551E+3	1.542E+3	2	2.769E+3	2.764E+3	52	9.401E-2	9.401E-2
3	1.149E+3	1.147E+3	3	2.445E+3	2.442E+3	53	1.118E-1	1.118E-1
4	8.303E+2	8.304E+2	4	2.193E+3	2.191E+3	54	1.323E-1	1.323E-1
5	5.557E+2	5.545E+2	5	2.008E+3	2.007E+3	55	1.571E-1	1.571E-1
6	3.668E+2	3.669E+2	6	1.857E+3	1.856E+3	56	1.819E-1	1.819E-1
7	1.910E+2	1.910E+2	7	1.744E+3	1.744E+3	57	2.050E-1	2.050E-1
8	9.040E+1	9.040E+1	8	1.612E+3	1.612E+3	58	2.313E-1	2.313E-1
9	1.293E+1	1.293E+1	9	1.472E+3	1.471E+3	59	2.603E-1	2.603E-1
10	2.466E+0	2.466E+0	10	1.366E+3	1.366E+3	60	2.935E-1	2.935E-1
11	1.152E-1	1.152E-1	11	1.285E+3	1.285E+3	61	3.293E-1	3.293E-1
12	2.344E-1	2.344E-1	12	1.268E+3	1.268E+3	62	3.684E-1	3.684E-1
13	4.156E-1	4.156E-1	13	1.168E+3	1.168E+3	63	4.103E-1	4.103E-1
14	7.411E-1	7.411E-1	14	1.026E+3	1.026E+3	64	4.578E-1	4.578E-1
15	1.129E+0	1.129E+0	15	1.011E+3	1.011E+3	65	5.120E-1	5.120E-1
16	1.387E+0	1.387E+0	16	8.337E+2	8.337E+2	66	5.751E-1	5.751E-1
17	1.602E+0	1.602E+0	17	7.852E+2	7.852E+2	67	6.482E-1	6.482E-1
18	1.831E+0	1.831E+0	18	8.129E+2	8.130E+2	68	7.314E-1	7.314E-1
19	2.057E+0	2.057E+0	19	8.854E+2	8.854E+2	69	8.231E-1	8.231E-1
20	2.314E+0	2.314E+0	20	8.363E+2	8.363E+2	70	9.280E-1	9.280E-1
21	2.585E+0	2.585E+0	21	7.070E+2	7.069E+2	71	1.011E+0	1.011E+0
22	2.838E+0	2.838E+0	22	6.727E+2	6.727E+2	72	1.067E+0	1.067E+0
23	3.121E+0	3.121E+0	23	5.027E+2	5.026E+2	73	1.126E+0	1.126E+0
24	3.484E+0	3.487E+0	24	4.813E+2	4.813E+2	74	1.188E+0	1.188E+0
25	3.957E+0	3.985E+0	25	3.607E+2	3.606E+2	75	1.251E+0	1.251E+0
26	4.749E+0	4.784E+0	26	4.015E+2	4.031E+2	76	1.387E+0	1.387E+0
27	6.406E+0	6.353E+0	27	4.957E+2	4.957E+2	77	1.602E+0	1.602E+0
28	8.695E+0	8.590E+0	28	2.469E+2	2.469E+2	78	1.831E+0	1.831E+0
29	1.314E+1	1.216E+1	29	3.168E+2	3.168E+2	79	2.057E+0	2.057E+0
30	2.108E+1	2.007E+1	30	3.721E+2	3.721E+2	80	2.314E+0	2.314E+0
31	2.770E+1	2.748E+1	31	3.040E+2	3.040E+2	81	2.585E+0	2.585E+0
32	3.165E+1	3.152E+1	32	1.728E+2	1.728E+2	82	2.838E+0	2.838E+0
33	3.516E+1	3.505E+1	33	2.135E+2	2.135E+2	83	3.121E+0	3.121E+0
34	3.855E+1	3.846E+1	34	1.676E+2	1.676E+2	84	3.484E+0	3.487E+0
35	4.245E+1	4.229E+1	35	9.713E+1	9.713E+1	85	3.957E+0	3.985E+0
36	4.753E+1	4.732E+1	36	1.442E+2	1.442E+2	86	4.749E+0	4.784E+0
37	5.449E+1	5.408E+1	37	6.361E+1	6.361E+1	87	6.406E+0	6.353E+0
38	6.554E+1	6.453E+1	38	6.448E+1	6.448E+1	88	8.695E+0	8.590E+0
39	2.334E+2	9.698E+1	39	1.735E+2	1.735E+2	89	1.314E+1	1.216E+1
			40	6.232E+0	6.232E+0	90	2.108E+1	2.007E+1
			41	1.018E+1	1.018E+1	91	2.770E+1	2.748E+1
			42	1.426E+1	1.426E+1	92	3.165E+1	3.152E+1
			43	2.652E+1	2.652E+1	93	3.516E+1	3.505E+1
			44	7.947E+0	7.947E+0	94	3.855E+1	3.846E+1
			45	5.723E+0	5.723E+0	95	4.245E+1	4.229E+1
			46	3.889E+0	3.889E+0	96	4.753E+1	4.732E+1
			47	2.825E+0	2.825E+0	97	5.449E+1	5.408E+1
			48	4.120E+0	4.120E+0	98	6.554E+1	6.453E+1
			49	1.153E+0	1.153E+0	99	2.334E+2	9.698E+1
			50	3.410E-1	3.410E-1			

Table 16. Comparison of integrated DPA values at several locations of interest using the two different collapsed response functions and the multigroup neutron fluxes from DORT Run 5.

R mm	Z mm	DPA1 (dpa/year)	DPA2 (dpa/year)
135.00	308.50	33.51	33.43
135.00	248.50	36.91	36.83
135.00	191.59	39.72	39.63
135.00	155.72	40.81	40.71
135.00	101.91	40.70	40.61
135.00	50.00	37.23	37.14
135.00	0.00	36.96	36.87
332.94	308.50	9.99	9.92
332.94	248.50	10.95	10.87
332.94	191.59	11.47	11.39
332.94	155.72	11.59	11.51
332.94	101.91	11.12	11.04
332.94	50.00	9.50	9.41
332.94	0.00	8.10	8.01

Note: Z = distance above core midplane (mm)



6.0 THE PROGRESSION AND VERIFICATION OF THE DORT CALCULATIONS: LESSONS LEARNED

6.1 OVERVIEW

Details of the different models used, the different physical phenomena considered, and the different cross section datasets used, are all described in the preceding sections of this report. The purpose of this section is to show, more or less in chronological order, how and when the various pieces were brought together — i.e., to show the specific considerations that went into each of the DORT models, the specific cross sections used in each case, the testing that was done along the way to establish confidence in the various models, and to briefly document the lessons that were learned so that someone repeating similar calculations in the future can avoid some of the pitfalls described below. Those interested only in the final set of reference results should skip to the end of this section, which shows the 2-D flux maps for DORT Run 5, or go directly to Sect. 7 and/or Appendix E, which show the final reference results at each of 761 particular points of interest as organized in 26 different tables.

Figure 6 shows the chronological evolution of the global 2-D shielding calculations for the ANS core and reflector vessel. Much of the discussion below refers to the various calculational blocks in Fig. 6 which, chronologically speaking, is somewhat more accurate than the text in Sect. 4.

6.2 EARLY PROBLEMS WITH SLOW CONVERGENCE (DORT RUNS 1 AND 2)

DORT Runs 1 and 2 used the original reactor physics spatial mesh (cf. Fig. 2 and Table 3) and the original self-shielded cross sections as described in the first paragraph of Sect 4.1. [Because these calculations were never fully converged, however, they are not discussed anywhere else in this report.] The calculational strategy used was to start or restart each calculation three times. In the first step, one would perform only one outer iteration but use many inner iterations to tightly converge the fast neutron groups (1-14). In the second step, one would perform 10-20 outer iterations over the thermal neutron groups, with as many as 10 inner (spatial) iterations per outer iteration, to converge the thermal groups. This step may be restarted several times if more outer iterations are needed. In the third step, one would perform just one outer iteration but use many inner iterations to converge the gamma groups. Unfortunately, while 10-20 outer iterations are normally more than sufficient to provide highly converged results for most reactors, this was not the case for the ANS reactor. Convergence at that point was not good, and the convergence rate was extremely slow, taking 5 or 6 CPU hours per outer iteration on an IBM Model 530 workstation. Moreover, a very large number of outer iterations would be required to converge the thermal neutron upscatter terms in the thick D₂O reflector. J-P. Renier advised that 150 to 200 outer iterations might be required for good convergence based on his reactor physics work. Using the original calculational strategy, this would have taken up to 30 or 35 CPU days on an IBM Model 530 workstation. These calculations were therefore abandoned, and a new strategy was developed.

6.3 ERROR MODE ACCELERATION OF DORT RUN 3 USING SMURF DATA

The new calculational strategy for converging the upscatter source terms for the thermal neutron groups is discussed in Sect. 4.2, while the details of how to implement that strategy in the DORT calculations for Run 3 are outlined in Table 17. Basically, it involved using the SMURF code (cf. Table 8)

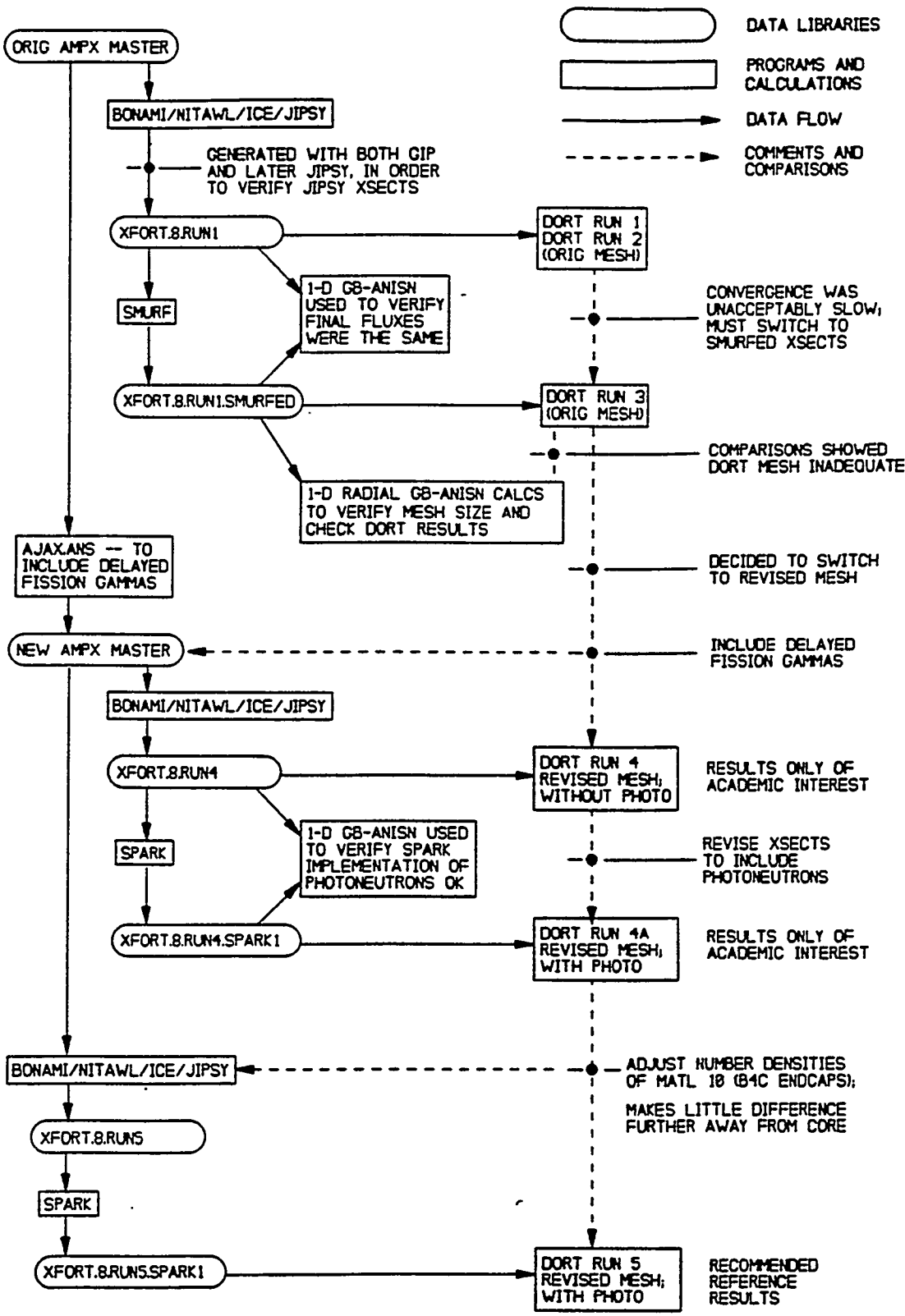


Fig. 6. Evolution of the global 2-D shielding calculations for the ANS core and reflector vessel.

Table 17. Calculational strategy for converging the upscatter source terms for the thermal neutron groups (15-39) in DORT Run 3. Basically, this table shows the recommended values for a number of the DORT input parameters during this stage of the analysis.

- 1) Use "smurfed" cross sections having a fake macro $nusigf=1.0E-10/cm$ for all thermal groups, and $nusigf=0.0$ for all of the fast neutron groups and all of the gamma groups (see explanation in text)
 - 2) Use the 1^{**} array to set $\chi(g)=1.0E-10$ (unnormalized) for group 1, and $\chi(g)=0.0$ for all other groups so that the negligible fission source created will go into group 1; while group 1 was previously converged, no additional inner iterations are being performed on it calculational step (so this negligibly small fission source will never be seen)
 - 3) Set $nofis=1$ so that the small fake $\chi(g)$ entered in the 1^{**} array will not be renormalized to 1.0
 - 4) Impose an unrealistically tight pointwise flux convergence criteria of $epp=1.0E-6$ so that it will never be met and the code will always use the maximum allowed number of inner iterations (which is set to 2 in the 28^{**} array so that one always gets the same number of inner iterations and the error-mode extrapolation will work well)
 - 5) Allow for many outer iterations, but set the maximum number of allowed inners to ...
 - 0 for the fast neutron groups (1-14) to save time when converging the thermal upscatter terms and to assure that the negligibly small fission source placed in group 1 will never be seen
 - 2 for the thermal neutron groups (15-39) to save time when converging onouters and to assure that this many inners are always used so that error-mode extrapolation will work well
 - 0 for all the gamma groups (which will be converged later in a separate DORT calculational step)
 - 6) Set the outer iteration flux criterion to $epo=1.0E-4$
-

Notes:

- a) $nusigf$ is the macroscopic fission cross section times the neutron yield.
- b) $\chi(g)$ refers to the fission yield spectrum; see the DORT 1^{**} array.
- c) $nofis$, epp , and epo are input parameters for the DORT transport code.

to add the equivalent of a negligibly small amount of fissionable material in each material mixture by modifying the value of $\nu\Sigma_p$ in each material. It also involved using a large number of outer iterations over energy groups 15-39 to make use of the Vondy error mode extrapolation technique while simultaneously using only 2 inner (spatial) iterations per outer iteration to save time.

Before using the modified cross sections produced by SMURF in the long-running DORT calculations, two separate 1-D calculations were performed using the group-banded version of the ANISN code (GB-ANISN)³⁰ to verify that both the modified and unmodified cross sections would yield the same results. These calculations were based on a 1-D radial model, halfway up the upper section of the core, and used the same 133 radial mesh intervals as used in the DORT analyses (cf. Table 3a). Because of the relatively few number of mesh intervals in these 1-D calculations, and because of the acceleration techniques built into the GB-ANISN code (especially the "group banding" applied to all 25 thermal neutron groups), the GB-ANISN code was able to fully converge this problem in about 2.1 minutes using either set of cross sections. Comparisons of these fully converged results using both the modified and unmodified cross sections showed the fluxes in all energy groups at all points of interest to be identical to 6 significant figures — thus confirming that the newly modified (SMURFed) cross sections were suitable for use in DORT Run 3, which employed the new calculational strategy described in Sect. 4.2 and Table 17.

Converging DORT Run 3 still required patience and vigilance. After the first 20 or 25 outer iterations, the Vondy error mode extrapolation algorithm would "kick in" automatically about once every 5 to 10 outer iterations. [It only "kicks in" after a semi-stable solution is obtained.] The effect of this, when it happens, is quite dramatic. Between kicks, the fluxes at the reflector vessel may change by a few percent (generally not more than 25 or 30%) between outer iterations while, immediately after one of these flux extrapolations, the flux there may change by a factor of 2 or 3, or even by as much as a factor of 6 or 7 in some energy groups, thus bypassing the dozen or more outer iterations that would otherwise have been required to get to that same point if this technique had not been invoked. Still, even with this technique, a great many outer iterations were required to achieve convergence. Multidimensional 2-D plots of the neutron flux in various energy groups were made after 10, 71, 130, and 150 outer iterations. Over the first 130 outer iterations, for example, one could readily see the contours of constant flux migrating outward and pushing deeper into the reflector. (See, for example, the thermal flux contours for $1.0E17$ and $1.0E18 \text{ s}^{-1}\text{m}^{-2}$ in Figs. 7a, 7b, and 7c for groups 20-39.) To aid in determining when convergence was achieved, a utility program called CHKCON³¹ was written to compare the multigroup fluxes at the reflector vessel, directly across from the upper and lower portion of the core as the DORT calculations progressed from one outer iteration to the next. Convergence was assumed, and the DORT calculation(s) terminated when the flux in each group had changed by less than 0.05% at these two key flux locations over the last 20 outer iterations. This was achieved after 150 outer iterations over the thermal neutron groups. [Moreover, by using the calculational strategy described in Sect 4.2 and Table 17, we were able to obtain this degree of convergence in only 5.5 CPU days rather than the 30-35 days that might otherwise have been required using the previous calculational strategy.] The gamma groups were then converged as noted above.

6.4 QA CHECK OF DORT RUN 3: PROBLEM WITH MESH

To determine the adequacy of the DORT model and the quality of the fluxes corresponding to DORT Run 3, those fluxes were first compared against the results for the previous GB-ANISN calculation based on a 1-D radial trace halfway up the upper section of the core using the same radial mesh as in the DORT calculations (cf. Table 3a). While the results for all 39 neutron energy groups are shown in Table 18, the

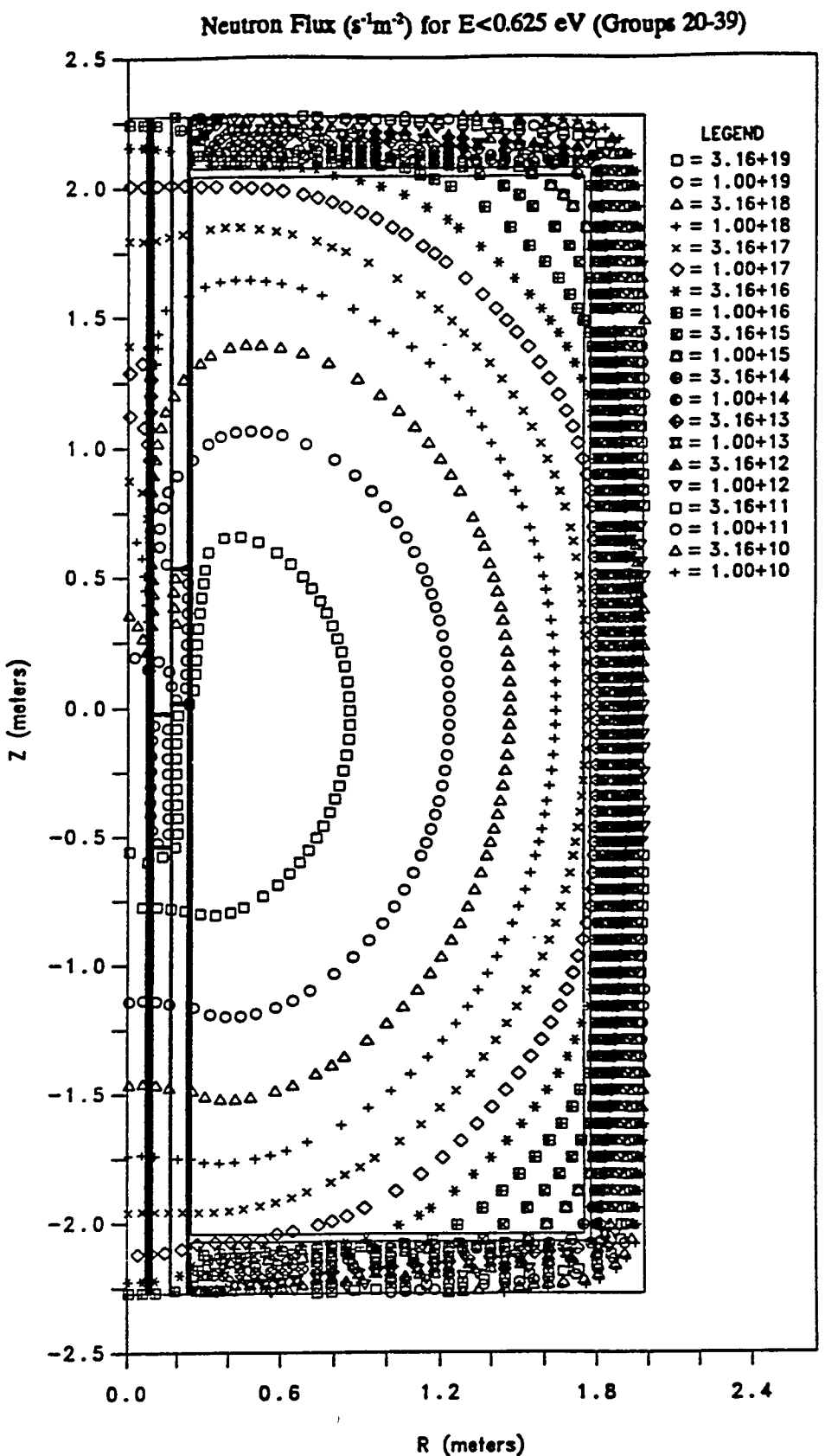


Fig. 7a. Contours showing the 2-D spatial distribution of the thermal neutron flux below 0.625 eV as given by DORT Run 3 after 10 outer iterations over all groups for which thermal upscattering is possible.

Neutron Flux ($s^{-1}m^{-2}$) for $E < 0.625$ eV (Groups 20-39)

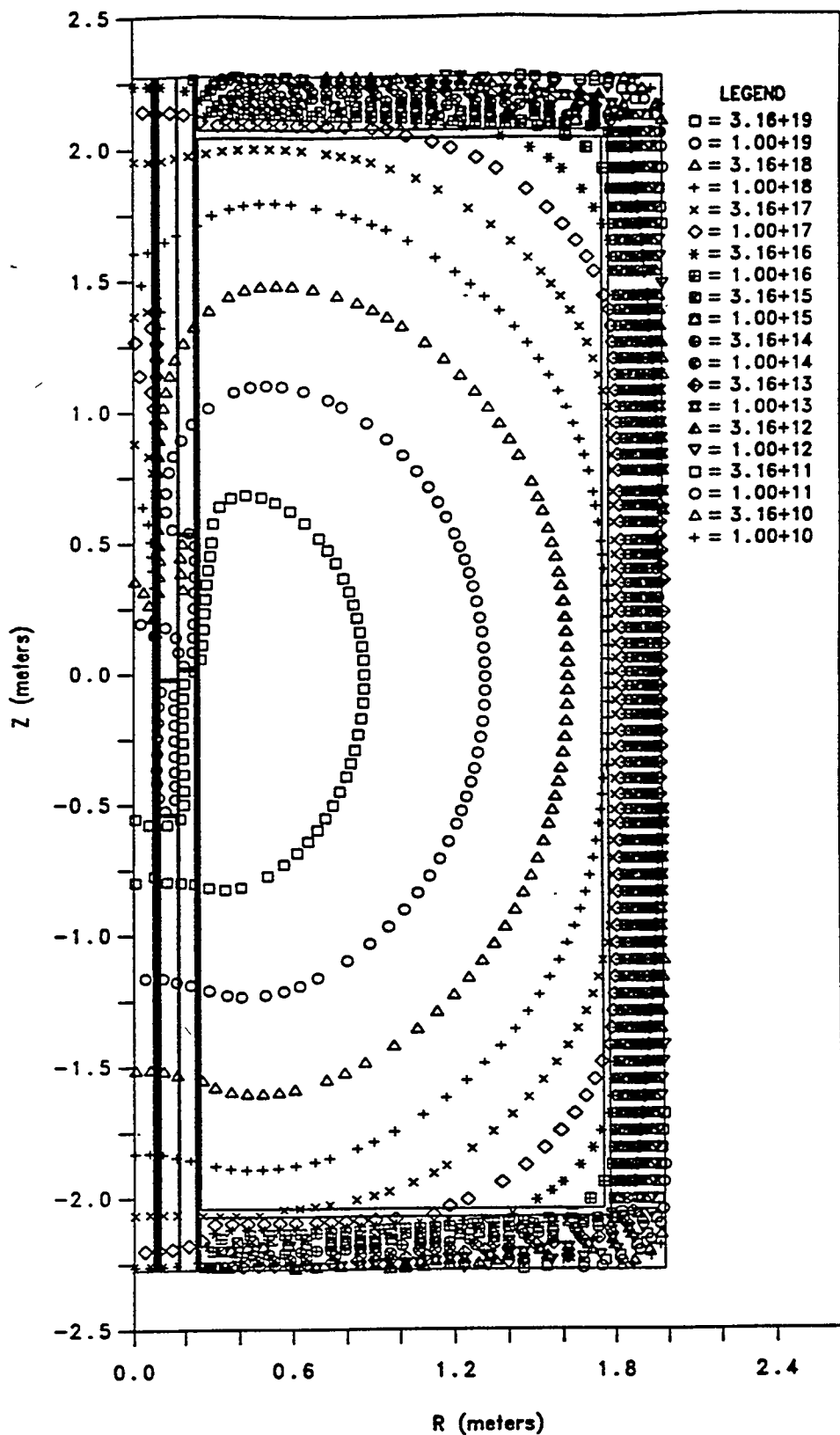


Fig. 7b. Contours showing the 2-D spatial distribution of the thermal neutron flux below 0.625 eV as given by DORT Run 3 after 71 outer iterations over all groups for which thermal upscattering is possible.

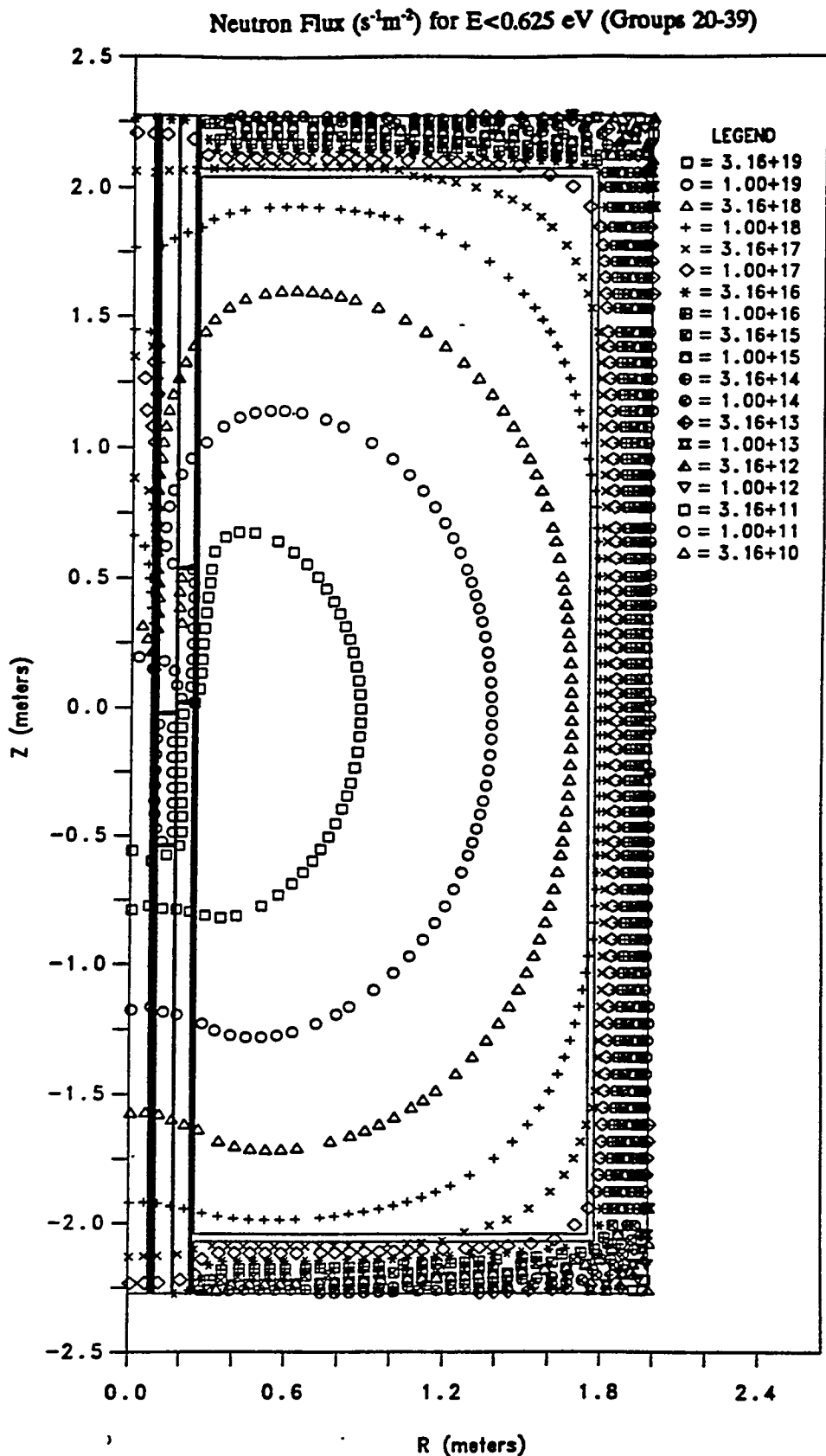


Fig. 7c. Contours showing the 2-D spatial distribution of the thermal neutron flux below 0.625 eV as given by DORT Run 3 after 130 outer iterations over all groups for which thermal upscattering is possible.

results for neutron groups 1 through 18 were both enlightening and disturbing. They showed that, at the reflector vessel, the 2-D DORT fluxes in these 18 fast energy groups were about a factor of 2 or so higher than the 1-D ANISN fluxes where the core was modeled as an infinite cylinder -- even though the same materials, cross sections, and source terms were used in both calculations. Physically, of course, that result is quite impossible (at least for the fast groups) since the finite core in the 2-D model would have to yield (fast neutron) flux levels that are at least slightly lower than those obtained using an infinite cylindrical model of the core. To pursue this matter, we first tripled the number of mesh intervals used in the GB-ANISN calculation (i.e., increased the number of mesh intervals from 133 to 399) and then tripled the number again (to 1197). These GB-ANISN results are also shown in Table 18. In the first case, the GB-ANISN fluxes in groups 1-18 increased by 25 to 35%, while in the second refinement, they increased by another 3 or 4%. While this tended to moderate the above anomaly and showed that the original mesh used in both calculations was clearly inadequate, the 2-D DORT fluxes remained higher than the fine mesh 1-D results which, as noted above, is physically impossible (at least for the fast energy groups). Unfortunately, restrictions on disk space and computer time precluded the use of a much finer mesh in the 2-D DORT analyses.

Examination of the DORT mesh specifications (cf. Tables 3a and 3b, which were originally developed for reactor physics analyses of the core) revealed that:

1. use of a fine axial mesh in the core and a coarse radial mesh deep in the side reflector would give rise to long thin flat mesh intervals having aspect ratios of about 6:1 deep in the side reflector, while
2. use of a fine radial mesh in the core and a coarse axial mesh in the upper and lower reflector regions would give rise to tall thin mesh intervals above and below the core.

Based on prior experience with shielding calculations for the MHTGR program (cf. Sect. 2.5.3 of Ref. 32), it was thought that use of such mesh intervals in the side reflector could quite possibly cause the DORT calculation to overestimate the fast flux deep in the side reflector. This process, known as artificial numerical diffusion, is illustrated in Fig. 8. Consider the uncollided component of the directional flux entering the left side of a standard (almost square) mesh interval and passing out the top surface of that mesh interval as shown in the top portion of Fig. 8. While it is true that the uncollided component going out the top of one mesh interval enters the bottom of the adjacent mesh interval, it is also true that this uncollided component will advance radially by half a mesh space (ΔR_1) in the process. In the case of a long thin mesh interval, the same is also true, except that now it will advance by a much greater distance (ΔR_2), thus getting a free (unattenuated) ride over the distance ($\Delta R_2 - \Delta R_1$). If the bulk of the side reflector is composed of a multitude of such mesh intervals, the effect will be compounded many times over, resulting in an overestimate of the flux deep in the side reflector as evidenced by the DORT fluxes for Run 3. This anomalous effect can be reduced two ways: (1) one can reduce the size of the radial mesh intervals or (2) one can increase the size of the mesh in the axial direction. While the former is always preferable if one can afford many more mesh intervals in the calculation (which we cannot), the latter is also effective insofar as it reduces the uncollided component of the flux passing through each mesh interval and advancing radially outward in an unnatural fashion.

With these observations in mind, the radial and axial mesh distributions used in the original DORT models (cf. Tables 3a and 3b and Figs. 2a-2f) were carefully reevaluated. For shielding studies, as opposed to core physics studies, it became apparent that one needed far fewer radial mesh intervals in the source region (i.e., in the core) and more in the reflector. Likewise, it became apparent that one needed far fewer axial mesh intervals in the core and more in the upper and lower axial reflectors. Based on that,

Table 18. Comparison of the neutron fluxes (s-&a-30V-1-&a+30Vm-&a-30V-2-&a+30V) for DORT Run 3 and Run 4 at 10.4 mm past the outside of the reflector vessel (halfway up the top section of the core) against the corresponding 1-D radial GB-ANISN results using 1, 3, and 9 times as many radial mesh intervals as in the DORT Run 3 analysis. Note that the results shown here are for comparison purposes only, and do not represent the final reference values. See text.

Neutron Group	DORT RUN 3	GB-ANISN-1x	GB-ANISN-3x	GB-ANISN-9x	DORT RUN 4
1	1.261E+10	6.904E+09	9.158E+09	9.441E+09	5.030E+09
2	1.459E+10	7.505E+09	1.004E+10	1.037E+10	5.865E+09
3	9.898E+09	4.774E+09	6.432E+09	6.650E+09	3.830E+09
4	4.277E+09	2.073E+09	2.795E+09	2.891E+09	1.641E+09
5	5.083E+09	2.543E+09	3.399E+09	3.517E+09	2.004E+09
6	8.257E+09	4.093E+09	5.454E+09	5.641E+09	3.274E+09
7	1.191E+10	5.835E+09	7.415E+09	7.683E+09	4.929E+09
8	1.735E+10	8.016E+09	9.415E+09	9.822E+09	7.431E+09
9	2.145E+10	9.347E+09	1.107E+10	1.148E+10	8.974E+09
10	2.662E+10	1.144E+10	1.402E+10	1.446E+10	1.112E+10
11	3.385E+10	1.435E+10	1.801E+10	1.858E+10	1.421E+10
12	2.969E+10	1.194E+10	1.519E+10	1.569E+10	1.200E+10
13	3.179E+10	1.243E+10	1.600E+10	1.654E+10	1.267E+10
14	4.071E+10	1.558E+10	2.026E+10	2.096E+10	1.624E+10
15	2.072E+10	7.835E+09	1.031E+10	1.066E+10	8.251E+09
16	1.337E+10	5.027E+09	6.349E+09	6.619E+09	5.401E+09
17	1.228E+10	4.574E+09	5.955E+09	6.168E+09	4.890E+09
18	1.530E+10	8.771E+09	9.569E+09	9.881E+09	7.564E+09
19	6.763E+10	1.242E+11	1.074E+11	1.087E+11	7.334E+10
20	6.569E+11	1.378E+12	1.192E+12	1.215E+12	7.814E+11
21	8.354E+12	1.815E+13	1.619E+13	1.635E+13	1.006E+13
22	7.431E+13	1.618E+14	1.468E+14	1.478E+14	8.917E+13
23	5.282E+14	1.152E+15	1.060E+15	1.064E+15	6.305E+14
24	3.091E+15	6.740E+15	6.289E+15	6.293E+15	3.667E+15
25	1.608E+16	3.506E+16	3.320E+16	3.309E+16	1.897E+16
26	9.274E+16	2.022E+17	1.938E+17	1.923E+17	1.089E+17
27	3.992E+17	8.704E+17	8.334E+17	8.267E+17	4.693E+17
28	3.021E+17	6.586E+17	6.305E+17	6.250E+17	3.553E+17
29	3.248E+17	7.081E+17	6.787E+17	6.722E+17	3.820E+17
30	5.412E+16	1.180E+17	1.143E+17	1.126E+17	6.349E+16
31	7.052E+15	1.538E+16	1.502E+16	1.473E+16	8.259E+15
32	2.980E+15	6.499E+15	6.370E+15	6.231E+15	3.488E+15
33	1.694E+15	3.695E+15	3.628E+15	3.544E+15	1.982E+15
34	1.107E+15	2.413E+15	2.375E+15	2.316E+15	1.294E+15
35	9.155E+14	1.996E+15	1.969E+15	1.917E+15	1.070E+15
36	6.296E+14	1.373E+15	1.357E+15	1.319E+15	7.355E+14
37	4.839E+14	1.055E+15	1.045E+15	1.014E+15	5.652E+14
38	3.318E+14	7.235E+14	7.167E+14	6.946E+14	3.875E+14
39	2.140E+14	4.665E+14	4.609E+14	4.471E+14	2.501E+14

Note: Groups 1 to 18 extend from 20 MeV down to 0.765 eV.

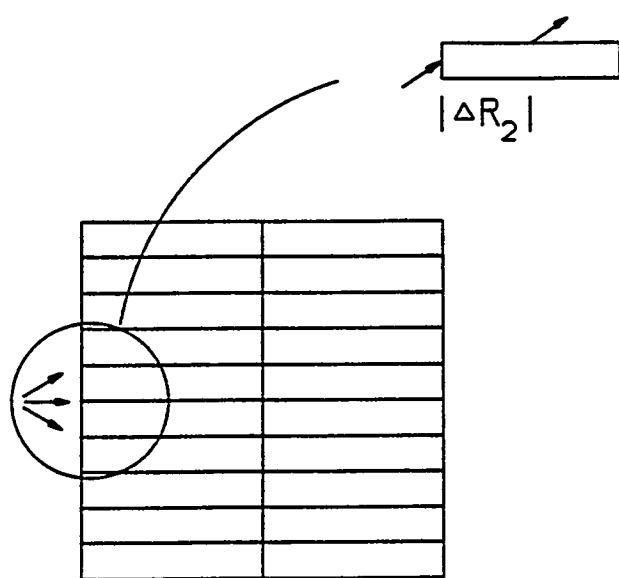
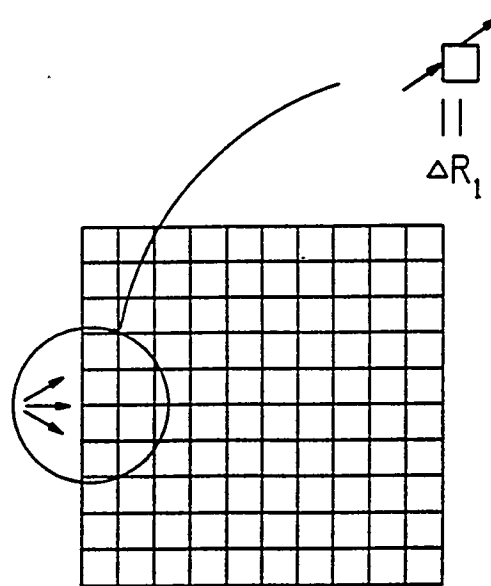


Fig. 8. Illustration showing the unnatural advancement of the flux via artificial numerical diffusion in the direction of elongation when numerous long thin mesh intervals are used.

a new set of mesh specifications were developed with the intent of keeping the mesh intervals as close to square as possible throughout the bulk of the reflector while at the same time retaining all of the original (physical) material boundaries listed in Table 1. These revised mesh specifications are described in Tables 4a and 4b and in Figs. 3a-3f. Note that instead of having 133x236 mesh intervals, we now have 138x266 mesh intervals in the global 2-D RZ model. While the number of mesh intervals (especially in the radial direction) is not that much different, the distribution of the mesh intervals is significantly different, with many more "closer-to-square" intervals throughout the reflector. These revised mesh specifications were subsequently used in DORT Runs 4, 4a, and 5. Subsequent results from DORT Run 4 (without photoneutrons, like DORT Run 3, but with the revised mesh) strongly suggest that this redistribution fixed the malady described above. DORT Run 4 results on the surface of the reflector vessel directly across from a point halfway up the top section of the core are shown in Table 18 along with the earlier DORT Run 3 results and the 1-D GB-ANISN results. There, one can see that the fast fluxes for groups 1-18 are now slightly lower than the 1-D GB-ANISN results (as they should be), rather than being a factor of 2 or more higher, like the physically impossible results shown for DORT Run 3.

6.5 MODIFICATIONS TO INCLUDE DELAYED FISSION GAMMAS (NEW AJAX DATA FOR DORT RUN 4)

After DORT Run 3 but prior to DORT Run 4, it became clear that prompt fission gammas were being properly accounted for in the cross section processing codes and in the shielding analysis but that the delayed fission gammas were not being accounted for at all. While delayed fission gammas include everything out to 1.0E13 seconds after fission, the bulk of these are generated in the first 1 to 10 seconds, and indeed in the first few hundredths of a second after fission. (By contrast, prompt fission gammas normally include only those gammas generated in the first 50 to 100 nanoseconds after fission). Moreover, while the number of delayed fission gammas is comparable to the number of prompt fission gammas, the spectra for the delayed fission gammas is somewhat softer. In any event, both should be included in the reactor shielding analysis. To rectify this, the original ANSL-V AMPX master cross section library was processed through a modified version of the AJAX code (as explained in the second paragraph of Sect. 4.1 above) and a new AMPX master cross section library was produced in which the MT number associated with the delayed fission yield data for U-235 and U-238 had been changed to MT=18 so that the NITAWL code would now fold that yield data with the fission cross sections and include that data in the subsequent working cross section libraries.

Subsequent investigations using the 1-D group-banded ANISN code have shown that while the lower energy gamma fluxes in groups 54 to 83 (i.e., gamma groups 15 to 44) are 50 to 250% higher in the fuel, and on the outer surface of the fuel, when one includes the delayed fission gammas than they are when one does not, the gamma fluxes in these same groups further out in the reflector (at the interface between the D₂O and the reflector vessel) are only a few percent higher than they would have been had one not included the delayed fission gammas.

Plots of the 2-D neutron and gamma fluxes and dose rates for DORT Run 4 (with delayed fission gammas but without photoneutrons) are shown in Figs. 9a-9h. While later plots for DORT Run 5 show the recommended reference results, comparisons against these earlier results for DORT Run 4 are most interesting and will be discussed later. In both cases, however, it should be noted that these are "unperturbed fluxes" and, as such, do not account for local effects caused by the presence of beam tubes and other components in the reflector which could not be modeled in a global 2-D RZ analysis.

Neutron Flux ($s^{-1}m^{-3}$) for $E > 0.1$ MeV (Groups 1-7)

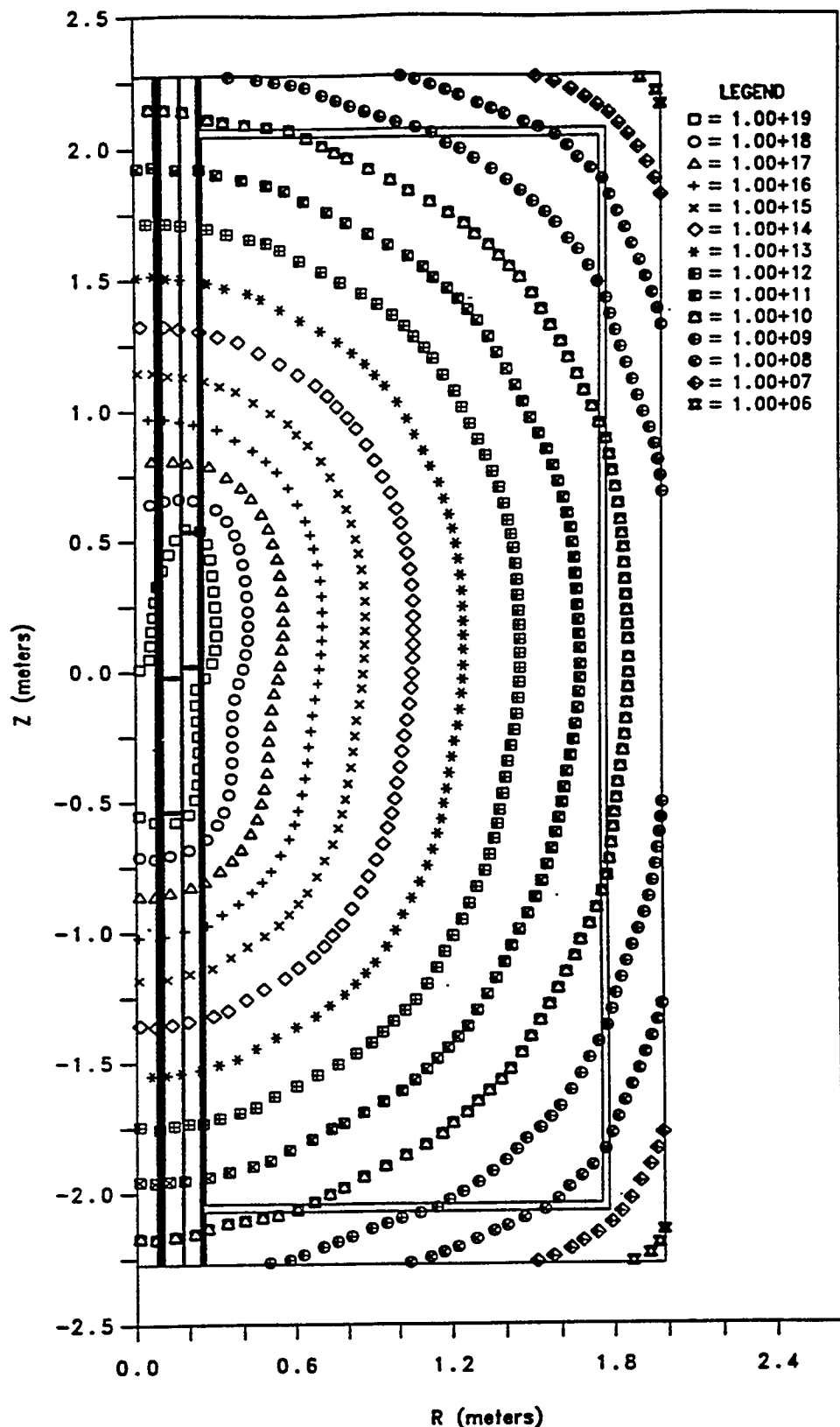


Fig. 9a. Contours showing the 2-D spatial distribution of the fast neutron flux in the ANS core and reflector ($E > 0.1$ MeV), as given by DORT Run 4, which did not account for photoneutrons.

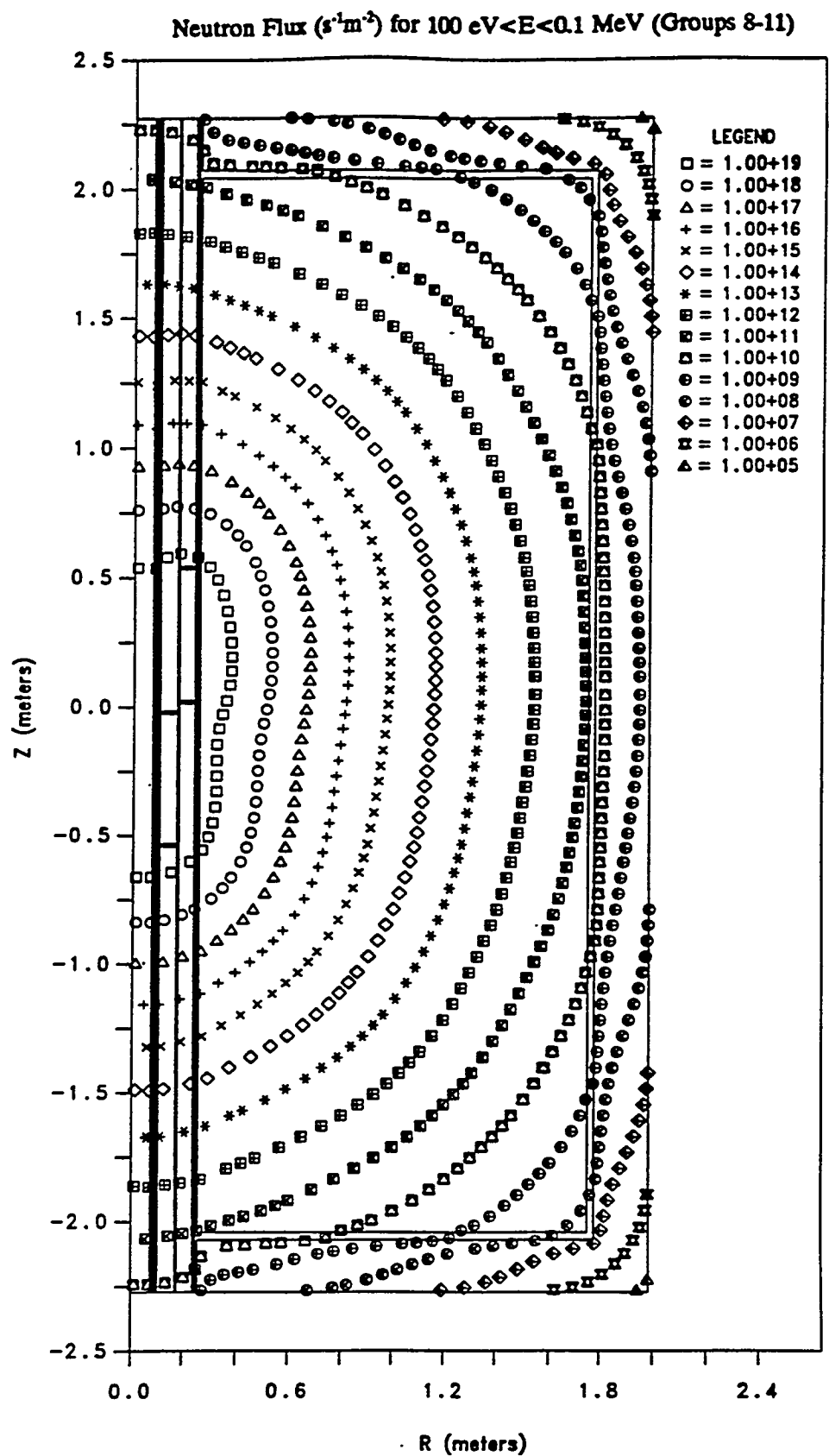


Fig. 9b. Contours showing the 2-D spatial distribution of the intermediate-energy neutron flux in the ANS core and reflector ($100 \text{ eV} < E < 0.1 \text{ MeV}$), as given by DORT Run 4, which did not account for photoneutrons.

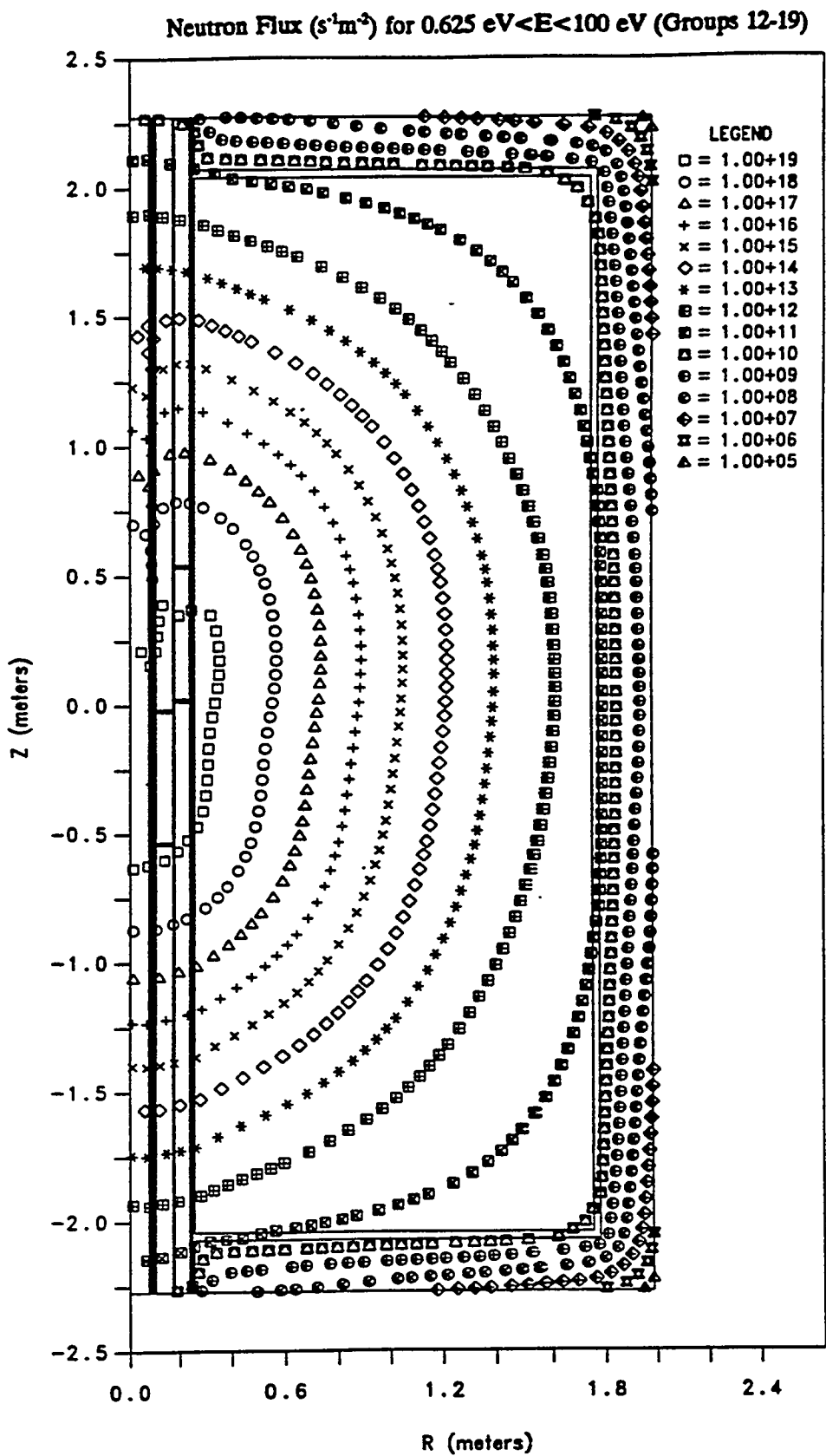


Fig. 9c. Contours showing the 2-D spatial distribution of the epithermal neutron flux in the ANS core and reflector ($0.625 \text{ eV} < E < 100 \text{ eV}$), as given by DORT Run 4, which did not account for photoneutrons.

Neutron Flux ($s^{-1}m^{-3}$) for $E < 0.625$ eV (Groups 20-39)

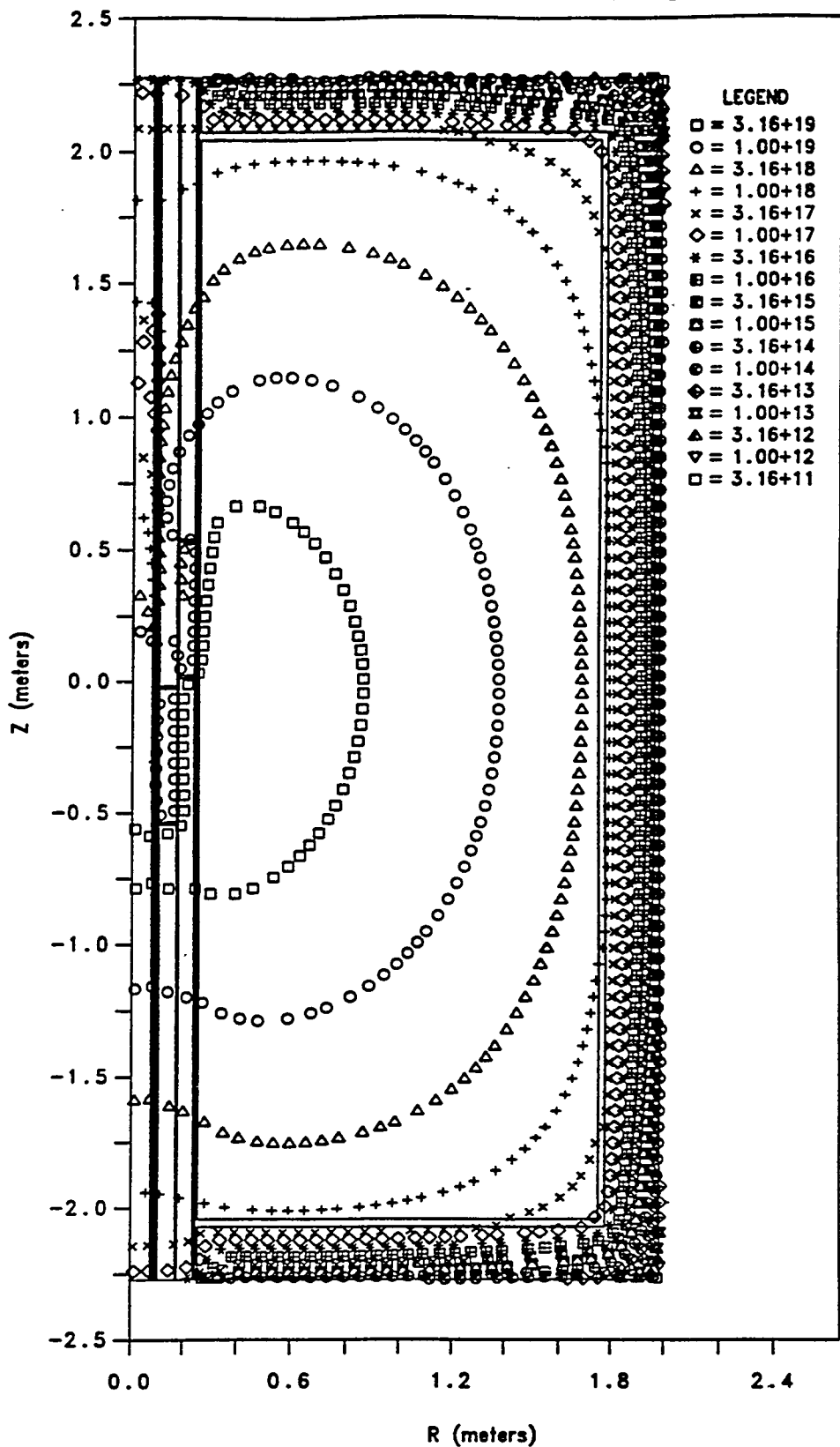


Fig. 9d. Contours showing the 2-D spatial distribution of the thermal neutron flux in the ANS core and reflector ($E < 0.625$ eV), as given by DORT Run 4, which did not account for photoneutrons.

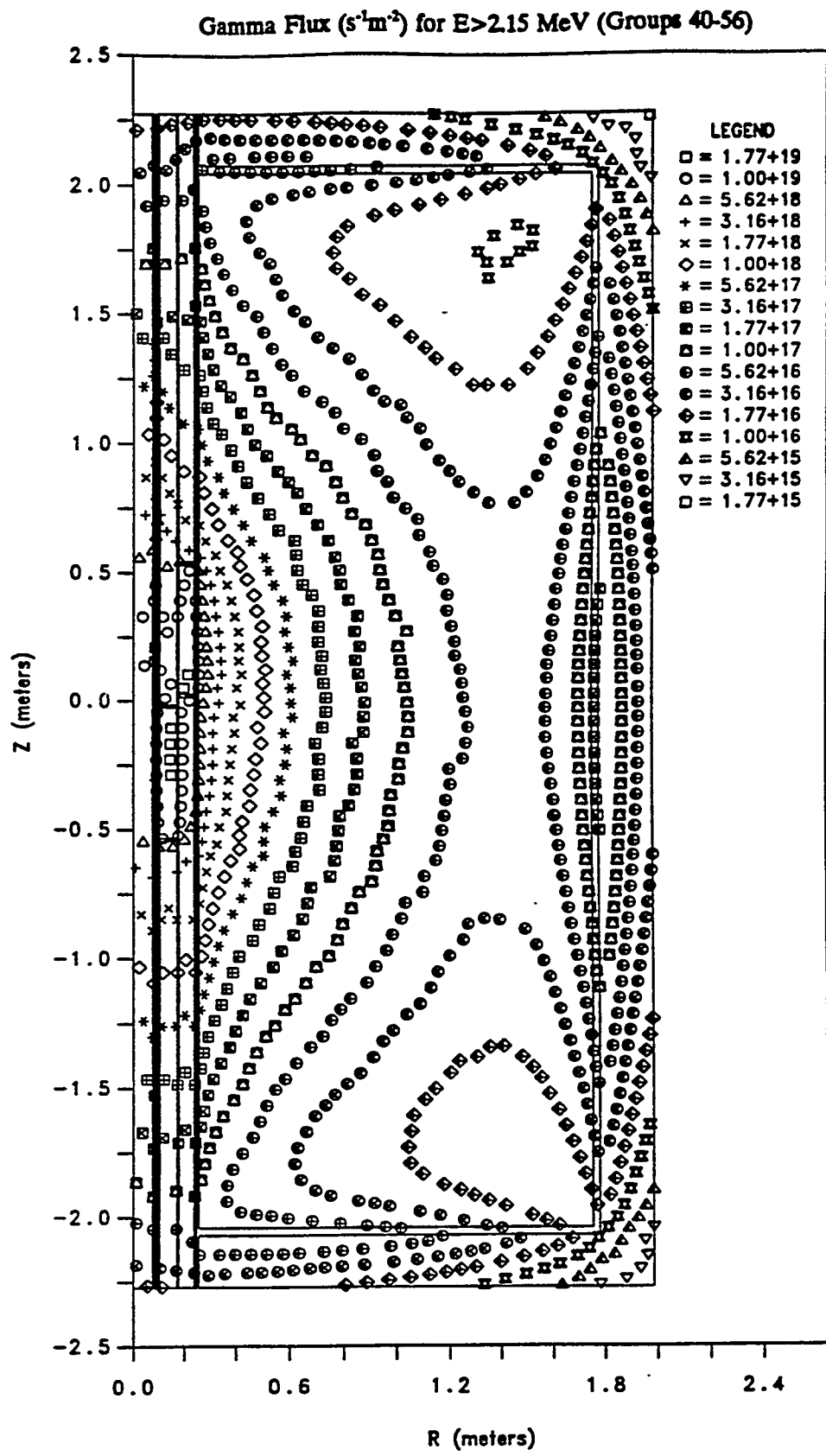


Fig. 9e. Contours showing the 2-D spatial distribution of the high-energy gamma flux above 2.15 MeV in the ANS core and reflector, as given by DORT Run 4, which did not account for photoneutrons. [Note that most of these photons (i.e., those above 2.25 MeV) had sufficient energy to create fast photoneutrons in the heavy water.]

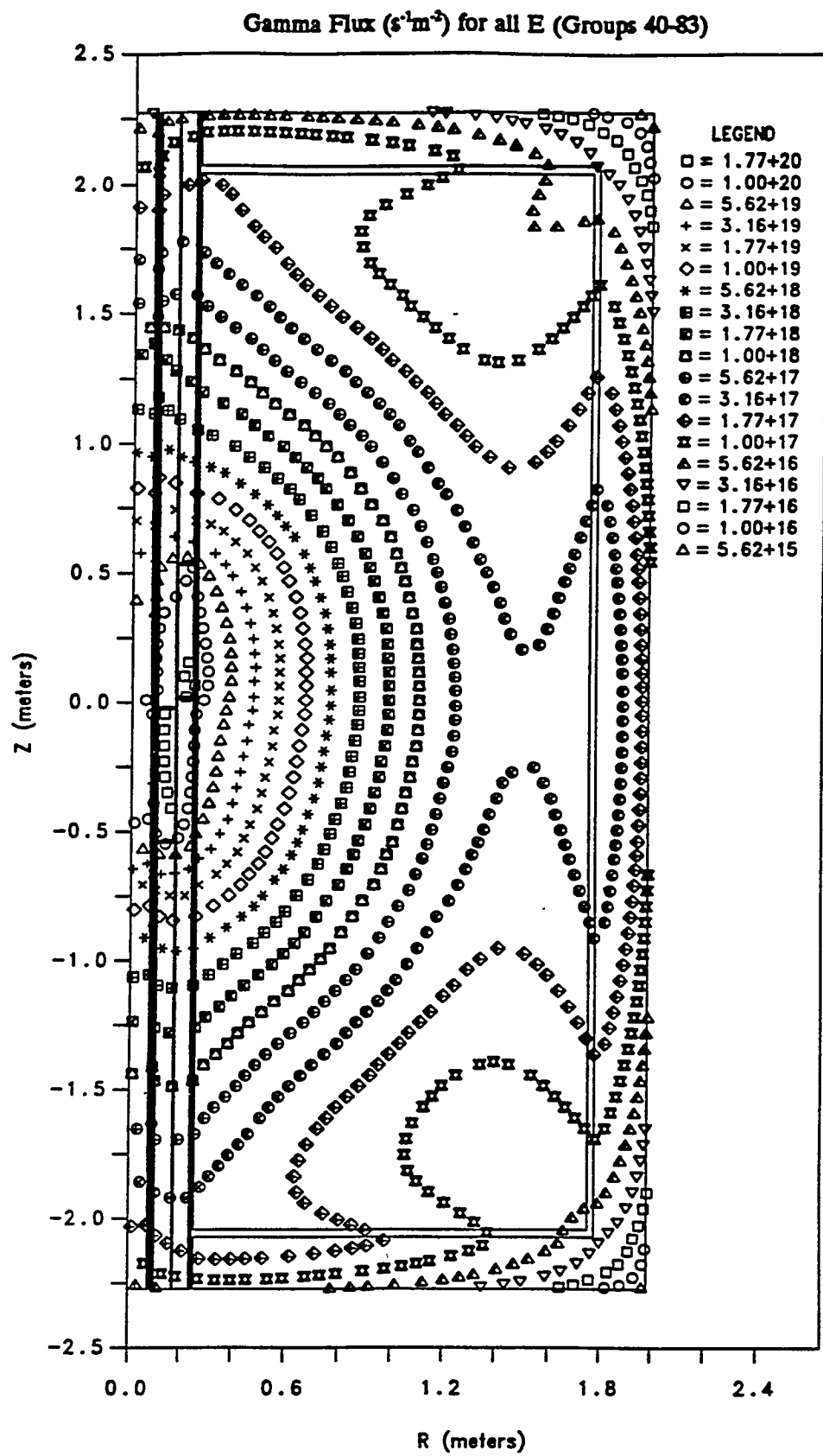


Fig. 9f. Contours showing the 2-D spatial distribution of the total gamma flux in the ANS core and reflector (summed over all gamma energy groups), as given by DORT Run 4, which did not account for photoneutrons.

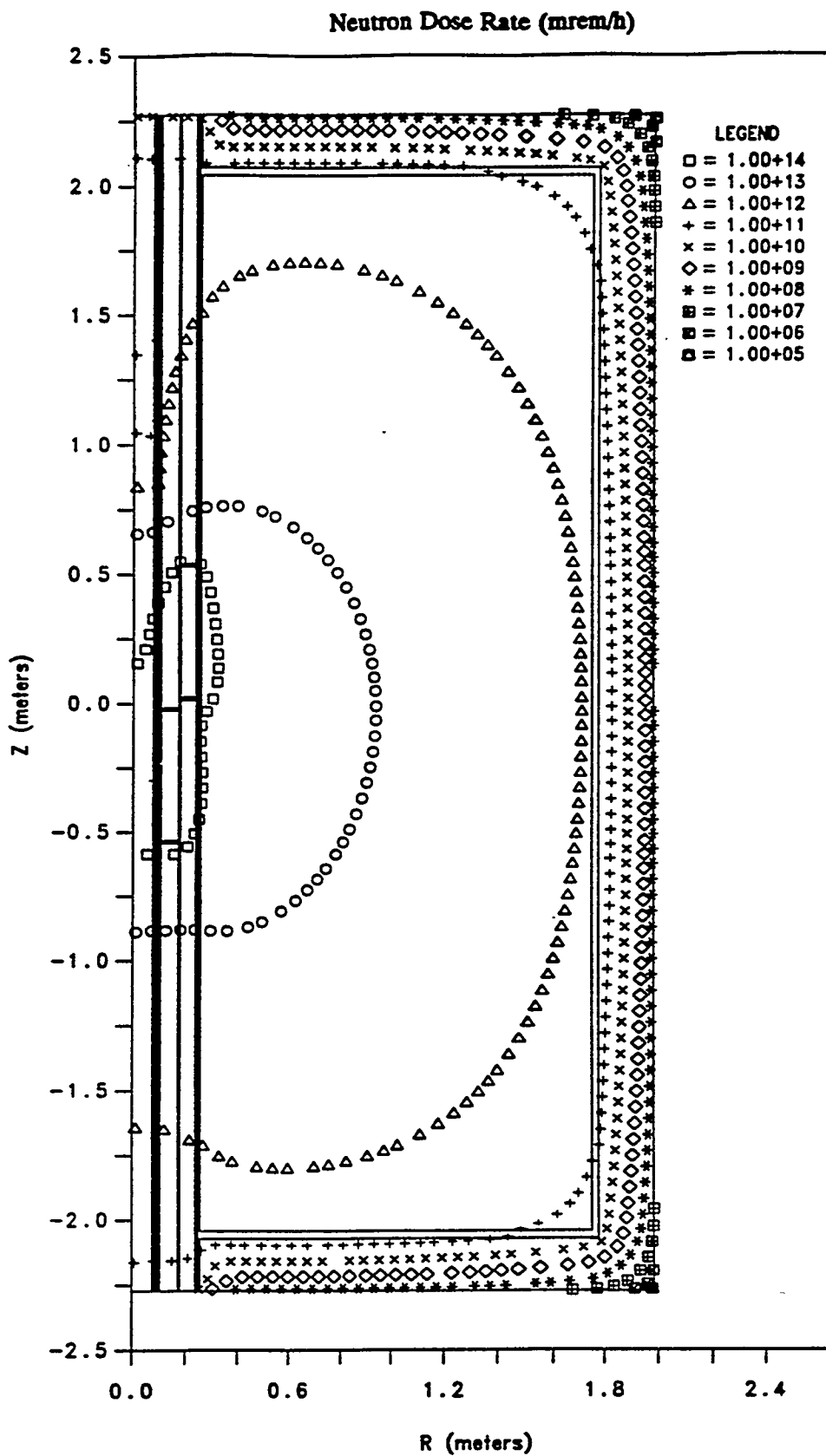


Fig. 9g. Contours showing the 2-D spatial distribution of the neutron dose rate (mrem/h) in the ANS core and reflector, as given by DORT Run 4, which did not account for photoneutrons.

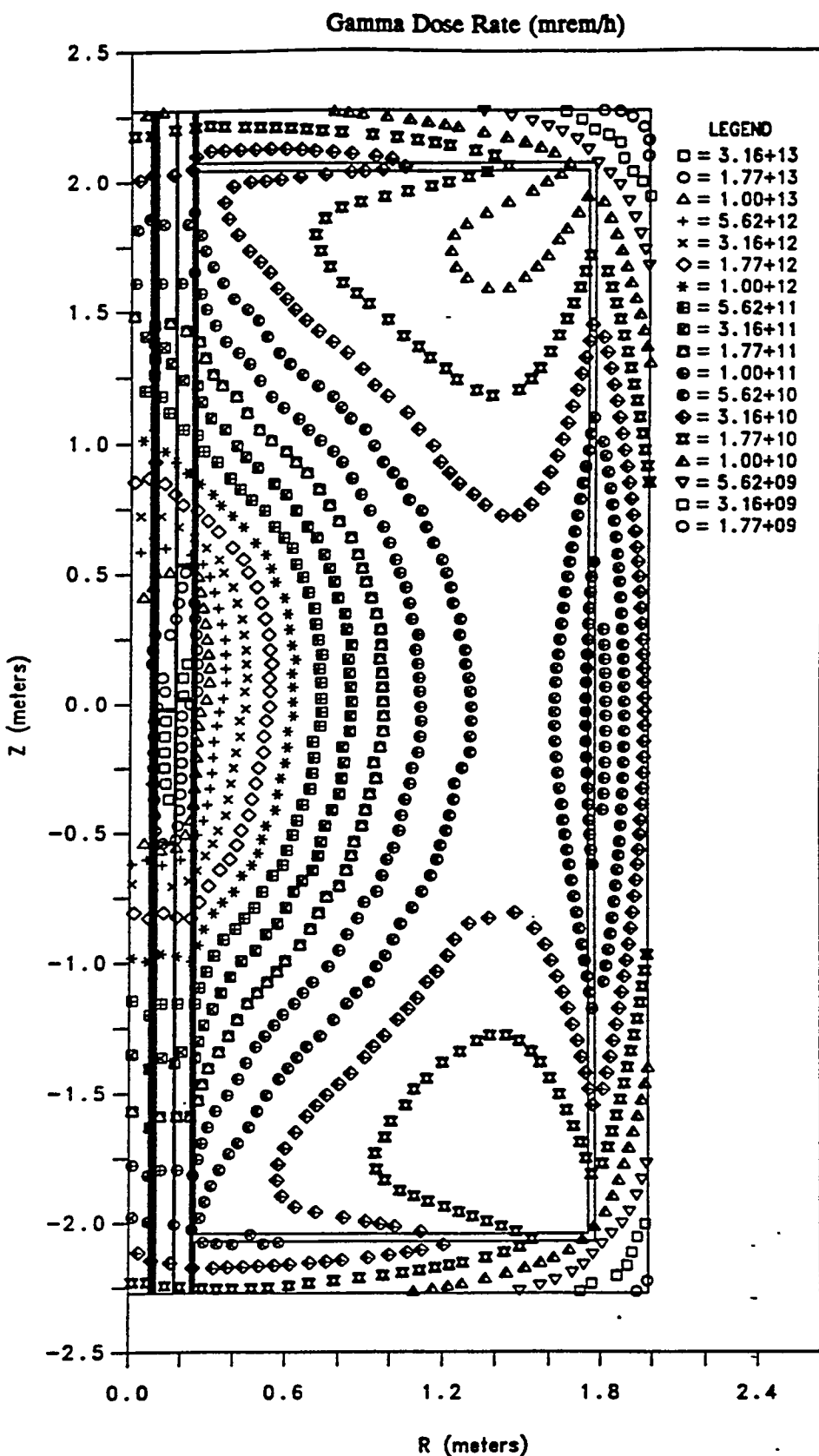


Fig. 9h. Contours showing the 2-D spatial distribution of the gamma dose rate (in rem/h) in the ANS core and reflector, as given by DORT Run 4, which did not account for photoneutrons.

6.6 TREATMENT OF PHOTONEUTRONS (PHOTOX/SPARK DATA IN DORT RUNS 4A AND 5)

After DORT Run 4 but prior to DORT Runs 4a and 5, we began to account explicitly for the presence of photoneutrons. Section 4.3 alludes to the potential importance of photoneutrons and then goes on to describe the PHOTOX program for determining the group-to-group photoneutron production matrix and the SPARK program for reading an existing DORT-ready cross section library, modifying it to include that data, and writing out a new DORT-ready cross section library with that data. The next few paragraphs illustrate the potential importance of photoneutrons in a more quantitative fashion and explain how the cross section library produced by the SPARK program was verified prior to its use in DORT, as well as how the calculational strategy was modified to make effective use of that data in the DORT analysis.

To understand how the SPARK-modified cross sections (with photoneutrons) and the calculational procedures for utilizing that data were verified, it is useful to review the cruder and more cumbersome preliminary procedures that were used to investigate the effects of photoneutrons in 1-D calculations before we had the PHOTOX and SPARK codes. These initial fixed-source GB-ANISN calculations were performed using the standard DORT-ready cross section library "xfort.8.run4" without photoneutrons (cf. Fig. 6) to determine the gamma fluxes everywhere. Based purely on a crude visual inspection of Fig. 5 (overlaid with the gamma group structure from Table 7a), the photoneutron production cross sections for the first 17 gamma groups were assumed to be 1.0, 1.0, 1.25, 1.6, 1.8, 1.9, 2.0, 2.08, 2.18, 2.22, 2.27, 2.3, 2.2, 2.0, 1.6, 1.1, and 0.45 millibarns, respectively. Assuming that all gammas in a given energy group were at the mid-point energy for that group, gammas in any one group would produce neutrons in only one neutron group corresponding to $E_n = 0.5(E_\gamma - 2.23 \text{ MeV})$. Using a small PC program to read the multigroup gamma fluxes at each point and fold that data with these crude cross sections, the resulting multigroup photoneutron sources were calculated at each point and then fed to the next group-banded ANISN calculation as a fixed source. More precisely, the logic for an entire sequence of 1-D calculations would proceed as follows:

1. Run one GB-ANISN calculation with ONLY the fission neutron source in the core to get the resulting gamma flux everywhere and save it as $\text{flux}(a)$.
2. Run the PC-based program described above to get the resulting (crude) multigroup photoneutron source terms everywhere.
3. Run another GB-ANISN calculation with the ONLY source being the multigroup photoneutron source from Step 2. This will generate a new neutron and gamma flux field that is due only to the last round of photoneutrons.
4. Repeat Steps 2 and 3 nine or ten times. Note that with each round of "manual iterations" the source terms and the resulting neutron and gamma fluxes will be getting smaller and smaller.
5. When done, add together all of the fluxes from all of the GB-ANISN runs to get the final flux distribution:

$$\text{flux}(\text{final}) = \text{flux}(a) + \text{flux}(b) + \dots + \text{flux}(j) \quad . \quad (8)$$

6. For reference, calculate and save the ratio of the final fluxes with photoneutrons to the original fluxes without photoneutrons:

$$ratio(R,E) = flux(final) / flux(a) . \quad (9)$$

Table 19 shows a partial listing of the ratios of the group-banded ANISN neutron fluxes with/without the photoneutrons generated in the D₂O as a function of energy and position, as determined by using the standard DORT-ready cross section library (xfort.8.run4) and the series of fixed source calculations as described above, for a 1-D radial trace halfway up the top section of the ANS core. Deep in the D₂O reflector, close to the reflector vessel where the fast flux would otherwise be quite depressed, the fast neutron flux levels were 2, 3, or 4 thousand times greater than what one would have erroneously estimated had one not accounted for photoneutron production. Whether or not that is significant will depend on the situation one is analyzing (subpile room: yes; bulk shielding: maybe; beam tubes: no). That, however, is a separate topic.

The above 1-D analysis of photoneutrons using the original cross section library and a series of "manual iterations" using fixed source calculations where the source for each iteration is based on a straightforward stand-alone application of the crude photoneutron production cross sections described above also provides a good independent benchmark that can be (and was) used to verify the revised DORT-ready cross section library produced by the SPARK code (xfort.8.run4.spark1), as well as the newer and more automated calculational procedures employing that data. To that end, the revised DORT-ready cross section library with photoneutrons was then used in conjunction with a new 1-D group-banded ANISN analysis in which we simply entered the original neutron sources in the core and allowed the GB-ANISN code to perform a series of outer iterations over all neutron and gamma energy groups while using the data in the new library to converge the photoneutron sources and the resulting fluxes. After only 4 outer iterations and 7.4 minutes of CPU time, that calculation was fully converged. The resulting multigroup fluxes in each spatial mesh interval were then compared with those obtained using the off-line manual iteration technique employing the preliminary (less refined) photoneutron production cross sections described above (based on visual inspection of Fig. 5). The agreement was absolutely excellent – i.e., generally within 1 or 2% of the values obtained using the manual iteration technique with the less precise photoneutron production cross sections and quite frequently within 0.1% for the same mesh locations and energy ranges shown in Table 19. In the most extreme cases, a handful (< 5 or 6) of the newer (more precise) values differed by at most 6 to 7% from the values obtained using the manual iteration technique and the preliminary (less refined) photoneutron production cross sections described above. [Moreover, even those differences can be explained by the fact that the newer more refined data based on the PHOTOX and SPARK codes allowed gammas in some energy groups to produce photoneutrons in a range of neutron groups, whereas the cruder preliminary data mentioned above assumed there was a unique one-to-one correspondence between each gamma group and each neutron group.] Based on these comparisons, one may safely conclude that the PHOTOX cross section generation program, the SPARK cross section insertion program, the resulting cross section data library, and the technique for automatically applying that data in the GB-ANISN and DORT programs have all been adequately verified.

DORT Run 4a (with the revised spatial mesh distribution, with delayed fission gammas, and with the new cross section library including photoneutrons) was successfully run and converged. While those results are available upon request, they will not be presented here since they differ almost imperceptibly from the final reference results for DORT Run 5, which superseded DORT Run 4a.

Table 19. Partial listing of the ratios of the group-banded ANISN neutron fluxes with/without the photoneutrons generated in the D₂O as a function of energy and position, as determined by using a standard cross section library and a series of manual iterations as described in the text. This GB-ANISN calculation is for a 1-D radial slice, halfway up the top section of the core, using 3 times as many mesh intervals as shown in Table 3a.

Position		Neutron energy range(*)				
Mesh	R(mm)	>6.434MeV	>0.9 MeV <6.434MeV	>0.1 MeV <0.9 MeV	>17 keV <0.1 MeV	>550 eV <17 keV
354	1576.31	1.00086	381.1	755.5	635.0	497.4
355	1594.59	1.00098	477.2	954.5	795.3	618.2
356	1612.88	1.00111	599.9	1208.5	994.4	764.9
357	1631.16	1.00125	756.6	1531.1	1238.6	940.2
358	1649.44	1.00141	955.7	1936.4	1532.0	1145.3
359	1667.73	1.00158	1206.6	2436.6	1874.9	1378.7
360	1686.01	1.00176	1515.7	3034.6	2258.5	1634.4
361	1704.29	1.00192	1877.8	3709.4	2658.1	1899.6
362	1722.58	1.00202	2248.7	4380.4	3020.6	2152.3
363	1740.86	1.00196	2308.4	4708.3	3222.9	2332.7
364	1752.08	1.00181	2090.0	4610.3	3246.9	2396.2
365	1756.25	1.00173	1964.5	4477.3	3235.8	2398.9
366	1760.42	1.00165	1861.5	4361.3	3226.4	2403.6
367	1764.58	1.00159	1774.1	4255.8	3218.6	2410.4
368	1768.75	1.00153	1696.8	4155.2	3212.6	2419.5
369	1772.92	1.00148	1625.0	4054.0	3208.3	2431.1
370	1778.47	1.00142	1475.2	3819.6	3207.7	2514.1
371	1785.40	1.00135	1266.0	3427.7	3184.5	2672.1
372	1792.33	1.00130	1113.9	3089.3	3097.2	2746.8
373	1799.27	1.00125	993.9	2779.7	2946.6	2770.8
374	1806.20	1.00121	894.6	2498.4	2750.2	2717.5
375	1813.13	1.00118	810.0	2244.7	2527.5	2603.7
376	1820.07	1.00115	736.8	2017.5	2298.2	2439.6
377	1827.00	1.00113	672.6	1815.0	2075.6	2247.5
378	1833.93	1.00110	615.8	1635.0	1867.9	2045.2
379	1840.87	1.00108	565.2	1475.3	1678.9	1847.1
380	1847.80	1.00106	519.9	1333.7	1509.4	1661.8
381	1854.73	1.00105	479.1	1208.0	1359.0	1493.3
382	1861.67	1.00103	442.3	1096.4	1225.8	1342.8
383	1868.60	1.00102	409.0	997.2	1108.3	1209.4
384	1875.53	1.00100	378.8	908.9	1004.5	1091.9
385	1882.47	1.00099	351.3	830.1	912.7	988.5
386	1889.40	1.00098	326.1	759.7	831.5	897.4
387	1896.33	1.00097	303.2	696.7	759.4	817.1
388	1903.27	1.00096	282.3	640.3	695.4	746.2
389	1910.20	1.00094	263.1	589.8	638.5	683.5
390	1917.13	1.00093	245.5	544.4	587.8	628.0
391	1924.07	1.00093	229.3	503.7	542.7	579.0
392	1931.00	1.00092	214.6	467.2	502.7	535.7
393	1937.93	1.00091	201.0	434.6	467.2	497.7
394	1944.87	1.00090	188.7	405.5	435.9	464.6
395	1951.80	1.00089	177.4	379.8	408.7	436.1
396	1958.73	1.00089	167.3	357.4	385.4	412.0
397	1965.67	1.00088	158.3	338.5	366.2	392.6
398	1972.60	1.00087	150.6	323.9	351.4	377.6
399	1979.53	1.00087	144.5	318.8	344.7	369.6

* Note: The calculations were actually performed using the 39n/44g library structure, with the results being reported here in this group structure for the sake of compactness.

6.7 CORRECTION OF A MINOR DATA ERROR PRIOR TO DORT RUN 5

Subsequent to DORT Run 4a but prior to DORT Run 5, an input data error was discovered in the description of material 10 (the 10-mm-thick homogenized poison plates at the top and bottom of the upper and lower fuel elements in the core). Fortunately, it was discovered, corrected, and found to have very little effect on the global 2-D shielding analysis and no effect at all on the 1-D analyses since material 10 was never used in the 1-D analyses. While the correct specifications for material 10 are listed in Table 2 and in the right hand column of Table 20, the erroneous specifications initially used by the SCALE/CSASI (BONAMI/NITAWL/ICE/JIPSY) codes to prepare the cross section data for DORT Runs 1-4 are shown on the left hand side of Table 20 along with the (incorrect) resulting number densities. [Basically, the 0.0 in each line of the material specifications tells the SCALE codes to treat the following data item as a nuclide number density, whereas without that 0.0 data flag (as on the left of Table 20), the next item is treated as a volume fraction.] This error resulted in the number densities for this one material being about an order of magnitude too low in DORT Runs 1-4. This error was corrected prior to DORT Run 5, subsequent to which, inspection of the results has shown that it made very little difference for several reasons:

1. Material 10 was never used in any of the 1-D calculations, only in the 2-D calculations.
2. Because the 2-D RZ calculations were "fixed source" calculations, as opposed to eigenvalue calculations, the source distribution (cf. Sect. 3 and/or Table 6b) was correct and was not affected by this material in any of the 2-D calculations.
3. This relatively thin 10-mm-thick region of material 10 (comprised mainly of aluminum, heavy water, and some boron) is relatively transparent to fast neutrons so that the fast neutron fluxes above and below these plates are relatively unaffected, as evidenced by the fact that differences in the fast flux (if any) are so small that they cannot be seen at all in the corresponding 2-D plots of the final results.
4. Because these thin thermal-neutron-absorbing poison plates were located immediately adjacent to the highly absorptive fuel elements, the effect on even the thermal flux in that immediate region was rather marginal. Basically, the long, highly absorptive fuel elements immediately adjacent to these poison plates caused such a large dip in the thermal flux there that the presence or absence of these thin poison plates in that particular location made very little difference in these fixed source calculations. [In an eigenvalue calculation, of course, their presence or absence would have had a large effect on the shape of the source in that region, but this is not the case with a fixed-source calculation.] At the axial midplane, in the radial aluminum separator between the upper and lower fuel elements immediately adjacent to two such poison plates, the thermal neutron flux below 0.625 eV as given by DORT Run 4a ($1.989E19 \text{ s}^{-1}\text{m}^{-2}$), for example, was only 1.28 times higher than the corresponding value for DORT Run 5 ($1.550E19 \text{ s}^{-1}\text{m}^{-2}$) where material 10 was correctly represented. Further away, near the hot end of a horizontal beam tube (at $R=430.2 \text{ mm}$, just 177.2 mm past the core pressure boundary tube) the thermal neutron flux based on DORT Run 4a ($7.048E19 \text{ s}^{-1}\text{m}^{-2}$) was only 2% higher than the more accurate value from DORT Run 5 ($6.914E19 \text{ s}^{-1}\text{m}^{-2}$) where material 10 was correctly represented.

Based on these observations, it is safe to say that the unfortunate error noted above made very little appreciable difference in the global 2-D shielding analysis. Nevertheless, in the interest of rigor, the DORT Run 5 results (with the revised spatial mesh, with delayed fission gammas, and with photoneutrons) must be considered as the final recommended reference solution.

Table 20. Erroneous and correct material specifications for material 10, which represents the 10 mm thick homogenized poison plates at the top and bottom of the upper and lower fuel elements in the core.

SCALE material specifications (erroneous; runs 1-4)				SCALE material specifications (correct; run 5)			
' mix 10 = homogenized poison plates at ends of fuel:				' mix 10 = homogenized poison plates at ends of fuel:			
' homogenized densities due to boron itself:				' homogenized densities due to boron itself:			
b-10	10	2.980e-04	339.2	end	b-10	10	0.0
b-11	10	1.199e-03	339.2	end	b-11	10	0.0
' homogenized densities due to cladding:				' homogenized densities due to cladding:			
mg	10	1.337e-04	339.2	end	mg	10	0.0
al	10	2.868e-02	339.2	end	al	10	0.0
si	10	1.440e-04	339.2	end	si	10	0.0
ti	10	1.018e-05	339.2	end	ti	10	0.0
cr	10	1.250e-05	339.2	end	cr	10	0.0
mn	10	1.311e-05	339.2	end	mn	10	0.0
fe	10	8.241e-05	339.2	end	fe	10	0.0
cu	10	2.247e-05	339.2	end	cu	10	0.0
cu	10	1.955e-05	339.2	end	cu	10	0.0
' homogenized densities due to heavy water:				' homogenized densities due to heavy water:			
d	10	3.265e-02	339.2	end	d	10	0.0
o	10	1.632e-02	339.2	end	o	10	0.0
end comp				end comp			
Resulting number densities (erroneous; runs 1-4)				Resulting number densities (correct; run 5)			
Mixture number	Isotope name	Isotope Z/A ID	Number density atoms/(barn*cm)	Mixture number	Isotope name	Isotope Z/A ID	Number density atoms/(barn*cm)
10	b-10	5010	3.934E-05	10	b-10	5010	2.980E-04
10	b-11	5011	1.583E-04	10	b-11	5011	1.199E-03
10	mg	12000	3.314E-06	10	mg	12000	1.337E-04
10	al	13027	1.728E-03	10	al	13027	2.868E-02
10	si	14000	7.173E-06	10	si	14000	1.440E-04
10	ti	22000	5.815E-07	10	ti	22000	1.018E-05
10	cr	24000	1.041E-06	10	cr	24000	1.250E-05
10	mn	25055	1.069E-06	10	mn	25055	1.311E-05
10	fe	26000	6.997E-06	10	fe	26000	8.241E-05
10	cu	29000	3.537E-06	10	cu	29000	4.202E-05
10	d	1002	9.762E-03	10	d	1002	3.265E-02
10	o	8016	6.146E-04	10	o	8016	1.632E-02

6.8 DISCUSSION OF THE FINAL SOLUTION (DORT RUN 5: STRATEGY AND QUALITATIVE RESULTS)

DORT Run 5 [with the revised spatial mesh distribution, with delayed fission gammas, and with the new cross section library (xfort.8.run5.spark1) including the photoneutron production cross sections and a correct description of material 10] was successfully run and converged and is currently considered the recommended reference solution. A detailed description of those results is presented in Sect. 7 and Appendix E, while the remainder of Sect. 6 will focus primarily on the solution strategy employed and a qualitative discussion of the results obtained.

In the interest of efficiency, the flux solution for DORT Run 4a (with photoneutrons) was used as the initial flux guess for DORT Run 5. Both used a similar solution strategy, as shown in Tables 21a and 21b, and both required restarting the problem several times to converge efficiently the flux in different energy groups and account for different effects. Unlike the small fast 1-D calculations where one can easily afford to account for photoneutrons in the course of each outer iteration over all energy groups, it was much more efficient in the large 2-D calculations to first converge the fast neutron groups, then the thermal neutron groups, and later the gamma groups, before beginning to perform additional outer iterations for the photoneutrons. This is possible because the large thermal neutron population deep in the reflector is several orders of magnitude larger than the fast neutron population there (even after one accounts for fast photoneutrons). Moreover, the strategy employed here is also much more efficient because the first series of outer iterations to converge the thermal neutron groups (Step B1) only needs to span groups 15 to 39, whereas the second series of outer iterations needed to converge the photoneutrons (Step D1) has to span groups 1 to 56 -- i.e., all 39 neutron groups plus the first 17 gamma groups. The calculational strategy for converging the photoneutrons in Step D1 of DORT Run 4a and DORT Run 5 is described further in Table 22.

To aid in determining when a particular calculational step (or a whole series of calculational steps) was adequately converged, a simple on-line utility program called CHKCON was written and used extensively in parallel with the DORT code. This simple routine reads the printed output listing file produced by DORT and saves all key fluxes requested by the user and printed by DORT in the following order:

((flux(inner,igrp,iouter), inner=1,maxin), igrp=1,maxgrp), iouter=1,maxout) .

It then sorts all the key flux data and prints it out as

((flux(inner,igrp,iouter), inner=1,maxin), iouter=1,maxout), igrp=1,maxgrp) ,

which is much more useful insofar as one can then look at the results for any given group (all in one place) and see how the results are converging, not only from one inner iteration to the next, but also from one outer iteration to the next. Careful monitoring of this history file then allowed us to continue performing outer iterations over all energy groups of interest until the key fluxes (at $I_r=119$, $J_z=150$ and $I_r=119$, $J_z=117$) in each group had changed by less than 0.1% over the last 10 or 20 outer iterations. At this point, the given calculational steps (B1 and D1) were terminated manually.

Flux and dose rate contours for DORT Run 5 with photoneutrons are shown in Figs. 10a-10h, and may be compared to the earlier results for DORT Run 4 without photoneutrons, as shown in Figs. 9a-9h. Characteristic differences are as follows: Without photoneutrons (Figs. 9a-9h), the flux contours are more or less oval shaped and evenly spaced as one moves outward from the core to the reflector vessel. With

Table 21a. Description of the calculational steps for DORT Run 4a with photoneutrons, where each step used the flux moment file generated by the previous step as the initial flux guess, and step A1 was run from scratch. Note that these 9 steps required a total of 139.9 CPU hours (5.83 CPU days) on an IBM Model 530 workstation.

Step	Groups Covered	Number of Outer Iterations Over Energy Groups	Total Number of Inner (Spatial) Iterations	Average Number of inners/group/outer (allowed, used)	Purpose of this Step
A-1	1 - 39	1	420	(50,18.5) grps 1-14 (8, 6.5) grps 15-39	Converge all neutron groups, especially the fast groups
A2	1 - 39	1	372	(50,15.3) grps 1-14 (8, 6.3) grps 15-39	Converge all neutron groups, especially the fast groups
B1	15 - 39	150	7500	(2, 2.0)	Converge thermal neutron groups
C1	40 - 83	1	177	(50, 4.0)	Converge gamma groups
C2	1 - 83	1	251	(10, 3.0)	Converge all groups
D1	1 - 56	28	3136	(2, 2.0)	Converge photoneutrons
E1	1 - 83	3	398	(10, 1.6)	Converge everything
E2	1 - 83	3	349	(10, 1.4)	Converge everything tighter
F1	1 - 83	1	178	(4, 2.1)	Converge everything (final check; one last outer)

Table 21b. Description of the calculational steps for DORT Run 5 with photoneutrons, where each step used the flux moment file generated by the previous step as the initial flux guess, except for step A1 which used step F1 of DORT Run 4a as its initial flux guess. Note that these 7 steps required a total of 78.1 CPU hours (3.25 CPU days) on an IBM Model 530 workstation.

Step	Groups Covered	Number of Outer Iterations Over Energy Groups	Total Number of Inner (Spatial) Iterations	Average Number of inners/group/outer (allowed, used)	Purpose of this Step
A1	1 - 39	1	244	(50, 9.6) grps 1-14 (8, 4.4) grps 15-39	Converge all neutron groups, especially the fast groups
B1	15 - 39	20	1000	(2, 2.0)	Converge thermal neutron groups
C1	40 - 83	1	145	(50, 3.3)	Converge gamma groups
C2	1 - 83	1	154	(10, 1.9)	Converge all groups
D1	1 - 56	42	4704	(2, 2.0)	Converge photoneutrons
E1	1 - 83	6	715	(10, 1.4)	Converge everything tightly
F1	1 - 83	1	178	(4, 2.1)	Converge everything (final check; one last outer)

Table 22. Calculational strategy for converging the fast photoneutrons in Step D1 of DORT Run 4a and DORT Run 5. Note that this table shows the recommended values for a number of the DORT input parameters during this stage of the analysis. For the overall (multistep) calculational strategy, see Tables 21a and 21b.

- 1) Use "spark1" cross sections having a fake macro nusigf=1.0E-15/cm for all 39 neutron groups and all 44 gamma groups in all materials
 - 2) Use the 1** array to enter chi(g)=1.0E-10 (unnormalized) for group 83, and 0 for all other groups, so that the negligible fission source created will go into group 83 (ie, gamma group 44) on which no inner iterations are being performed in this calculational step (so it will never be seen)
 - 3) Set nofis=1 so that the small fake chi(g) entered in the 1** array will not be renormalized to 1.0
 - 4) Impose an unrealistically tight pointwise flux convergence criteria of epp=1.0E-6 so that it will never be met and the code will always use the maximum allowed number of inner iterations (which is set to 2 in the 28\$\$ array so that one always gets the same number of inner iterations and the error-mode extrapolation will work well)
 - 5) Allow for many outer iterations, but set the maximum number of allowed inners to ...
 - 2 for all fast and thermal neutron groups (1 to 39) to save time when converging onouters and to assure that this many inners are always used so that error-mode extrapolation works well
 - 2 for groups 40 to 56 (ie, gamma groups 1-17) to save time when converging onouters and to assure that this many inners are always used so that error-mode extrapolation works well
 - 0 for groups 57 to 83 (ie, gamma groups 18-44) which have insufficient energy to create photoneutrons; these will converge later in a separate DORT calculational step
 - 6) Set the outer iteration flux criterion to epo=1.0E-4
-

Notes:

- a) nusigf is the macroscopic fission cross section times the neutron yield.
- b) chi(g) refers to the fission yield spectrum; see the DORT 1** array.
- c) nofis, epp, and epo are input parameters for the DORT transport code.
- d) This procedure works best if the earlier procedures (see Table 17, and/or Steps B1, B2, ..., in Tables 21a and 21b) are first used to pre-converge the thermal neutron flux in groups 15 to 39 before attempting to account for photoneutrons; final convergence of these groups will occur naturally as the photoneutrons are being converged.

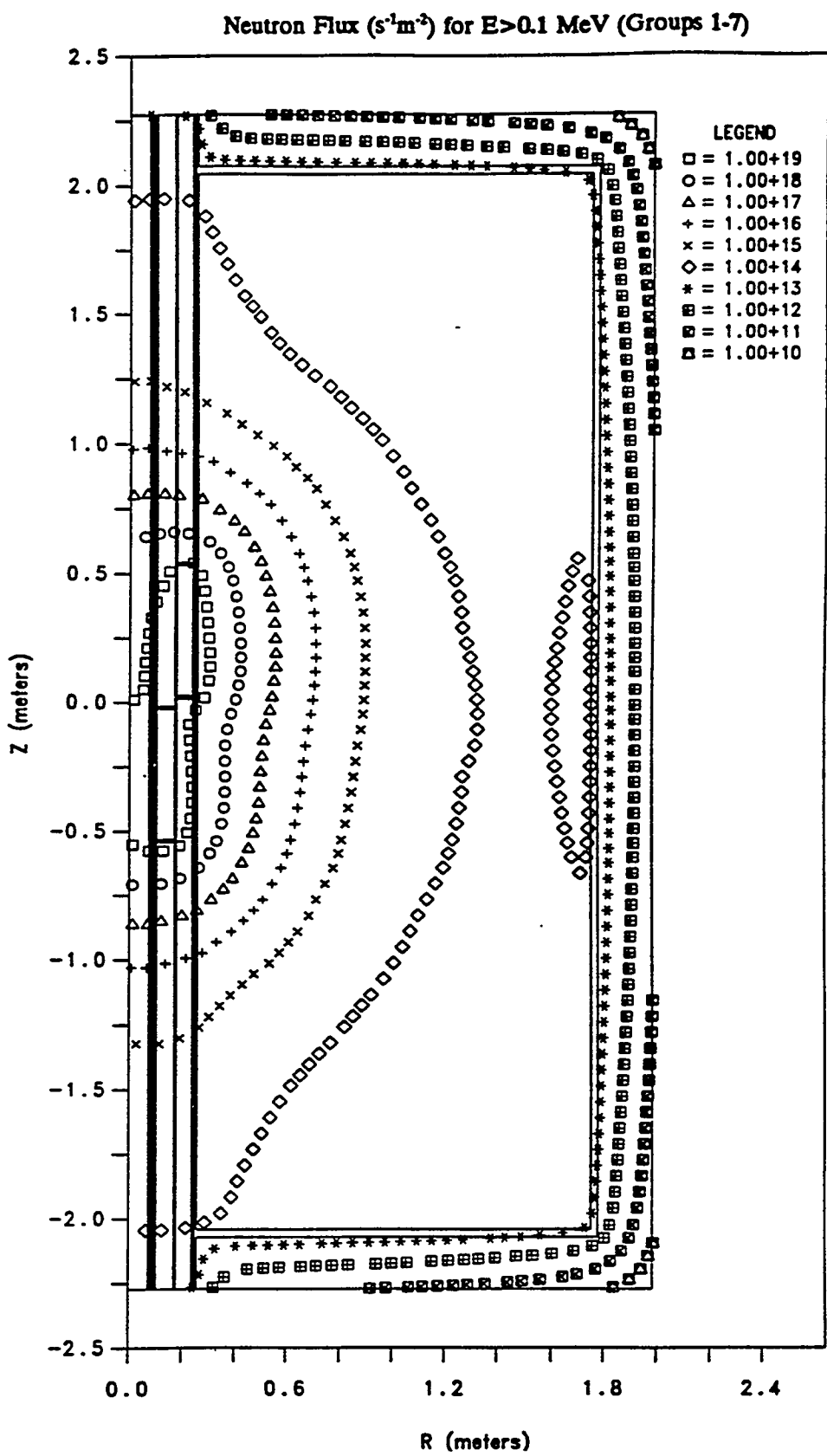


Fig. 10a. Contours showing the 2-D spatial distribution of the fast neutron flux in the ANS core and reflector ($E > 0.1$ MeV), as given by DORT Run 5, which did not account for photoneutrons and is considered the final reference solution.

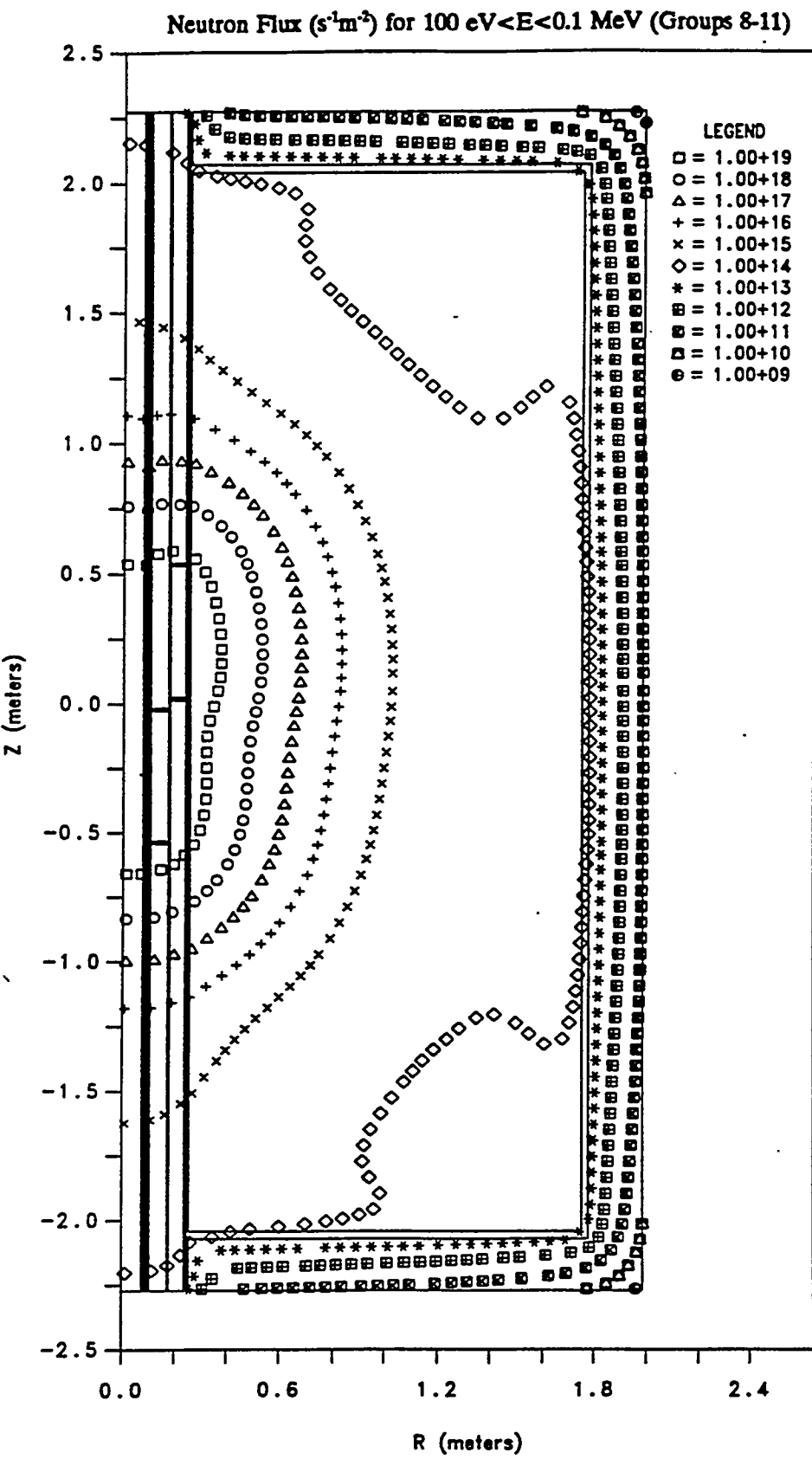


Fig. 10b. Contours showing the 2-D spatial distribution of the intermediate-energy neutron flux in the ANS core and reflector ($100 \text{ eV} < E < 0.1 \text{ MeV}$), as given by DORT Run 5, which did account for photoneutrons and is considered the final reference solution.

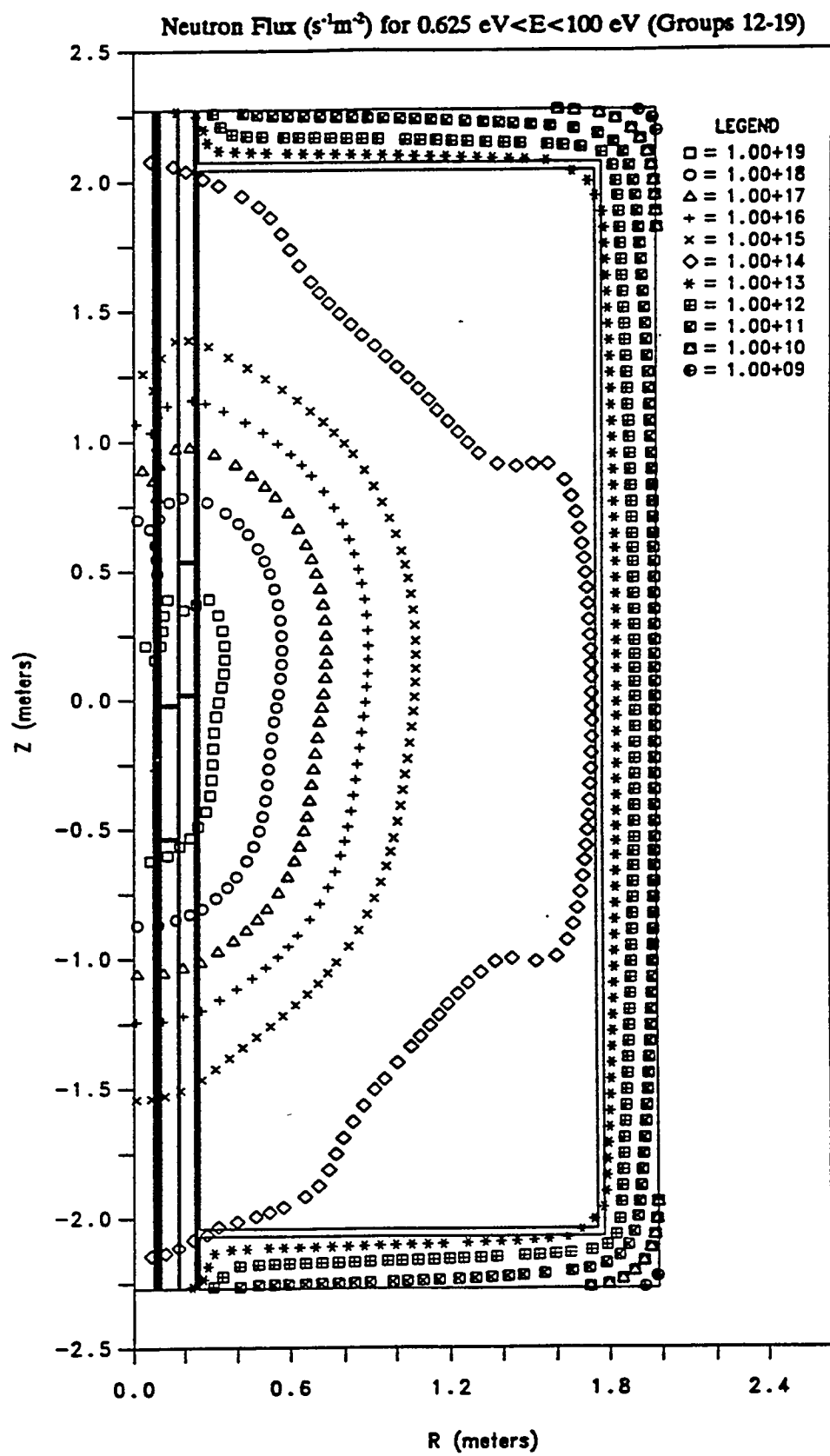


Fig. 10c. Contours showing the 2-D spatial distribution of the epithermal neutron flux in the ANS core and reflector ($0.625 \text{ eV} < E < 100 \text{ MeV}$), as given by DORT Run 5, which did account for photoneutrons and is considered the final reference solution.

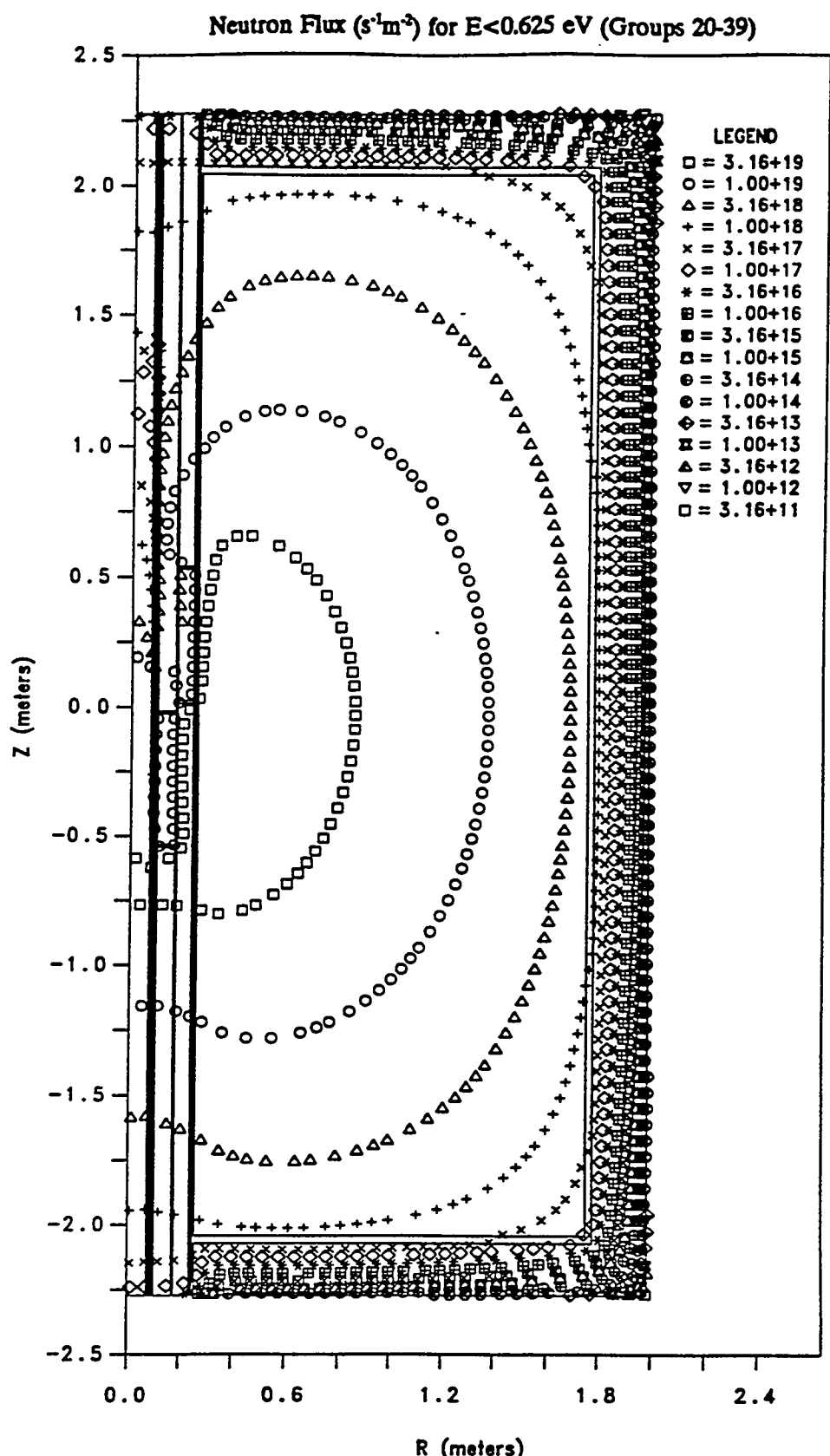


Fig. 10d. Contours showing the 2-D spatial distribution of the thermal neutron flux in the ANS core and reflector ($E < 0.625$ eV), as given by DORT Run 5, which did account for photoneutrons and is considered the final reference solution.

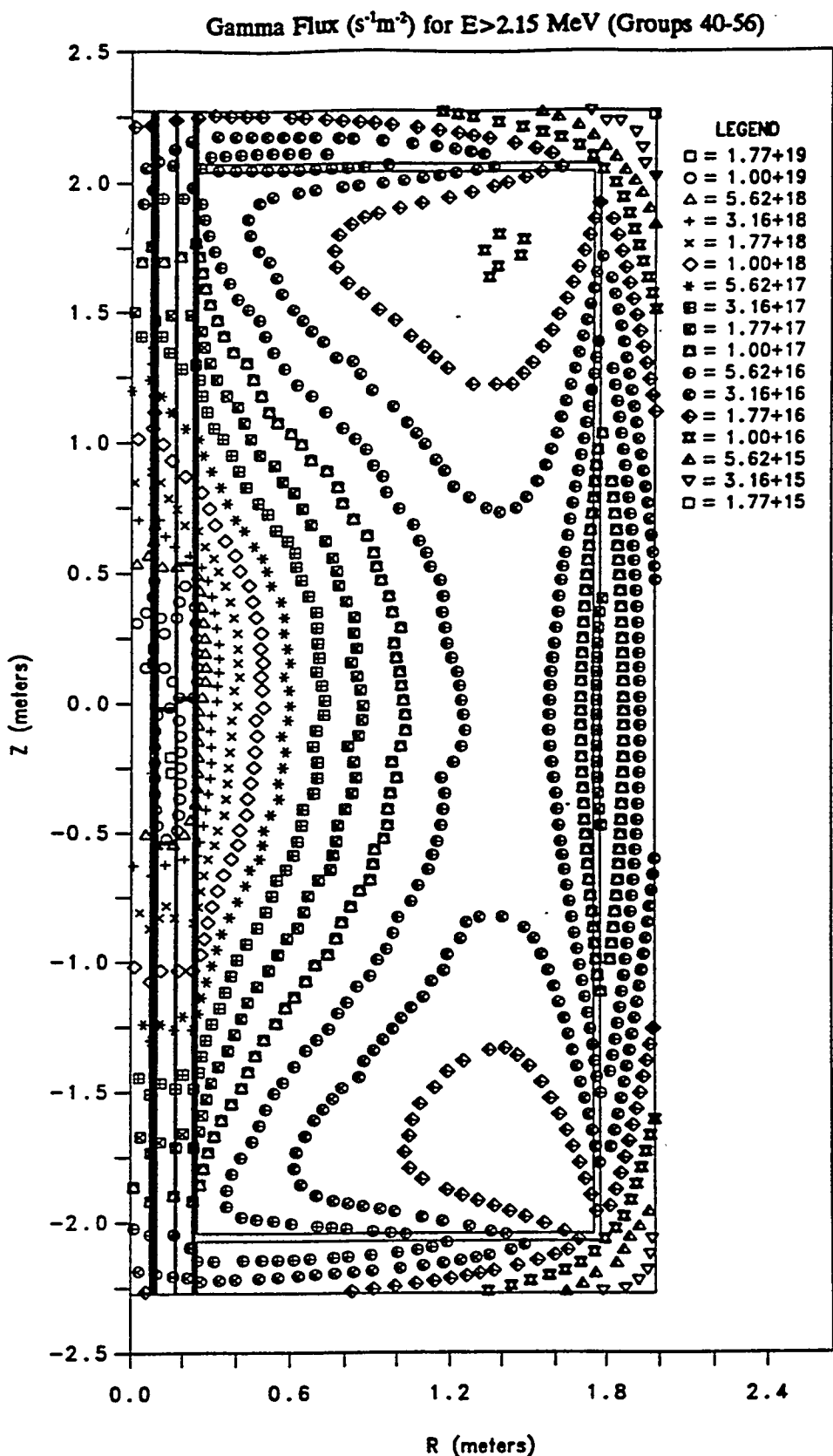


Fig. 10e. Contours showing the 2-D spatial distribution of the high-energy gamma flux above 2.15 MeV in the ANS core and reflector, as given by DORT Run 5, which did account for photoneutrons and is considered the final reference solution. [Note that most of these photons (i.e., those above 2.25 MeV) have sufficient energy to create fast photoneutrons in the heavy water.]

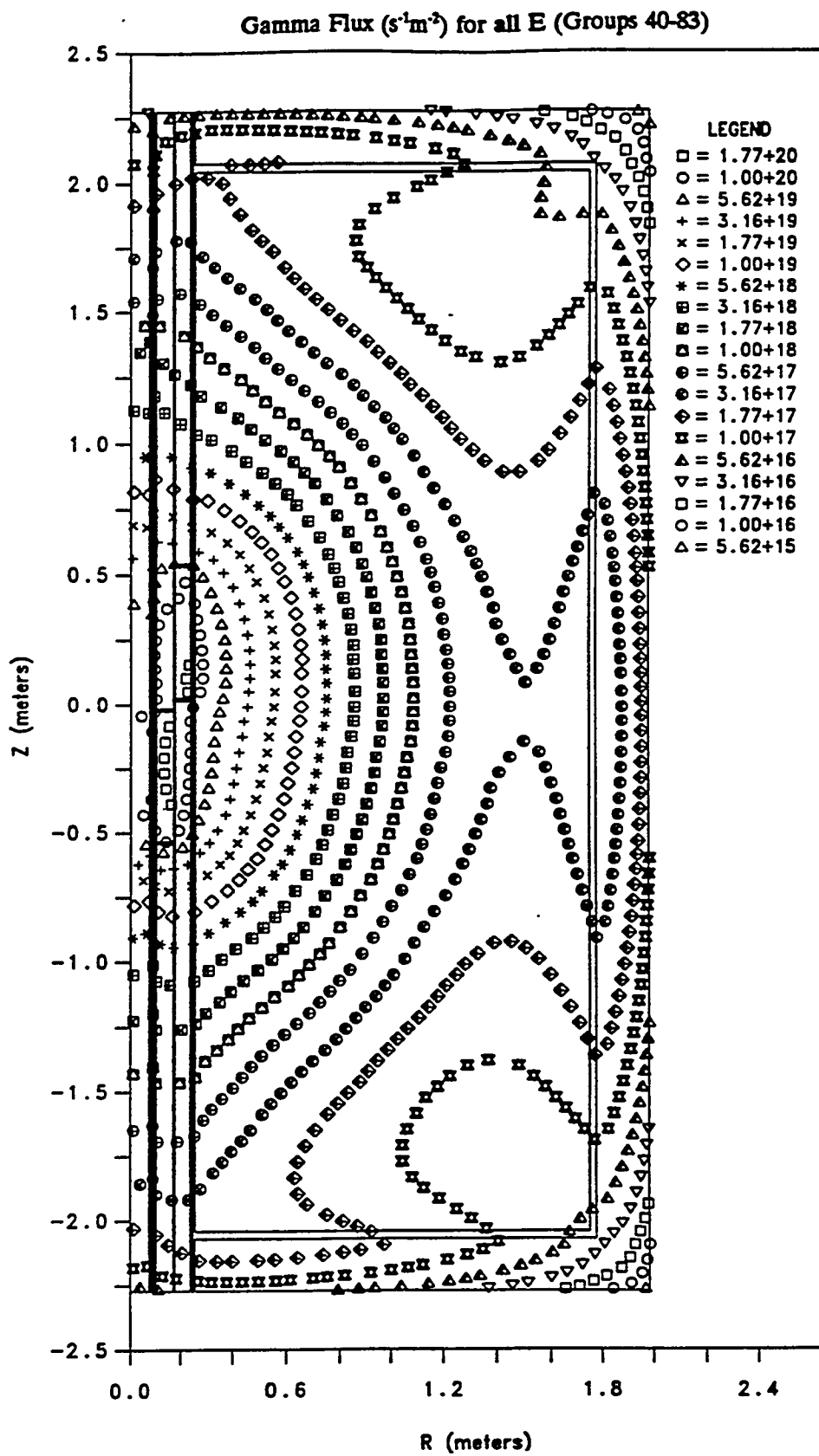


Fig. 10f. Contours showing the 2-D spatial distribution of the total gamma flux in the ANS core and reflector (summed over all gamma energy groups), as given by DORT Run 5, which did account for photoneutrons and is considered the final reference solution.

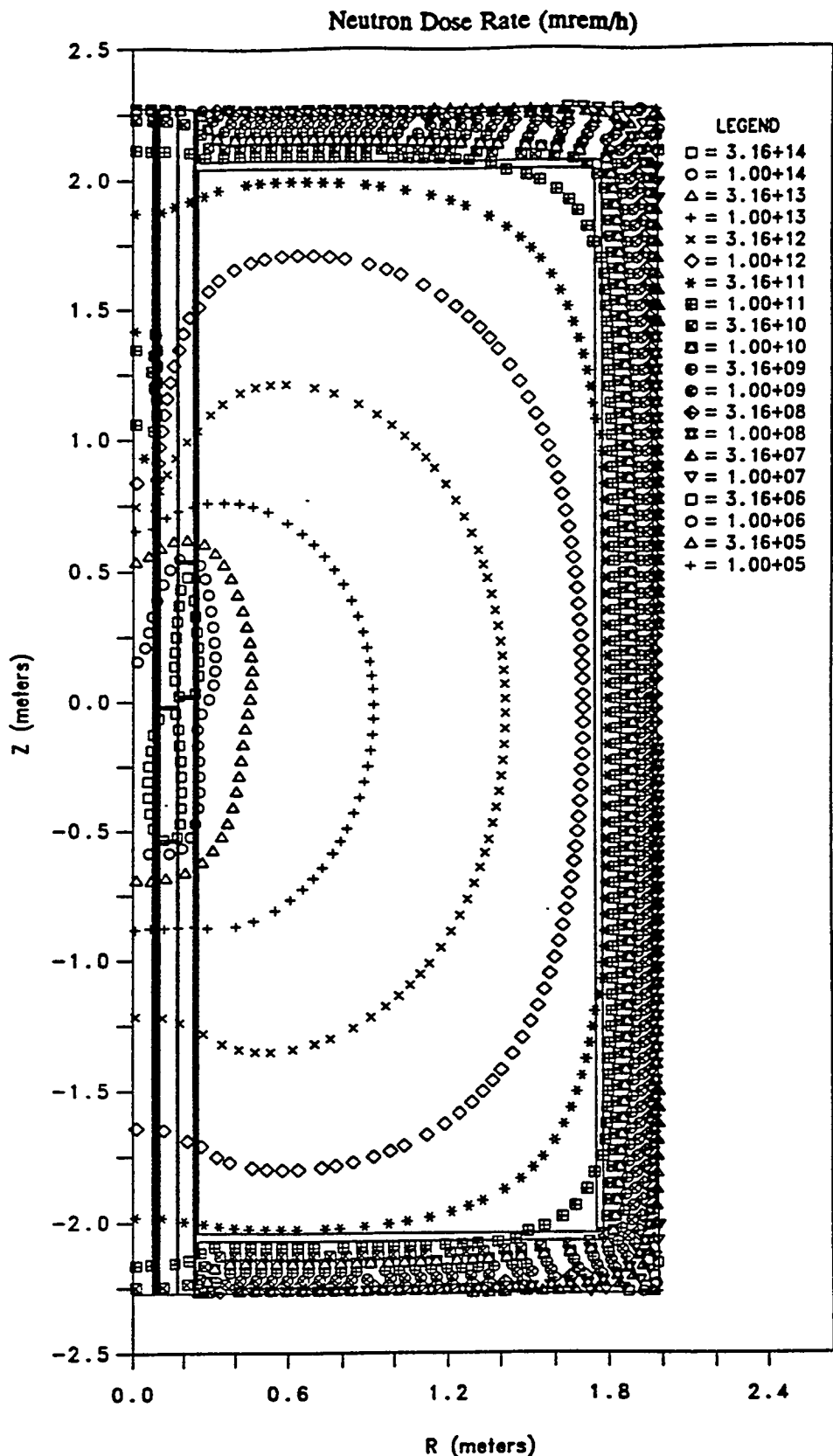


Fig. 10g. Contours showing the 2-D spatial distribution of the neutron dose rate (mrem/h) in the ANS core and reflector, as given by DORT Run 5, which did account for photoneutrons and is considered the final reference solution.

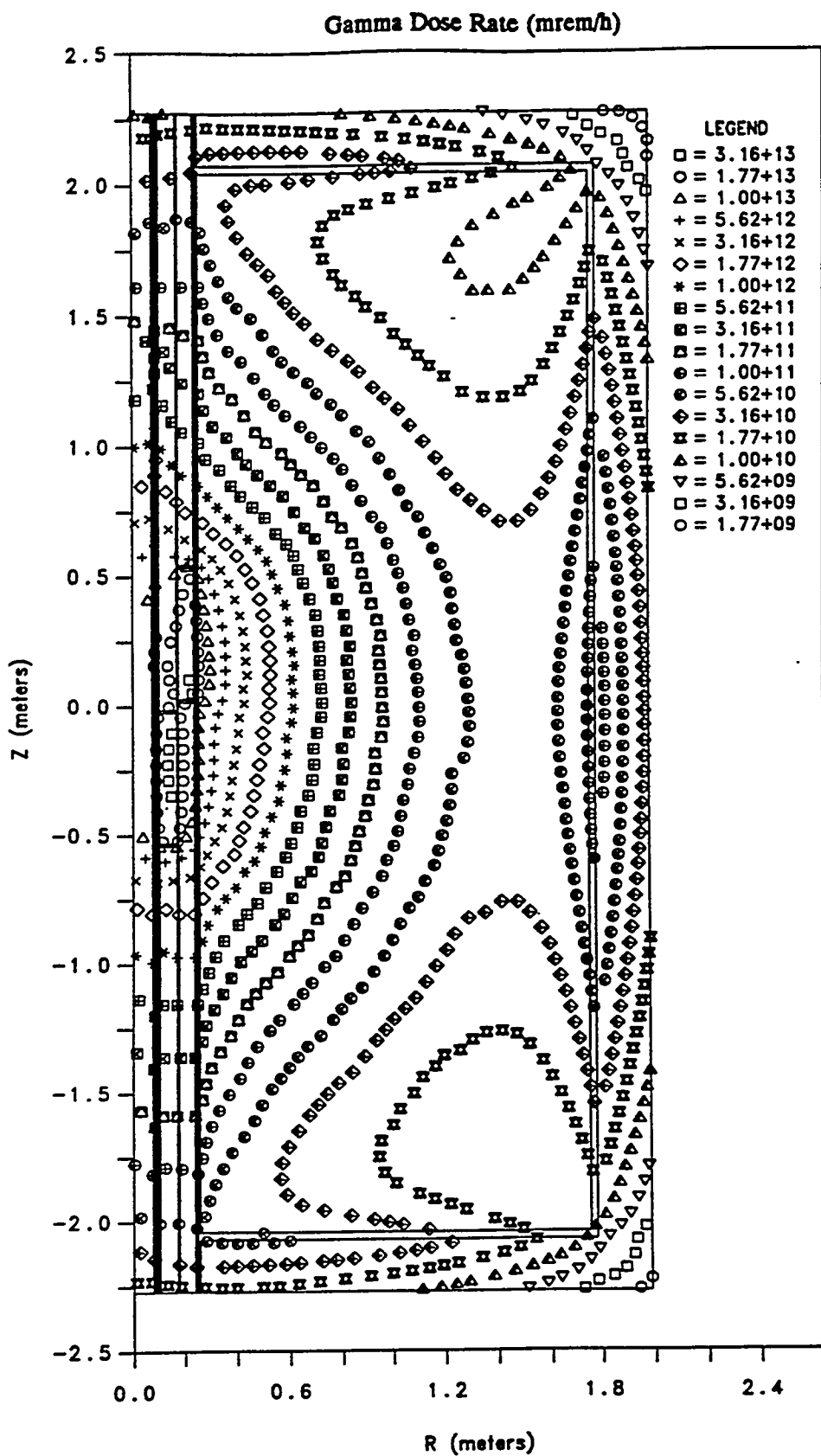


Fig. 10h. Contours showing the 2-D spatial distribution of the gamma dose rate (mrem/h) in the ANS core and reflector, as given by DORT Run 5, which did account for photoneutrons and is considered the final reference solution.

photoneutrons, the fast neutron flux contours become somewhat more distorted. While there is not much difference in near the core, the fast flux out in the reflector close to the vessel is now much higher—up to 3300 times higher near the vessel wall, where the fast flux would otherwise normally be quite depressed. Also, the fast flux contours with photoneutrons are more elongated axially, becoming more "football shaped." This is due to the thermal (n,g) reactions in the aluminum core pressure boundary tube which then produce gammas of sufficiently high energy to cause fast photoneutrons to be produced in this region. (Continued photoneutron production in the lower portion of the CPBT near the top of the subpile room below the reactor should therefore be factored into any shielding designed for the upper portion of the subpile room.) With or without photoneutrons, plots of the gamma fluxes and dose rates show high gamma fluxes near the corners of the aluminum D₂O reflector vessel due to the proximity of the aluminum in both the radial and axial directions. Moreover, the plots of the high-energy gamma flux levels ($E > 2.15$ MeV) in these corner regions, coupled with the lower fast neutron flux levels otherwise present in these regions if one did not account for photoneutrons, visually explain why the fast neutron flux contours become so distorted once one accounts for photoneutron production. Basically, the high-energy gamma flux in these outer regions establishes a minimum fast neutron flux field in these regions. Thus, as one moves outward from the core through the D₂O, the fast neutron flux initially appears to attenuate normally until it reaches this "minimum," after which it appears to remain roughly constant until one passes through the vessel and enters the light water outside the vessel.

Depending upon the particular problem one is addressing, the consequences of these higher flux levels associated with photoneutron production may be important or they may be negligible: (1) If one were interested in fast neutron radiation damage in ferritic test specimens placed in the outermost irradiation facilities (such as PT-1), this effect could be quite important, while if one were concerned about radiation damage over the entire energy range, it might not be important. (2) If one were interested in dose rates several meters down along any of the horizontal beam tubes whose hot ends are close to the core, the effect would be almost negligible since most of the neutrons that successfully stream down such a tube are almost monodirectional and have their origin (i.e., point of last scatter) in the D₂O close to the core where the additional fast neutrons due to photoneutron production are negligible relative to the normal fast neutron population close to the core. (3) If one is interested in the overall vessel heating rates, the effect of photoneutron production will be almost completely negligible because (a) most of this is due to gamma heating and (b) most of the remaining heating is due to thermal neutron activation of the aluminum and the subsequent beta and gamma decay of the Al-28 that is produced, while the "thermal" neutron population here is so large that it is virtually unaffected by the few additional neutrons coming from photoneutron production. (4) If one is interested in the dose rates in the subpile room, one should certainly consider the photoneutron production already described plus any additional photoneutron production that may occur in the lower portion of the core pressure boundary tube near the top of the subpile room below the reactor. Subsequent calculations outside the scope of this report have since shown that if one neglects photoneutron production in this region, the neutron dose rates in the subpile room would be 8 to 10 orders of magnitude below the gamma dose rate there. With photoneutron production, the neutron dose rate may only be 2 or 3 orders of magnitude lower than the gamma dose rate there. If one were to include additional gamma shielding and no additional neutron shielding, it is conceivable that the final neutron and gamma dose rates there may ultimately be comparable.

7.0 FINAL RESULTS

DORT Run 5, as described in Sect. 6, is considered the final reference solution. It uses the revised spatial mesh shown in Fig. 3; it includes delayed fission gammas; and, most notably, it includes the effect of photoneutron production in the D₂O. Plots showing the corresponding neutron fluxes in each of four broad energy groups

- A: E ≥ 0.1 MeV ,
- B: 100 eV ≤ E ≤ 0.1 MeV ,
- C: 0.625 eV ≤ E ≤ 100 eV ,
- D: E ≤ 0.625 eV .

are shown in Sect. 6 (cf. Figs. 10a-10d). Other plots included there (cf. Figs. 10e-10h) show the gamma flux above 2.15 MeV, the total gamma flux (summed over all energies), the neutron dose rate in mrem/h, and the gamma dose rate in mrem/h. Some qualitative discussion of these results is also provided at the end of Sect. 6. More precise numerical results at 761 particular points of interest are provided in Appendix E. For easier reference, these results have been organized into 26 different tables corresponding to full and part-length radial and axial traverses at and near the reflector vessel, the core pressure boundary tube, the core itself, and at various locations in the reflector corresponding to each of the major experimental facilities. This tabulated data also show the total neutron plus gamma heating rate in aluminum at each point, as well as the displacements per atom (per year) that would be produced in small steel specimens that one might insert at many of these locations. Note, however, that most of the local pointwise data in Appendix E should be interpreted with caution in light of the original modeling assumptions. Recall, for example, that these values are based on the lifetime-averaged power distribution described in Sect. 3 and the fixed geometric model described in Sect. 2. In reality, the motion of the outer control rods above the core (not modeled here) and/or the motion of the central control rod (modeled here in a fixed location) would both affect the fluxes and reaction rates close to the centerline of the system. Likewise, deep in the side reflector near the axial midplane, it must be remembered that the dose rates and other data given in Appendix E are based on the "unperturbed fluxes" that would be present if the beam tubes did not exist. In reality, the fluxes and dose rates along the axis of an empty beam tube would be considerably higher. (Appendix F, for example, discusses a simple solid angle routine for estimating fluxes and dose rates down a long void-filled beam tube based on the unperturbed fluxes at the hot end and along the surface of the beam tube.) Within the context of the above remarks and limitations, however, it is hoped that the detailed results presented in Appendix E will be useful to a broad range of interested parties, including designers and experimenters alike.

In addition to the local pointwise data in Appendix E, integral parameters such as the volume-averaged heating rates in the aluminum reflector vessel and core pressure boundary tube are also of interest. To facilitate the reporting of such data, the reflector vessel was divided into 9 different zones (A-I) as described in Table 23 and illustrated schematically in Fig. 11, while the inner and outer core pressure boundary tubes were each divided into 7 axial zones (J-P). The fine mesh multigroup fluxes for DORT Run 5 were then used in conjunction with the kerma factors listed in Table 14a to obtain the volume-averaged neutron and gamma heating rates (watts/gm) in each zone, as well as the total (n+g) volume-integrated heating rates for each zone. These results are also shown in Table 23. Based on the simplified geometric model used throughout this study, these results would indicate that the total volume-integrated nuclear heat load on the reflector vessel may be as high as 1.36 megawatts, and as high as 1.18 and 1.71 megawatts for the inner and outer core pressure boundary tubes, respectively. In the case of the reflector

Table 23. Volume-averaged neutron and gamma heating rates, and the total volume-integrated heating rate, in 9 different regions of the reflector vessel and 14 different regions of the core pressure boundary tube.

Zone	ZMIN mm	ZMAX mm	RMIN mm	RMAX mm	VOL m ³	NEUTRON HEATING watts/g	GAMMA HEATING watts/g	VOL INTEGRATED TOTAL HEATING watts
Refl vessel:								
A	-2072.00	-2042.00	253.00	1001.50	8.84980E-02	1.46990E-01	1.26936E-01	6.54532E+04
B	-2072.00	-2042.00	1001.50	1750.00	1.94103E-01	6.74682E-02	5.79123E-02	6.57092E+04
C	-2072.00	-1292.00	1750.00	1775.00	2.15945E-01	7.81380E-02	6.26909E-02	8.21106E+04
D	-1292.00	-542.00	1750.00	1775.00	2.07640E-01	2.43678E-01	1.82475E-01	2.38913E+05
E	-542.00	542.00	1750.00	1775.00	3.00108E-01	3.64493E-01	2.71075E-01	5.14996E+05
F	542.00	1292.21	1750.00	1775.00	2.07698E-01	2.22410E-01	1.66702E-01	2.18208E+05
G	1292.21	2072.00	1750.00	1775.00	2.15887E-01	6.67351E-02	5.34406E-02	7.00498E+04
H	2042.00	2072.00	1001.50	1750.00	1.94103E-01	5.50451E-02	4.70346E-02	5.34978E+04
I	2042.00	2072.00	253.00	1001.50	8.84980E-02	1.11075E-01	9.46539E-02	4.91578E+04
								1.35810E+06
Inner CBPT:								
J	-2272.00	-2072.00	235.00	240.00	1.49226E-03	4.71348E-02	7.87193E-02	5.07079E+02
K	-2072.00	-1292.00	235.00	240.00	5.81980E-03	7.17780E-01	4.15774E-01	1.78121E+04
L	-1292.00	-542.00	235.00	240.00	5.59596E-03	5.21203E+00	4.10921E+00	1.40835E+05
M	-542.00	542.00	235.00	240.00	8.08803E-03	8.44105E+00	3.36864E+01	9.19966E+05
N	542.00	1292.21	235.00	240.00	5.59753E-03	2.72965E+00	3.28237E+00	9.08616E+04
O	1292.21	2072.00	235.00	240.00	5.81823E-03	4.24287E-01	2.73373E-01	1.09597E+04
P	2072.00	2272.00	235.00	240.00	1.49226E-03	3.22556E-02	5.39051E-02	3.47150E+02
							inner:	1.18129E+06
Outer CBPT:								
J	-2272.00	-2072.00	245.00	253.00	2.50322E-03	4.55659E-02	8.14368E-02	8.58372E+02
K	-2072.00	-1292.00	245.00	253.00	9.76255E-03	7.23643E-01	4.00592E-01	2.96336E+04
L	-1292.00	-542.00	245.00	253.00	9.38707E-03	5.23511E+00	3.81675E+00	2.29420E+05
M	-542.00	542.00	245.00	253.00	1.35674E-02	8.72798E+00	2.63260E+01	1.28410E+06
N	542.00	1292.21	245.00	253.00	9.38971E-03	2.80298E+00	3.07688E+00	1.49067E+05
O	1292.21	2072.00	245.00	253.00	9.75992E-03	4.32088E-01	2.62747E-01	1.83101E+04
P	2072.00	2272.00	245.00	253.00	2.50322E-03	3.11862E-02	5.60866E-02	5.89850E+02
							outer:	1.71198E+06

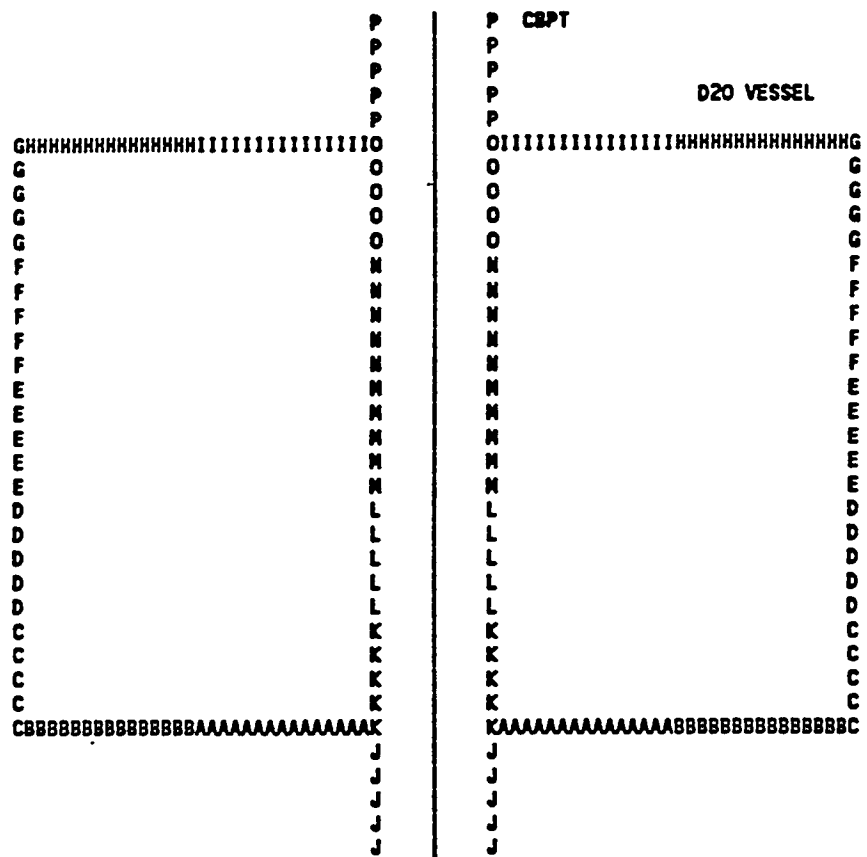


Fig. 11. Relative location of the 9 zones in the reflector vessel and 7 zones in the inner and outer core boundary pressure tubes for which the volume-averaged neutron and gamma heating rates are reported in Table 23.

vessel in particular, the geometric model employed in this study may be overly simplistic (especially near the top and bottom of the vessel), and the specific neutron and gamma heating rates (watts/gm) may be more credible than the volume-integrated heating rate, which depends more directly on the geometric modeling approximations. In the case of the reflector vessel, the neutron heating rate (which is almost entirely due to thermal neutrons) accounts for about 55% of the total nuclear heating ($n+g$), whereas for the inner and outer core pressure boundary tubes, the neutron heating accounts for only 20-25% of the total. In all three cases, however, it should be remembered that the total neutron kerma factor used here is equal to the basic prompt kerma plus the total decay energy associated with the β or γ disintegration of the Al-28 formed by (thermal) neutron activation of the Al-27 (see Sect. 5). Moreover, the bulk of the energy ascribed to neutron heating (especially in the reflector vessel) is really associated with this radioactive decay. As such, much of this energy is actually transported away from the aluminum by the β and γ radiation and deposited in the surrounding D₂O or other nearby components rather than being deposited exclusively in the reflector vessel or core pressure boundary tubes as implied in Table 23. By contrast, the gamma heating shown in Table 23 is due to direct gamma heating of the reflector vessel or core pressure boundary tube by gamma radiation coming directly from the core, or by prompt secondary gammas (not decay gammas) generated in other components. As such, this heat load, as well as some fraction of the neutron heat load, will have to be dissipated directly by these components. Lastly, it must be remembered that the ANS reactor system has a large number of aluminum beam tubes and other irradiation facilities in the D₂O reflector which were not included in the basic geometric model used here (cf. Fig. 1). While a substantial amount of neutron and gamma heating will occur in these components due to neutron and gamma interactions with them, the shielding provided by these components will tend to reduce the number of neutrons and gammas available to interact with the reflector vessel, thus reducing the neutron and gamma heating in the vessel by a similar amount. It is therefore expected that the neutron and gamma heating rates shown for the vessel in Table 23 will be higher than one might calculate in a rigorous 3-D analysis where all the beam tubes and other irradiation facilities are explicitly modeled. Qualitatively, at least, this is consistent with the February 1993 finding by INEL³³ that the total neutron plus gamma heat load on the beam tubes, cold source, cold source guides, hydraulic tubes, slant tube, long slant beam tube, isotope target facility, and the reflector vessel, came to a total of 1.64 megawatts, while they estimated the total neutron plus gamma heat load on the reflector vessel itself to be only 0.50 megawatts (which is 2.72 times lower than the ORNL estimate of 1.36 megawatts cited above). For the moment at least, this qualitatively consistent explanation for that difference remains a matter of speculation.

8.0 SUMMARY

This document describes the initial global 2-D shielding analyses for the ANS core, the D₂O reflector, the reflector vessel, and the first 200 mm of light water beyond the reflector vessel. It is intended that the directional and scalar flux files generated in the course of this study will serve as the basis for many of the source terms to be used in subsequent shielding analyses involving other portions of the facility or the various subsystems. In addition to reporting the fluxes and other parameters at key points of interest, a major objective of this report was to document how these analyses were performed, the phenomena that were included, and checks that were made to verify that these phenomena were properly modeled.

Because this was a shielding analysis as opposed to a physics analysis, the "lifetime-averaged" spatial power distribution in the core (based on burnup-dependent distributions previously reported by the Physics Task) was used to determine the fixed neutron source distribution in the core subsequently used in the shielding analyses described here.

Prior to the final analysis, the master cross section library was modified so that the secondary gamma production terms in the fuel would include the delayed fission gammas as well as the prompt fission gammas. While 1-D studies have shown that this increased the calculated low-energy gamma fluxes in and close to the fuel by 50 to 250%, the gamma fluxes in these same energy groups were found to increase by only a few percent next to the reflector vessel, while the gamma fluxes in the higher energy groups at this location were virtually unchanged.

All of the shielding analyses reported here were performed using the ANSL-V 39n/44g coupled library in order to obtain a rigorous representation of the thermal neutron spectrum throughout the reflector. Because of thermal neutron upscatter from all the thermal neutron groups into group 15, these calculations were exceedingly slow to converge. Convergence was accelerated, however, by placing a negligibly small amount of fissile material throughout the reflector, eliminating further neutron production in the core due to fission, and treating this as an eigenvalue problem, thereby allowing the calculation to benefit from the Vondy error-mode extrapolation technique embedded in the DORT code. Rapidly converging 1-D calculations with and without this modified cross section data were used to verify that the final results obtained were identical in both cases.

Sensitivity studies with respect to mesh size were performed using the 1-D group-banded version of the ANISN code. These studies showed that the original radial mesh sizes used in the side reflector and the original axial mesh sizes used in the upper and lower axial reflectors were too large relative to the extremely fine mesh originally used in the core. A new 2-D mesh scheme for shielding analyses was then developed which used fewer mesh intervals in the core and more mesh intervals in the reflector while maintaining a mesh cell aspect ratio that was as close to square as possible. Unlike the original mesh scheme, the revised scheme yielded results deep in the reflector that were physically consistent with the 1-D studies.

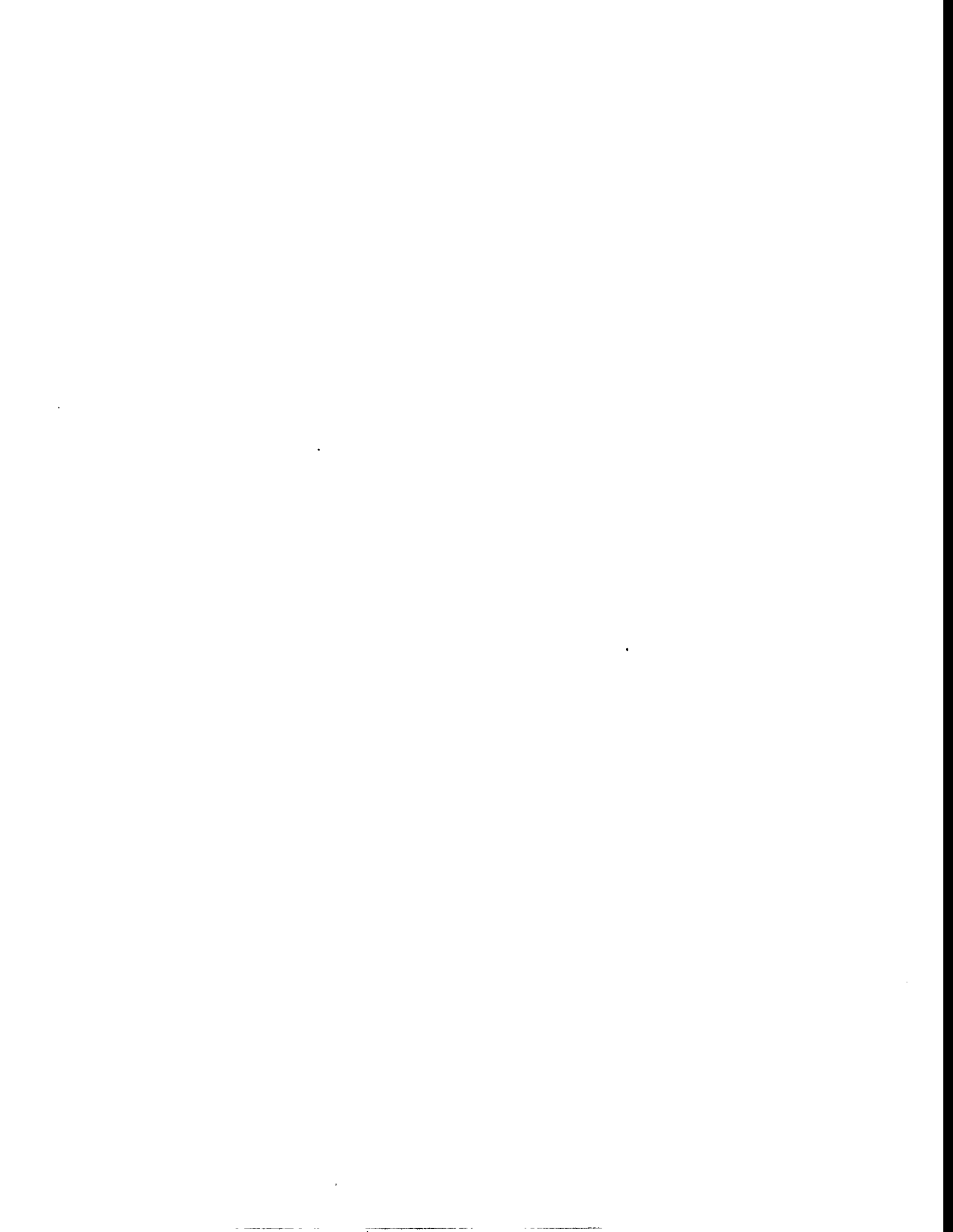
The inclusion of photoneutron production in the heavy water was found to have a profound effect on the fast neutron flux levels deep in the reflector where those flux levels would otherwise be fairly depressed. Deep in the reflector close to the vessel, for example, the calculated fast flux above 0.1 MeV was found to be over 3300 times higher than it would be if one did not account for photoneutron production. This is exacerbated by the fact that thermal neutron (n,g) reactions with the aluminum vessel can yield prompt secondary gammas of sufficient energy to trigger photoneutron production in the heavy water.

The preliminary 2-D analyses described in the earlier portions of this report did not account for photoneutron production because those data were not available in the ANSL-V cross section library and because none of the ORNL cross section codes could process those data. The PHOTOX and SPARK programs were therefore written to generate the group-to-group photoneutron production cross sections and to insert the data into the DORT-ready working cross section library as an enlarged scattering matrix. The 1-D GB-ANISN code was then used to verify that calculations performed with this new working library would yield the same results that one would have obtained with the original library if one had performed a series of fixed source calculations and manually calculated the multigroup photoneutron production terms at the end of each calculation and used those as fixed sources in the next calculational step.

While the inclusion of photoneutron production in the D₂O was found to have a pronounced effect on the fast neutron flux levels deep in the reflector, the significance of that is strongly dependent on the particular situation one is interested in analyzing: (1) If one is interested in fast neutron radiation damage in ferritic test specimens placed in the outermost irradiation facilities (such as PT-1), this effect could be quite important, while if one were concerned about radiation damage over the entire energy range, it might not be important. (2) If one is interested in dose rates several meters down along any of the horizontal beam tubes whose hot ends are close to the core, the effect would be almost negligible since most of the neutrons that successfully stream down such a tube are almost monodirectional and have their origin (i.e., point of last scatter) in the D₂O close to the core where the additional fast neutrons due to photoneutron production are negligible relative to the normal fast neutron population close to the core. (3) If one is interested in the overall vessel heating rates, the effect of photoneutron production is almost completely negligible because (a) most of this is due to gamma heating and (b) most of the remaining heating is due to thermal neutron activation of the aluminum and the subsequent beta and gamma decay of the Al-28 that is produced, while the "thermal" neutron population here is so large that it is virtually unaffected by the few additional neutrons coming from photoneutron production. (4) If one is interested in the dose rates in the subpile room, one should certainly consider the photoneutron production already described plus any additional photoneutron production that may occur in the lower portion of the core pressure boundary tube near the top of the subpile room below the reactor. Subsequent calculations outside the scope of this study have since shown that if one neglects photoneutron production in that region, the neutron dose rates in the subpile room would be 8 to 10 orders of magnitude below the gamma dose rate there. With photoneutron production, the neutron dose rate may only be 2 or 3 orders of magnitude lower than the gamma dose rate there. If one were to include additional gamma shielding and no additional neutron shielding, it is conceivable that the final neutron and gamma dose rates there may ultimately be comparable.

The final reference solution corresponds to DORT Run 5, which is very tightly converged, includes delayed fission gammas, employs the revised spatial mesh, and properly accounts for photoneutron production. Two-dimensional flux maps showing the fast, intermediate, epithermal, and thermal flux contours for DORT Run 5 are shown and qualitatively discussed in Sect. 6.8. Plots showing the high-energy gamma flux, the total gamma flux, and the neutron and gamma dose rates are also presented there. In Appendix E, tabulated results for these quantities are presented at each of 761 particular points of interest. These numerical results are organized into 26 separate tables corresponding to radial and axial traces of interest throughout the system, including all the main structural components as well as locations specifically identified as being close to the various beam tubes and irradiation facilities. In addition to fluxes and dose rates, these tabulated results also show the total neutron plus gamma heating rates (watts/gm) that would exist in any aluminum that might be present at these locations, as well as the displacements per atom (per year) that could be produced in small ferritic test specimens that might

eventually be placed at many of these locations. A more complete discussion of these parameters and all the associated caveats may be found in Sect. 7 or Appendix E. Integral quantities such as the volume-averaged neutron and gamma heating rates (watts/gm) in various portions of the reflector vessel and core pressure boundary tube are given in Sect. 7. There, the volume-integrated total heating rates for the reflector vessel and the inner and outer portions of the core pressure boundary tube were found to be 1.36, 1.18, and 1.71 megawatts, respectively. With respect to this data, however, one is urged to read the special caveats in Sect. 7. Lastly, Appendix F describes a simple solid angle procedure for estimating the fluxes and dose rates several meters down the horizontal beam tubes.



REFERENCES

1. W. A. Rhoades and R. L. Childs, *DORT/TORT: The Two- and Three-Dimensional Discrete Ordinates Transport Codes* [computer program], available from the Radiation Shielding Information Center at ORNL as Code Package CCC-543, Version 1.5.15, Martin Marietta Energy Systems, Inc., Oak Ridge Natl. Lab., January 1992.
2. *ANS Conceptual Safety Analysis Report*, ORNL/ANS/INT-33/V2, Martin Marietta Energy Systems, Inc., Oak Ridge Natl. Lab., June 1992.
3. W. E. Ford et al., *ANSL-V: ENDF/B-V Based Multigroup Cross-Section Libraries for Advanced Neutron Source (ANS) Reactor Studies*, ORNL-6618, Martin Marietta Energy Systems, Inc., Oak Ridge Natl. Lab., September 1990.
4. **PERFUME**: A Module to Correct Legendre Polynomial Fits to Scattering Matrices, as described in Sect. 3 of Ref. 5 (below).
5. N. M. Greene et al., *AMPX-77: A Modular Code System for Generating Coupled Multigroup Neutron-Gamma Cross-Section Libraries from ENDF/B-IV and/or ENDF-B-V*, ORNL/CSD/TM-238, Martin Marietta Energy Systems, Inc., Oak Ridge Natl. Lab., October 1992.
6. N. M. Greene, L. M. Petrie, and R. M. Westfall, "NITAWL-II: SCALE System Module for Performing Resonance Shielding and Working Library Production," as described in Sect. F2 of ref. 10 (below).
7. **AJAX**: A Module to Merge, Collect, Assemble, Reorder, Join, and/or Copy Selected Datasets from AMPX Master Interfaces, as described in Sect. 3 of ref. 5 (above).
8. **CSASI**: An Option in Table C4.4.1 of the SCALE CSAS Module, "CSAS: An Enhanced Criticality Safety Analysis Module With Search Options," as described in Sect. C4 of ref. 10 (below).
9. **JIPSY**: A Simplified Version of the GIP Program to be Used With the SCALE Driver, as described in Sect. 4.1 of this report, ORNL/TM-12672.
10. **SCALE**: A Modular Code System for Performing Standardized Computer Analyses for Licensing Evaluation, NUREG/CR-0200, rev. 4 (ORNL/NUREG/CSD-2/R4), Vols. I, II, and III, Martin Marietta Energy Systems, Inc., Oak Ridge Natl. Lab., February 1995. Available from the Radiation Shielding Information Center at ORNL as Code Package CCC-545.
11. N. M. Greene, "BONAMI: Resonance Self-Shielding by the Bondarenko Method," as described in Sect. F1 of ref. 10 (above).
12. N. M. Greene, "ICE: Module to Mix Multigroup Cross Sections," as described in Sect. F8 of ref. 10 (above).

13. W. A. Rhoades, "GIP: Group-Organized Cross Section Input Program," distributed as part of ref. 1 (above) and documented in Sect. 3 of *DOS: The Discrete Ordinates System*, ORNL/TM-8362, Martin Marietta Energy Systems, Inc., Oak Ridge Natl. Lab., September 1982.
14. E. P. Blizzard, ed., Vol. III, Part B on Radiation Shielding in the *Reactor Handbook*, Interscience Publishers, a Division of John Wiley and Sons, 1962.
15. G. R. Keepin, *Physics of Nuclear Kinetics*, Addison-Wesley Publishing Co., 1965.
16. R. D. Evans, *The Atomic Nucleus*, McGraw-Hill Publishing Co., 1955.
17. R. E. MacFarlane and D. W. Muir, *The NJOY Nuclear Data Processing System, Version 91*, LA-12740-M, University of California, Los Alamos Natl. Lab., October 1994.
18. W. W. Engle, Jr., *A User's Manual for ANISN, A One-Dimensional Discrete Ordinates Transport Code with Anisotropic Scattering*, K-1693, Oak Ridge Gaseous Diffusion Plant, Union Carbide Corp., 1967. Available from the Radiation Shielding Information Center at ORNL as Code Package CCC-254 (updated April 1991).
19. G. C. Haynes, "The AXMIX Program for Cross Section Mixing and Library Arrangement," December 1974. Available from the Radiation Shielding Information Center at ORNL as part of Code Package PSR-75 (updated October 1984).
20. W. A. Rhoades, "VISTA: A Vehicle Input Source Transformation and Assembly Code," distributed as part of ref. 1 (above); since renamed VISA and documented in Sect. II of *The TORSED Method for Construction of TORT Boundary Sources from External DORT Flux Files*, ORNL/TM-12359, Martin Marietta Energy Systems, Inc., Oak Ridge Natl. Lab., August 1993.
21. R. A. Lillie, "DTD: A Coupling Code for Two-Dimensional R-Z Cylindrical Geometries," *Transactions of the American Nuclear Society* 61, 381 (June 1990).
22. *Neutron and Gamma-Ray Flux-to-Dose-Rate Factors*, an American National Standard, ANSI/ANS-6.1.1-1977, American Nuclear Society, 1977.
23. *Neutron and Gamma-Ray Fluence-to-Dose Factors*, an American National Standard, ANSI/ANS-6.1.1-1991, American Nuclear Society, 1991.
24. J. A. Bucholz, "Recommended Quality Factors and Methodology for Calculating Neutron Dose Rates," personal correspondence to B. A. Worley of Oak Ridge Natl. Lab., February 28, 1994.
25. SMUG: A Module for Generating Multigroup Photon Cross Sections, as described in Sect. 3 of ref. 5 (above).
26. PAL: A Module to Punch 1-D Cross Sections from AMPX Libraries, as described in Sect. 3 of ref. 5 (above).

27. *KAOS/LIB-V: A Library of Nuclear Response Functions Generated by the KAOS-V Code from ENDF/B-V and Other Data Files*, ANL/FPP/TM-241, Argonne Natl. Lab., April 1991. Available through the Radiation Shielding Information Center at ORNL as Data Library DLC-160.
28. C. R. Weisbin et al., *VITAMIN-E: An ENDF/B-V Multigroup Cross Section Library for LMFBR Core and Shield, LWR Shield, Dosimetry and Fusion-Blanket Technology*, ORNL-5505, 1979. Available from the Radiation Shielding Information Center at ORNL as Data Library DLC-113B, August 1985.
29. *Standard Practice for Characterizing Neutron Exposures in Ferritic Steels in Terms of Displacements Per Atom*, ASTM Std E693-79, American Society for Testing and Materials, 1979.
30. R. L. Childs, "GB-ANISN: A Group-Banded Version of the ANISN Code for One-Dimensional Transport Problems With Thermal Neutron Upscatter," unpublished but available from R. L. Childs, C. O. Slater, or J. A. Bucholz of Oak Ridge Natl. Lab., 1992.
31. J. A. Bucholz, "CHKCON: A Utility Program for Checking the Convergence of DORT Calculations Involving Numerous Outer Iterations Over Multiple Energy Groups," as described in Sect. 6.8 of this report, ORNL/TM-12672.
32. J. A. Bucholz and R. L. Childs, *Preconceptual Shielding Design Analyses for the Lower Portion of the MHTGR Reactor System Incorporating a 350-MW_{th} Annular Prismatic Core*, ORNL/GCR-86/1, Martin Marietta Energy Systems, Inc., Oak Ridge Natl. Lab., June 1986.
33. C. A. Wemple, "Component Heat Load Evaluations, Methods and Results," presented at the Advanced Neutron Source Reactor Physics Review, Oak Ridge, Tenn., February 8-10, 1993.



APPENDIX A

Listing of the PHOTOX program for generating a (g)group-to-(n)group scattering matrix that represents the microscopic photoneutron production cross section for deuterium (in barns).

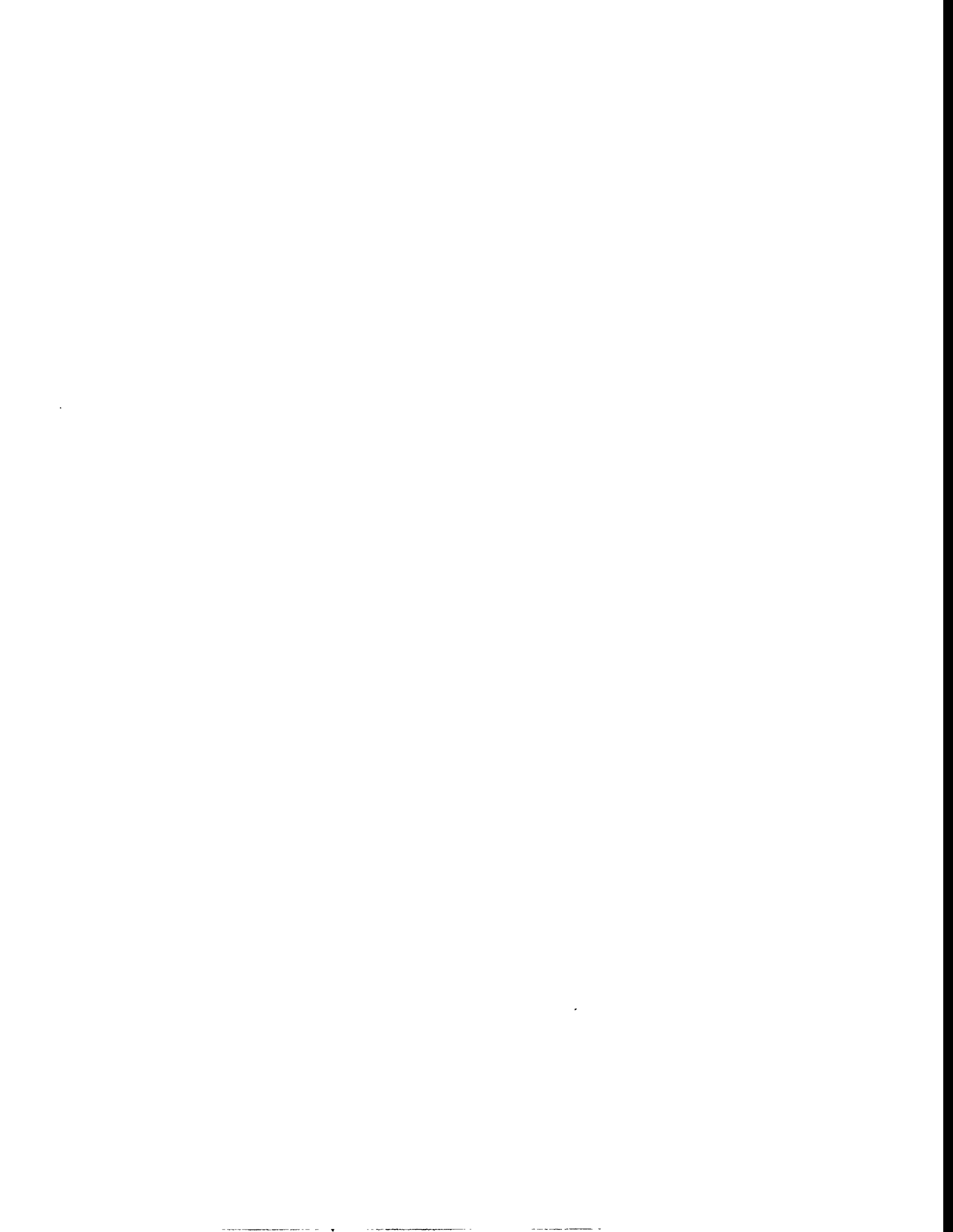


Table A.1. Listing of the PHOTOX program for generating a (gamma)group-to-(neutron)group scattering matrix that represents the microscopic photoneutron production cross section for deuterium (in barns).

Table A.1 (continued)

```

c   data ebgamm/ ! energy bounds for gammas in 39n/44g library:
*   2.0000e+07,1.40000e+07,1.20000e+07,1.00000e+07,8.00000e+06,
*   7.5000e+06,7.00000e+06,6.50000e+06,6.00000e+06,5.50000e+06,
*   5.00000e+06,4.50000e+06,4.00000e+06,3.50000e+06,3.00000e+06,
*   2.50000e+06,2.35000e+06,2.15000e+06,2.00000e+06,1.80000e+06,
*   1.66000e+06,1.57000e+06,1.50000e+06,1.44000e+06,1.33000e+06,
*   1.20000e+06,1.00000e+06,8.00000e+05,7.00000e+05,6.00000e+05,
*   5.12000e+05,5.10000e+05,4.50000e+05,4.00000e+05,3.00000e+05,
*   2.00000e+05,1.50000e+05,1.00000e+05,7.50000e+04,7.00000e+04,
*   6.00000e+04,4.50000e+04,3.00000e+04,2.00000e+04,1.00000e+04,/
```

c Approximate deuterium (g,n) photoneutron production xsect in barns:

c These approximate results are based on eyeballing plot in Keppins book.

c They may be used later to perform a rough check of the analytic results.

```

data xgna/ 39*0.0, 1.0e-3, 1.0e-3, 1.25e-3, 1.6e-3, 1.8e-3,
*   1.9e-3, 2.0e-3, 2.08e-3, 2.18e-3, 2.22e-3, 2.27e-3, 2.3e-3,
*   2.2e-3, 2.0e-3, 1.6e-3, 1.1e-3, 0.45e-3, 27*0.0 /
```

c b0=2.225e6 ! threshold energy for photoneutron reaction

c npts=100 ! number of points used to integrate across each gamma source group

c do 10 ifrom=1,83
do 10 iio=1,83
10 xprnt(iio,ifrom)=0.0

c do 29 igam=1,44
if (emaxg(igam).le.b0) go to 29 ! note: only gamma groups 1 to 17 can create photoneutrons [emaxg(igam=18)=2.15 MeV]
ifrom=39+igam
wtint=0.0
degam=(emaxg(igam)-emng(igam))/float(npts)

c do 28 igpt=1,npts
egam=emng(igam)+(float(igpt)-0.5)*degam
! avg energy of photoneutron generated (b0=threshold energy)
eneut=(egam-b0)/2.0
call xpnd2o (egam, sigma) ! get deuterium (g,n) photoneutron production xsect in barns
if (igpt.eq.50)
* write (*, '(1x,i2,1p,3e15.5)') igam, egam, eneut, sigma
wtint=wtint+wfunc(egam) ! integrate wfunc over source gamma group

Table A.1 (continued)

```

c      do iio=1,39 ! find energy group (iio) that the photoneutron is born into, and register result
      if (eneut.gt.eminn(iio) .and. eneut.lt.emaxn(iio)) then
        xpn(iio,ifrom)=xpn(iio,ifrom)+wfuns(egam)*sigma*degam
        go to 28
      endif
    enddo
    continue
c      do iio=1,39
      xpn(iio,ifrom)=xpn(iio,ifrom)/wtint
    enddo
    continue
c      do ig=1,83
      ifrom=ig
      xups(ig)=-xpn(ig,ig)
      do iio=1,ig
        xups(ig)=xups(ig)+xpn(iio,ifrom) ! xups(ig)=(photoneutron) upscatter xsect from group ig to all higher energy groups
      enddo
    enddo

c      Following block was put in after code had been run once, just to get a nice listing of the results:
c      write (6,30) (ineut,ineut=1,10)          ! having run the code once, we know everything else is zero
30     format (/////, 'PHOTONEUTRON PRODUCTION XSECTS (IN',
      * 'BARNs) FOR DEUTERIUM IN THE ANSL-V 39N/44G LIBRARY',/
      * 'GAMMA ---',29'---')/; GROUP '10' TO NGRP';3)/
      do igam=1,17
        ! note: only gamma groups 1 to 17 can create photoneutrons [emaxg(igam=18)=2.15 MeV]
        ifrom=igam+39
        write (6,31) igam,(xpn(iio,ifrom),iio=1,10) ! having run the code once, we know everything else is zero
31     format (1x,i3,4x,1p,10e12.5)
        enddo
        write (6,'(//)')

c      do igam=1,17
      ifrom=igam+39
      do iio=1,10
        if (xpn(iio,ifrom).gt.0.0) then
          write (6,'(1x,i3,i4,1pe15.5)') ifrom,iio,xpn(iio,ifrom)
        endif
      enddo
    enddo
  enddo
enddo

```

Table A.1 (continued)

Table A.1 (continued)

```

c      do iio=1,83
c      write (6,'(a,i2,3x,8ji1)')
c      *     , iio=,iio,(ixpn(iio,ifrom),ifrom = iio,83)
c      enddo
c
c      write (6,'(1x,5i5)' ) iit1,ih1,ihm1,nabov1,nbelow1
c      write (6,'(1x,5i5)' ) iit2,ih2,ihm2,nabov2,nbelow2
c
c      ccc20   read (*,* ) egam
c      ccc    egam=egam*1.0e6
c      ccc    if (egam.le.0.0) stop
cccc
ccc    call xpnd2o (egam,sigma) ! get deuterium (g,n) photoneutron production xsect in barns
ccc
ccc30  write (*,'(1x,1p,2e15.5)' ) egam,sigma
ccc    go to 20
c
c      Perform a simple check to see if these xsects look reasonable:
c      do 34 ifrom=1,83
c          xgnb(ifrom)=0.0
c          do 33 iio=1,83
c              xgnb(ifrom)=xgnb(ifrom)+xpnd2o(ifrom,ifrom)
c              write (*,'(1x,13,1p,2e15.5)' ) ifrom,xgna(ifrom),xgnb(ifrom)
c              continue
c
c          stop
c          end
c          subroutine xpnd2o (egam,sigma)
c
c      subroutine to calculate the deuterium photoneutron production
c      xsect in barns, given the gamma energy in eV
c
c      dimension xplot(29),yplot(29),energy(29),sigxgn(29),u(29)
c      dimension sigx2(29),sigx3(29)
c
c      save b0,fac,energy,sigxgn
c
c      data fac/0.0/

```

Table A.1 (continued)

```

c      data xplot/
*   0.30, 0.35, 0.40, 0.50, 0.61, 0.80, 1.0, 1.5, 2.0,
*   2.5, 3.0, 3.5, 4.0, 4.5, 5.0, 5.5, 6.0, 6.5, 7.0,
*   7.5, 8.0, 9.0, 10.0, 11.0, 12.0, 13.0, 14.0, 15.0, 15.5/
c      data yplot/
*   0.0, 1.0, 2.0, 3.0, 4.0, 5.0, 5.8, 7.07, 7.85,
*   8.3, 8.6, 8.7, 8.65, 8.6, 8.4, 8.2, 8.0, 7.77,
*   7.55, 7.31, 7.07, 6.6, 6.1, 5.66, 5.25, 4.88,
*   4.47, 4.12, 3.96/
c      if (fac>0.0) go to 20
c
pi=2.0*asin(1.0)
rho=4.31e-13
rho2=rho*rho*1.0e24
fac=1.0/(1.0-0.394)
fac=rho2*fac/137.0
fac=8.0*pi*fac/3.0
b0=2.225e6 ! threshold energy for photoneutron reaction
c      do i=1,29
c
This data represents the empirical data graphically displayed in Fig 5.7 on pp 143 of Keipin's book,
the "Physics of Nuclear Kinetics" (and/or from Fig. 3.6 on pp 56 of Goldstein's book "Fundamental Aspects
of Reactor Shielding" -- which is identical, but lists more of the original detailed references.)
energy(i)=(2.0 + (13.0*2.0)*(xplot(i)/16.31))*(1.0e6) ! energy in eV
sigxgn(i)= 3.0 * (yplot(i)/11.42) * (1.0e-3) ! deuterium sigma(g,n) in barns; better fit than theoretical xsect
c
Following equations from pages 334-336 of "The Atomic Nucleus" by Evans
show that sigxgn(E) could vary as sigxgn = a*u + b*u**3.
g=b0*(energy(i)-b0)
if (g.le.0) g=0.0
u(i)=(sqrt(g))/energy(i)
sig2(i)=fac*(u(i)**3)
pm=0.008672*u(i)*0.037e6/(0.037e6+energy(i)-b0)
pm=0.006237*u(i)*0.07388e6/(0.07388e6+energy(i)-b0)
sig3(i)=sig2(i)+pm
c
! photoelectric component on photoneutron xsect, based on Eq 4.20
! photomagnetic component based on Eq 4.19; old; mistake in book ?
! photomagnetic component based on Eq 4.19; new, better
! total theoretical photoneutron xsect for disintegration of deuterium

```

Table A.1 (continued)

```

c      write (*,'(1x,1p,3e15.5)') energy(i),sigxgn(i),sigx3(i)
enddo
c
c
20    sigma=0.0
      g=b0*(egam-b0)
      if (g.le.0.0) go to 30      ! xsect=0 below threshold
      if (egam.gt.energy(27)) then ! use theoretical formula for high energies
         uu=(sqrt(g))/egam
         sig2=fac*(uu**3)
         pm=0.006237*uu**0.07388e6/(0.07388e6+egam-b0)
         sigma=sig2+pm
         go to 30
      endif
      do i=1,26 ! interpolate empirical data in Keepin's book for all other energies
      if (egam.ge.energy(i) .and. egam.le.energy(i+1)) then
         sigma=(egam-energy(i))/(energy(i+1)-energy(i))
         sigma=sigxgn(i)+(sigxgn(i+1)-sigxgn(i))*sigma
         go to 30
      endif
      enddo
c
30    return
end

```

Table A.2. Group-to-group photoneutron production cross sections for deuterium in the ANSL-V 39n/44g library energy group structure (cf Table 7a), as calculated by the PHOTOX program in Table A.1.

FROM GAMMA GROUP	PHOTONEUTRON PRODUCTION XSECTS (IN BARNS) FOR DEUTERIUM IN THE ANSL-V 39N/44G LIBRARY (*)															
	TO NGRP 1	TO NGRP 2	TO NGRP 3	TO NGRP 4	TO NGRP 5	TO NGRP 6	TO NGRP 7	TO NGRP 8	TO NGRP 9	TO NGRP 10						
1	5.7901e-4	1.59937e-4	0.0	0.0	0.0	0.0	0.0	0.0	0.0	0.0	0.0	0.0	0.0	0.0	0.0	0.0
2	0.0	1.01982e-3	0.0	0.0	0.0	0.0	0.0	0.0	0.0	0.0	0.0	0.0	0.0	0.0	0.0	0.0
3	0.0	1.24817e-3	0.0	0.0	0.0	0.0	0.0	0.0	0.0	0.0	0.0	0.0	0.0	0.0	0.0	0.0
4	0.0	1.37300e-3	1.89845e-4	0.0	0.0	0.0	0.0	0.0	0.0	0.0	0.0	0.0	0.0	0.0	0.0	0.0
5	0.0	0.0	1.79236e-3	0.0	0.0	0.0	0.0	0.0	0.0	0.0	0.0	0.0	0.0	0.0	0.0	0.0
6	0.0	0.0	1.88451e-3	0.0	0.0	0.0	0.0	0.0	0.0	0.0	0.0	0.0	0.0	0.0	0.0	0.0
7	0.0	0.0	1.97719e-3	0.0	0.0	0.0	0.0	0.0	0.0	0.0	0.0	0.0	0.0	0.0	0.0	0.0
8	0.0	0.0	2.06519e-3	0.0	0.0	0.0	0.0	0.0	0.0	0.0	0.0	0.0	0.0	0.0	0.0	0.0
9	0.0	0.0	3.17202e-4	1.83059e-3	0.0	0.0	0.0	0.0	0.0	0.0	0.0	0.0	0.0	0.0	0.0	0.0
10	0.0	0.0	0.0	2.11254e-3	1.13003e-4	0.0	0.0	0.0	0.0	0.0	0.0	0.0	0.0	0.0	0.0	0.0
11	0.0	0.0	0.0	0.0	2.27029e-3	0.0	0.0	0.0	0.0	0.0	0.0	0.0	0.0	0.0	0.0	0.0
12	0.0	0.0	0.0	0.0	2.16166e-3	1.12834e-4	0.0	0.0	0.0	0.0	0.0	0.0	0.0	0.0	0.0	0.0
13	0.0	0.0	0.0	0.0	0.0	2.19128e-3	0.0	0.0	0.0	0.0	0.0	0.0	0.0	0.0	0.0	0.0
14	0.0	0.0	0.0	0.0	0.0	1.90334e-3	9.28385e-5	0.0	0.0	0.0	0.0	0.0	0.0	0.0	0.0	0.0
15	0.0	0.0	0.0	0.0	0.0	0.0	0.0	1.58033e-3	0.0	0.0	0.0	0.0	0.0	0.0	0.0	0.0
16	0.0	0.0	0.0	0.0	0.0	0.0	0.0	5.77769e-4	4.82154e-4	0.0	0.0	0.0	0.0	0.0	0.0	0.0
17	0.0	0.0	0.0	0.0	0.0	0.0	0.0	0.0	2.97099e-4	4.32129e-5	3.99949e-6					

(*) All other terms not shown are zero. Used 100 energy points to integrate across each gamma source group.

APPENDIX B

Listing of the SPARK program used to augment a premixed DORT-ready cross section library (previously produced by GIP or JIPSY) by expanding the scattering matrix and "adding in" the (g)group-to-(n)group upscatter terms that represent the photoneutron production cross sections for deuterium in the various mixtures as needed.



Table B.1. Listing of the SPARK program used to augment a premixed DORT-ready cross section library (previously produced by GIP or JIPSY) by expanding the scattering matrix and "adding in" the (g)-group-to-(n)-group upscatter terms that represent the photoneutron production cross sections for deuterium in the various mixtures as needed.

```

*****  

c  

c SPARK.F (dated 5-6-93, by J. A. Bucholz)  

c  

c This is a simple program to take a premixed dort-ready xsect library previously produced by GIP  

c or JIPSY and "add in" the (gamma)-group-to-(neutron)group scattering matrix that represents the  

c photoneutron production cross section for deuterium (in barns) for the various mixtures (as needed).  

c This version of SPARK is for xsect sets based on the ANSL-V 39n/44g library.  

c  

c One may also want to turn off the fission source in the fuel (if you later plan to do only fixed source  

c calculations) and put a negligibly small amount of fission everywhere (in all materials and in all  

c energy groups) so that the DORT code can take advantage of Vondy's "error mode extrapolation technique"  

c to accelerate convergence. (If so, set ivon=1; if not set ivon=0).  

c  

c A typical input dataset would be as follows:  

c  

c title card for the spark program  

c 83 / igm = total number of energy groups (must be 83 for the ANSL-V 39n/44g library)  

c 3 / iit1 = position of sigma total in the input dataset  

c 28 / ihs1 = position of the within-group (g-to-g) scattering xsect in the input dataset  

c 110 / ihm1 = length of the input xsect dataset (actually dort sets are 1 element longer, but we don't count that)  

c 10 / nmat = number of real material mixtures in the input xsect dataset (10 real mats with p3 yield matm=40, but nmat=10)  

c 3 / isct = order of scattering for materials in the input xsect dataset  

c 1 / ivon = Vondy flag; ivon=1 means "set nr$igf=1.0e-15 for all materials and all groups"; ivon=0 means don't mess  

c 1 5.95609e-02 / says that: (real) mixture 1 has deuterium density of 5.95609e-02 atoms/(barn*cm)  

c 2 5.94656e-02 / says that: (real) mixture 2 has deuterium density of 5.94656e-02 atoms/(barn*cm)  

c 8 2.94852e-02 / says that: (real) mixture 8 has deuterium density of 2.94852e-02 atoms/(barn*cm)  

c 9 2.94852e-02 / says that: (real) mixture 9 has deuterium density of 2.94852e-02 atoms/(barn*cm)  

c 10 3.26488e-02 / says that: (real) mixture 10 has deuterium density of 3.26488e-02 atoms/(barn*cm)  

c 0 0 / flag card indicating that this is the end of the input data  

c  

c  

c The first and second parameters on the command line are the names of the input and output dort-ready binary xsect files.  

c (If not specified, the input xsect file is assumed to be fort.11 and the output xsect file is assumed to be fort.12).  

c To run the program, one would say:  

c  

c spark xsect.bin.inp xsect.bin.out <input >output  

c or simply:  

c  

c
```

Table B.1 (continued)

```

c spark <input> >output
c
c where "input" and "output" are the names of the card-image input and the printed output files.
c ****
c
c dimension aden(1000),d(100000) 1 d(limit)
c dimension xpn(83,83),xpn0(26),ifrom0(26),ito0(26),xupsn(83)
c character*128 inpf1,outfil 1 command-line arguments; names of input/output xsect files
c character*80 title
c data limit/ 100000 /
c
c
c xpn0(n)=micorscopic photoneutron production xsect (in barns) where
c igam=ifrom0(n) and ineut=ito0(n) are the respective group numbers in
c the 39n/44g library for that particular cross section [xpnnic(n)]:
c dimension xpn0(26),ifrom0(26),ito0(26)
c
c
c data xpn0/ 5.79901e-4, 1.59937e-4, 1.01982e-3, 1.24817e-3,
c 1.37300e-3, 1.89845e-4, 1.79236e-3, 1.88451e-3, 1.97719e-3,
c 2.06519e-3, 3.17202e-4, 1.83059e-3, 2.11254e-3, 1.13003e-4,
c 2.27029e-3, 2.16166e-3, 1.12834e-4, 2.19128e-3, 1.90334e-3,
c 9.28385e-5, 1.58033e-3, 5.77769e-4, 4.82154e-4, 2.97095e-4,
c 4.32129e-5, 3.99949e-6/
c
c data ifrom0/40,40,41,42,43,43,44,45,46,47,48,48,
c 49,49,50,51,51,52,53,53,54,55,55,56,56,56/
c
c data ito0/ 1,2,2,2,2,3,3,3,3,3,4,
c 4,5,5,5,6,6,6,7,7,7,8,8,9,10/
c
c
c xupsn(ig)=micorscopic photoneutron upscatter xsect from
c group ig to all higher groups (in barns):
c dimension xupsn(83)
c
c data xupsn/ 39*0.0, 7.39837e-4, 1.01982e-3, 1.24817e-3,
c 1.56284e-3, 1.79236e-3, 1.88451e-3, 1.97719e-3, 2.06519e-3,
c 2.14779e-3, 2.22555e-3, 2.27029e-3, 2.27450e-3, 2.19128e-3,
c 1.99617e-3, 1.58033e-3, 1.05992e-3, 3.44311e-4, 27*0.0 /
c
c
c do 10 ifrom=1,83
c do 10 ito=1,83
c xpn(ito,ifrom)=0.0
10

```

Table B.1 (continued)

```

c      do 11 n=1,26
      ifrom=ifrom0(n)
      iio=ito0(n)
      xpn(iio,ifrom)=xpn0(n)
11
c
c      read the card-image input data:
c
read (5,'(80)') title ! dummy title card
read (5,*),igm ! total number of energy groups (must be 83 for the ANSL-V 39n/44g library)
if (igm.ne.83) stop 7771
read (5,*),ih1 ! position of sigma total in the input dataset
read (5,*),ihs1 ! position of the within-group (g-to-g) scattering xsect in the input dataset
read (5,*),ihs2 ! position of the between-group (g-to-g) scattering xsect in the input dataset
read (5,*),ihs3 ! position of the total cross section in the input dataset
read (5,*),ihs4 ! position of the total cross section in the input dataset
read (5,*),ihs5 ! position of the total cross section in the input dataset
read (5,*),ihs6 ! position of the total cross section in the input dataset
read (5,*),ihs7 ! position of the total cross section in the input dataset
read (5,*),ihs8 ! position of the total cross section in the input dataset
read (5,*),ihs9 ! position of the total cross section in the input dataset
read (5,*),ihs10 ! position of the total cross section in the input dataset
read (5,*),ihs11 ! position of the total cross section in the input dataset
read (5,*),ihs12 ! position of the total cross section in the input dataset
read (5,*),ihs13 ! position of the total cross section in the input dataset
read (5,*),ihs14 ! position of the total cross section in the input dataset
read (5,*),ihs15 ! position of the total cross section in the input dataset
read (5,*),ihs16 ! position of the total cross section in the input dataset
read (5,*),ihs17 ! position of the total cross section in the input dataset
read (5,*),ihs18 ! position of the total cross section in the input dataset
read (5,*),ihs19 ! position of the total cross section in the input dataset
read (5,*),ihs20 ! position of the total cross section in the input dataset
read (5,*),ihs21 ! position of the total cross section in the input dataset
read (5,*),ihs22 ! position of the total cross section in the input dataset
read (5,*),ihs23 ! position of the total cross section in the input dataset
read (5,*),ihs24 ! position of the total cross section in the input dataset
read (5,*),ihs25 ! position of the total cross section in the input dataset
read (5,*),ihs26 ! position of the total cross section in the input dataset
read (5,*),ihs27 ! position of the total cross section in the input dataset
read (5,*),ihs28 ! position of the total cross section in the input dataset
read (5,*),ihs29 ! position of the total cross section in the input dataset
read (5,*),ihs30 ! position of the total cross section in the input dataset
read (5,*),ihs31 ! position of the total cross section in the input dataset
read (5,*),ihs32 ! position of the total cross section in the input dataset
read (5,*),ihs33 ! position of the total cross section in the input dataset
read (5,*),ihs34 ! position of the total cross section in the input dataset
read (5,*),ihs35 ! position of the total cross section in the input dataset
read (5,*),ihs36 ! position of the total cross section in the input dataset
read (5,*),ihs37 ! position of the total cross section in the input dataset
read (5,*),ihs38 ! position of the total cross section in the input dataset
read (5,*),ihs39 ! position of the total cross section in the input dataset
read (5,*),ihs40 ! position of the total cross section in the input dataset
read (5,*),ihs41 ! position of the total cross section in the input dataset
read (5,*),ihs42 ! position of the total cross section in the input dataset
read (5,*),ihs43 ! position of the total cross section in the input dataset
read (5,*),ihs44 ! position of the total cross section in the input dataset
read (5,*),ihs45 ! position of the total cross section in the input dataset
read (5,*),ihs46 ! position of the total cross section in the input dataset
read (5,*),ihs47 ! position of the total cross section in the input dataset
read (5,*),ihs48 ! position of the total cross section in the input dataset
read (5,*),ihs49 ! position of the total cross section in the input dataset
read (5,*),ihs50 ! position of the total cross section in the input dataset
read (5,*),ihs51 ! position of the total cross section in the input dataset
read (5,*),ihs52 ! position of the total cross section in the input dataset
read (5,*),ihs53 ! position of the total cross section in the input dataset
read (5,*),ihs54 ! position of the total cross section in the input dataset
read (5,*),ihs55 ! position of the total cross section in the input dataset
read (5,*),ihs56 ! position of the total cross section in the input dataset
read (5,*),ihs57 ! position of the total cross section in the input dataset
read (5,*),ihs58 ! position of the total cross section in the input dataset
read (5,*),ihs59 ! position of the total cross section in the input dataset
read (5,*),ihs60 ! position of the total cross section in the input dataset
read (5,*),ihs61 ! position of the total cross section in the input dataset
read (5,*),ihs62 ! position of the total cross section in the input dataset
read (5,*),ihs63 ! position of the total cross section in the input dataset
read (5,*),ihs64 ! position of the total cross section in the input dataset
read (5,*),ihs65 ! position of the total cross section in the input dataset
read (5,*),ihs66 ! position of the total cross section in the input dataset
read (5,*),ihs67 ! position of the total cross section in the input dataset
read (5,*),ihs68 ! position of the total cross section in the input dataset
read (5,*),ihs69 ! position of the total cross section in the input dataset
read (5,*),ihs70 ! position of the total cross section in the input dataset
read (5,*),ihs71 ! position of the total cross section in the input dataset
read (5,*),ihs72 ! position of the total cross section in the input dataset
read (5,*),ihs73 ! position of the total cross section in the input dataset
read (5,*),ihs74 ! position of the total cross section in the input dataset
read (5,*),ihs75 ! position of the total cross section in the input dataset
read (5,*),ihs76 ! position of the total cross section in the input dataset
read (5,*),ihs77 ! position of the total cross section in the input dataset
read (5,*),ihs78 ! position of the total cross section in the input dataset
read (5,*),ihs79 ! position of the total cross section in the input dataset
read (5,*),ihs80 ! position of the total cross section in the input dataset
read (5,*),ihs81 ! position of the total cross section in the input dataset
read (5,*),ihs82 ! position of the total cross section in the input dataset
read (5,*),ihs83 ! position of the total cross section in the input dataset
enddo
read (5,*),endd=13,err=13 ),aden(i) ! aden(i) says: (real) mixture "i" has deut density of aden(i) atoms/(barn*cm)
12
      if (i.ne.0) go to 12 ! last data card should have two zeros (one integer and one real)
      continue
13
c
c
c      inpf1='fort.11' ! default name of dort-ready binary xsect input file
outf1='fort.12' ! default name of dort-ready binary xsect input file
niargs=jargc0 ! niargs = number of command line arguments detected
if (niargs.ge.1) call getarg (1,inpf1) ! get user-supplied name of dort-ready binary xsect input file
if (niargs.ge.2) call getarg (2,outf1) ! get user-supplied name of dort-ready binary xsect output file
c
open (11,file=inpf1,status='old',form='unformatted')
open (12,file=outf1,status='new',form='unformatted')
c
nblow=ihs1-1
nabove=ihs1-1-ih1
ih1=ihm1
if (nabove.gt.0) ih1=ihm1+1 ! real length of dort-ready xsect table with upscat, even though we tell the code it is ihm1

```

Table B.1 (continued)

```

c      nblow2=nblow1
c      nabov2=nabov1
c
c      nabovp=48 ! min number of positions reqd for photon-neutron production
c      (upsat) in the 39n4g library as given by the photox.f program.
c      In this case, two reactions require this many positions:
c      (1) photons in group 55 (gamma grp 16) can produce neutrons in group 7
c      (2) photons in group 56 (gamma grp 17) can produce neutrons in group 8
c      The logic below will check requirements for all groups and satisfy all.
c
c      do ito=1,igm
c          nabito=0
c          do ifrom=1,igm
c              if (xpn(ito,ifrom).gt.0.0) nabito=ifrom-ito
c          enddo
c          if (nabito.gt.nabov2) nabov2=nabito
c      enddo
c
c      iit2=iit1
c      iits2=iit2+nabov2+1
c      iim2=iis2+nblow2
c      iit2=iim2+1 ! actual length of dorb-ready xsect table, even though we still tell dorb it is iim2
c
c      need=iit2*nmat2
c      if (need.gt.limit) stop 7773
c
c      write (6,14) iit1,ihs1,iim1,itl1,nabov1,nblow1,
c                  iit2,ihs2,iim2,itl2,nabov2,nblow2
c
c      format (f,
c              *     ' For input xsect dataset: iit1='i3,' ihs1='i3,
c              *     ' iim1='i3,' itl1='i3,' nabov1='i3,' nblow1='i3//,
c              *     ' For output xsect dataset: iit2='i3,' ihs2='i3,
c              *     ' iim2='i3,' itl2='i3,' nabov2='i3,' nblow2='i3)
c
c      do ig=1,igm
c          call addpxn (d(1),xpn,xupspn,aden,
c                      ign,itl1,nabov1,itl1,ihs2,itl2,nabov2,itl2,
c                      nmat,nmat2,isctivon,ig)
c      enddo
c

```

Table B.1 (continued)

```

15      write (6,15)
c      format(1,' The output xsect dataset was successfully written.')
c      stop
c      end
c      subroutine addpxn (xsect,xpn,xupspn,aden,
c      igm,ih1,nabov1,ih1,ih2,nabov2,ih2,
c      nmat,nmat2,isc1,ivon,ig)
c
c      dimension xsec(ih2,nmat2)           ! xpn(lto,ifrom)
c      dimension xpn(igm,igm)             ! total upscatter out of each group
c      dimension xupspn(igm)
c      dimension aden(1000)
c
c      do 10 imat=1,nmat2
c      do 10 ipos=1,ih2
c      xsec(ipos,imat)=0.0
10
c      ih1a=ih1+1
c      read (11) ((xsec(ipos,imat),ipos=1,ih1),
c      (xsec(ipos+nabov2-nabov1,imat),ipos=ih1a,ih1),
c      imat=1,nmat2)
c
c      do 12 m=1,nmat
c      mat=m*(isc1+1)-isc1
c      xsec(ih2,mat)=xsec(ih2,mat)+aden(m)*xupspn(ig)
c      ipos=ig
c      ifrom=ig
c      ipos=ih2
c      ifrom=ifrom+1
c      ipos=ipos-1
c      if (ipos>ih2) then
c      xsec(ipos,mat)=xsec(ipos,mat)+aden(m)*xpn(lto,ifrom)
c      go to 11
c      endif
c      continue
12
c      Photoneutron production cross sections have all been "added in" at this point.
c
c      One may (?) now want to turn off the fission source in the fuel (if you later
c      plan to do only fixed source calculations) and put a negligibly small amount
c      of fission everywhere (in all materials and in all energy groups) so that the
c      DORT code can take advantage of Vondy's "error mode extrapolation technique"
c      to accelerate convergence. (If so, set ivon=1; if not set ivon=0)
c
c

```

Table B.1 (continued)

```

if (ivon.eq.1) then
  nusigf=ih2-1
  do mat=1,nmat2
    xsect(nusigf,mat)=0.0          ! set nu*sigf=0.0
  enddo
  do m=1,nmat
    mat=m*(isct+1)-isct           ! go back for all "real" materials corresponding to the
    xsect(nusigf,mat)=1.0e-15      ! P0 components and set nu*sigf=1.0e-15 for all groups
  enddo
endif

c
c
c   write (12)((xsect(ipos,jmat),ipos=1,ih2),imat=1,nmat2)

c   Early debug print (formerly in the smurf program).
c   if (ig.eq.18)
c     if (ig.ge.40 .and. ig.le.60)
c       write (6,21) (ig,mat,xsect(1,mat),xsect(2,mat),xsect(3,mat),
c                   xsect(28,mat),xsect(134,mat),xsect(135,mat),mat=1,40)
c       *
c       format (i///,(1x,'ig='',i3,' mat='',i3,p,6e16.5))
21
c
c   return
end

```

APPENDIX C

Listing of the ANSIDOSE program for calculating neutron and gamma flux-to-dose-rate conversion factors as prescribed in ANSI Std. ANSI-6.1.1-1977 (Ref. 22).

This stand-alone utility program was originally available as the DOSE module of the AMPX code system in the late 1970s. While it is no longer included as a stand-alone code in the newer (1992) release of the AMPX-77 code system, the same functionality can be achieved by running the JERGENS, VEL, and CASTROL modules^{C.1-C.3} (sequentially) in the AMPX-77 code system.⁵



Table C.1. Listing of the ANSIDOSE program for calculating neutron and gamma flux-to-dose-rate conversion factors as prescribed in ANSI Std. ANSI-6.1.1-1977

```

c ****
c ****
c
c ANSIDOSE.F -- Calculates multigroup neutron & gamma flux-to-dose-rate
c conversion factors as prescribed in ANSI/ANS-6.1.1-1977
c
c This utility program was originally written by Dr. John R. Knight
c and was called the DOSE program in the AMPX System as it existed in
c the late 1970's. Code reads std input (5) and writes std output (6).
c
c Input data:
c
c The first record gives the number of neutron energy groups (IGMN).
c The second record gives the number of gamma energy groups (IGMG).
c If IGMN.gt.0, one then enters the energy group boundaries for the
c neutron groups in free-form input as follows:
c   Emax(ngrp 1), Emin(ngrp 1), Emin(ngrp 2), ... Emin(for last ngrp)
c If IGMG.gt.0, one then enters the energy group boundaries for the
c gamma groups in free-form input as follows:
c   Emax(ggrp 1), Emin(ggrp 1), Emin(ggrp 2), ... Emin(for last ggrp)
c
c All energy bounds are given in eV.
c
c ****
c ****
c
* common /data/ d(1),lp,lebn,lebg,ldfn,ldfg,igmn,igmg,ipun,itype,
*           x(1000)
c
c read (*,*) igmn ! number of neutron groups
c read (*,*) igmg ! number of gamma groups
c
c igmn1=igmn+1
c igmg1=igmg+1
c
c lp=7
c lebn=11
c lebg=lebn+igmn1
c ldfn=lebg+igmg1
c ldfg=ldfn+igmn
c
c if (igmn.gt.0) read (*,*) (d(lebn-1+ig),ig=1,igmn1) ! neut grp bounds
c if (igmg.gt.0) read (*,*) (d(lebg-1+ig),ig=1,igmg1) ! gamma grp bounds
c
c ipun=0
c if (igmn.gt.0) itype=1
c if (igmg.gt.0) itype=2
c if (igmn.gt.0 .and. igmg.gt.0) itype=3
c
c call dose(d(lebn),d(lebg),d(ldfn),d(ldfg))
c
c stop
c end
c subroutine dose(ebn,ebg,dofn,dofg)
c
c Calculate neutron & gamma dose factors as per ANSI/ANS-6.1.1-1977
c

```

Table C.1 (continued)

```

dimension ebn(1),ebg(1),dofn(1),dofg(1)
common /data/ d(1),lp,lebn,lebg,ldfn,ldfg,igmn,igmg,ipun,itype,
*      x(1000)
      real*8 ansa,ansb,eb1,eb2
c
c      external dfn,dfg,wt
c
c      igmn1=igmn+1
c      igmg1=igmg+1
c
c      do 100 i=1,igmn1
100    ebn(i)=1.e-6*ebn(i)
      do 110 i=1,igmg1
110    ebg(i)=1.e-6*ebg(i)
c
c      if (itype.eq.1 .or. itype.eq.3) then
c          **** neutron ****
c          do 130 i=1,igmn
c              eb1=ebn(i+1)
c              eb2=ebn(i)
c              call gauss(eb1,eb2,1,ansa,dfn,24)
c              call gauss(eb1,eb2,1,ansb,wt,24)
130    dofni(i)=ansa/ansb
c      endif
c
c      if (itype.eq.2 .or. itype.eq.3) then
c          **** gamma ****
c          do 150 i=1,igmg
c              eb1=ebg(i+1)
c              eb2=ebg(i)
c              call gauss(eb1,eb2,1,ansa,dfg,24)
150    dofgi(i)=ansa/(ebg(i)-ebg(i+1))
c      endif
c
c      do 170 i=1,igmn1
170    ebn(i)=1.e+6*ebn(i)
      do 180 i=1,igmg1
180    ebg(i)=1.e+6*ebg(i)
c
c      if (itype.eq.1 .or. itype.eq.3)
*        write(6,191) (i,ebn(i),ebn(i+1),dofn(i),i=1,igmn)
191    format (1x,i3,3x,1p,e12.4,' -- ',e12.4,' ev, ',e12.4,
*           '(mrem/hr)/(n/sec/cm2)')
c
c      if (itype.eq.2. .or. itype.eq.3)
*        write(6,192) (i,ebg(i),ebg(i+1),dofg(i),i=1,igmg)
192    format (1x,i3,3x,1p,e12.4,' -- ',e12.4,' ev, ',e12.4,
*           '(mrem/hr)/(p/sec/cm2)')
c
c      return
c      end
c      function wt(ee)
c          double precision wt,ee
c          e=ee
c**** E in MeV ****
c      if (e.gt.6.74e-2) go to 100
c      if (e.lt.1.265e-7) go to 110
c**** 1/E weight ****
c      wt=1.6633e-2/e
c      go to 120

```

Table C.1 (continued)

```

c**** fission spectrum weight ****
100 wt=sqrt(e)*exp(-e/1.33)
      go to 120
c**** maxwell weight ****
110 wt=sqrt(e)*exp(-e/2.53e-8)*5.4866e10
120 return
end
function dfg(ee)
      double precision dfg,ee
c**** gamma ray dose factors - E in MeV (mrem/hr)/(gammas/cm**2-sec) **
dimension a(4),b(4),c(4),d(4)
data a,b,c,d/-20.477,-13.626,-13.133,-12.791,-1.7454,-.57117,
* .72008, .28309,0.,-1.0954,-.033603,.10873,0.,-24897,2*0./
      e=ee
if (e.lt.03) i=1
if (e.ge..03.and.e.lt.5) i=2
if (e.ge..5.and.e.lt.5.) i=3
if (e.ge.5.) i=4
x=alog(e)
dfg=1000.0*exp(a(i)+b(i)*x+c(i)*x**2+d(i)*x**3)          00000110
return
end
function dfn(ee)
      double precision dfn,wt,ee
c**** neutron dose factors - E in MeV (mrem/hr)/(n/cm**2-sec) ****
dimension a(11),b(11),c(11),d(11)
data a,b,c,d/-12.514,-12.21,-8.9302,-8.6632,2*-8.9359,-9.2822,
* -8.4741,-8.8247,-11.208,-9.1202,0.,.17165,.7844,.90037,.56096,
* -.055979,.32193,-.18018,0.,1.0352,.24395,0.,.026034,9*0.,0.,
* 1.0273e-3,9*0./
      e=ee
if (e.lt.1.e-7) i=1
if (e.ge.1.e-7.and.e.lt.01) i=2
if (e.ge..01.and.e.lt..1) i=3
if (e.ge..1.and.e.lt..5) i=4
if (e.ge..5.and.e.lt.1.) i=5
if (e.ge.1..and.e.lt.2.5) i=6
if (e.ge.2.5.and.e.lt.5.) i=7
if (e.ge.5..and.e.lt.7.) i=8
if (e.ge.7..and.e.lt.10.) i=9
if (e.ge.10..and.e.lt.14.) i=10
if (e.ge.14.) i=11
x=alog(e)
dfn=1000.0*exp(a(i)+b(i)*x+c(i)*x**2+d(i)*x**3)*wt(ee)
return
end
subroutine gauss(xl,xu,nfold2,answ,fun,np12)                00000010
implicit real*8(a-h,o-z)                                      00000020
00000030
c.....                                                 00000040
c Program author E. B. Harris
c Gaseous Diffusion Development Division, Union Carbide Corp., 00000050
c Nuclear Div.,                                              00000060
c Oak Ridge,Tenn.                                            00000070
c                                                       00000080
c      xl=lower limit of integral (double precision)        00000090
c      xu=upper limit of integral (double precision)       00000100
c      nfold2=number of equal subintervals that (xl,xu) is to be 00000110
c      subdivided into                                         00000120
c      answ=approximate value of the integral as evaluated by this 00000130
c      subroutine (double precision)                           00000140
c      fun=the name of the double precision function subprogram that 00000150
c      defines the integrand function. fun has one double precision 00000160

```

Table C.1 (continued)

c	variable, say x, as an argument and returns the value of the integrand at x (where x is the variable of integration). the name passed to fun must be declared external in the calling program.	00000170 00000180 00000190 00000200 00000210 00000220 00000230 00000240 00000250 00000260 00000270 00000280 00000290 00000300 00000310 00000320 00000330 00000340 00000350
c	npt2=number of points (order) at which the integrand is to be evaluated in each subinterval, i.e., total number of evaluations = npt2*nfold2. permissible values of npt2 are 2, 3, 4, 5, 6, 7, 8, 9, 10, 12, 16, 20, 24, 32, 40, 48, 64, 80, and 96. if npt2 is .lt. 2, 2 points are used. if npt2 is .gt. 96, 96 points are used. within the range of 2-96, if npt2 is not one of the permissible values, the next higher permissible value is used.	
c	the data statements beginning with an2 and ending with an96d are the abscissas and weight factors for the gaussian integration and are taken from the handbook of mathematical functions edited by milton abramowitz and irene a. stegun, applied mathematics series 55, u. s. department of commerce, national bureau of standards, 1964, pages 916-919.	
:	: (details not shown here for this standard Gaussian integration routine)	
return		00003400
end		00003410

APPENDIX C. REFERENCES

- C-1. JERGENS: A Module to Generate Weight Functions and to Combine ENDF/B TAB1 Records, as described in Sect. 3 of Ref. 5 (above).
- C-2. VEL: A Module for Group-Averaging Point Data, as described in Sect. 3 of Ref. 5 (above).
- C-3. CASTROL: A Module to Write "TAB1" Records With Cross Sections Input from Cards, as described in Sect. 3 of Ref. 5 (above).



APPENDIX D

Neutron and gamma kerma factors in aluminum and iron for the ANSL-V 39n/44g and 99n/44g energy group structures. See discussion in Sect. 5 for additional details.



Table D.1. Recommended "prompt" kerma factors (alone) for Al-27 as given by the KAOS-V data library, extracted using the KAOS/RETRIEVE program, and expressed here in units of eV*barns for each of the 99 neutron energy groups in Table 7b.

Groups 01-07:	4.428E+06	4.756E+06	4.396E+06	1.587E+06	7.006E+05	3.858E+05	4.545E+05
Groups 08-14:	4.049E+05	3.692E+05	3.409E+05	3.159E+05	3.126E+05	2.545E+05	2.923E+05
Groups 15-21:	2.657E+05	2.350E+05	2.391E+05	2.125E+05	2.238E+05	2.096E+05	1.794E+05
Groups 22-28:	1.981E+05	1.856E+05	1.449E+05	1.370E+05	1.850E+05	1.318E+05	1.264E+05
Groups 29-35:	1.188E+05	1.171E+05	7.781E+04	5.963E+04	5.929E+04	8.000E+04	2.841E+04
Groups 36-42:	5.275E+04	7.942E+03	2.843E+04	9.628E+03	1.085E+03	1.095E+03	8.899E+02
Groups 43-49:	9.531E+02	6.116E+02	3.355E+02	2.400E+02	1.700E+02	1.212E+02	8.872E+01
Groups 50-56:	6.254E+01	4.526E+01	3.366E+01	2.398E+01	1.823E+01	1.411E+01	1.147E+01
Groups 57-63:	1.006E+01	9.102E+00	8.520E+00	8.237E+00	8.213E+00	8.391E+00	8.734E+00
Groups 64-70:	9.230E+00	9.871E+00	1.074E+01	1.181E+01	1.308E+01	1.456E+01	1.627E+01
Groups 71-77:	1.811E+01	1.811E+01	2.006E+01	2.042E+01	2.173E+01	2.416E+01	2.771E+01
Groups 78-84:	3.159E+01	3.549E+01	3.994E+01	8.232E+01	8.235E+01	8.235E+01	8.235E+01
Groups 85-91:	8.235E+01	8.235E+01	1.701E+02	1.704E+02	1.704E+02	1.704E+02	1.704E+02
Groups 92-98:	1.704E+02						
Group 99:	1.704E+02						

* Multiply these kerma factors by 3.57554E-21 to put them in units of W*s*cm²/g, or (assuming an aluminum density of 2.70 g/cc), multiply by 9.65397E-21 to put them in units of W*s/cm. The resulting kerma factors may then be folded directly with the multigroup photon particle fluxes (s-&a-20V-1-&a+20Vcm-&a-20V-2-&a+20V) to obtain the local gamma heating rates in units of W/g or W/cc.

Table D.2. Recommended prompt kerma factors for Al-27 plus the "charged particle" decay heat associated with its activation products (i.e. the beta decay of Al-28 produced from activation of the Al-27) as given by the KAOS-V data library, extracted using the KAOS/RETRIEVE program, and expressed here in units of eV*barns for each of the 99 neutron energy groups in Table 7b.

Groups 01-07:	4.503E+06	4.879E+06	4.526E+06	1.689E+06	7.593E+05	4.177E+05	4.720E+05
Groups 08-14:	4.143E+05	3.744E+05	3.435E+05	3.165E+05	3.129E+05	2.547E+05	2.925E+05
Groups 15-21:	2.659E+05	2.352E+05	2.393E+05	2.127E+05	2.240E+05	2.098E+05	1.796E+05
Groups 22-28:	1.983E+05	1.858E+05	1.451E+05	1.372E+05	1.853E+05	1.322E+05	1.268E+05
Groups 29-35:	1.194E+05	1.180E+05	7.885E+04	6.057E+04	6.047E+04	8.276E+04	3.167E+04
Groups 36-42:	5.566E+04	9.347E+03	4.122E+04	1.713E+04	4.710E+03	4.805E+03	5.315E+03
Groups 43-49:	2.677E+04	1.603E+04	5.601E+03	4.266E+03	3.322E+03	2.666E+03	2.422E+03
Groups 50-56:	2.610E+03	2.875E+03	3.156E+03	3.536E+03	3.903E+03	4.321E+03	4.836E+03
Groups 57-63:	5.466E+03	6.178E+03	6.974E+03	7.871E+03	8.872E+03	9.906E+03	1.105E+04
Groups 64-70:	1.230E+04	1.369E+04	1.538E+04	1.733E+04	1.952E+04	2.200E+04	2.480E+04
Groups 71-77:	2.775E+04	2.775E+04	3.085E+04	3.143E+04	3.350E+04	3.733E+04	4.291E+04
Groups 78-84:	4.896E+04	5.506E+04	6.199E+04	1.280E+05	1.280E+05	1.280E+05	1.280E+05
Groups 85-91:	1.280E+05	1.280E+05	2.645E+05	2.649E+05	2.649E+05	2.649E+05	2.649E+05
Groups 92-98:	2.649E+05						
Group 99:	2.649E+05						

* Multiply these kerma factors by 3.57554E-21 to put them in units of W*s*cm²/g, or (assuming an aluminum density of 2.70 g/cc), multiply by 9.65397E-21 to put them in units of W*s/cm. The resulting kerma factors may then be folded directly with the multigroup photon particle fluxes (s-&a-20V-1-&a+20Vcm-&a-20V-2-&a+20V) to obtain the local gamma heating rates in units of W/g or W/cc.

Table D.3. Recommended prompt kerma factors for Al-27 plus the "total decay heat" associated with its activation products (i.e. the beta and gamma decay of Al-28 produced from activation of the Al-27) as given by the KAOS-V data library, extracted using the KAOS/RETRIEVE program, and expressed here in units of eV*barns for each of the 99 neutron energy groups in Table 7b.

Groups 01-07:	4.834E+06	5.456E+06	5.127E+06	2.042E+06	8.999E+05	4.645E+05	4.946E+05
Groups 08-14:	4.265E+05	3.811E+05	3.469E+05	3.173E+05	3.131E+05	2.549E+05	2.927E+05
Groups 15-21:	2.661E+05	2.354E+05	2.395E+05	2.129E+05	2.242E+05	2.100E+05	1.798E+05
Groups 22-28:	1.985E+05	1.860E+05	1.453E+05	1.375E+05	1.858E+05	1.327E+05	1.275E+05
Groups 29-35:	1.201E+05	1.193E+05	8.035E+04	6.194E+04	6.216E+04	8.677E+04	3.638E+04
Groups 36-42:	5.986E+04	1.138E+04	5.971E+04	2.795E+04	9.947E+03	1.017E+04	1.171E+04
Groups 43-49:	6.408E+04	3.831E+04	1.321E+04	1.008E+04	7.875E+03	6.343E+03	5.793E+03
Groups 50-56:	6.289E+03	6.963E+03	7.666E+03	8.609E+03	9.516E+03	1.054E+04	1.181E+04
Groups 57-63:	1.335E+04	1.509E+04	1.704E+04	1.923E+04	2.167E+04	2.420E+04	2.699E+04
Groups 64-70:	3.006E+04	3.346E+04	3.758E+04	4.235E+04	4.772E+04	5.377E+04	6.058E+04
Groups 71-77:	6.780E+04	6.780E+04	7.539E+04	7.680E+04	8.185E+04	9.121E+04	1.048E+05
Groups 78-84:	1.196E+05	1.346E+05	1.515E+05	3.126E+05	3.127E+05	3.127E+05	3.127E+05
Groups 85-91:	3.127E+05	3.127E+05	6.463E+05	6.473E+05	6.473E+05	6.473E+05	6.473E+05
Groups 92-98:	6.473E+05						
Group 99:	6.473E+05						

* Multiply these kerma factors by 3.57554E-21 to put them in units of W*s*cm²/g, or (assuming an aluminum density of 2.70 g/cc), multiply by 9.65397E-21 to put them in units of W*s/cm. The resulting kerma factors may then be folded directly with the multigroup photon particle fluxes (s-&a-20V-1-&a+20Vcm-&a-20V-2-&a+20V) to obtain the local gamma heating rates in units of W/g or W/cc.

Table D.4. Recommended "prompt" kerma factors (alone) for Al-27 as given by the KAOS-V data library, extracted using the KAOS/RETRIEVE program, and expressed here in units of eV*barns for each of the 39 neutron energy groups in Table 7a.

Groups 01-07:	4.743E+06	3.830E+05	2.877E+05	2.240E+05	1.691E+05	1.358E+05	6.102E+04
Groups 08-14:	1.986E+04	7.770E+02	1.366E+02	2.707E+01	9.475E+00	8.884E+00	1.329E+01
Groups 15-21:	1.968E+01	2.416E+01	2.771E+01	3.159E+01	3.549E+01	3.994E+01	8.232E+01
Groups 22-28:	8.235E+01	8.235E+01	8.235E+01	8.235E+01	8.235E+01	1.701E+02	1.704E+02
Groups 29-35:	1.704E+02						
Groups 36-39:	1.704E+02	1.704E+02	1.704E+02	1.704E+02			

* Multiply these kerma factors by 3.57554E-21 to put them in units of W*s*cm²/g, or (assuming an aluminum density of 2.70 g/cc), multiply by 9.65397E-21 to put them in units of W*s/cm. The resulting kerma factors may then be folded directly with the multigroup photon particle fluxes (s-&a-20V-1-&a+20Vcm-&a-20V-2-&a+20V) to obtain the local gamma heating rates in units of W/g or W/cc.

Table D.5. Recommended prompt kerma factors for Al-27 plus the "charged particle" decay heat associated with its activation products (i.e. the beta decay of Al-28 produced from activation of the Al-27) as given by the KAOS-V data library, extracted using the KAOS/RETRIEVE program, and expressed here in units of eV*barns for each of the 39 neutron energy groups in Table 7a.

Groups 01-07:	4.866E+06	3.929E+05	2.879E+05	2.242E+05	1.693E+05	1.364E+05	6.285E+04
Groups 08-14:	2.549E+04	1.170E+04	3.059E+03	3.557E+03	6.268E+03	1.115E+04	1.981E+04
Groups 15-21:	3.026E+04	3.733E+04	4.291E+04	4.896E+04	5.506E+04	6.199E+04	1.280E+05
Groups 22-28:	1.280E+05	1.280E+05	1.280E+05	1.280E+05	1.280E+05	2.645E+05	2.649E+05
Groups 29-35:	2.649E+05						
Groups 36-39:	2.649E+05	2.649E+05	2.649E+05	2.649E+05			

* Multiply these kerma factors by 3.57554E-21 to put them in units of W*s*cm²/g, or (assuming an aluminum density of 2.70 g/cc), multiply by 9.65397E-21 to put them in units of W*s/cm. The resulting kerma factors may then be folded directly with the multigroup photon particle fluxes (s-&a-20V-1-&a+20Vcm-&a-20V-2-&a+20V) to obtain the local gamma heating rates in units of W/g or W/cc.

Table D.6. Recommended prompt kerma factors for Al-27 plus the "total decay heat" associated with its activation products (i.e. the beta and gamma decay of Al-28 produced from activation of the Al-27) as given by the KAOS-V data library, extracted using the KAOS/RETRIEVE program, and expressed here in units of eV*barns for each of the 39 neutron energy groups in Table 7a.

Groups 01-07:	5.442E+06	4.063E+05	2.883E+05	2.244E+05	1.695E+05	1.371E+05	6.551E+04
Groups 08-14:	3.362E+04	2.749E+04	7.279E+03	8.655E+03	1.531E+04	2.725E+04	4.840E+04
Groups 15-21:	7.393E+04	9.121E+04	1.048E+05	1.196E+05	1.346E+05	1.515E+05	3.126E+05
Groups 22-28:	3.127E+05	3.127E+05	3.127E+05	3.127E+05	3.127E+05	6.463E+05	6.473E+05
Groups 29-35:	6.473E+05						
Groups 36-39:	6.473E+05	6.473E+05	6.473E+05	6.473E+05			

* Multiply these kerma factors by 3.57554E-21 to put them in units of W*s*cm²/g, or (assuming an aluminum density of 2.70 g/cc), multiply by 9.65397E-21 to put them in units of W*s/cm. The resulting kerma factors may then be folded directly with the multigroup photon particle fluxes ($s \leftarrow \&a-20V-1 \leftarrow \&a+20V cm \leftarrow \&a-20V-2 \leftarrow \&a+20V$) to obtain the local gamma heating rates in units of W/g or W/cc.

Table D.7. Kerma factors for gammas interacting with Al-27 as calculated by the SMUG module of the AMPX cross section processing code system, stored in the ANSL-V 39n/44g cross section library (as nuclide 13027, MT-process 1527), subsequently extracted using the PAL module of the AMPX code system, and expressed here in units of eV*barns for each of the 44 gamma energy groups in Table 7a.

Groups 01-06:	1.38746E+7	1.03221E+7	8.67200E+6	7.09214E+6	6.13066E+6	5.75062E+6
Groups 07-12:	5.38195E+6	5.02370E+6	4.66673E+6	4.31279E+6	3.96312E+6	3.61826E+6
Groups 13-18:	3.27416E+6	2.93155E+6	2.58391E+6	2.35455E+6	2.23064E+6	2.10482E+6
Groups 19-24:	1.97312E+6	1.84219E+6	1.75183E+6	1.68756E+6	1.63339E+6	1.56137E+6
Groups 25-30:	1.45744E+6	1.30565E+6	1.10608E+6	9.43956E+5	8.28495E+5	7.14614E+5
Groups 31-36:	6.58371E+5	6.18704E+5	5.47134E+5	4.46919E+5	3.11940E+5	2.16874E+5
Groups 37-42:	1.74221E+5	1.84507E+5	2.20468E+5	2.58835E+5	3.80555E+5	7.63444E+5
Groups 43-44:	1.78921E+6	5.59453E+6				

* Note that above values are indeed in eV*barns, not MeV*barns as incorrectly stated in some versions of the AMPX-77 documentation for the SMUG module.

Multiply these kerma factors by 3.57554E-21 to put them in units of W*s*cm²/g, or (assuming an aluminum density of 2.70 g/cc), multiply by 9.65397E-21 to put them in units of W*s/cm. The resulting kerma factors may then be folded directly with the multigroup photon particle fluxes ($s \leftarrow \&a-20V-1 \leftarrow \&a+20V cm \leftarrow \&a-20V-2 \leftarrow \&a+20V$) to obtain the local gamma heating rates in units of W/g or W/cc.

Table D.8. Recommended "prompt" kerma factors (alone) for natural iron as given by the KAOS-V data library, extracted using the KAOS/RETRIEVE program, and expressed here in units of eV*barns for each of the 99 neutron energy groups in Table 7b.

Groups 01-07:	2.387E+06	1.542E+06	1.347E+06	8.097E+05	6.238E+05	5.023E+05	4.317E+05
Groups 08-14:	3.561E+05	2.933E+05	2.564E+05	2.259E+05	2.139E+05	1.764E+05	1.504E+05
Groups 15-21:	1.469E+05	1.292E+05	1.118E+05	1.152E+05	1.182E+05	1.102E+05	1.035E+05
Groups 22-28:	1.002E+05	7.404E+04	7.309E+04	5.553E+04	7.144E+04	7.388E+04	3.681E+04
Groups 29-35:	4.859E+04	6.040E+04	4.172E+04	2.409E+04	3.063E+04	2.615E+04	1.140E+04
Groups 36-42:	1.891E+04	7.986E+03	8.585E+03	2.426E+04	8.795E+02	1.340E+03	2.394E+03
Groups 43-49:	3.182E+03	1.175E+03	8.581E+02	6.291E+02	5.054E+02	5.125E+02	4.039E+02
Groups 50-56:	2.307E+02	1.766E+02	1.360E+02	1.023E+02	7.941E+01	6.413E+01	5.437E+01
Groups 57-63:	4.927E+01	4.625E+01	4.495E+01	4.509E+01	4.651E+01	4.884E+01	5.208E+01
Groups 64-70:	5.619E+01	6.112E+01	6.734E+01	7.470E+01	8.323E+01	9.305E+01	1.043E+02
Groups 71-77:	1.163E+02	1.163E+02	1.290E+02	1.314E+02	1.399E+02	1.557E+02	1.788E+02
Groups 78-84:	2.039E+02	2.291E+02	2.577E+02	5.236E+02	5.238E+02	5.238E+02	5.238E+02
Groups 85-91:	5.238E+02	5.238E+02	1.084E+03	1.086E+03	1.086E+03	1.086E+03	1.086E+03
Groups 92-98:	1.086E+03						
Group 99:	1.086E+03						

* Multiply these kerma factors by 1.72755E-21 to put them in units of W*s*cm²/g, or (assuming a density of 7.874 g/cc for iron), multiply by 1.36027E-20 to put them in units of W*s/cm. The resulting kerma factors may then be folded directly with the multigroup photon particle fluxes (s-&a-20V-1-&a+20Vcm-&a-20V-2-&a+20V) to obtain the local gamma heating rates in units of W/g or W/cc.

Table D.9. Recommended prompt kerma factors for natural iron plus the "charged particle" decay heat associated with its activation products as given by the KAOS-V data library, extracted using the KAOS/RETRIEVE program, and expressed here in units of eV*barns for each of the 99 neutron energy groups in Table 7b.

Groups 01-07:	2.441E+06	1.627E+06	1.434E+06	8.543E+05	6.469E+05	5.114E+05	4.336E+05
Groups 08-14:	3.562E+05	2.933E+05	2.564E+05	2.259E+05	2.139E+05	1.764E+05	1.504E+05
Groups 15-21:	1.469E+05	1.292E+05	1.118E+05	1.152E+05	1.182E+05	1.102E+05	1.035E+05
Groups 22-28:	1.002E+05	7.404E+04	7.309E+04	5.553E+04	7.144E+04	7.388E+04	3.681E+04
Groups 29-35:	4.859E+04	6.040E+04	4.172E+04	2.409E+04	3.063E+04	2.615E+04	1.140E+04
Groups 36-42:	1.891E+04	7.986E+03	8.585E+03	2.426E+04	8.795E+02	1.340E+03	2.394E+03
Groups 43-49:	3.182E+03	1.175E+03	8.581E+02	6.291E+02	5.054E+02	5.125E+02	4.039E+02
Groups 50-56:	2.307E+02	1.766E+02	1.360E+02	1.023E+02	7.941E+01	6.413E+01	5.437E+01
Groups 57-63:	4.927E+01	4.625E+01	4.495E+01	4.509E+01	4.651E+01	4.884E+01	5.208E+01
Groups 64-70:	5.619E+01	6.112E+01	6.734E+01	7.470E+01	8.323E+01	9.305E+01	1.043E+02
Groups 71-77:	1.163E+02	1.163E+02	1.290E+02	1.314E+02	1.399E+02	1.557E+02	1.788E+02
Groups 78-84:	2.039E+02	2.291E+02	2.577E+02	5.236E+02	5.238E+02	5.238E+02	5.238E+02
Groups 85-91:	5.238E+02	5.238E+02	1.084E+03	1.086E+03	1.086E+03	1.086E+03	1.086E+03
Groups 92-98:	1.086E+03						
Group 99:	1.086E+03						

* Multiply these kerma factors by 1.72755E-21 to put them in units of W*s*cm²/g, or (assuming a density of 7.874 g/cc for iron), multiply by 1.36027E-20 to put them in units of W*s/cm. The resulting kerma factors may then be folded directly with the multigroup photon particle fluxes (s-&a-20V-1-&a+20Vcm-&a-20V-2-&a+20V) to obtain the local gamma heating rates in units of W/g or W/cc.

Table D.10. Recommended prompt kerma factors for natural iron plus the "total decay heat" associated with either charged particle or gamma decay (of all isotopes produced by neutron activation) as given by the KAOS-V data library, extracted using the KAOS/RETRIEVE program, and expressed here in units of eV*barns for each of the 99 neutron energy groups in Table 7b.

Groups 01-07:	2.566E+06	1.836E+06	1.650E+06	9.639E+05	7.037E+05	5.336E+05	4.383E+05
Groups 08-14:	3.565E+05	2.933E+05	2.564E+05	2.259E+05	2.139E+05	1.764E+05	1.504E+05
Groups 15-21:	1.469E+05	1.292E+05	1.118E+05	1.152E+05	1.182E+05	1.102E+05	1.035E+05
Groups 22-28:	1.002E+05	7.404E+04	7.309E+04	5.553E+04	7.144E+04	7.388E+04	3.681E+04
Groups 29-35:	4.859E+04	6.040E+04	4.172E+04	2.409E+04	3.063E+04	2.615E+04	1.140E+04
Groups 36-42:	1.891E+04	7.986E+03	8.585E+03	2.426E+04	8.795E+02	1.340E+03	2.394E+03
Groups 43-49:	3.182E+03	1.175E+03	8.581E+02	6.291E+02	5.054E+02	5.125E+02	4.039E+02
Groups 50-56:	2.307E+02	1.766E+02	1.360E+02	1.023E+02	7.941E+01	6.413E+01	5.437E+01
Groups 57-63:	4.927E+01	4.625E+01	4.495E+01	4.509E+01	4.651E+01	4.884E+01	5.208E+01
Groups 64-70:	5.619E+01	6.112E+01	6.734E+01	7.470E+01	8.323E+01	9.305E+01	1.043E+02
Groups 71-77:	1.163E+02	1.163E+02	1.290E+02	1.314E+02	1.399E+02	1.557E+02	1.788E+02
Groups 78-84:	2.039E+02	2.291E+02	2.577E+02	5.236E+02	5.238E+02	5.238E+02	5.238E+02
Groups 85-91:	5.238E+02	5.238E+02	1.084E+03	1.086E+03	1.086E+03	1.086E+03	1.086E+03
Groups 92-98:	1.086E+03						
Group 99:	1.086E+03						

* Multiply these kerma factors by 1.72755E-21 to put them in units of W*s*cm²/g, or (assuming a density of 7.874 g/cc for iron), multiply by 1.36027E-20 to put them in units of W*s/cm. The resulting kerma factors may then be folded directly with the multigroup photon particle fluxes (s-&a-20V-1-&a+20Vcm-&a-20V-2-&a+20V) to obtain the local gamma heating rates in units of W/g or W/cc.

Table D.11. Recommended "prompt" kerma factors (alone) for natural iron as given by the KAOS-V data library, extracted using the KAOS/RETRIEVE program, and expressed here in units of eV*barns for each of the 39 neutron energy groups in Table 7a.

Groups 01-07:	1.538E+06	3.382E+05	1.818E+05	1.169E+05	8.127E+04	5.822E+04	2.679E+04
Groups 08-14:	1.207E+04	1.795E+03	4.564E+02	1.118E+02	4.797E+01	5.292E+01	8.452E+01
Groups 15-21:	1.266E+02	1.557E+02	1.788E+02	2.039E+02	2.291E+02	2.577E+02	5.236E+02
Groups 22-28:	5.238E+02	5.238E+02	5.238E+02	5.238E+02	5.238E+02	1.084E+03	1.086E+03
Groups 29-35:	1.086E+03						
Groups 36-39:	1.086E+03	1.086E+03	1.086E+03	1.086E+03			

* Multiply these kerma factors by 1.72755E-21 to put them in units of W*s*cm²/g, or (assuming a density of 7.874 g/cc for iron), multiply by 1.36027E-20 to put them in units of W*s/cm. The resulting kerma factors may then be folded directly with the multigroup photon particle fluxes (s-&a-20V-1-&a+20Vcm-&a-20V-2-&a+20V) to obtain the local gamma heating rates in units of W/g or W/cc.

Table D.12. Recommended prompt kerma factors for natural iron plus the "charged particle" decay heat associated with its activation products as given by the KAOS-V data library, extracted using the KAOS/RETRIEVE program, and expressed here in units of eV*barns for each of the 39 neutron energy groups in Table 7a.

Groups 01-07:	1.623E+06	3.395E+05	1.818E+05	1.169E+05	8.127E+04	5.822E+04	2.679E+04
Groups 08-14:	1.207E+04	1.795E+03	4.564E+02	1.118E+02	4.797E+01	5.292E+01	8.452E+01
Groups 15-21:	1.266E+02	1.557E+02	1.788E+02	2.039E+02	2.291E+02	2.577E+02	5.236E+02
Groups 22-28:	5.238E+02	5.238E+02	5.238E+02	5.238E+02	5.238E+02	1.084E+03	1.086E+03
Groups 29-35:	1.086E+03						
Groups 36-39:	1.086E+03	1.086E+03	1.086E+03	1.086E+03			

* Multiply these kerma factors by 1.72755E-21 to put them in units of W*s*cm²/g, or (assuming a density of 7.874 g/cc for iron), multiply by 1.36027E-20 to put them in units of W*s/cm. The resulting kerma factors may then be folded directly with the multigroup photon particle fluxes (s-&a-20V-1-&a+20Vcm-&a-20V-2-&a+20V) to obtain the local gamma heating rates in units of W/g or W/cc.

Table D.13. Recommended prompt kerma factors for natural iron plus the "total decay heat" associated with either charged particle or gamma decay (of all isotopes produced by neutron activation) as given by the KAOS-V data library, extracted using the KAOS/RETRIEVE program, and expressed here in units of eV*barns for each of the 39 neutron energy groups in Table 7a.

Groups 01-07:	1.832E+06	3.426E+05	1.818E+05	1.169E+05	8.127E+04	5.822E+04	2.679E+04
Groups 08-14:	1.207E+04	1.795E+03	4.564E+02	1.118E+02	4.797E+01	5.292E+01	8.452E+01
Groups 15-21:	1.266E+02	1.557E+02	1.788E+02	2.039E+02	2.291E+02	2.577E+02	5.236E+02
Groups 22-28:	5.238E+02	5.238E+02	5.238E+02	5.238E+02	5.238E+02	1.084E+03	1.086E+03
Groups 29-35:	1.086E+03						
Groups 36-39:	1.086E+03	1.086E+03	1.086E+03	1.086E+03			

* Multiply these kerma factors by 1.72755E-21 to put them in units of W*s*cm²/g, or (assuming a density of 7.874 g/cc for iron), multiply by 1.36027E-20 to put them in units of W*s/cm. The resulting kerma factors may then be folded directly with the multigroup photon particle fluxes ($s \leftarrow \&a-20V-1 \leftarrow \&a+20Vcm \leftarrow \&a-20V-2 \leftarrow \&a+20V$) to obtain the local gamma heating rates in units of W/g or W/cc.

Table D.14. Kerma factors for gammas interacting with natural iron as calculated by the SMUG module of the AMPX cross section processing code system, stored in the ANSL-V 39n/44g cross section library (as nuclide 26000, MT-process 1527), subsequently extracted using the PAL module of the AMPX code system, and expressed here in units of eV*barns for each of the 44 gamma energy groups in Table 7a.

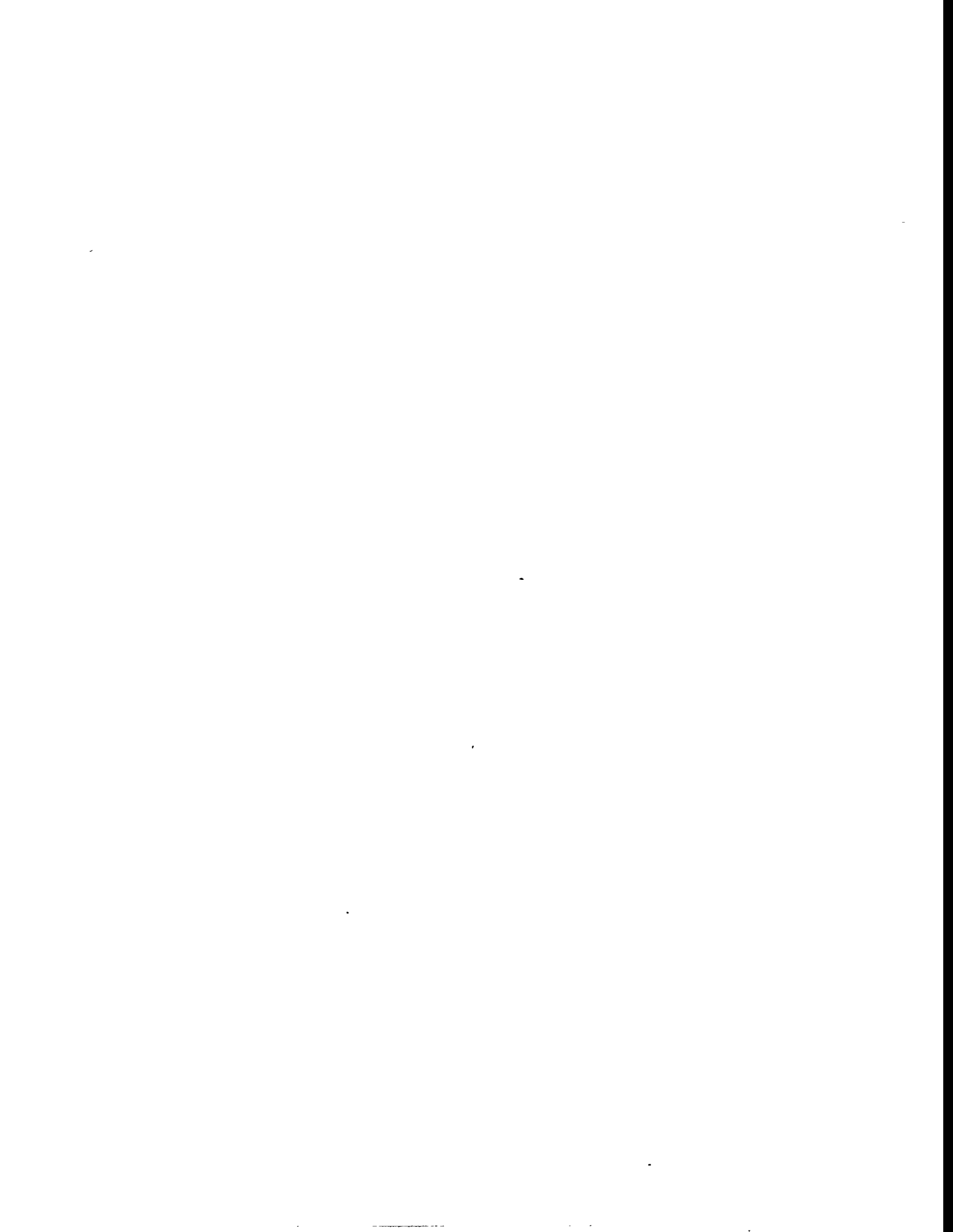
Groups 01-06:	4.31796E+7	3.05255E+7	2.47625E+7	1.93491E+7	1.61191E+7	1.48642E+7
Groups 07-12:	1.36644E+7	1.25180E+7	1.13934E+7	1.02998E+7	9.24415E+6	8.23349E+6
Groups 13-18:	7.25893E+6	6.33163E+6	5.43705E+6	4.87544E+6	4.58792E+6	4.30420E+6
Groups 19-24:	4.01092E+6	3.72796E+6	3.53859E+6	3.40605E+6	3.29282E+6	3.14597E+6
Groups 25-30:	2.93932E+6	2.63895E+6	2.24611E+6	1.93008E+6	1.70814E+6	1.49331E+6
Groups 31-36:	1.38939E+6	1.31812E+6	1.19326E+6	1.03602E+6	9.00130E+5	9.87179E+5
Groups 37-42:	1.47901E+6	2.67975E+6	3.76936E+6	4.69598E+6	7.28250E+6	1.44207E+7
Groups 43-44:	3.13706E+7	8.45638E+7				

* Note that above values are indeed in eV*barns, not MeV*barns as incorrectly stated in some versions of the AMPX-77 documentation for the SMUG module.

Multiply these kerma factors by 1.72755E-21 to put them in units of W*s*cm²/g, or (assuming a density of 7.874 g/cc for iron), multiply by 1.36027E-20 to put them in units of W*s/cm. The resulting kerma factors may then be folded directly with the multigroup photon particle fluxes ($s \leftarrow \&a-20V-1 \leftarrow \&a+20Vcm \leftarrow \&a-20V-2 \leftarrow \&a+20V$) to obtain the local gamma heating rates in units of W/g or W/cc.

APPENDIX E

Tabulated numerical results at particular points of interest.



E. TABULATED NUMERICAL RESULTS AT PARTICULAR POINTS OF INTEREST

DORT Run 5, as described in Sect. 6, is considered the final reference solution. It uses the revised spatial mesh shown in Fig. 3; it includes delayed fission gammas; and, most notably, it includes the effect of photoneutron production in the D₂O. Plots showing the corresponding neutron fluxes for each of four broad energy groups

- A: E ≥ 0.1 MeV ,
- B: 100 eV ≤ E ≤ 0.1 MeV ,
- C: 0.625 eV ≤ E ≤ 100 eV ,
- D: E ≤ 0.625 eV .

are shown in Sect. 6 (cf. Figs. 10a-10d). Other plots included there (Figs. 10e-10h) show the gamma flux above 2.15 MeV, the total gamma flux (summed over all energies), the neutron dose rate in mrem/h, and the gamma dose rate in mrem/h. Some qualitative discussion of these results is also provided at the end of Sect. 6. More precise numerical results at 761 particular points of interest are presented here in Appendix E. These points are denoted by small black squares superimposed on the original material mesh map, as shown in Figs. E1a-E1h. For easier reference, these results have been organized into 26 different tables:

Table Description

E.01	Radial trace along top of reflector vessel (at mid-thickness)
E.02	Radial trace about 1.20 m above the midplane
E.03	Radial trace about 0.30 m above the midplane, roughly halfway up the upper fuel element
E.04	Radial trace exactly at the axial midplane (by HB-1,2,3,4 and HB-6,7,8,9)
E.05	Radial trace about 0.30 m below the midplane, by the horizontal through tube (HB-5 / HB-10), roughly halfway up bottom fuel element
E.06	Radial trace about 1.20 m below the midplane
E.07	Radial trace along bottom of reflector vessel (at mid-thickness)
E.08	Partial axial trace along system centerline
E.09	Partial axial trace near inner surface of lower fuel element
E.10	Full axial trace at radial midpoint of lower (inner) fuel element
E.11	Partial axial trace near outer surface of lower fuel element
E.12	Partial axial trace near inner surface of upper fuel element
E.13	Full axial trace at radial midpoint of upper (outer) fuel element
E.14	Partial axial trace near outer surface of upper fuel element
E.15	Partial axial trace corresponding to radial location for lower portion of HT-2
E.16	Partial axial trace corresponding to radial location for lower portion of SH-1 and SH-2
E.17	Partial axial trace corresponding to radial location for lower portion of HT-4
E.18	Full axial trace at radial location corresponding to HT-1 and HT-3
E.19	Axial trace up through VT-1,2,3,4
E.20	Axial trace up through PT-1
E.21	Axial trace through side of reflector vessel (at mid-thickness)
E.22	Partial axial trace corresponding to radial location for lower portion of PF-1
E.23	Partial axial trace corresponding to radial location for lower portion of PF-2
E.24	Trace along axis of the long slanted beam tube (LSBT)
E.25	Trace along axis of PT-2 and PT-5
E.26	Trace along axis of PT-3 and PT-4

Each of the 26 tables show:

IR,JZ the radial and axial mesh intervals corresponding to the results

R the radial location (in mm) corresponding to the center of that mesh interval

Z the axial location (in mm) corresponding to the center of that mesh interval relative to the core midplane as shown in Fig. 1a

Note: In the actual DORT input data and the computer generated flux files that have since been archived to tape, R and Z are necessarily given in cm (not mm), and the core midplane was located at Z=227.2 cm. Also, those fluxes are in terms of neutrons or photons per second, per square centimeter. This is significant only if one needs to access that data in the future.

FLUX-A . . . neutron flux ($s^{-1}m^{-2}$) for $E \geq 0.1$ MeV

FLUX-B . . . neutron flux ($s^{-1}m^{-2}$) for 100 eV $\leq E \leq 0.1$ MeV

FLUX-C . . . neutron flux ($s^{-1}m^{-2}$) for 0.625 eV $\leq E \leq 100$ eV

FLUX-D . . . neutron flux ($s^{-1}m^{-2}$) for $E \leq 0.625$ eV

GFLUX>2 . . . gamma (photon) flux ($s^{-1}m^{-2}$) for $E \geq 2.15$ MeV (gamma groups 1 to 17)

DOSE-N . . . neutron dose rate (mrem/h) due to neutrons of all energies

DOSE-G . . . gamma dose rate (mrem/h) due to gammas of all energies

DPA1/Y . . . displacements per atom per year (365.25 days at full power) in a ferritic test specimen (irradiation sample) if located here and the flux remained unperturbed; based on the standard ASTM dpa function (cf. ASTM Std. E693-79).

HT RATE . . . total neutron plus gamma heat generation rate (watts/gm) in aluminum that would exist at this location; includes the gamma heating rate plus the total neutron heating rate due to the basic prompt kerma factor plus the total (charged particle+gamma) decay energy due to temporary neutron activation of the aluminum.

While all of the above data have been provided at all 761 points of interest, the data must be interpreted with caution. Obviously the heating rates would apply to points located on the body of the aluminum reflector vessel or in the body of the core boundary pressure tube, but they would not apply to points in the D₂O reflector or in the core where there is no aluminum. Likewise, the dpa values cited here would apply to small steel irradiation specimens that one might insert at various locations, but they are certainly not applicable to the aluminum in the vessel, for example. Likewise, it must also be noted that these values (based on the lifetime-averaged power distribution described in Sect. 3 and the fixed geometric model described in Sect. 2) are also based on the unperturbed fluxes at the point of interest. Insertion of a large (thick) irradiation specimen in a thick-walled capsule would certainly depress the flux levels locally and result in somewhat lower dpa values. Likewise, the motion of the outer control rods above the core (not modeled here) and/or the motion of the central control rod (modeled here in a fixed location) would affect the fluxes and hence the dpa values close to the centerline of the system.

Lastly, the neutron and gamma dose rates tabulated here must be interpreted with extreme caution. Note that the dose rates tabulated here at each location are based on the unperturbed fluxes that would exist if, for example, the beam tubes did not exist or were flooded with heavy water. Inside a large 200 mm x 100 mm beam tube extending inward toward the center of the core, for example, the dose rates would actually be much closer to those that would exist at the hot end of the beam tube close to the core. Moreover, down along the inside of the beam tube (far from the hot end), the actual neutron and gamma dose rates will tend to vary as $[D_o \pi r^2 / (4\pi X^2)]$ where r is the effective radius of the beam tube ($r=0.5\sqrt{ab}$, where "a" and "b" are the major and minor diameters of an elliptically shaped beam tube), D_o is the dose rate at the hot end of the beam tube, and X is the distance down along the beam tube from the hot end to the point of interest ($X \gg r$). Appendix F, for example, discusses a simple solid angle routine for estimating fluxes and dose rates down a long void-filled beam tube based on the unperturbed fluxes at the hot end and along the surface of the beam tube. [More precise calculations may also be made using the VISTA and DTD codes^{20,21} in conjunction with a second DORT calculation along the axis of the beam tube.] The point here is that while the unperturbed fluxes and dose rates at the hot end of a beam tube (as tabulated below) may be useful for some applications at some future time, the fluxes and dose rates along the axis of a (flooded) beam tube as given here are certainly not applicable to an empty beam tube where the fluxes and dose rates would be considerably higher. Within the context of the above remarks and limitations, however, it is hoped that the broad range of detailed results presented here will be useful to a broad range of interested parties, including designers and experimenters alike.

66
65
64
63
62
61
60
59
58
57
56
55
54
53
52
51
50
49
48
47
46
45
44
43
42
41
40
39
38
37
36
35
34
33
32
31
30
29
28
27
26
25
24
23
22
21

Fig. E.1a. Points of particular interest in the global 2-D RZ analysis of the ANS core and reflector vessel in DORT Run 5 ($Ir=1$ to 138, $Jz=1$ to 266). This is similar to Fig. 3 except that the small solid black squares shown here denote particular points at which tabulated results are presented in Tables E.1 to E.26. For a description of each material and the coordinates at each point, see Tables 2 and 4.

Fig. E.1b. Points of particular interest in the global 2-D RZ analysis of the ANS core and reflector vessel in DORT Run 5 ($I_1=1$ to 138, $J_2=1$ to 266). This is similar to Fig. 3 except that the small solid black squares shown here denote particular points at which tabulated results are presented in Tables E.1 to E.26. For a description of each material and the coordinates at each point, see Tables 2 and 4.

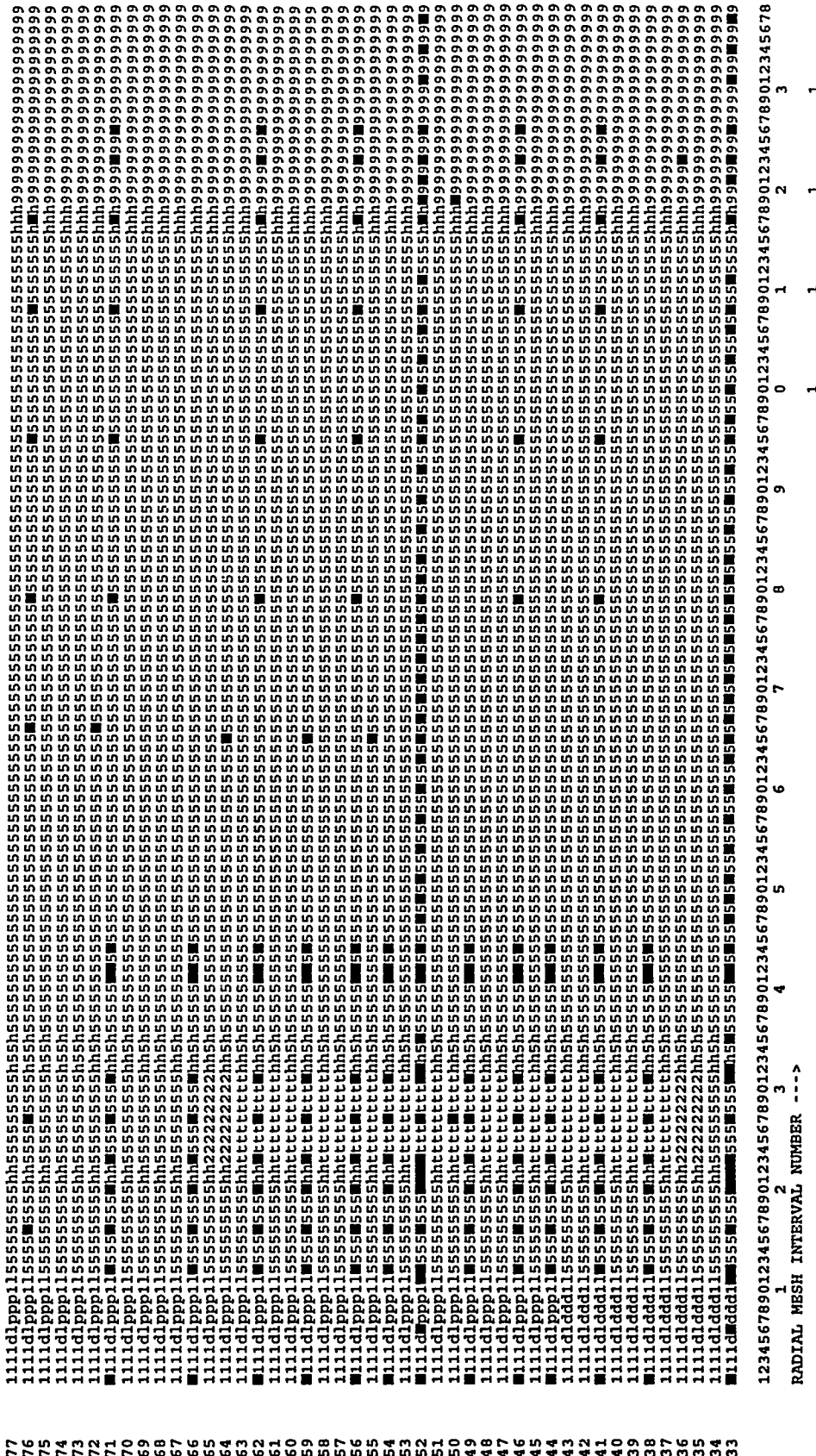


Fig. E.1c. Points of particular interest in the global 2-D RZ analysis of the ANS core and reflector vessel in DORT Run 5 (Ir=1 to 138, Jz=1 to 266). This is similar to Fig. 3 except that the small solid black squares shown here denote particular points at which tabulated results are presented in Tables E.1 to E.26. For a description of each material and the coordinates at each point, see Tables 2 and 4.

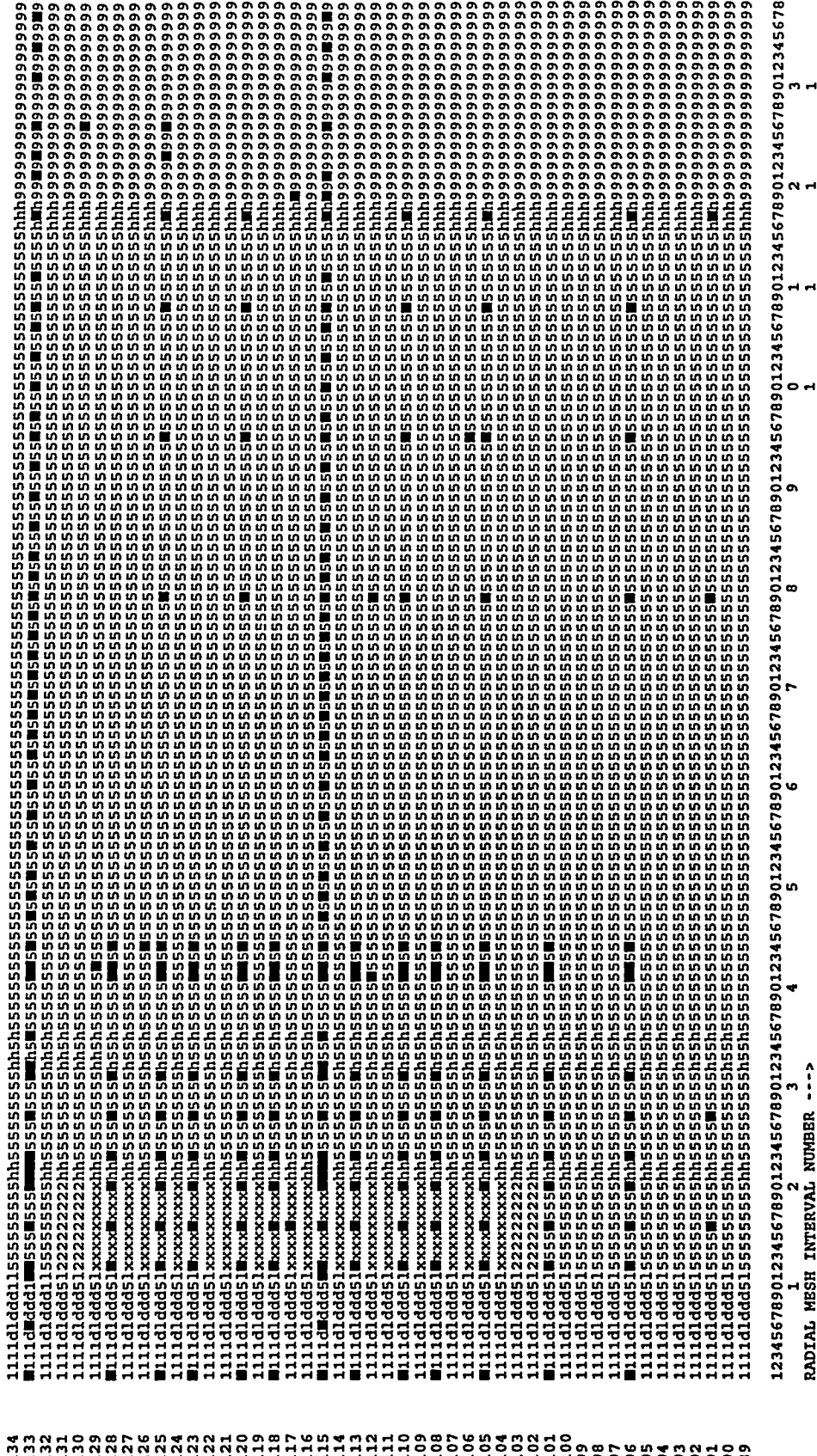


Fig. E.1d. Points of particular interest in the global 2-D RZ analysis of the ANS core and reflector vessel in DORT Run 5 ($1r=1$ to 138, $Jz=1$ to 266). This is similar to Fig. 3 except that the small solid black squares shown here denote particular points at which tabulated results are presented in Tables E.1 to E.26. For a description of each material and the coordinates at each point, see Tables 2 and 4.

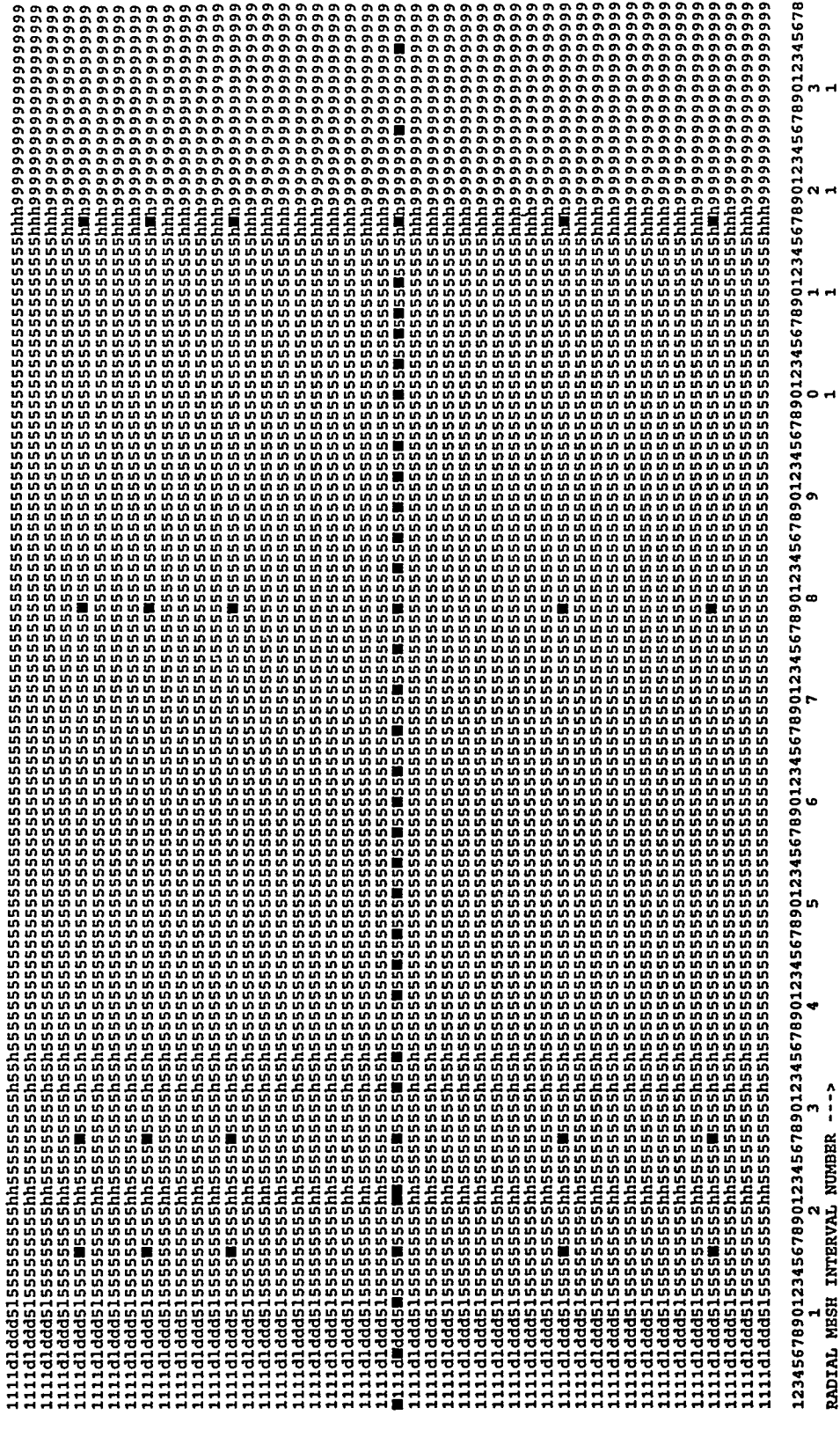


Fig. E.1e. Points of particular interest in the global 2-D RZ analysis of the ANS core and reflector vessel in DORT Run 5 (Ir=1 to 138, Jz=1 to 266). This is similar to Fig. 3 except that the small solid black squares shown here denote particular points at which tabulated results are presented in Tables E.1 to E.26. For a description of each material and the coordinates at each point, see Tables 2 and 4.

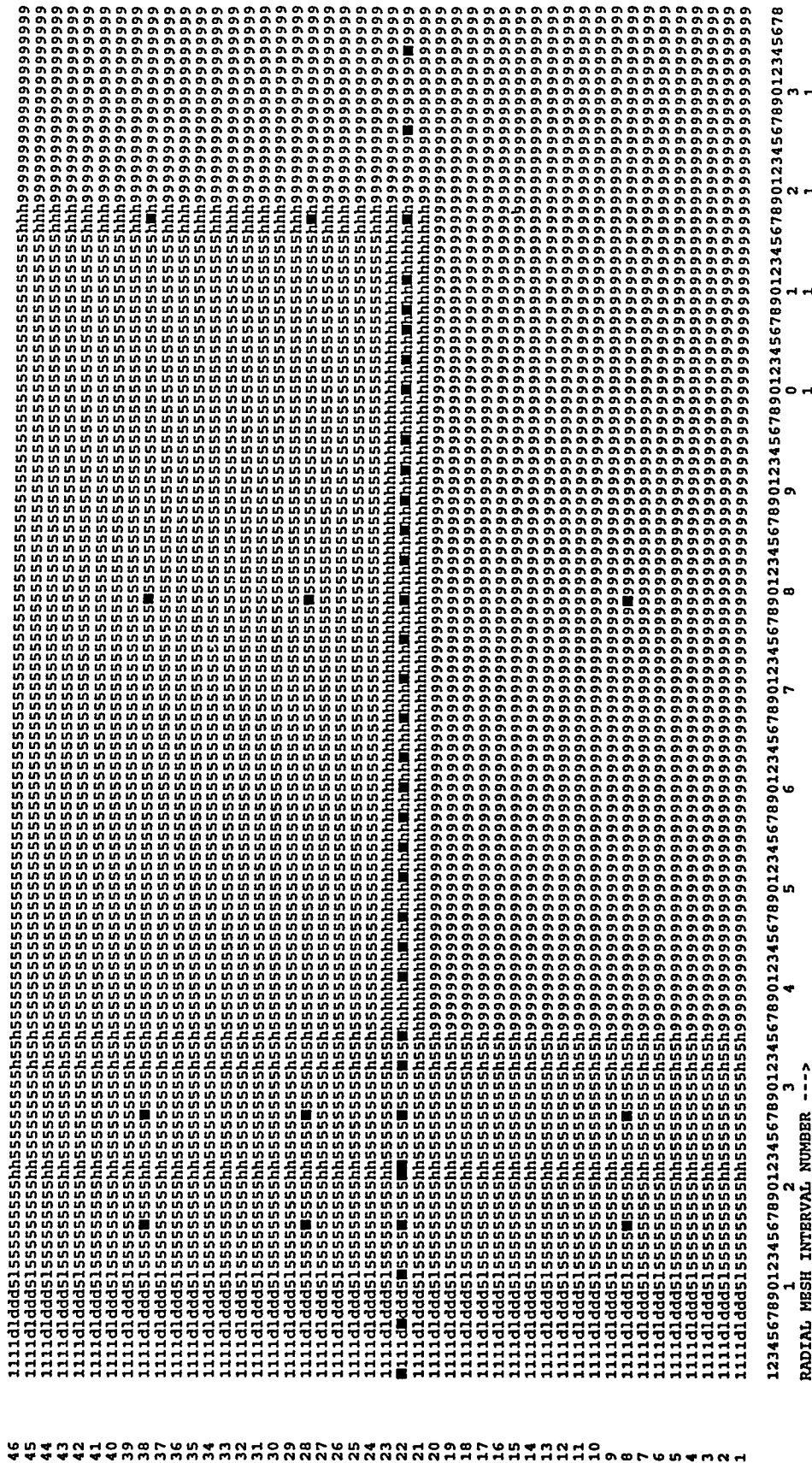


Fig. E.1f. Points of particular interest in the global 2-D RZ analysis of the ANS core and reflector vessel in DORT Run 5 ($I_1=1$ to 138, $J_1=1$ to 266). This is similar to Fig. 3 except that the small solid black squares shown here denote particular points at which tabulated results are presented in Tables E.1 to E.26. For a description of each material and the coordinates at each point, see Tables 2 and 4.

Table E.01. Radial trace along top of reflector vessel (at mid-thickness).

IR	JZ	R	Z mm	FLUX-A s ⁻¹ m ⁻²	FLUX-B s ⁻¹ m ⁻²	FLUX-C s ⁻¹ m ⁻²	FLUX-D s ⁻¹ m ⁻²	GFLUX>2 s ⁻¹ m ⁻²	DOSE-N mrem/h	DOSE-G mrem/h	DPA/Y dp/gyr	HT RATE Watts/g
1	245	9.4	2057.0	6.133E+13	1.615E+14	1.135E+14	3.854E+17	3.011E+16	1.428E+11	2.445E+10	1.193E-02	1.437E-01
6	245	79.6	2057.0	6.308E+13	1.578E+14	1.084E+14	3.722E+17	3.614E+16	1.380E+11	2.780E+10	1.140E-02	1.490E-01
11	245	98.5	2057.0	6.295E+13	1.566E+14	1.071E+14	3.760E+17	3.588E+16	1.394E+11	2.808E+10	1.153E-02	1.509E-01
16	245	135.0	2057.0	6.207E+13	1.512E+14	1.024E+14	3.941E+17	3.205E+16	1.450E+11	2.601E+10	1.218E-02	1.502E-01
21	245	169.7	2057.0	6.157E+13	1.421E+14	9.524E+13	3.954E+17	3.650E+16	1.465E+11	2.856E+10	1.216E-02	1.566E-01
22	245	173.2	2057.0	6.156E+13	1.421E+14	9.495E+13	3.953E+17	3.659E+16	1.444E+11	2.857E+10	1.216E-02	1.567E-01
27	245	205.0	2057.0	5.897E+13	1.293E+14	8.710E+13	4.075E+17	3.513E+16	1.509E+11	2.760E+10	1.257E-02	1.570E-01
32	245	237.5	2057.0	5.362E+13	1.112E+14	7.763E+13	4.081E+17	4.445E+16	1.511E+11	3.300E+10	1.245E-02	1.701E-01
35	245	249.0	2057.0	5.061E+13	1.046E+14	7.486E+13	4.115E+17	5.089E+16	1.523E+11	3.678E+10	1.249E-02	1.801E-01
41	245	313.0	2057.0	3.787E+13	7.931E+13	6.066E+13	4.420E+17	6.052E+16	1.634E+11	4.200E+10	1.335E-02	1.995E-01
44	245	372.9	2057.0	3.383E+13	6.788E+13	5.170E+13	4.700E+17	6.141E+16	1.737E+11	4.224E+10	1.419E-02	2.062E-01
47	245	432.7	2057.0	3.189E+13	6.128E+13	4.582E+13	4.947E+17	6.231E+16	1.828E+11	4.253E+10	1.493E-02	2.123E-01
51	245	512.5	2057.0	2.939E+13	5.572E+13	4.033E+13	5.189E+17	6.752E+16	1.907E+11	4.251E+10	1.566E-02	2.177E-01
54	245	572.4	2057.0	2.939E+13	5.279E+13	3.729E+13	5.297E+17	6.315E+16	1.957E+11	4.257E+10	1.598E-02	2.202E-01
57	245	632.3	2057.0	2.833E+13	4.999E+13	3.479E+13	5.346E+17	6.263E+16	1.955E+11	4.202E+10	1.613E-02	2.199E-01
60	245	692.2	2057.0	2.724E+13	4.761E+13	3.282E+13	5.338E+17	6.113E+16	1.972E+11	4.088E+10	1.610E-02	2.170E-01
63	245	752.0	2057.0	2.631E+13	4.546E+13	3.073E+13	5.277E+17	5.997E+16	1.992E+11	3.999E+10	1.592E-02	2.135E-01
67	245	831.9	2057.0	2.500E+13	4.273E+13	2.897E+13	5.122E+17	5.752E+16	1.882E+11	3.824E+10	1.545E-02	2.058E-01
71	245	911.7	2057.0	2.364E+13	4.017E+13	2.697E+13	4.895E+17	5.485E+16	1.808E+11	3.639E+10	1.476E-02	1.963E-01
75	245	991.5	2057.0	2.217E+13	3.750E+13	2.512E+13	4.607E+17	5.168E+16	1.720E+11	3.427E+10	1.389E-02	1.848E-01
79	245	1071.3	2057.0	2.064E+13	3.503E+13	2.331E+13	4.270E+17	4.780E+16	1.577E+11	3.170E+10	1.288E-02	1.711E-01
83	245	1151.2	2057.0	1.887E+13	3.220E+13	2.150E+13	3.920E+17	4.046E+16	1.498E+11	2.905E+10	1.174E-02	1.564E-01
86	245	1211.1	2057.0	1.751E+13	2.986E+13	2.005E+13	3.589E+17	4.046E+16	1.323E+11	2.687E+10	1.082E-02	1.444E-01
89	245	1270.9	2057.0	1.607E+13	2.763E+13	1.869E+13	3.273E+17	3.706E+16	1.209E+11	2.466E+10	9.875E-03	1.320E-01
92	245	1330.8	2057.0	1.495E+13	2.595E+13	1.760E+13	2.948E+17	3.363E+16	1.089E+11	2.246E+10	8.893E-03	1.195E-01
95	245	1390.7	2057.0	1.359E+13	2.376E+13	1.616E+13	2.614E+17	3.021E+16	9.652E+10	2.024E+10	7.889E-03	1.068E-01
100	245	1490.5	2057.0	1.134E+13	2.045E+13	1.401E+13	2.056E+17	2.456E+16	7.598E+10	1.660E+10	6.206E-03	8.563E-02
103	245	1550.3	2057.0	1.029E+13	1.857E+13	1.271E+13	1.721E+17	2.123E+16	6.361E+10	1.447E+10	5.196E-03	7.307E-02
106	245	1610.2	2057.0	9.053E+12	1.620E+13	1.101E+13	1.396E+17	1.822E+16	5.160E+10	1.254E+10	4.216E-03	6.119E-02
108	245	1650.1	2057.0	8.115E+12	1.421E+13	9.544E+12	1.186E+17	1.608E+16	4.382E+10	1.117E+10	3.583E-03	5.321E-02
111	245	1705.0	2057.0	6.517E+12	1.085E+13	7.370E+12	9.171E+16	1.362E+16	1.011E+16	2.588E+10	9.547E+09	4.330E-02
117	245	1762.5	2057.0	3.496E+12	6.542E+12	4.932E+12	7.006E+16	1.011E+16	1.011E+16	2.588E+10	6.983E+09	2.122E-03
126	245	1853.0	2057.0	2.495E+11	2.358E+11	2.371E+11	3.592E+15	5.665E+15	1.327E+09	4.127E+09	1.103E-04	1.077E-02
134	245	1936.2	2057.0	3.530E+10	2.619E+10	2.175E+10	1.989E+14	3.203E+15	7.376E+07	2.595E+09	6.151E-06	6.341E-03

See text in Appendix E for a more complete description of the parameters, the associated energy ranges, and any applicable caveats.

Table E.02. Radial trace about 1.20 m above the midplane.

IR	JZ	R mm	Z mm	FLUX-A s ⁻¹ m ⁻²	FLUX-B s ⁻¹ m ⁻²	FLUX-C s ⁻¹ m ⁻²	FLUX-D s ⁻¹ m ⁻²	GFLUX>2 s ⁻¹ m ⁻²	DOSE-N mrem/h	DOSE-G mrem/h	DPA/I/Y dpa/y _r	HT RATE Watts/g
1	200	9.4	1199.4	1.277E+15	3.997E+15	2.050E+15	8.425E+16	5.623E+17	4.575E+10	5.322E+11	4.777E-03	1.239E+00
6	200	79.6	1199.4	1.279E+15	3.308E+15	8.885E+14	4.553E+16	6.656E+17	3.067E+10	5.991E+11	3.384E-03	1.385E+00
11	200	98.5	1199.4	1.255E+15	3.780E+15	3.254E+15	1.315E+18	7.147E+17	5.003E+11	6.294E+11	4.148E-02	1.751E+00
16	200	135.0	1199.4	1.199.4	1.255E+15	4.001E+15	4.978E+15	1.024E+12	4.328E+11	8.582E-02	1.623E+00	
21	200	169.7	1199.4	1.067E+15	4.048E+15	5.962E+15	3.721E+18	4.428E+17	1.387E+12	3.954E+11	1.154E-01	1.759E+00
22	200	173.2	1199.4	1.090E+15	4.050E+15	5.958E+15	3.748E+18	4.292E+17	1.397E+12	3.832E+11	1.163E-01	1.737E+00
27	200	205.0	1199.4	9.900E+14	3.738E+15	6.003E+15	4.564E+18	3.799E+17	6.697E+12	3.431E+11	1.417E-01	1.830E+00
32	200	237.5	1199.4	9.219E+14	3.587E+15	6.125E+15	5.58E+18	4.053E+17	9.915E+12	3.454E+11	1.589E-01	1.963E+00
35	200	249.0	1199.4	8.893E+14	3.521E+15	6.083E+15	5.296E+18	3.826E+17	9.966E+12	3.256E+11	1.622E-01	1.955E+00
41	200	313.0	1199.4	6.448E+14	2.488E+15	4.433E+15	6.729E+18	2.081E+17	2.491E+12	2.069E+11	2.082E-01	1.994E+00
44	200	372.9	1199.4	5.015E+14	1.820E+15	3.229E+15	7.664E+18	1.583E+17	2.833E+12	1.684E+11	2.369E-01	2.108E+00
47	200	432.7	1199.4	3.687E+14	2.297E+15	8.291E+15	8.291E+18	1.274E+17	3.059E+12	1.394E+11	2.556E-01	2.173E+00
51	200	512.5	1199.4	2.519E+14	8.717E+14	1.426E+14	8.717E+18	8.628E+16	3.218E+12	9.948E+10	2.684E-01	2.175E+00
54	200	572.4	1199.4	1.925E+14	6.344E+14	9.854E+14	8.818E+18	6.976E+16	3.254E+12	8.154E+10	2.718E-01	2.150E+00
57	200	632.3	1199.4	1.577E+14	4.781E+14	6.766E+14	8.767E+18	6.224E+16	3.235E+12	7.133E+10	2.701E-01	2.113E+00
60	200	692.2	1199.4	1.288E+14	3.775E+14	4.695E+14	8.544E+18	5.385E+16	3.171E+12	6.099E+10	2.647E-01	2.048E+00
63	200	752.0	1199.4	1.060E+14	2.975E+14	3.381E+14	8.326E+18	4.560E+16	3.072E+12	5.165E+10	2.556E-01	1.965E+00
67	200	831.9	1199.4	8.614E+13	2.241E+14	2.291E+14	7.859E+18	4.049E+16	2.899E+12	4.343E+10	2.421E-01	1.842E+00
71	200	911.7	1199.4	6.880E+13	1.778E+14	1.621E+14	7.304E+18	2.971E+16	2.694E+12	3.326E+10	2.249E-01	1.694E+00
75	200	991.5	1199.4	5.749E+13	1.474E+14	1.261E+14	6.691E+18	2.650E+16	2.468E+12	2.842E+10	2.060E-01	1.546E+00
76	200	1011.5	1199.4	5.549E+13	1.387E+14	1.182E+14	6.532E+18	2.605E+16	2.409E+12	2.764E+10	2.010E-01	1.507E+00
79	200	1071.3	1199.4	5.004E+13	1.232E+14	1.020E+14	6.045E+18	2.482E+16	2.230E+12	2.542E+10	1.861E-01	1.396E+00
83	200	1151.2	1199.4	4.371E+13	1.066E+14	8.661E+13	5.383E+18	2.102E+16	1.986E+12	2.117E+10	1.658E-01	1.240E+00
86	200	1211.1	1199.4	4.602E+13	9.800E+13	7.930E+13	7.304E+18	1.954E+16	1.802E+12	1.928E+10	1.504E-01	1.125E+00
89	200	1270.9	1199.4	3.726E+13	9.190E+13	4.339E+13	4.398E+18	1.812E+16	1.812E+12	1.758E+10	1.351E-01	1.012E+00
92	200	1330.8	1199.4	3.620E+13	8.819E+13	7.056E+13	3.898E+18	1.794E+16	1.438E+12	1.722E+10	1.200E-01	9.028E+00
95	200	1390.7	1199.4	3.495E+13	8.695E+13	6.979E+13	3.415E+18	1.846E+16	1.260E+12	1.728E+10	1.052E-01	7.964E-01
100	200	1490.5	1199.4	3.596E+13	9.131E+13	7.057E+13	2.632E+18	1.945E+16	9.714E+11	1.775E+10	8.110E-02	6.250E-01
103	200	1550.3	1199.4	3.981E+13	9.768E+13	7.151E+13	2.177E+18	2.202E+16	8.035E+11	1.939E+10	6.709E-02	5.286E-01
106	200	1610.2	1199.4	4.375E+13	1.028E+14	6.902E+13	1.734E+18	2.636E+16	6.399E+11	2.223E+10	5.344E-02	4.376E-01
108	200	1650.1	1199.4	4.794E+13	1.028E+14	6.381E+13	1.444E+18	3.118E+16	5.334E+11	2.523E+10	4.454E-02	3.811E-01
111	200	1705.0	1199.4	5.210E+13	8.804E+13	5.033E+13	1.055E+18	4.290E+16	3.896E+11	3.221E+10	3.251E-02	3.120E-01
117	200	1762.5	1199.4	2.987E+13	5.033E+13	3.368E+13	6.976E+16	2.576E+17	7.415E+11	4.847E+10	2.110E-02	2.714E-01
126	200	1853.0	1199.4	1.940E+12	1.789E+12	1.843E+12	3.873E+16	4.531E+16	1.430E+10	2.950E+10	1.186E-03	7.987E-02
134	200	1936.2	1199.4	2.658E+11	1.931E+11	1.589E+11	1.912E+15	2.189E+16	7.084E+08	1.626E+10	5.895E-05	3.985E-02

See text in Appendix E for a more complete description of the parameters, the associated energy ranges, and any applicable caveats.

Table E.03. Radial trace about 0.30 m above the midplane, roughly half way up the upper fuel element.

IR	JZ	R mm	Z mm	FLUX-A s ⁻¹ m ⁻²	FLUX-B s ⁻¹ m ⁻²	FLUX-C s ⁻¹ m ⁻²	FLUX-D s ⁻¹ m ⁻²	GFLUX>2 s ⁻¹ m ⁻²	DOSE-N mmr/h	DOSE-G mmr/h	DPA/Y dp/yr	HT RATE Watts/g
1	152	9.4	308.5	6.359E+18	2.381E+19	8.344E+18	3.686E+18	9.900E+18	7.634E+13	1.203E+13	1.309E+01	2.831E+01
6	152	79.6	308.5	6.060E+19	2.375E+19	3.855E+18	1.042E+18	1.295E+19	1.131E+14	1.379E+13	2.026E+01	3.225E+01
11	152	98.5	308.5	1.208E+19	2.991E+19	8.475E+18	1.183E+19	1.336E+19	1.554E+13	2.352E+13	3.633E+01	3.633E+01
12	152	105.1	308.5	1.246E+19	3.101E+19	9.468E+18	4.122E+18	1.062E+19	1.384E+14	1.528E+13	2.437E+01	3.580E+01
16	152	135.0	308.5	1.713E+19	3.611E+19	1.260E+19	6.225E+18	9.267E+18	1.883E+14	1.566E+13	3.350E+01	3.712E+01
20	152	164.9	308.5	2.864E+19	3.174E+19	1.213E+19	4.854E+18	1.005E+19	1.770E+13	1.701E+01	4.211E+01	4.375E+01
21	152	169.8	308.5	3.174E+19	3.860E+19	1.174E+19	4.356E+18	1.046E+19	3.411E+14	1.830E+13	6.393E+01	6.393E+01
22	152	173.7	308.5	3.396E+19	3.860E+19	1.156E+19	4.150E+18	1.096E+19	3.659E+14	1.925E+13	6.928E+01	4.580E+01
23	152	177.8	308.5	3.859E+19	3.691E+19	1.133E+19	3.747E+18	1.157E+19	3.987E+14	2.036E+13	7.642E+01	4.844E+01
27	152	205.0	308.5	4.279E+19	3.472E+19	1.052E+19	3.765E+18	1.354E+19	4.632E+14	2.451E+13	9.036E+01	5.814E+01
31	152	232.2	308.5	3.507E+19	3.124E+19	1.103E+19	1.179E+19	1.299E+19	2.450E+13	7.355E+01	5.899E+01	5.899E+01
32	152	237.5	308.5	3.363E+19	3.238E+19	1.127E+19	1.489E+19	1.131E+19	3.421E+14	2.133E+13	6.448E+01	5.238E+01
35	152	249.0	308.5	2.423E+19	1.830E+19	1.170E+19	1.844E+19	8.337E+18	2.667E+14	1.567E+13	4.852E+01	4.036E+01
41	152	313.0	308.5	6.207E+18	1.512E+18	1.085E+19	4.498E+19	3.386E+18	8.908E+13	7.249E+12	1.367E+01	2.674E+01
42	152	332.9	308.5	4.195E+19	9.769E+18	1.096E+19	4.989E+19	5.366E+18	8.186E+13	6.143E+12	9.994E+00	2.539E+01
44	152	372.9	308.5	1.973E+18	8.674E+18	7.371E+18	5.584E+19	2.083E+18	4.690E+13	4.592E+12	5.846E+00	2.307E+01
47	152	432.7	308.5	6.765E+17	3.766E+18	4.256E+18	5.788E+19	1.350E+18	3.164E+13	3.265E+00	1.987E+01	1.987E+01
49	152	472.6	308.5	3.422E+17	2.098E+18	2.777E+18	5.646E+19	1.036E+18	2.644E+13	2.504E+00	1.792E+01	1.792E+01
51	152	512.5	308.5	1.779E+17	1.748E+18	5.283E+19	8.211E+17	2.211E+17	2.966E+13	1.756E+12	2.062E+00	2.674E+01
54	152	572.4	308.5	6.947E+16	4.613E+17	8.280E+17	4.889E+19	5.866E+17	1.933E+13	1.208E+12	1.665E+00	1.376E+01
57	152	632.3	308.5	2.850E+16	1.833E+17	3.739E+17	4.370E+19	4.346E+17	1.667E+13	8.522E+12	1.411E+00	1.176E+01
60	152	692.2	308.5	1.212E+16	7.321E+16	1.635E+17	3.880E+19	3.204E+17	1.454E+13	6.025E+11	1.222E+00	1.007E+01
63	152	752.0	308.5	5.510E+15	2.962E+16	3.377E+19	5.464E+19	2.495E+17	1.277E+13	4.369E+11	1.070E+00	8.638E+00
65	152	792.0	308.5	3.205E+15	1.653E+16	3.944E+16	3.169E+16	2.114E+17	1.174E+13	3.601E+11	9.830E+01	7.898E+00
67	152	831.9	308.5	9.375E+15	6.947E+16	2.226E+16	2.922E+19	1.851E+17	1.081E+13	2.997E+11	9.041E-01	7.200E+00
69	152	871.8	308.5	1.243E+15	5.454E+15	1.261E+16	2.694E+19	1.586E+17	9.959E+12	2.465E+11	8.324E-01	6.564E+00
71	152	911.7	308.5	8.058E+14	3.272E+15	7.213E+15	2.185E+19	1.372E+17	1.677E+11	7.668E-01	1.222E+00	1.007E+01
73	152	951.6	308.5	5.471E+14	4.034E+15	4.174E+15	2.291E+19	1.152E+17	8.459E+11	7.066E-01	5.476E+00	5.476E+00
75	152	991.5	308.5	3.850E+14	1.321E+15	2.463E+15	2.112E+19	9.92E+16	7.796E+12	1.396E+11	6.511E-01	5.010E+00
77	152	1031.4	308.5	9.704E+13	9.040E+14	1.498E+15	8.809E+16	7.182E+12	1.187E+11	5.997E-01	4.591E+00	4.591E+00
79	152	1071.3	308.5	2.186E+14	6.513E+14	9.533E+14	1.791E+19	1.589E+17	6.611E+12	4.452E+11	1.022E+01	6.564E+00
81	152	1111.3	308.5	1.752E+14	4.936E+14	6.364E+14	1.647E+19	7.012E+16	6.079E+12	8.765E+10	5.076E-01	3.854E+00
83	152	1151.2	308.5	1.455E+14	3.920E+14	4.996E+14	1.513E+19	6.292E+16	5.582E+12	7.597E+10	4.661E-01	3.527E+00
86	152	1211.1	308.5	1.146E+14	3.000E+14	3.000E+14	1.327E+19	5.303E+16	4.896E+12	6.154E+10	4.087E-01	3.081E+00
89	152	1270.9	308.5	9.484E+14	9.040E+14	1.498E+15	1.946E+19	8.809E+16	5.097E+12	5.997E-01	3.564E-01	2.680E+00
92	152	1330.8	308.5	8.554E+13	2.170E+14	1.871E+14	1.001E+19	4.128E+16	3.695E+12	4.452E+10	3.095E-01	2.321E+00
95	152	1390.7	308.5	7.328E+13	2.021E+14	1.684E+14	8.583E+18	3.954E+16	3.166E+12	4.085E+10	2.643E-01	1.995E+00
97	152	1430.6	308.5	7.747E+13	1.983E+14	1.623E+14	7.686E+18	3.965E+16	2.835E+12	3.978E+10	2.367E-01	1.794E+00
100	152	1490.5	308.5	7.823E+13	2.018E+14	1.592E+14	6.418E+18	4.186E+16	2.368E+12	4.009E+10	1.977E-01	1.515E+00
103	152	1550.3	308.5	8.379E+13	2.122E+14	1.574E+14	5.233E+18	4.699E+16	1.931E+12	4.280E+10	1.612E-01	1.261E+00
106	152	1610.2	308.5	9.498E+13	2.251E+14	1.510E+14	4.119E+18	5.705E+16	1.520E+12	4.890E+10	1.269E-01	1.030E+00
108	152	1650.1	308.5	1.051E+14	2.259E+14	1.396E+14	3.410E+18	6.867E+16	1.259E+12	5.602E+10	1.051E-01	8.909E-01
111	152	1705.0	308.5	1.155E+14	1.972E+14	1.112E+14	2.473E+18	9.703E+16	9.134E+11	7.286E+10	7.621E-02	7.248E-01

continued

Table E.03 (cont.)

IR	JZ	R	Z	FLUX-A s ⁻¹ m ⁻²	FLUX-B s ⁻¹ m ⁻²	FLUX-C s ⁻¹ m ⁻²	FLUX-D s ⁻¹ m ⁻²	GFLUX>2 s ⁻¹ m ⁻²	DOSE-N mrem/h	DOSE-G mrem/h	DPA/Y dpa/yr	HT RATE Watts/g
111	152	1705.0	308.5	1.155E+14	1.972E+14	1.112E+14	2.473E+18	9.703E+16	9.134E+11	7.286E+10	7.621E-02	7.248E-01
117	152	1762.5	308.5	6.698E+13	1.115E+14	7.387E+13	1.627E+18	1.711E+17	6.009E+11	1.115E+11	4.922E-02	6.295E-01
119	150	1780.2	268.5	4.110E+13	7.971E+13	6.308E+13	1.390E+18	1.882E+17	5.131E+11	1.120E+11	4.243E-02	5.771E-01
119	152	1780.2	308.5	4.041E+13	7.842E+13	6.202E+13	1.367E+18	1.851E+17	5.048E+11	1.102E+11	4.174E-02	5.677E-01
121	152	1801.0	308.5	1.870E+13	2.889E+13	3.116E+13	6.273E+17	1.692E+17	2.315E+11	9.928E+10	1.914E-02	3.776E-01
123	152	1821.8	308.5	1.005E+13	1.193E+13	1.368E+13	2.875E+17	1.409E+17	1.061E+11	8.513E+10	8.774E-03	2.686E-01
126	152	1853.0	308.5	4.345E+12	3.982E+12	4.047E+12	9.019E+16	1.022E+17	3.331E+10	6.603E+10	2.764E-03	1.794E-01
131	152	1905.0	308.5	1.222E+12	9.308E+11	8.022E+11	1.281E+16	6.156E+16	4.740E+09	4.407E+10	3.929E-04	1.096E-01
134	152	1936.2	308.5	5.883E+11	4.273E+11	3.478E+11	4.083E+15	4.746E+16	1.512E+09	3.519E+10	1.258E-04	8.612E-02
137	152	1967.4	308.5	2.846E+11	1.804E+11	1.378E+11	1.002E+15	3.770E+16	3.730E+08	2.802E+10	3.112E-05	6.788E-02

See text in Appendix E for a more complete description of the parameters, the associated energy ranges, and any applicable caveats.

Table E.04. Radial trace exactly at the axial midplane (by HB-1,2,3,4 and HB-6,7,8,9).

IR	JZ	R	Z	FLUX-A s ⁻¹ m ⁻²	FLUX-B s ⁻¹ m ⁻²	FLUX-C s ⁻¹ m ⁻²	FLUX-D s ⁻¹ m ⁻²	GFLUX>2 s ⁻¹ m ⁻²	DOSE-N mrem/h	DOSE-G mrem/h	DPAI/Y dpayr	HT RATE Watts/g
1	133	9.4	0.0	1.045E+19	3.751E+19	2.408E+19	2.692E+19	7.247E+18	1.376E+14	1.316E+13	2.194E+01	3.515E+01
6	133	79.6	0.0	1.616E+19	4.010E+19	2.102E+19	1.752E+19	6.876E+18	1.893E+14	1.175E+13	3.182E+01	3.043E+01
11	133	98.5	0.0	4.043E+19	4.080E+19	2.025E+19	1.573E+19	7.466E+18	2.010E+14	1.457E+13	3.433E+01	3.629E+01
12	133	105.1	0.0	1.734E+19	4.082E+19	1.570E+19	1.570E+19	7.946E+18	1.997E+14	1.528E+13	3.413E+01	3.809E+01
16	133	135.0	0.0	1.871E+19	4.094E+19	1.908E+19	1.407E+19	9.026E+18	2.121E+14	1.743E+13	3.696E+01	4.261E+01
20	133	164.9	0.0	2.097E+19	3.960E+19	1.746E+19	1.554E+19	8.334E+18	2.349E+14	1.652E+13	4.157E+01	4.098E+01
21	133	169.7	0.0	2.152E+19	3.928E+19	1.708E+19	1.547E+19	8.302E+18	2.407E+14	1.640E+13	4.274E+01	4.073E+01
22	133	173.2	0.0	2.146E+19	3.921E+19	1.702E+19	1.551E+19	8.293E+18	2.400E+14	1.630E+13	4.260E+01	4.055E+01
23	133	177.8	0.0	2.095E+19	3.892E+19	1.705E+19	1.652E+19	8.311E+18	2.347E+14	1.630E+13	4.151E+01	4.082E+01
27	133	205.0	0.0	1.903E+19	3.519E+19	1.607E+19	2.311E+19	8.147E+18	2.166E+14	1.607E+13	3.820E+01	4.171E+01
31	133	232.2	0.0	1.520E+19	2.979E+19	1.482E+19	3.366E+19	7.147E+18	1.830E+14	1.364E+13	3.139E+01	3.843E+01
32	133	237.5	0.0	1.521E+19	2.892E+19	1.452E+19	3.456E+19	7.202E+18	1.870E+14	1.336E+13	3.102E+01	3.800E+01
35	133	249.0	0.0	1.353E+19	2.748E+19	1.425E+19	3.713E+19	6.513E+18	1.644E+14	1.176E+13	3.777E+01	3.511E+01
41	133	313.0	0.0	4.179E+18	1.461E+19	1.087E+19	6.125E+19	3.403E+18	7.433E+13	6.937E+12	1.038E+01	2.966E+01
42	133	332.9	0.0	2.927E+18	1.148E+19	9.481E+18	6.530E+19	2.940E+18	6.190E+13	6.075E+12	8.096E+00	2.860E+01
44	133	372.9	0.0	1.427E+18	6.865E+18	6.947E+19	6.947E+19	2.622E+18	4.618E+13	4.622E+12	2.622E+01	2.622E+01
47	133	432.7	0.0	5.198E+17	2.996E+18	3.821E+18	6.913E+19	1.464E+18	3.377E+13	3.109E+12	3.295E+00	2.270E+01
49	133	472.6	0.0	2.700E+17	1.682E+18	2.462E+18	6.638E+19	1.135E+18	2.908E+13	2.404E+12	2.659E+00	2.046E+01
51	133	512.5	0.0	1.436E+17	9.325E+17	1.539E+18	6.261E+19	9.002E+17	2.568E+13	1.875E+12	2.258E+00	1.840E+01
54	133	572.4	0.0	5.808E+16	3.798E+17	7.262E+17	6.449E+17	1.308E+17	2.866E+12	1.308E+12	1.866E+00	1.563E+01
57	133	632.3	0.0	2.469E+16	1.539E+17	3.290E+17	4.990E+19	4.862E+17	1.868E+13	6.929E+11	1.594E+00	1.333E+01
60	133	692.2	0.0	1.086E+16	6.287E+16	1.447E+17	4.404E+19	3.697E+17	1.645E+13	6.679E+11	1.381E+00	1.139E+01
63	133	752.0	0.0	4.909E+15	2.612E+16	6.241E+16	3.879E+19	2.891E+17	1.440E+13	4.899E+11	1.205E+00	9.793E+00
65	133	792.0	0.0	2.948E+15	2.482E+16	3.550E+16	3.565E+19	2.404E+17	1.326E+13	3.954E+11	8.862E+00	8.862E+00
67	133	831.9	0.0	1.884E+15	8.579E+15	2.020E+16	3.276E+19	2.034E+17	1.211E+13	3.233E+11	1.104E+00	8.043E+00
69	133	871.8	0.0	1.209E+15	5.089E+15	1.155E+16	3.011E+19	1.734E+17	1.122E+13	2.655E+11	9.299E-01	7.314E+00
71	133	911.7	0.0	7.990E+14	3.115E+15	6.666E+15	2.769E+19	1.468E+17	1.022E+13	2.179E+11	8.541E-01	6.658E+00
73	133	951.6	0.0	5.509E+14	1.954E+15	2.545E+15	2.545E+19	1.810E+17	9.37E+12	1.848E+11	6.072E+00	6.072E+00
75	133	991.5	0.0	3.970E+14	1.321E+15	2.350E+15	2.340E+19	1.105E+17	8.636E+12	1.526E+11	7.211E+01	5.546E+00
77	133	1031.4	0.0	2.990E+14	9.274E+14	1.461E+15	2.150E+19	9.794E+16	7.944E+12	1.299E+11	6.625E+01	5.069E+00
79	133	1071.3	0.0	2.348E+14	6.858E+14	9.503E+14	1.974E+19	8.712E+16	7.285E+12	1.112E+11	6.082E-01	4.634E+00
81	133	1111.3	0.0	1.914E+14	5.309E+14	6.506E+14	1.811E+19	2.765E+16	1.022E+13	2.179E+11	8.541E-01	6.658E+00
83	133	1151.2	0.0	1.608E+14	4.289E+14	4.703E+14	1.659E+19	6.976E+16	1.623E+12	8.336E+10	5.112E-01	3.869E+00
86	133	1211.1	0.0	1.292E+14	3.331E+14	3.192E+14	1.451E+19	6.049E+16	5.352E+12	6.897E+10	4.469E-01	3.373E+00
89	133	1270.9	0.0	1.101E+14	2.772E+14	2.445E+14	1.262E+19	1.262E+16	5.655E+12	5.862E+10	3.886E-01	2.929E+00
92	133	1330.8	0.0	9.715E+13	2.446E+14	2.059E+14	1.089E+19	5.370E+16	4.098E+12	5.155E+10	3.355E-01	2.531E+00
95	133	1390.7	0.0	8.968E+13	2.264E+14	1.953E+14	9.215E+18	4.920E+16	6.638E+12	4.707E+10	2.869E-01	2.172E+00
97	133	1430.6	0.0	8.699E+13	2.213E+14	1.785E+14	8.331E+18	4.667E+16	3.036E+12	4.536E+10	2.565E-01	1.950E+00
100	133	1490.5	0.0	8.694E+13	2.231E+14	1.742E+14	6.945E+18	4.606E+16	2.562E+12	4.483E+10	2.139E-01	1.643E+00
103	133	1550.3	0.0	9.202E+13	2.331E+14	1.715E+14	5.655E+18	4.730E+16	2.085E+12	4.717E+10	1.742E-01	1.364E+00
106	133	1610.2	0.0	1.034E+14	2.453E+14	1.642E+14	4.445E+18	5.206E+16	1.640E+12	5.344E+10	1.370E-01	1.113E+00
108	133	1650.1	0.0	1.141E+14	2.454E+14	1.514E+14	3.678E+18	6.252E+16	1.357E+12	6.093E+10	1.134E-01	9.621E-01
111	133	1705.0	0.0	1.250E+14	2.141E+14	1.207E+14	2.666E+18	7.482E+16	9.846E+11	7.886E+10	8.214E-02	7.820E-01

continued

Table E.04 (cont.)

IR	I2	R	Z	FLUX-A s ⁻¹ m ⁻²	FLUX-B s ⁻¹ m ⁻²	FLUX-C s ⁻¹ m ⁻²	FLUX-D s ⁻¹ m ⁻²	GFLUX>2 s ⁻¹ m ⁻²	DOSE-N mrem/h	DOSE-G mrem/h	DPA/I/Y dpa/yr	HT RATE Watts/g
111	133	1705.0	0.0	1.250E+14	2.141E+14	1.207E+14	2.666E+18	1.050E+17	9.846E+11	7.886E+10	8.214E-02	7.820E-01
117	133	1762.5	0.0	7.235E+13	1.207E+14	7.987E+13	1.753E+18	1.846E+17	6.475E+11	1.203E+11	5.304E-02	6.787E-01
121	133	1801.0	0.0	2.025E+13	3.138E+13	3.372E+13	6.759E+17	1.825E+17	2.495E+11	1.070E+11	2.062E-02	4.070E-01
123	133	1821.8	0.0	1.085E+13	1.292E+13	1.475E+13	3.097E+17	1.519E+17	1.143E+11	9.175E+10	9.451E-03	2.894E-01
126	133	1853.0	0.0	4.701E+12	4.329E+12	4.437E+12	9.684E+16	1.100E+17	3.577E+10	7.109E+10	2.967E-03	1.930E-01
131	133	1905.0	0.0	1.316E+12	1.008E+12	8.609E+11	1.414E+16	6.618E+16	5.233E+09	4.735E+10	4.335E-04	1.178E-01
134	133	1936.2	0.0	6.351E+11	4.598E+11	3.863E+11	4.438E+15	5.098E+16	1.643E+09	3.778E+10	1.368E-04	5.244E-02
137	133	1967.4	0.0	3.052E+11	1.952E+11	1.465E+11	1.081E+15	4.049E+16	4.233E+08	3.008E+10	3.357E-05	7.284E-02

See text in Appendix E for a more complete description of the parameters, the associated energy ranges, and any applicable caveats.

Table E.05. Radial trace about 0.30 m below the midplane, by the horizontal thru tube (HB-5), roughly half way up bottom fuel element.

IR	JZ	R mm	Z mm	FLUX-A s ⁻¹ m ⁻²	FLUX-B s ⁻¹ m ⁻²	FLUX-C s ⁻¹ m ⁻²	FLUX-D s ⁻¹ m ⁻²	GFLUX>2 s ⁻¹ m ⁻²	DOSE-N mrem/h	DOSE-G mrem/h	DPA/IY dpa/yr	HT RATE Watts/g
1	115	9.4	-308.5	2.194E+19	5.827E+19	2.633E+19	2.083E+19	7.966E+18	2.532E+14	1.582E+13	4.290E+01	4.046E+01
6	115	79.6	-308.5	3.944E+19	5.684E+19	2.003E+19	1.082E+19	8.976E+18	4.224E+14	1.638E+13	7.542E+01	4.081E+01
11	115	98.5	-308.5	4.934E+19	5.600E+19	1.783E+19	7.845E+18	1.238E+19	5.277E+14	2.303E+13	9.805E+01	5.570E+01
12	115	105.1	-308.5	5.785E+19	5.251E+19	1.719E+19	6.789E+18	1.406E+19	6.611E+14	5.773E+14	1.092E+02	6.280E+01
16	115	135.0	-308.5	5.791E+19	5.251E+19	1.545E+19	5.942E+18	1.693E+19	6.251E+14	5.154E+13	1.209E+02	7.510E+01
20	115	164.9	-308.5	4.346E+19	4.645E+19	1.565E+19	1.587E+19	1.579E+19	4.768E+14	3.017E+13	9.014E+01	7.288E+01
21	115	169.7	-308.5	3.894E+19	4.551E+19	1.589E+19	1.948E+19	1.390E+19	4.265E+14	2.651E+13	7.977E+01	6.532E+01
22	115	173.2	-308.5	4.513E+19	5.627E+19	1.603E+19	2.053E+19	1.231E+19	3.931E+14	2.336E+13	7.267E+01	5.847E+01
23	115	177.8	-308.5	3.196E+19	4.419E+19	1.627E+19	2.332E+19	1.100E+19	3.886E+14	2.091E+13	6.388E+01	5.350E+01
27	115	205.0	-308.5	1.652E+19	3.486E+19	1.619E+19	3.953E+19	7.585E+18	1.967E+14	1.438E+13	3.329E+01	4.168E+01
31	115	232.2	-308.5	9.668E+18	2.55E+19	1.444E+19	4.947E+19	6.197E+18	1.286E+14	1.103E+13	2.042E+01	3.603E+01
32	115	237.5	-308.5	8.952E+18	2.447E+19	1.412E+19	5.033E+19	6.088E+18	1.215E+14	1.049E+13	1.909E+01	3.492E+01
35	115	249.0	-308.5	7.488E+18	2.227E+19	1.354E+19	5.229E+19	5.495E+18	1.205E+14	1.633E+12	3.249E+01	3.249E+01
41	115	313.0	-308.5	2.172E+18	1.008E+19	8.859E+18	6.605E+19	2.774E+18	5.387E+13	5.243E+12	6.562E+00	2.680E+01
42	115	332.9	-308.5	1.497E+18	7.626E+18	7.428E+18	6.767E+19	2.335E+18	4.629E+13	4.499E+12	5.262E+00	2.548E+01
44	115	372.9	-308.5	7.307E+17	4.283E+18	5.017E+18	6.822E+19	1.653E+18	3.656E+13	3.310E+12	3.702E+00	2.292E+01
47	115	432.7	-308.5	2.627E+17	1.750E+18	2.580E+18	6.492E+19	1.096E+18	2.854E+13	2.205E+12	2.590E+00	1.967E+01
49	115	472.6	-308.5	1.384E+17	9.533E+17	5.94E+18	6.133E+19	8.698E+17	2.581E+13	1.726E+12	2.203E+00	1.777E+01
51	115	512.5	-308.5	5.173E+17	9.572E+16	9.627E+17	5.731E+19	7.168E+17	2.259E+13	1.385E+12	1.939E+00	1.606E+01
54	115	572.4	-308.5	3.103E+16	2.068E+17	4.365E+17	5.118E+19	5.232E+17	1.949E+13	9.780E+11	1.647E+00	1.373E+01
57	115	632.3	-308.5	8.359E+16	1.923E+17	4.540E+17	5.504E+19	5.963E+17	1.701E+13	7.072E+11	1.429E+00	1.179E+01
60	115	692.2	-308.5	6.277E+15	3.449E+16	8.322E+16	4.019E+19	3.262E+17	1.494E+13	5.363E+11	1.251E+00	1.021E+01
63	115	752.0	-308.5	2.981E+15	1.473E+16	3.580E+16	3.556E+19	2.543E+17	1.377E+13	3.972E+11	1.101E+00	8.847E+00
65	115	792.0	-308.5	8.592E+15	2.041E+16	3.279E+19	2.147E+17	2.112E+13	3.255E+11	1.013E+00	8.054E+00	8.054E+00
67	115	831.9	-308.5	1.306E+15	2.068E+15	3.023E+19	5.118E+19	5.232E+17	1.949E+13	9.780E+11	1.647E+00	1.373E+01
69	115	871.8	-308.5	8.000E+14	3.148E+15	6.785E+15	2.788E+19	1.551E+17	2.215E+13	1.833E+11	8.602E+00	6.710E+00
71	115	911.7	-308.5	5.567E+14	2.017E+15	3.999E+15	2.571E+19	1.323E+17	9.494E+12	7.929E+01	6.135E+00	6.135E+00
73	115	951.6	-308.5	4.013E+14	1.350E+15	2.421E+15	2.371E+19	1.142E+17	8.752E+12	1.536E+11	7.308E+01	5.618E+00
75	115	991.5	-308.5	3.085E+14	9.456E+15	2.151E+15	2.186E+19	9.522E+16	9.522E+12	5.066E+12	5.148E+00	5.148E+00
77	115	1031.4	-308.5	2.365E+14	6.947E+14	9.849E+14	2.013E+19	8.553E+16	7.450E+12	1.089E+11	6.704E+00	4.716E+00
79	115	1071.3	-308.5	1.908E+14	5.350E+14	6.696E+14	1.853E+19	1.034E+19	7.561E+16	4.126E+11	3.646E+00	3.186E+01
81	115	1111.3	-308.5	1.599E+14	4.286E+14	4.800E+14	1.704E+19	6.727E+16	6.289E+12	8.088E+10	5.249E+01	3.962E+00
83	115	1151.2	-308.5	1.367E+14	3.562E+14	3.636E+14	1.565E+19	6.004E+16	5.773E+12	7.022E+10	4.819E+01	3.628E+00
86	115	1211.1	-308.5	1.129E+14	2.886E+14	2.694E+14	1.371E+19	5.115E+16	5.061E+12	5.783E+10	4.225E+01	3.171E+00
89	115	1270.9	-308.5	9.693E+13	2.448E+14	2.132E+14	1.196E+19	4.533E+16	4.412E+12	4.943E+10	3.683E+01	2.762E+00
92	115	1330.8	-308.5	8.729E+13	2.194E+14	1.850E+14	1.034E+19	4.126E+16	3.817E+12	4.362E+10	3.186E+01	2.391E+00
95	115	1390.7	-308.5	8.136E+13	2.068E+14	1.711E+14	8.862E+18	4.026E+16	3.259E+12	4.088E+10	2.057E+01	2.057E+00
97	115	1430.6	-308.5	7.993E+13	2.042E+14	1.665E+14	7.934E+18	4.078E+16	2.927E+12	4.026E+10	2.443E+01	1.850E+00
100	115	1490.5	-308.5	8.106E+13	2.077E+14	1.630E+14	6.623E+18	4.327E+16	2.433E+12	4.095E+10	2.040E+01	1.563E+00
103	115	1550.3	-308.5	8.687E+13	2.199E+14	1.627E+14	5.398E+18	4.879E+16	1.992E+12	4.404E+10	1.663E+01	1.300E+00
106	115	1610.2	-308.5	9.848E+13	2.324E+14	1.557E+14	4.248E+18	5.211E+16	1.567E+12	5.048E+10	1.309E+01	1.062E+00
108	115	1650.1	-308.5	1.089E+14	2.332E+14	1.441E+14	3.517E+18	7.113E+16	1.298E+12	5.782E+10	1.084E+01	9.188E-01
111	115	1705.0	-308.5	1.195E+14	2.044E+14	1.152E+14	2.549E+18	1.003E+17	9.416E+11	7.520E+10	7.856E-02	7.474E-01

continued

Table E.05 (cont.)

IR	JZ	R	Z	FLUX-A s ⁻¹ m ⁻²	FLUX-B s ⁻¹ m ⁻²	FLUX-C s ⁻¹ m ⁻²	FLUX-D s ⁻¹ m ⁻²	GFLUX>2 s ⁻¹ m ⁻²	DOSE-N mrem/h	DOSE-G mrem/h	DPA/Y dpa/yr	HT RATE Watts/g
111	115	1705.0	-308.5	1.195E+14	2.044E+14	1.152E+14	2.549E+18	1.003E+17	9.416E+11	7.520E+10	7.856E-02	7.474E-01
117	115	1762.5	-308.5	6.936E+13	1.152E+14	7.632E+13	1.677E+18	1.768E+17	6.195E+11	1.151E+11	5.074E-02	6.493E-01
117	115	1780.2	-268.5	4.241E+13	8.211E+13	6.479E+13	1.427E+18	1.936E+17	5.270E+11	1.152E+11	4.357E-02	5.931E-01
119	115	1780.2	-308.5	4.187E+13	8.105E+13	6.394E+13	1.410E+18	1.911E+17	5.205E+11	1.137E+11	4.304E-02	5.857E-01
119	115	1801.0	-308.5	1.931E+13	2.980E+13	3.213E+13	6.471E+17	1.747E+17	2.388E+11	1.025E+11	1.974E-02	3.897E-01
121	115	1853.0	-308.5	4.521E+12	4.108E+12	4.150E+12	9.302E+16	1.055E+17	3.435E+10	6.817E+10	2.851E-03	1.851E-01
126	115	1905.0	-308.5	1.260E+12	9.616E+11	8.217E+11	1.320E+16	6.359E+16	4.885E+16	4.548E+10	4.043E-04	1.131E-01
131	115	1936.2	-308.5	6.035E+11	4.412E+11	3.642E+11	4.150E+15	4.904E+16	1.537E+09	3.633E+10	1.281E-04	8.888E-02
134	115	1936.2	-308.5	2.925E+11	1.866E+11	1.392E+11	9.919E+14	3.897E+16	3.590E+08	2.894E+10	3.077E-05	7.009E-02
137	115	1967.4	-308.5									

See text in Appendix E for a more complete description of the parameters, the associated energy ranges, and any applicable caveats.

Table E.06. Radial trace about 1.20 m below the midplane.

IR	JZ	R mm	Z mm	FLUX-A s ⁻¹ m ⁻²	FLUX-B s ⁻¹ m ⁻²	FLUX-C s ⁻¹ m ⁻²	FLUX-D s ⁻¹ m ⁻²	GFLUX>2 s ⁻¹ m ⁻²	DOSE-N mrem/h	DOSE-G mrem/h	DPA/I/Y dpa/yr	HT RATE Watts/g
1	67	9.4	-1199.4	1.919E+15	8.148E+15	1.683E+16	8.938E+18	5.908E+17	3.326E+12	4.664E+11	2.779E-01	3.099E+00
6	67	79.6	-1199.4	2.014E+15	9.054E+15	1.718E+16	8.656E+18	7.516E+17	3.224E+12	5.638E+11	2.665E-01	3.275E+00
11	67	98.5	-1199.4	1.905E+15	8.278E+15	1.717E+16	8.765E+18	7.179E+17	3.263E+12	5.444E+11	2.701E-01	3.262E+00
16	67	135.0	-1199.4	1.812E+15	7.296E+15	1.477E+16	9.222E+18	5.964E+17	3.447E+12	4.701E+11	2.876E-01	3.201E+00
21	67	169.7	-1199.4	1.719E+15	6.809E+15	1.363E+16	9.399E+18	6.736E+17	3.492E+12	5.144E+11	2.900E-01	3.341E+00
22	67	173.2	-1199.4	1.755E+15	6.052E+15	1.193E+16	9.030E+18	6.662E+17	3.491E+12	5.090E+11	2.902E-01	3.329E+00
27	67	205.0	-1199.4	1.635E+15	5.612E+15	1.097E+16	9.926E+18	6.600E+17	3.683E+12	4.996E+11	3.043E-01	3.286E+00
32	67	237.5	-1199.4	1.516E+15	5.485E+15	1.074E+16	9.988E+18	6.312E+17	3.705E+12	4.776E+11	3.053E-01	3.424E+00
35	67	249.0	-1199.4	1.445E+15	3.713E+15	9.698E+15	1.181E+19	3.357E+17	4.140E+12	3.873E+11	3.068E-01	3.384E+00
41	67	313.0	-1199.4	1.025E+15	7.087E+14	2.570E+15	4.638E+15	1.179E+19	4.224E+12	3.460E+11	3.184E+00	
44	67	372.9	-1199.4	7.087E+14	2.570E+15	4.638E+15	1.206E+19	1.673E+17	4.455E+12	1.606E+11	3.722E-01	3.066E+00
47	67	432.7	-1199.4	5.093E+14	1.790E+15	3.054E+15	1.204E+19	1.215E+17	4.445E+12	1.205E+11	3.713E-01	2.961E+00
51	67	512.5	-1199.4	3.423E+14	1.111E+15	1.744E+15	1.204E+19	1.827E+16	4.360E+12	9.954E+10	3.642E+01	2.857E+00
54	67	572.4	-1199.4	2.679E+14	8.045E+14	1.160E+15	1.181E+19	8.432E+16	4.224E+12	8.600E+10	3.530E+01	2.743E+00
57	67	632.3	-1199.4	2.142E+14	6.032E+14	7.874E+14	1.145E+19	7.302E+16	4.057E+12	7.399E+10	3.388E+01	2.611E+00
60	67	692.2	-1199.4	1.712E+14	4.594E+14	5.259E+14	1.099E+19	2.332E+17	4.122E+12	3.642E+11	3.722E-01	3.066E+00
63	67	752.0	-1199.4	1.339E+14	3.651E+14	3.855E+14	1.046E+19	6.043E+16	3.861E+12	6.119E+10	3.224E-01	2.462E+00
67	67	831.9	-1199.4	1.087E+14	2.756E+14	2.644E+14	9.686E+18	4.787E+16	3.577E+12	4.823E+10	2.983E-01	2.257E+00
71	67	911.7	-1199.4	8.749E+13	2.180E+14	1.907E+14	8.857E+18	4.006E+16	3.267E+12	3.943E+10	2.728E-01	2.052E+00
75	67	991.5	-1199.4	7.272E+13	1.770E+14	1.499E+14	8.006E+18	3.427E+16	2.957E+12	3.358E+10	2.465E-01	1.849E+00
79	67	1071.3	-1199.4	6.207E+13	1.491E+14	1.212E+14	7.154E+18	2.951E+16	2.639E+12	2.831E+10	2.203E-01	1.648E+00
83	67	1151.2	-1199.4	5.441E+13	1.287E+14	1.036E+14	6.312E+18	2.682E+16	2.323E+12	2.527E+10	1.944E-01	1.455E+00
86	67	1211.4	-1199.4	4.878E+13	1.171E+14	9.304E+13	5.594E+18	2.415E+16	2.108E+12	1.753E+10	1.312E+00	
89	67	1270.9	-1199.4	4.524E+13	1.095E+14	8.724E+13	5.090E+18	2.247E+16	1.877E+12	2.089E+10	1.567E-01	1.174E+00
92	67	1330.8	-1199.4	4.255E+13	1.026E+14	8.288E+13	4.501E+18	2.121E+16	1.660E+12	1.976E+10	1.386E-01	1.042E+00
95	67	1390.7	-1199.4	4.093E+13	1.010E+14	8.035E+13	3.928E+18	2.098E+16	1.449E+12	1.928E+10	1.210E-01	9.146E-01
100	67	1490.5	-1199.4	4.151E+13	1.046E+14	8.181E+13	3.012E+18	2.214E+16	1.111E+12	1.989E+10	7.141E-01	
103	67	1550.3	-1199.4	4.437E+13	1.111E+14	8.122E+13	2.483E+18	2.483E+16	9.172E+11	2.172E+10	7.658E-02	6.024E-01
106	67	1610.2	-1199.4	5.007E+13	1.175E+14	7.852E+13	1.975E+18	2.962E+16	7.291E+11	2.484E+10	6.089E-02	4.975E-01
108	67	1650.1	-1199.4	5.468E+13	1.173E+14	7.247E+13	1.644E+18	3.549E+16	6.070E+11	2.855E+10	5.070E-02	4.334E-01
111	67	1705.0	-1199.4	5.913E+13	1.013E+14	5.865E+13	1.199E+18	4.888E+16	4.430E+11	3.658E+10	3.696E-02	3.546E-01
117	67	1762.5	-1199.4	3.398E+13	5.715E+13	3.821E+13	7.926E+17	8.437E+16	2.927E+11	5.509E+10	2.398E-02	3.085E-01
126	67	1853.0	-1199.4	2.225E+12	2.053E+12	2.088E+12	4.385E+16	5.139E+16	1.619E+10	3.338E+10	1.344E-03	9.039E-02
134	67	1936.2	-1199.4	3.043E+11	2.163E+11	1.780E+11	2.059E+15	2.471E+16	7.629E+08	1.833E+10	6.352E-05	4.490E-02

See text in Appendix E for a more complete description of the parameters, the associated energy ranges, and any applicable caveats.

Table E.07. Radial trace along bottom of reflector vessel (at mid-thickness).

	IR	JZ	R	Z	FLUX-A s ⁻¹ m ⁻²	FLUX-B s ⁻¹ m ⁻²	FLUX-C s ⁻¹ m ⁻²	FLUX-D s ⁻¹ m ⁻²	GFLUX>2 s ⁻¹ m ⁻²	DOSE-N mrneth	DOSE-G mrneth	DPA/Y dpayr	HT RATE Watts/g
1	22	9.4	-2057.0	9.385E+13	2.463E+14	1.739E+14	5.762E+17	4.614E+16	3.711E+11	1.784E-02	2.164E-01		
6	22	79.6	-2057.0	9.593E+13	2.403E+14	1.659E+14	5.546E+17	5.492E+16	2.056E+11	4.200E+10	1.699E-02	2.236E-01	
11	22	98.5	-2057.0	9.583E+13	2.378E+14	1.634E+14	5.597E+17	5.417E+16	2.075E+11	4.208E+10	1.717E-02	2.255E-01	
16	22	135.0	-2057.0	9.407E+13	2.291E+14	1.565E+14	5.884E+17	4.633E+16	2.163E+11	3.884E+10	1.805E-02	2.234E-01	
21	22	169.7	-2057.0	9.300E+13	2.148E+14	1.452E+14	5.826E+17	5.489E+16	2.159E+11	4.258E+10	1.793E-02	2.322E-01	
22	22	173.2	-2057.0	9.288E+13	2.146E+14	1.446E+14	5.824E+17	5.473E+16	2.158E+11	4.242E+10	1.791E-02	2.318E-01	
27	22	205.0	-2057.0	8.887E+13	1.950E+14	1.325E+14	5.965E+17	5.256E+16	2.210E+11	4.090E+10	1.841E-02	2.313E-01	
32	22	237.5	-2057.0	8.054E+13	1.668E+14	1.172E+14	5.929E+17	6.569E+16	2.196E+11	4.845E+10	1.810E-02	2.448E-01	
35	22	249.0	-2057.0	7.485E+13	1.571E+14	1.134E+14	5.967E+17	7.384E+16	2.200E+11	5.322E+10	1.812E-02	2.511E-01	
41	22	313.0	-2057.0	5.634E+13	1.182E+14	9.124E+13	6.316E+17	8.811E+16	2.336E+11	6.095E+10	1.909E-02	2.877E-01	
44	22	372.9	-2057.0	4.983E+13	1.001E+14	7.692E+13	6.625E+17	8.814E+16	2.449E+11	6.049E+10	2.001E-02	2.933E-01	
47	22	432.7	-2057.0	4.628E+13	8.925E+13	6.725E+13	6.881E+17	8.801E+16	2.541E+11	5.999E+10	2.077E-02	2.976E-01	
51	22	512.5	-2057.0	4.324E+13	7.958E+13	5.810E+13	7.096E+17	8.771E+16	2.622E+11	5.933E+10	2.142E-02	3.007E-01	
54	22	572.4	-2057.0	4.090E+13	7.379E+13	5.271E+13	7.157E+17	8.619E+16	2.644B+11	5.801E+10	2.160E-02	2.988E-01	
57	22	632.3	-2057.0	3.891E+13	6.897E+13	4.848E+13	7.139E+17	8.369E+16	2.637E+11	5.611E+10	2.154E-02	2.938E-01	
60	22	692.2	-2057.0	3.692E+13	6.474E+13	4.502E+13	7.048E+17	8.146E+16	2.642E+11	5.442E+10	2.126E-02	2.877E-01	
63	22	752.0	-2057.0	3.520E+13	6.090E+13	4.179E+13	6.898E+17	7.902E+16	2.548E+11	5.263E+10	2.081E-02	2.800E-01	
67	22	831.9	-2057.0	3.292E+13	5.684E+13	3.849E+13	6.611E+17	7.502E+16	2.442E+11	4.985E+10	1.994E-02	2.669E-01	
71	22	911.7	-2057.0	3.082E+13	5.263E+13	3.555E+13	6.244E+17	7.050E+16	2.306E+11	4.679E+10	1.883E-02	2.514E-01	
75	22	991.5	-2057.0	2.878E+13	4.883E+13	3.267E+13	5.831E+17	6.351E+16	2.277E+11	4.354E+10	1.775E-02	2.432E-01	
79	22	1071.3	-2057.0	2.633E+13	4.481E+13	2.979E+13	5.336E+17	6.011E+16	1.971E+11	3.985E+10	1.610E-02	2.145E-01	
83	22	1151.2	-2057.0	2.390E+13	4.071E+13	2.728E+13	4.824E+17	5.469E+16	1.728E+11	3.632E+10	1.455E-02	1.946E-01	
86	22	1211.1	-2057.0	2.201E+13	3.776E+13	2.544E+13	4.423E+17	5.015E+16	1.634E+11	3.334E+10	1.334E-02	1.785E-01	
89	22	1270.9	-2057.0	2.057E+13	3.486E+13	2.367E+13	4.030E+17	4.567E+16	1.427E+11	3.042E+10	1.210E-02	1.624E-01	
92	22	1330.8	-2057.0	1.849E+13	3.200E+13	2.170E+13	3.597E+17	4.127E+16	1.328E+11	2.756E+10	1.085E-02	1.462E-01	
95	22	1390.7	-2057.0	1.667E+13	2.922E+13	2.000E+13	3.178E+17	3.687E+16	1.174E+11	2.470E+10	9.590E-03	1.300E-01	
100	22	1490.5	-2057.0	1.399E+13	2.504E+13	1.729E+13	2.485E+17	2.981E+16	9.182E+10	2.016E+10	7.500E-03	1.037E-01	
103	22	1550.3	-2057.0	1.251E+13	2.247E+13	1.542E+13	2.075E+17	2.569E+16	7.659E+10	1.752E+10	6.264E-03	8.828E-02	
106	22	1610.2	-2057.0	1.092E+13	1.964E+13	1.327E+13	1.678E+17	2.181E+16	6.203E+10	1.503E+10	5.068E-03	7.346E-02	
108	22	1650.1	-2057.0	9.842E+12	1.726E+13	1.149E+13	1.423E+17	1.947E+16	5.267E+10	1.352E+10	4.300E-03	6.416E-02	
111	22	1705.0	-2057.0	7.779E+12	1.310E+13	8.919E+12	1.102E+17	1.632E+16	4.074E+10	1.142E+10	3.328E-03	5.193E-02	
117	22	1762.5	-2057.0	4.056E+12	7.962E+12	6.060E+12	8.403E+16	3.103E+10	8.332E+09	2.543E-03	3.847E-02		
126	22	1853.0	-2057.0	3.027E+11	7.841E+11	4.326E+15	6.822E+15	1.598E+09	4.967E+09	1.325E-04	1.296E-02		
134	22	1936.2	-2057.0	4.335E+10	3.242E+10	2.667E+10	2.610E+14	4.042E+15	9.674E+07	3.263E+09	8.067E-06	7.970E-03	

See text in Appendix E for a more complete description of the parameters, the associated energy ranges, and any applicable caveats.

Table E.08. Partial axial trace along system centerline.

IR	JZ	R mm	Z mm	FLUX-A s ⁻¹ m ⁻²	FLUX-B s ⁻¹ m ⁻²	FLUX-C s ⁻¹ m ⁻²	FLUX-D s ⁻¹ m ⁻²	GFLUX>2 s ⁻¹ m ⁻²	DOSE-N mrem/h	DOSE-G mrem/h	DPA/I/Y dpas/yr	HT RATE Watts/g
1	171	9.4	602.0	1.353E+18	5.876E+18	2.339E+18	1.224E+18	4.354E+18	1.704E+13	4.820E+12	2.844E+00	1.125E+01
1	166	9.4	547.0	2.367E+18	9.279E+18	3.420E+18	1.532E+18	5.440E+18	2.893E+13	6.256E+12	4.960E+00	1.462E+01
1	162	9.4	507.0	3.151E+18	1.209E+19	4.287E+18	1.779E+18	5.962E+18	3.801E+13	7.007E+12	6.496E+00	1.639E+01
1	159	9.4	451.3	4.325E+18	1.597E+19	5.514E+18	2.170E+18	7.332E+18	5.177E+13	8.778E+12	8.962E+00	2.055E+01
1	156	9.4	389.7	5.318E+18	1.976E+19	6.772E+18	2.659E+18	8.284E+18	6.357E+13	1.006E+13	1.095E+01	2.359E+01
1	154	9.4	348.7	5.889E+18	2.192E+19	7.558E+18	3.079E+18	9.101E+18	7.048E+13	1.107E+13	1.213E+01	2.601E+01
1	152	9.4	308.5	6.359E+18	2.381E+19	8.344E+18	3.688E+18	9.900E+18	7.634E+13	1.203E+13	1.309E+01	2.831E+01
1	149	9.4	248.5	6.996E+18	2.626E+19	9.770E+18	5.542E+18	1.118E+19	8.486E+13	1.344E+13	1.444E+01	3.194E+01
1	146	9.4	191.6	7.432E+18	2.871E+19	1.273E+19	1.029E+19	1.109E+19	9.318E+13	1.381E+13	1.545E+01	3.368E+01
1	144	9.4	155.7	7.611E+18	3.055E+19	1.601E+19	1.558E+19	9.335E+18	9.909E+13	1.284E+13	1.594E+01	3.238E+01
1	141	9.4	101.9	8.055E+18	3.306E+19	2.103E+19	2.396E+19	8.241E+18	1.103E+14	1.273E+13	1.731E+01	3.366E+01
1	138	9.4	50.0	8.539E+18	3.499E+19	2.354E+19	2.782E+19	6.580E+18	1.178E+14	1.155E+13	1.806E+01	3.167E+01
1	133	9.4	0.0	1.045E+19	3.751E+19	2.408E+19	2.622E+19	7.612E+18	1.376E+14	1.316E+13	2.194E+01	3.515E+01
1	128	9.4	-45.0	1.249E+19	4.10E+19	2.424E+19	2.459E+19	6.914E+18	1.565E+14	1.323E+13	2.508E+01	3.483E+01
1	125	9.4	-105.7	1.604E+19	4.664E+19	2.467E+19	2.244E+19	8.004E+18	1.922E+14	1.540E+13	3.183E+01	3.541E+01
1	123	9.4	-146.8	1.792E+19	5.022E+19	2.519E+19	2.170E+19	8.034E+18	2.116E+14	1.584E+13	3.537E+01	4.033E+01
1	120	9.4	-208.2	2.015E+19	5.475E+19	2.036E+19	2.136E+19	8.221E+18	2.321E+14	1.627E+13	3.965E+01	4.140E+01
1	118	9.4	-248.5	2.111E+19	5.690E+19	2.639E+19	2.121E+19	8.156E+18	2.449E+14	1.619E+13	4.131E+01	4.126E+01
1	115	9.4	-308.5	2.194E+19	5.827E+19	2.633E+19	2.033E+19	7.966E+18	2.532E+14	1.582E+13	4.290E+01	4.146E+01
1	113	9.4	-348.7	2.191E+19	5.764E+19	2.575E+19	2.045E+19	7.772E+18	2.524E+14	1.538E+13	4.287E+01	3.944E+01
1	110	9.4	-410.2	2.080E+19	5.381E+19	2.387E+19	2.002E+19	7.215E+18	2.392E+14	1.413E+13	4.072E+01	3.658E+01
1	108	9.4	-451.2	1.894E+19	4.394E+19	2.197E+19	2.039E+19	6.508E+18	2.184E+14	1.261E+13	3.698E+01	3.222E+01
1	105	9.4	-507.0	1.446E+19	3.905E+19	1.870E+19	2.316E+19	5.220E+18	1.709E+14	9.806E+12	2.838E+01	2.740E+01
1	101	9.4	-547.0	1.088E+19	3.033E+19	1.602E+19	2.725E+19	4.841E+18	1.327E+14	8.336E+12	2.187E+01	2.497E+01
1	96	9.4	-602.3	5.363E+18	1.876E+19	1.207E+19	3.319E+19	3.483E+18	7.719E+13	5.312E+12	1.170E+01	1.932E+01

See text in Appendix E for a more complete description of the parameters, the associated energy ranges, and any applicable caveats.

Table E.09. Partial axial trace near inner surface of lower fuel element.

R	JZ	R	Z	FLUX-A s ⁻¹ m ⁻²	FLUX-B s ⁻¹ m ⁻²	FLUX-C s ⁻¹ m ⁻²	FLUX-D s ⁻¹ m ⁻²	GFLUX>2 s ⁻¹ m ⁻²	DOSE-N mrem/h	DOSE-G mrem/h	DPA/IY dp/yr	HT RATE Watts/g
12	171	105.1	602.0	2.123E+18	7.181E+18	3.171E+18	6.076E+18	4.674E+18	2.715E+13	5.654E+12	4.435E+00	1.425E+01
12	166	105.1	547.0	4.307E+18	1.189E+19	4.368E+18	4.761E+18	5.790E+18	5.028E+13	7.613E+12	8.687E+00	1.841E+01
12	162	105.1	507.0	6.174E+18	1.583E+19	5.267E+18	3.870E+18	6.340E+18	6.968E+13	1.213E+12	2.076E+01	2.076E+01
12	159	105.1	451.3	8.600E+18	2.107E+19	6.548E+18	3.479E+18	7.707E+18	9.096E+13	1.096E+12	2.575E+01	2.575E+01
12	156	105.1	389.7	1.050E+19	2.593E+19	7.906E+18	3.736E+18	9.062E+18	1.166E+18	1.301E+12	2.053E+01	3.047E+01
12	154	105.1	348.7	1.155E+19	2.865E+19	8.730E+18	4.051E+18	9.852E+18	1.283E+14	1.416E+13	2.260E+01	3.316E+01
12	152	105.1	308.5	1.246E+19	3.101E+19	9.468E+18	4.422E+18	1.068E+19	1.384E+14	1.528E+13	2.437E+01	3.580E+01
12	149	105.1	248.5	1.371E+19	3.398E+19	1.050E+19	5.197E+18	5.197E+18	1.199E+19	1.524E+14	2.682E+01	3.982E+01
12	146	105.1	191.6	1.468E+19	3.632E+19	1.201E+19	7.031E+18	1.285E+19	1.641E+14	1.823E+13	2.875E+01	4.306E+01
12	144	105.1	155.7	1.508E+19	3.809E+19	1.453E+19	1.030E+19	1.198E+19	1.713E+14	1.783E+13	2.973E+01	4.281E+01
12	141	105.1	101.9	1.507E+19	4.019E+19	1.974E+19	1.747E+19	8.794E+18	1.772E+14	1.530E+13	2.998E+01	3.836E+01
12	138	105.1	50.0	1.466E+19	4.029E+19	2.117E+19	1.956E+19	7.038E+18	1.743E+14	1.354E+13	2.899E+01	3.483E+01
12	133	105.1	0	1.734E+19	4.092E+19	2.025E+19	1.570E+19	7.946E+18	1.997E+14	1.538E+13	3.413E+01	3.809E+01
12	128	105.1	-45.0	2.970E+19	4.241E+19	1.758E+19	8.020E+18	1.204E+19	3.281E+14	2.259E+13	6.078E+01	5.331E+01
12	125	105.1	-105.7	4.007E+19	4.626E+19	1.7093E+19	7.256E+18	1.356E+19	4.362E+14	2.533E+13	8.213E+01	6.003E+01
12	123	105.1	-146.8	4.316E+19	4.889E+19	1.713E+19	7.097E+18	1.385E+19	4.670E+14	2.592E+13	8.775E+01	6.150E+01
12	120	105.1	-208.2	4.779E+19	5.259E+19	1.733E+19	7.004E+18	1.412E+19	5.146E+14	2.638E+13	9.678E+01	6.288E+01
12	118	105.1	-248.5	5.208E+19	5.456E+19	1.740E+19	6.939E+18	1.423E+19	5.608E+14	2.651E+13	1.061E+02	6.353E+01
12	115	105.1	-308.5	5.375E+19	5.572E+19	1.719E+19	6.789E+18	1.406E+19	5.773E+14	2.611E+13	1.092E+02	6.280E+01
12	113	105.1	-348.7	5.306E+19	5.506E+19	1.675E+19	6.654E+18	1.365E+19	5.691E+14	2.538E+13	1.075E+02	6.110E+01
12	110	105.1	-410.2	5.129E+19	5.156E+19	1.553E+19	6.455E+18	1.287E+19	5.497E+14	2.390E+13	1.040E+02	5.770E+01
12	108	105.1	-451.2	4.904E+19	4.722E+19	1.439E+19	6.548E+18	1.225E+19	5.264E+14	2.267E+13	1.001E+02	5.491E+01
12	105	105.1	-507.0	4.222E+19	3.848E+19	1.269E+19	7.743E+18	1.061E+19	4.593E+14	1.956E+13	8.859E+01	4.795E+01
12	101	105.1	-547.0	2.022E+19	3.052E+19	1.214E+19	1.647E+19	5.789E+18	2.209E+14	1.037E+13	3.945E+01	2.779E+01
12	96	105.1	-602.3	6.661E+18	1.810E+19	1.037E+19	3.046E+19	3.696E+18	8.743E+13	5.461E+12	1.372E+01	1.933E+01

See text in Appendix E for a more complete description of the parameters, the associated energy ranges, and any applicable caveats.

Table E.10. Full axial trace at radial midpoint of lower (inner) fuel element.

IR	JZ	R	Z	FLUX-A s ⁻¹ m ⁻²	FLUX-B s ⁻¹ m ⁻²	FLUX-C s ⁻¹ m ⁻²	FLUX-D s ⁻¹ m ⁻²	GFLUX>2 s ⁻¹ m ⁻²	DOSE-N mrem/h	DOSE-G mrem/h	DPAI/Y dp/a/yr	HT RATE Watts/g	
16	259	135.0	2197.0	3.205E+13	6.355E+13	3.814E+13	1.243E+17	2.218E+16	4.620E+10	1.722E+10	3.862E-03	6.941E-02	
16	245	135.0	2057.0	6.207E+13	1.512E+14	1.024E+14	3.541E+17	3.203E+16	1.456E+11	2.601E+10	1.218E-02	1.502E-01	
16	239	135.0	1997.0	8.352E+13	1.988E+14	1.361E+14	5.471E+17	4.621E+16	2.02E+11	3.630E+10	1.691E-02	2.098E-01	
16	229	135.0	1796.6	1.499E+14	3.657E+14	2.609E+14	1.159E+18	7.751E+16	4.295E+11	6.137E+10	3.579E-02	4.066E-01	
16	219	135.0	1590.9	2.455E+14	6.248E+14	4.594E+14	1.811E+18	1.342E+17	6.708E+11	2.302E+11	1.098E+11	5.593E-02	6.668E-01
16	210	135.0	1405.7	4.511E+14	1.135E+15	4.001E+15	8.202E+15	2.738E+18	4.694E+17	1.024E+12	4.328E+11	5.972E-02	9.720E-01
16	196	135.0	1199.4	7.645E+15	4.463E+16	6.769E+16	4.947E+18	8.652E+17	1.955E+12	8.423E+11	1.680E-01	1.623E+00	
16	190	135.0	993.1	889.9	2.960E+16	1.861E+17	2.477E+17	6.845E+18	1.276E+18	3.018E+12	2.766E-01	3.064E+00	
16	185	135.0	807.4	9.773E+16	1.884E+17	6.557E+17	8.903E+18	1.716E+18	4.785E+12	4.926E-01	6.221E+00	6.221E+00	
16	181	135.0	704.2	4.684E+17	2.352E+18	1.930E+18	1.118E+19	2.438E+18	1.065E+13	2.907E+12	1.364E+00	9.145E+00	
16	176	135.0	602.0	2.352E+18	8.048E+18	4.409E+18	1.057E+19	3.587E+18	3.198E+13	4.997E+12	5.036E+00	1.373E+01	
16	171	135.0	547.0	5.549E+18	1.374E+19	5.966E+18	7.603E+18	4.842E+18	6.498E+13	7.350E+12	1.120E+01	1.845E+01	
16	166	135.0	507.0	8.622E+18	1.886E+19	7.087E+18	5.988E+18	5.630E+18	7.603E+13	9.000E+12	1.701E+01	2.178E+01	
16	162	135.0	451.3	1.215E+19	2.471E+19	8.748E+18	4.875E+18	7.071E+18	1.335E+14	2.383E+13	2.746E+01	2.746E+01	
16	159	135.0	389.7	1.453E+19	3.027E+19	1.054E+19	5.277E+18	8.176E+18	1.596E+14	1.353E+13	2.842E+01	3.207E+01	
16	156	135.0	348.7	1.588E+19	3.339E+19	1.163E+19	5.721E+18	8.855E+18	1.748E+14	1.474E+13	3.109E+01	3.492E+01	
16	154	135.0	308.5	1.712E+19	3.611E+19	2.012E+19	1.225E+19	9.267E+18	1.888E+14	1.566E+13	3.260E+01	3.712E+01	
16	152	135.0	248.5	1.886E+19	3.951E+19	1.390E+19	7.206E+18	1.026E+19	2.078E+14	1.719E+13	3.691E+01	4.085E+01	
16	149	135.0	191.6	2.031E+19	4.201E+19	1.543E+19	9.133E+18	1.063E+19	2.338E+14	1.805E+13	3.972E+01	4.322E+01	
16	146	135.0	155.7	2.082E+19	4.309E+19	1.696E+19	1.144E+19	1.004E+19	2.308E+14	1.785E+13	4.080E+01	4.320E+01	
16	144	135.0	101.9	2.064E+19	4.336E+19	1.926E+19	1.388E+19	9.258E+18	2.328E+14	1.745E+13	4.070E+01	4.300E+01	
16	141	135.0	50.0	1.885E+19	4.199E+19	2.019E+19	1.725E+19	9.886E+18	2.151E+14	1.622E+13	3.722E+01	4.048E+01	
16	138	135.0	0.0	1.871E+19	4.094E+19	1.908E+19	1.607E+19	9.026E+18	2.128E+14	1.749E+13	3.696E+01	4.261E+01	
16	133	135.0	-45.0	3.260E+19	4.109E+19	1.594E+19	5.689E+18	1.398E+19	3.598E+14	2.611E+13	6.818E+01	6.992E+01	
16	128	135.0	-105.7	4.364E+19	4.401E+19	1.549E+19	6.533E+18	6.144E+19	1.004E+19	2.308E+14	1.785E+13	4.080E+01	4.320E+01
16	125	135.0	-146.8	4.650E+19	4.620E+19	1.561E+19	6.128E+18	1.683E+19	5.057E+14	3.146E+13	9.737E+01	7.396E+01	
16	123	135.0	-208.2	5.120E+19	4.950E+19	1.556E+19	6.091E+18	1.717E+19	5.538E+14	3.207E+13	1.066E+02	7.567E+01	
16	120	135.0	-248.5	5.618E+19	5.139E+19	1.566E+19	6.091E+18	1.719E+19	6.078E+14	3.208E+13	1.177E+02	7.617E+01	
16	118	135.0	-268.5	5.710E+19	5.202E+19	1.564E+19	6.060E+18	1.715E+19	6.171E+14	3.199E+13	1.194E+02	7.603E+01	
16	117	135.0	-308.5	5.791E+19	5.407E+19	1.545E+19	5.942E+18	1.693E+19	6.251E+14	3.154E+13	1.209E+02	7.510E+01	
16	115	135.0	-348.7	5.704E+19	5.519E+19	1.504E+19	5.779E+18	1.648E+19	6.146E+14	3.071E+13	1.187E+02	7.316E+01	
16	113	135.0	-410.2	5.553E+19	4.873E+19	1.394E+19	5.515E+18	1.556E+19	5.980E+14	2.896E+13	1.158E+02	6.917E+01	
16	110	135.0	-451.2	5.339E+19	4.478E+19	1.290E+19	5.317E+18	1.455E+19	5.753E+14	2.708E+13	1.117E+02	6.485E+01	
16	108	135.0	-507.0	4.707E+19	3.655E+19	1.137E+19	5.390E+18	1.228E+19	5.134E+14	2.27E+13	1.012E+02	5.508E+01	
16	105	135.0	-547.0	2.008E+19	2.885E+19	1.111E+19	1.566E+19	2.216E+14	1.148E+13	4.033E+01	3.014E+01	3.014E+01	
16	101	135.0	-602.3	5.837E+18	1.635E+19	9.720E+18	3.328E+19	3.582E+18	7.988E+13	5.806E+12	1.252E+01	2.068E+01	
16	96	135.0	-705.2	8.683E+17	4.612E+18	4.648E+18	2.150E+19	2.565E+18	1.071E+13	2.550E+12	2.871E+00	1.379E+01	
16	91	135.0	-808.2	1.676E+17	1.178E+18	1.685E+18	2.898E+19	1.673E+18	1.363E+13	1.618E+12	1.248E+00	1.023E+01	
16	86	135.0	-890.5	4.950E+16	3.774E+17	6.721E+17	2.301E+19	1.357E+18	9.460E+12	1.198E+12	8.121E+01	7.962E+00	
16	82	135.0	-993.5	1.268E+16	9.047E+16	1.945E+17	1.688E+19	1.030E+18	6.486E+12	8.545E+11	5.444E+01	5.888E+00	
16	77	135.0	-1199.4	1.812E+15	7.296E+15	1.477E+16	9.272E+18	5.964E+17	3.447E+12	4.701E+11	2.876E+01	3.201E+00	
16	67	135.0	-1405.2	7.251E+14	1.883E+15	1.933E+15	3.488E+17	1.983E+12	2.703E+11	1.653E+01	1.347E+00	1.347E+00	

continued

Table E.10 (cont.)

IR	JZ	R	Z	FLUX-A s ⁻¹ m ⁻²	FLUX-B s ⁻¹ m ⁻²	FLUX-C s ⁻¹ m ⁻²	FLUX-D s ⁻¹ m ⁻²	GFLUX>2 s ⁻¹ m ⁻²	DOSE-N mrem/h	DOSE-G mrem/h	DPA/IY dpalyr	HT RATE Watts/g
16	57	135.0	-1405.2	7.251E+14	1.883E+15	1.913E+15	5.354E+18	3.488E+17	1.983E+12	2.703E+11	1.653E-01	1.847E+00
16	48	135.0	-1590.5	7.248E+14	1.030E+15	7.721E+14	5.303E+18	2.160E+17	1.666E+11	1.019E-01	1.139E+00	
16	38	135.0	-1796.4	2.415E+14	5.847E+14	4.169E+14	1.820E+18	1.243E+17	6.742E+11	9.630E+10	5.622E-02	6.393E-01
16	28	135.0	-1997.0	1.271E+14	3.035E+14	2.095E+14	8.163E+17	6.987E+16	3.025E+11	5.441E+10	2.523E-02	3.138E-01
16	22	135.0	-2057.0	9.407E+13	2.291E+14	1.565E+14	5.838E+17	4.833E+16	2.163E+11	3.884E+10	1.805E-02	2.234E-01
16	8	135.0	-2197.0	4.731E+13	9.465E+13	5.749E+13	1.832E+17	3.221E+16	6.809E+10	2.502E+10	5.693E-03	1.012E-01

See text in Appendix E for a more complete description of the parameters, the associated energy ranges, and any applicable caveats.

Table E.11. Partial axial trace near outer surface of lower fuel element.

IR	JZ	R	Z	FLUX-A s ⁻¹ m ⁻²	FLUX-B s ⁻¹ m ⁻²	FLUX-C s ⁻¹ m ⁻²	FLUX-D s ⁻¹ m ⁻²	GFLUX>2 s ⁻¹ m ⁻²	DOSE-N mrem/h	DOSE-G mrem/h	DPA/IY dpalyr	HT RATE Watts/g
20	171	164.9	602.0	2.866E+18	8.599E+18	4.858E+18	1.359E+19	3.172E+18	3.864E+13	4.595E+12	6.148E+00	1.349E+01
20	166	164.9	547.0	8.206E+18	1.497E+19	6.179E+18	8.102E+18	4.514E+18	9.267E+13	7.334E+12	1.648E+01	1.863E+01
20	162	164.9	507.0	1.489E+19	2.007E+19	7.008E+18	4.480E+18	5.985E+18	1.671E+14	1.024E+13	2.999E+01	2.467E+01
20	159	164.9	451.3	2.095E+19	2.662E+19	8.492E+18	3.806E+18	7.427E+18	2.251E+13	4.195E+13	3.104E+01	3.104E+01
20	156	164.9	389.7	2.430E+19	3.245E+19	1.017E+19	4.140E+18	8.194E+18	2.609E+14	1.506E+13	4.837E+01	3.582E+01
20	154	164.9	348.7	2.642E+19	3.575E+19	1.120E+19	4.477E+18	9.319E+18	2.836E+14	1.644E+13	5.256E+01	3.910E+01
20	152	164.9	308.5	2.864E+19	3.865E+19	1.213E+19	4.854E+18	1.006E+19	3.051E+14	1.770E+13	7.701E+01	4.211E+01
20	149	164.9	248.5	3.132E+19	4.222E+19	1.334E+19	5.544E+18	1.094E+19	3.362E+14	1.931E+13	6.230E+01	4.601E+01
20	146	164.9	191.6	3.440E+19	4.468E+19	1.447E+19	6.625E+18	1.150E+19	3.655E+14	2.061E+13	6.862E+01	4.928E+01
20	144	164.9	155.7	3.526E+19	4.540E+19	1.530E+19	7.706E+18	1.148E+19	3.793E+14	2.111E+13	7.040E+01	5.062E+01
20	141	164.9	101.9	4.501E+19	4.485E+19	1.639E+19	9.451E+18	1.135E+19	1.745E+14	2.139E+13	5.152E+01	
20	138	164.9	50.0	3.121E+19	4.241E+19	1.704E+19	1.098E+19	9.990E+18	3.411E+14	1.945E+13	6.303E+01	4.724E+01
20	133	164.9	0.0	2.097E+19	3.960E+19	1.746E+19	1.554E+19	8.334E+18	2.339E+14	1.652E+13	4.157E+01	4.098E+01
20	128	164.9	-45.0	2.639E+19	3.831E+19	1.607E+19	1.362E+19	1.326E+19	2.953E+14	2.542E+13	5.483E+01	6.051E+01
20	125	164.9	-105.7	3.280E+19	3.961E+19	1.580E+19	1.562E+19	1.560E+19	3.616E+14	2.967E+13	6.865E+01	7.084E+01
20	123	164.9	-146.8	3.480E+19	4.119E+19	1.575E+19	1.612E+19	1.606E+19	3.606E+14	3.061E+13	7.019E+01	5.152E+01
20	120	164.9	-208.2	3.833E+19	4.388E+19	1.585E+19	1.634E+19	1.621E+19	4.205E+14	3.101E+13	7.927E+01	7.435E+01
20	118	164.9	-248.5	4.208E+19	4.547E+19	1.587E+19	1.625E+19	1.613E+19	4.613E+14	3.086E+13	8.765E+01	7.435E+01
20	115	164.9	-308.5	4.346E+19	4.645E+19	1.565E+19	1.587E+19	1.579E+19	4.798E+14	3.017E+13	9.014E+01	7.288E+01
20	113	164.9	-348.7	4.451E+19	4.601E+19	1.523E+19	1.546E+19	1.538E+19	4.865E+14	2.936E+13	9.282E+01	7.115E+01
20	110	164.9	-410.2	4.373E+19	4.322E+19	1.409E+19	1.469E+19	1.451E+19	4.774E+14	2.765E+13	9.143E+01	6.721E+01
20	108	164.9	-451.2	4.202E+19	3.964E+19	1.301E+19	1.426E+19	1.377E+19	4.592E+14	2.616E+13	8.830E+01	6.376E+01
20	105	164.9	-507.0	3.645E+19	3.209E+19	1.133E+19	1.460E+19	1.208E+19	4.056E+14	2.285E+13	7.869E+01	5.626E+01
20	101	164.9	-547.0	1.747E+19	2.475E+19	1.052E+19	2.298E+19	5.443E+18	1.789E+14	9.945E+12	3.178E+01	2.807E+01
20	96	164.9	-602.3	4.873E+18	1.413E+19	8.737E+18	3.548E+19	3.465E+18	6.938E+13	5.198E+12	1.062E+01	1.980E+01

See text in Appendix E for a more complete description of the parameters, the associated energy ranges, and any applicable caveats.

Table E.12. Partial axial trace near inner surface of upper fuel element.

IR	IZ	R	Z	FLUX-A s ⁻¹ m ⁻²	FLUX-B s ⁻¹ m ⁻²	FLUX-C s ⁻¹ m ⁻²	FLUX-D s ⁻¹ m ⁻²	GFLUX>2 s ⁻¹ m ⁻²	DOSE-N mrem/h	DOSE-G mrem/h	DPA/Y dp/yr	HT RATE Watts/g
23	171	177.8	602.0	2.868E+18	8.625E+18	4.938E+18	1.451E+19	2.973E+18	3.890E+13	4.416E+12	6.116E+00	1.335E+01
23	166	177.8	547.0	9.004E+18	1.522E+18	7.759E+18	4.380E+18	1.005E+14	7.410E+12	1.799E+01	1.870E+01	
23	162	177.8	507.0	1.999E+19	2.010E+19	6.590E+18	3.304E+18	7.120E+18	2.183E+14	1.233E+13	4.217E+01	2.962E+01
23	159	177.8	451.3	2.748E+19	2.661E+19	7.951E+18	2.938E+18	8.533E+18	2.974E+14	1.506E+13	5.738E+01	3.590E+01
23	156	177.8	389.7	3.108E+19	3.239E+19	9.500E+18	3.193E+18	9.876E+18	3.353E+14	1.739E+13	6.417E+01	4.133E+01
23	154	177.8	348.7	3.359E+19	3.568E+19	1.047E+19	3.462E+18	1.068E+19	3.623E+14	1.887E+13	6.923E+01	4.492E+01
23	152	177.8	308.5	3.691E+19	3.859E+19	1.133E+19	3.747E+18	1.157E+19	3.987E+14	2.036E+13	7.642E+01	4.844E+01
23	149	177.8	248.5	3.975E+19	4.212E+19	1.244E+19	4.243E+18	1.262E+19	4.286E+14	2.228E+13	8.185E+01	5.296E+01
23	146	177.8	191.6	4.473E+19	4.455E+19	1.344E+19	4.986E+18	1.334E+19	4.836E+14	2.387E+13	9.298E+01	5.699E+01
23	144	177.8	155.7	4.564E+19	4.518E+19	1.411E+19	5.665E+18	1.352E+19	4.935E+14	2.468E+13	9.478E+01	5.893E+01
23	141	177.8	101.9	4.534E+19	4.447E+19	1.494E+19	6.730E+18	1.387E+19	4.918E+14	2.569E+13	9.452E+01	6.131E+01
23	138	177.8	50.0	4.286E+19	4.188E+19	1.545E+19	7.632E+18	1.292E+19	4.711E+14	2.432E+13	9.146E+01	5.833E+01
23	133	177.8	0.0	2.095E+19	3.892E+19	1.705E+19	1.652E+19	8.311E+18	2.347E+14	1.630E+13	4.082E+01	
23	128	177.8	-45.0	2.019E+19	3.711E+19	1.677E+19	2.020E+19	9.346E+18	2.294E+14	1.818E+13	4.059E+01	4.578E+01
23	125	177.8	-105.7	2.396E+19	3.787E+19	1.643E+19	2.294E+19	1.094E+19	2.695E+14	2.09E+13	4.845E+01	5.285E+01
23	123	177.8	-146.8	2.565E+19	3.977E+19	1.638E+19	2.371E+19	1.134E+19	2.868E+14	2.162E+13	5.164E+01	5.460E+01
23	120	177.8	-208.2	2.840E+19	4.177E+19	1.646E+19	2.402E+19	1.130E+19	3.151E+14	2.156E+13	5.697E+01	5.776E+01
23	118	177.8	-248.5	3.050E+19	4.324E+19	1.649E+19	2.389E+19	1.122E+19	3.370E+14	2.141E+13	6.123E+01	5.458E+01
23	115	177.8	-308.5	3.186E+19	4.419E+19	1.627E+19	2.332E+19	1.100E+19	3.506E+14	2.091E+13	6.388E+01	5.350E+01
23	113	177.8	-348.7	3.224E+19	4.377E+19	1.584E+19	2.272E+19	1.074E+19	3.541E+14	2.035E+13	6.472E+01	5.217E+01
23	110	177.8	-410.2	3.159E+19	4.112E+19	1.465E+19	2.162E+19	1.011E+19	3.462E+14	1.906E+13	6.354E+01	4.908E+01
23	108	177.8	-451.2	3.008E+19	3.769E+19	1.352E+19	2.098E+19	9.482E+18	3.299E+14	1.778E+13	6.074E+01	4.604E+01
23	105	177.8	-507.0	2.418E+19	3.038E+19	1.171E+19	2.147E+19	7.667E+18	2.684E+14	1.422E+13	4.938E+01	3.790E+01
23	101	177.8	-547.0	1.350E+19	2.315E+19	1.047E+19	2.734E+19	5.155E+18	1.576E+14	8.890E+12	2.759E+01	2.676E+01
23	96	177.8	-602.3	4.608E+18	1.341E+19	8.401E+18	3.605E+19	3.404E+18	6.746E+13	4.933E+12	1.026E+01	1.942E+01

See text in Appendix E for a more complete description of the parameters, the associated energy ranges, and any applicable caveats.

Table E.13. Full axial trace at radial midpoint of upper (outer) fuel element.

IR	JZ	R	Z	FLUX-A s ⁻¹ m ⁻²	FLUX-B s ⁻¹ m ⁻²	FLUX-C s ⁻¹ m ⁻²	FLUX-D s ⁻¹ m ⁻²	GFLUX>2 s ⁻¹ m ⁻²	Dose-N mrn/m ⁻² /h	Dose-G mrn/m ⁻² /h	DPA/IY dpa/yr	HT RATE Watts/g
27	259	205.0	2197.0	2.686E+13	4.507E+13	2.735E+13	1.080E+17	2.395E+16	1.827E+10	3.357E-03	6.821E-02	
27	245	205.0	2057.0	5.897E+13	1.293E+14	8.710E+13	4.075E+17	3.513E+16	1.509E+10	1.257E-02	1.570E-01	
27	239	205.0	1997.0	8.203E+13	1.802E+14	1.211E+14	5.841E+17	4.810E+16	2.167E+11	3.751E+10	1.803E-02	2.212E-01
27	229	205.0	1796.6	1.452E+14	3.369E+14	2.388E+14	1.290E+18	7.817E+16	4.775E+11	6.133E+10	3.980E-02	4.361E-01
27	219	205.0	1509.9	5.656E+14	4.197E+14	2.117E+18	2.117E+18	1.302E+17	7.858E+11	1.052E+11	6.531E-02	7.253E-01
27	210	205.0	1405.7	3.975E+14	1.050E+15	9.015E+14	2.899E+18	2.124E+17	1.073E+12	1.073E+11	8.953E-02	1.083E+00
27	200	205.0	1199.4	9.900E+14	3.738E+15	6.003E+15	4.564E+18	3.799E+17	1.697E+12	3.431E+11	1.417E-01	1.830E+00
27	190	205.0	993.1	6.617E+15	4.297E+16	8.106E+16	8.139E+18	6.708E+17	3.125E+12	6.517E+11	2.640E-01	3.348E+00
27	185	205.0	889.9	2.478E+16	1.801E+17	2.930E+17	1.114E+19	9.275E+17	4.573E+12	9.566E+11	3.967E-01	4.721E+00
27	181	205.0	807.4	8.112E+16	5.685E+17	7.660E+17	1.422E+19	1.198E+18	6.651E+12	1.331E+12	6.141E-01	6.260E+00
27	176	205.0	704.2	4.138E+17	2.293E+18	2.219E+18	8.078E+19	1.639E+18	1.267E+13	2.113E+12	1.413E+00	8.975E+00
27	171	205.0	602.0	2.762E+18	2.296E+18	4.943E+18	1.776E+19	2.663E+18	3.890E+13	4.316E+12	6.003E+00	1.376E+01
27	166	205.0	547.0	9.739E+18	1.495E+19	5.887E+18	8.711E+18	4.333E+18	1.086E+14	7.810E+12	1.970E+01	1.983E+01
27	162	205.0	507.0	2.371E+19	1.962E+19	6.705E+18	8.303E+18	8.018E+19	3.502E+14	1.495E+13	5.110E+01	5.542E+01
27	159	205.0	451.3	3.228E+19	7.409E+18	2.933E+18	9.033E+19	1.018E+19	1.842E+13	6.882E+13	4.375E+01	
27	156	205.0	389.7	3.609E+19	1.454E+19	8.857E+18	3.278E+18	1.178E+19	3.903E+14	2.127E+13	7.610E+01	5.037E+01
27	154	205.0	348.7	3.889E+19	3.464E+19	9.746E+18	3.525E+18	1.274E+19	4.204E+14	2.298E+13	8.181E+01	5.438E+01
27	152	205.0	308.5	4.279E+19	1.747E+19	1.052E+19	1.652E+18	1.052E+19	4.654E+14	2.451E+13	9.036E+01	8.814E+01
27	150	205.0	268.5	4.482E+19	3.981E+19	1.120E+19	3.997E+18	1.439E+19	4.844E+14	2.600E+13	9.428E+01	6.160E+01
27	149	205.0	248.5	4.586E+19	4.084E+19	1.151E+19	4.118E+18	1.467E+19	4.95E+14	2.662E+13	9.631E+01	6.305E+01
27	146	205.0	191.6	5.157E+19	4.312E+19	1.227E+19	4.473E+18	1.574E+19	5.580E+14	2.859E+13	1.091E+02	6.797E+01
27	144	205.0	155.7	5.261E+19	4.360E+19	1.267E+19	4.736E+18	1.618E+19	5.960E+13	1.112E+02	7.030E+01	
27	141	205.0	101.9	5.220E+19	4.261E+19	1.310E+19	5.147E+19	1.642E+19	5.657E+14	3.030E+13	1.107E+02	7.186E+01
27	138	205.0	50.0	5.002E+19	3.955E+19	1.349E+19	5.729E+18	1.531E+19	5.494E+14	2.852E+13	1.089E+02	6.799E+01
27	133	205.0	0.0	1.903E+19	3.519E+19	1.607E+19	2.311E+19	8.147E+18	2.166E+14	1.607E+13	3.820E+01	4.171E+01
27	128	205.0	-405.7	1.227E+19	1.642E+19	1.642E+19	3.393E+19	7.179E+18	1.522E+13	1.420E+13	3.963E+01	
27	125	205.0	-105.7	1.281E+19	3.069E+19	1.642E+19	3.893E+19	7.272E+18	1.584E+14	2.616E+14	4.088E+01	
27	123	205.0	-146.8	1.357E+19	3.139E+19	1.634E+19	4.023E+19	7.453E+18	1.662E+14	1.444E+13	2.765E+01	4.168E+01
27	120	205.0	-208.2	1.493E+19	3.308E+19	1.638E+19	4.075E+19	7.650E+18	1.806E+14	1.477E+13	3.030E+01	4.252E+01
27	118	205.0	-245.5	1.579E+19	3.414E+19	1.640E+19	4.140E+19	7.706E+18	1.846E+14	1.477E+13	3.193E+01	4.258E+01
27	115	205.0	-308.5	1.652E+19	3.486E+19	1.619E+19	3.953E+19	7.585E+18	1.962E+14	1.438E+13	3.324E+01	4.168E+01
27	113	205.0	-348.7	1.662E+19	3.453E+19	1.576E+19	3.853E+19	7.319E+18	1.964E+14	1.387E+13	3.342E+01	4.033E+01
27	110	205.0	-410.2	1.609E+19	2.398E+19	1.455E+19	3.663E+19	6.785E+18	1.892E+14	1.273E+13	3.232E+01	3.738E+01
27	108	205.0	-451.2	1.510E+19	2.960E+19	1.336E+19	3.543E+19	6.412E+18	1.778E+14	1.184E+13	3.046E+01	3.512E+01
27	105	205.0	-507.0	1.165E+19	2.363E+19	1.137E+19	3.503E+19	5.214E+18	1.409E+14	9.346E+12	2.376E+01	2.932E+01
27	101	205.0	-547.0	7.681E+18	1.804E+19	9.828E+18	3.698E+19	4.324E+18	1.02E+14	7.189E+12	1.628E+01	2.480E+01
27	96	205.0	-602.3	3.151E+18	1.072E+19	7.476E+18	3.983E+19	3.104E+18	5.297E+13	4.545E+12	7.486E+00	1.931E+01
27	91	205.0	-705.2	6.132E+17	1.259E+17	3.241E+18	3.707E+19	2.291E+18	2.247E+13	2.647E+12	2.473E+00	1.437E+01
27	86	205.0	-808.2	1.259E+17	8.543E+17	1.286E+18	2.952E+19	1.685E+18	1.312E+13	1.642E+12	1.188E+00	1.043E+01
27	82	205.0	-890.5	3.894E+16	2.808E+17	5.181E+17	2.355E+19	1.353E+18	9.46E+12	1.214E+12	8.095E-01	8.130E+00
27	77	205.0	-993.5	1.017E+16	6.941E+16	1.515E+17	1.748E+19	9.956E+17	6.652E+12	8.337E+11	5.577E-01	5.896E+00
27	67	205.0	-1199.4	1.635E+15	6.052E+15	1.193E+16	9.824E+18	5.762E+17	3.677E+12	4.528E+11	3.043E-01	3.286E+00
27	57	205.0	-1405.2	6.728E+14	1.666E+15	1.641E+15	5.756E+18	3.381E+17	2.130E+12	2.599E+11	1.776E-01	1.914E+00

continued

Table E.13 (cont.)

IR	JZ	R	Z	FLUX-A s ⁻¹ m ⁻²	FLUX-B s ⁻¹ m ⁻²	FLUX-C s ⁻¹ m ⁻²	FLUX-D s ⁻¹ m ⁻²	GFLUX>2 s ⁻¹ m ⁻²	DOSE-N mrem/h	DOSE-G mrem/h	DPA/Y dp/yr	HT RATE Watts/g
27	57	205.0	-1405.2	6.728E+14	1.666E+15	1.641E+15	5.756E+18	3.381E+17	2.130E+12	2.599E+11	1.776E+01	1.914E+00
27	48	205.0	-1590.5	3.984E+14	9.234E+14	6.901E+14	3.576E+18	2.115E+17	1.323E+12	1.616E+11	1.103E+01	1.894E+00
27	38	205.0	-1796.4	2.292E+14	5.319E+14	3.782E+14	1.974E+18	1.230E+17	7.306E+11	9.444E+10	6.091E+02	6.695E+01
27	28	205.0	-1997.0	1.238E+14	2.738E+14	1.855E+14	8.590E+17	7.236E+16	3.181E+11	5.584E+10	2.653E+02	3.272E+01
27	22	205.0	-2057.0	8.887E+13	1.950E+14	1.325E+14	5.963E+17	5.256E+16	2.210E+11	4.090E+10	1.841E+02	2.313E+01
27	8	205.0	-2197.0	3.960E+13	6.691E+13	4.119E+13	1.588E+17	3.476E+16	5.888E+10	2.642E+10	4.925E+03	9.922E+02

See text in Appendix E for a more complete description of the parameters, the associated energy ranges, and any applicable caveats.

Table E.14. Partial axial trace near outer surface of upper fuel element.

IR	JZ	R	Z	FLUX-A s ⁻¹ m ⁻²	FLUX-B s ⁻¹ m ⁻²	FLUX-C s ⁻¹ m ⁻²	FLUX-D s ⁻¹ m ⁻²	GFLUX>2 s ⁻¹ m ⁻²	DOSE-N mrem/h	DOSE-G mrem/h	DPA/Y dp/yr	HT RATE Watts/g	
31	171	232.2	602.0	2.616E+18	7.606E+18	4.703E+18	2.061E+19	2.556E+18	3.821E+13	3.839E+12	5.782E+00	1.334E+01	
31	166	232.2	547.0	8.343E+18	5.839E+19	5.833E+18	3.819E+19	8.546E+18	9.433E+13	6.879E+12	1.660E+01	1.886E+01	
31	162	232.2	507.0	1.838E+19	1.780E+19	6.413E+18	9.419E+18	2.036E+18	1.606E+14	3.908E+13	3.868E+01	3.868E+01	
31	159	232.2	451.3	2.576E+19	2.357E+19	7.771E+18	9.602E+18	9.997E+18	2.824E+14	1.888E+13	5.441E+01	4.548E+01	
31	156	232.2	389.7	2.909E+19	2.872E+19	9.302E+18	1.049E+19	1.139E+19	3.177E+14	2.144E+13	6.067E+01	5.151E+01	
31	154	232.2	348.7	3.153E+19	3.167E+19	1.020E+19	1.020E+19	1.179E+19	3.442E+14	2.299E+13	6.522E+01	5.522E+01	
31	152	232.2	308.5	3.507E+19	3.426E+19	1.030E+19	1.030E+19	1.299E+19	3.835E+14	2.450E+13	7.355E+01	5.899E+01	
31	149	232.2	248.5	3.765E+19	3.731E+19	1.201E+19	1.201E+19	1.266E+19	1.393E+19	4.107E+14	2.643E+13	7.844E+01	6.356E+01
31	146	232.2	191.6	4.221E+19	3.92E+19	1.268E+19	1.344E+19	1.478E+19	4.611E+14	2.803E+13	8.872E+01	6.765E+01	
31	144	232.2	155.7	4.295E+19	4.952E+19	1.296E+19	1.316E+19	1.515E+19	4.684E+14	2.886E+13	9.017E+01	6.961E+01	
31	141	232.2	101.9	4.232E+19	3.829E+19	1.492E+19	1.492E+19	1.560E+19	4.641E+14	2.936E+13	9.936E+01	7.182E+01	
31	138	232.2	50.0	3.888E+19	3.494E+19	1.330E+19	1.609E+19	1.536E+19	4.320E+14	2.945E+13	8.393E+01	7.127E+01	
31	133	232.2	0.0	1.550E+19	2.979E+19	1.482E+19	3.366E+19	7.147E+18	1.830E+14	1.364E+13	3.139E+01	3.843E+01	
31	128	232.2	-45.0	9.434E+18	2.591E+19	1.522E+19	4.826E+19	6.265E+18	1.246E+14	1.151E+13	1.977E+01	3.557E+01	
31	125	232.2	-105.7	8.062E+18	2.386E+19	1.493E+19	4.888E+19	6.401E+18	1.246E+14	1.151E+13	1.741E+01	3.694E+01	
31	123	232.2	-146.8	8.266E+18	2.368E+19	1.478E+19	5.044E+19	6.602E+18	1.151E+14	1.181E+13	1.786E+01	3.783E+01	
31	120	232.2	-208.2	8.880E+18	2.468E+19	1.472E+19	5.105E+19	6.503E+18	1.215E+14	1.163E+13	1.901E+01	3.761E+01	
31	118	232.2	-248.5	9.283E+18	2.529E+19	1.469E+19	5.073E+19	6.346E+18	1.254E+14	1.137E+13	1.973E+01	3.699E+01	
31	115	232.2	-308.5	9.668E+18	2.568E+19	1.444E+19	4.947E+19	6.197E+18	1.286E+14	1.103E+13	2.042E+01	3.603E+01	
31	113	232.2	-348.7	9.717E+18	2.537E+19	1.403E+19	4.820E+19	6.113E+18	1.284E+14	1.077E+13	2.049E+01	3.519E+01	
31	110	232.2	-410.2	9.337E+18	2.368E+19	1.291E+19	4.582E+19	5.836E+18	1.227E+14	1.007E+13	1.968E+01	3.311E+01	
31	108	232.2	-451.2	8.573E+18	2.155E+19	1.183E+19	4.420E+19	5.355E+18	1.133E+14	9.094E+12	1.810E+01	3.056E+01	
31	105	232.2	-507.0	6.568E+18	1.722E+19	9.998E+18	4.261E+19	4.509E+18	9.072E+13	7.310E+12	1.410E+01	2.617E+01	
31	101	232.2	-547.0	4.715E+18	1.339E+19	8.524E+18	4.221E+19	4.121E+18	7.086E+13	6.183E+12	1.071E+01	2.357E+01	
31	96	232.2	-602.3	2.272E+18	8.340E+18	6.393E+18	4.117E+19	3.273E+18	4.385E+13	5.336E+12	5.864E+00	1.924E+01	

See text in Appendix E for a more complete description of the parameters, the associated energy ranges, and any applicable caveats.

Table E.15. Partial axial trace corresponding to radial location for lower portion of HT-2.

IR	JZ	R mm	Z mm	FLUX-A $s^1 m^2$	FLUX-B $s^1 m^2$	FLUX-C $s^1 m^2$	FLUX-D $s^1 m^2$	GFLUX>2 $s^1 m^2$	DOSE-N mrem/h	DOSE-G mrem/h	DPA/IY dpayr	HT RATE Watts/g
41	171	313.0	602.0	1.040E+18	4.254E+18	3.529E+18	3.053B+19	1.425B+18	2.479E+13	2.502E+12	3.079E+00	1.262E+01
41	166	313.0	547.0	2.118E+18	7.017E+18	4.930E+18	3.239E+19	1.895E+18	3.772E+13	3.579E+12	5.285E+00	1.551E+01
41	162	313.0	507.0	3.035E+18	9.322E+18	6.019E+18	2.128E+19	4.384E+18	7.052E+13	4.255E+12	1.738E+00	1.738E+01
41	159	313.0	451.3	4.250E+18	1.243E+19	7.553E+18	3.658E+19	2.631E+18	6.312E+13	5.409E+12	9.523E+00	2.063E+01
41	156	313.0	389.7	5.213E+18	1.531E+19	9.137E+18	4.022E+19	3.063E+18	7.566E+13	6.400E+12	1.154E+01	2.372E+01
41	154	313.0	348.7	5.748E+18	1.693E+19	1.007E+19	4.269E+19	3.250E+18	8.289E+13	6.871E+12	1.270E+01	2.536E+01
41	152	313.0	308.5	6.207E+18	1.830E+19	1.085E+19	4.498E+19	3.386E+18	8.908E+13	7.249E+12	1.367E+01	2.674E+01
41	149	313.0	248.5	6.814E+18	1.990E+19	1.174E+19	4.803E+19	3.695E+18	9.711E+13	7.831E+12	1.496E+01	2.877E+01
41	146	313.0	191.6	7.226E+18	2.073E+19	1.219E+19	5.050E+19	3.846E+18	1.025E+14	8.223E+12	1.583E+01	3.022E+01
41	144	313.0	155.7	7.306E+18	2.073E+19	1.225E+19	5.192E+19	3.903E+18	1.039E+14	8.324E+12	1.605E+01	3.078E+01
41	141	313.0	101.9	6.903E+18	1.970E+19	1.201E+19	5.422E+19	5.190E+18	1.003E+14	8.141E+12	1.532E+01	3.087E+01
41	138	313.0	50.0	5.678E+18	1.746E+19	1.150E+19	5.727E+19	3.365E+18	8.838E+13	7.301E+12	1.296E+01	2.961E+01
41	133	313.0	0.0	4.179E+18	1.461E+19	1.087E+19	6.125E+19	3.403E+18	7.433E+13	6.937E+12	1.038E+01	2.966E+01
41	128	313.0	-45.0	2.951E+18	1.235E+19	1.030E+19	6.478E+19	2.969E+18	6.253E+13	6.068E+12	8.066E+00	2.844E+01
41	125	313.0	-105.7	2.204E+18	1.005E+19	9.665E+18	6.786E+19	2.890E+18	5.890E+13	5.747E+12	6.703E+00	2.837E+01
41	123	313.0	-146.8	2.052E+18	1.007E+19	9.387E+18	6.876E+19	2.817E+18	5.395E+13	5.558E+12	6.402E+00	2.813E+01
41	120	313.0	-208.2	2.078E+18	9.988E+18	9.169E+18	6.872E+19	2.866E+18	5.407E+13	5.556E+12	6.463E+00	2.811E+01
41	118	313.0	-248.5	2.125E+18	1.006E+19	9.077E+18	6.800E+19	2.875E+18	5.424E+13	5.493E+12	6.532E+00	2.780E+01
41	115	313.0	-308.5	2.172E+18	1.008E+19	8.859E+18	6.605E+19	2.774E+18	5.387E+13	5.243E+12	6.562E+00	2.680E+01
41	113	313.0	-348.7	2.154E+18	9.897E+18	8.581E+18	6.423E+19	2.667E+18	5.280E+13	4.996E+12	6.460E+00	2.583E+01
41	112	313.0	-369.3	2.127E+18	9.716E+18	8.383E+18	6.316E+19	2.602E+18	5.197E+13	4.854E+12	6.370E+00	2.527E+01
41	110	313.0	-410.2	2.008E+18	9.149E+18	7.859E+18	6.079E+19	2.417E+18	4.941E+13	4.460E+12	6.028E+00	2.384E+01
41	108	313.0	-451.2	1.851E+18	8.286E+18	7.164E+18	5.818E+19	2.321E+18	4.633E+13	5.662E+12	4.172E+01	2.260E+01
41	105	313.0	-507.0	1.420E+18	6.678E+18	5.988E+18	5.444E+19	1.895E+18	3.945E+13	3.324E+12	4.608E+00	1.983E+01
41	101	313.0	-547.0	1.122E+18	5.342E+18	5.041E+18	5.168E+19	1.815E+18	3.465E+13	3.001E+12	3.967E+00	1.848E+01
41	96	313.0	-602.3	6.554E+17	3.558E+18	3.729E+18	4.768E+19	1.456E+18	2.722E+13	2.249E+12	2.846E+00	1.586E+01

See text in Appendix E for a more complete description of the parameters, the associated energy ranges, and any applicable caveats.

Table E.16. Partial axial trace corresponding to radial location for lower portion of SH-1 and SH-2.

IR	JZ	R mm	Z mm	FLUX-A s ⁻¹ m ⁻²	FLUX-B s ⁻¹ m ⁻²	FLUX-C s ⁻¹ m ⁻²	FLUX-D s ⁻¹ m ⁻²	GFLUX>2 s ⁻¹ m ⁻²	DOPEN mrem/h	DOSEG mrem/h	DPA/Y dpayr	HT RATE Watts/g
42	171	332.9	602.0	7.726E+17	3.452E+18	3.125E+18	3.241E+19	1.240E+13	2.245E+12	2.610E+00	1.246E+01	
42	166	332.9	547.0	1.476E+18	5.595E+18	4.392E+18	3.514E+19	1.624E+18	3.171E+13	3.120E+12	4.120E+00	1.507E+01
42	162	332.9	507.0	2.053E+18	7.380E+18	5.388E+18	3.722E+19	1.743E+18	3.915E+13	5.287E+12	5.286E+00	1.661E+01
42	159	332.9	451.3	2.853E+18	9.804E+18	6.787E+18	4.058E+19	2.154E+18	4.980E+13	4.540E+12	7.003E+00	1.953E+01
42	156	332.9	389.7	3.593E+18	1.209E+19	8.223E+18	4.467E+19	2.517E+18	5.934E+13	5.370E+12	8.464E+00	2.235E+01
42	154	332.9	348.7	3.868E+18	1.338E+19	9.064E+18	4.738E+19	2.696E+18	6.487E+13	5.819E+12	9.309E+00	2.399E+01
42	152	332.9	308.5	4.155E+18	1.446E+19	9.769E+18	4.989E+19	2.857E+18	6.951E+13	6.186E+12	9.994E+00	2.539E+01
42	149	332.9	248.5	4.611E+18	1.570E+19	1.055E+19	5.320E+19	3.150E+18	7.567E+13	6.716E+12	1.094E+01	2.736E+01
42	146	332.9	191.6	4.846E+18	1.631E+19	1.092E+19	5.585E+19	3.189E+18	7.930E+13	6.945E+12	1.147E+01	2.847E+01
42	144	332.9	155.7	4.880E+18	1.627E+19	1.095E+19	5.735E+19	3.199E+18	8.021E+13	6.967E+12	1.159E+01	2.886E+01
42	141	332.9	101.9	4.600E+18	1.542E+19	1.058E+19	5.963E+19	3.195E+18	7.792E+13	6.863E+12	1.112E+01	2.514E+01
42	138	332.9	50.0	3.781E+18	1.366E+19	1.014E+19	6.225E+19	2.756E+18	6.983E+13	6.121E+12	9.495E+00	2.802E+01
42	133	332.9	0.0	2.927E+18	1.148E+19	9.411E+18	6.530E+19	2.940E+18	6.190E+13	6.075E+12	8.096E+00	2.860E+01
42	129	332.9	-30.0	2.398E+18	1.025E+19	9.084E+18	6.712E+19	2.597E+18	5.570E+13	5.437E+12	6.834E+00	2.755E+01
42	128	332.9	-45.0	2.119E+18	8.723E+18	8.894E+18	6.791E+19	2.556E+18	5.394E+13	5.325E+12	6.515E+00	2.47E+01
42	125	332.9	-105.7	1.602E+18	8.235E+18	8.248E+18	7.020E+19	2.483E+18	4.893E+13	5.055E+12	5.579E+00	2.734E+01
42	123	332.9	-146.8	1.468E+18	7.790E+18	7.965E+18	7.083E+19	2.411E+18	4.749E+13	4.845E+12	5.302E+00	2.700E+01
42	120	332.9	-208.2	1.447E+18	7.628E+18	7.731E+18	7.056E+19	2.393E+18	4.702E+13	4.745E+12	5.247E+00	2.670E+01
42	118	332.9	-248.5	1.470E+18	7.651E+18	7.632E+18	6.973E+19	2.370E+18	4.690E+13	4.669E+12	5.269E+00	2.634E+01
42	115	332.9	-308.5	1.497E+18	7.626E+18	7.428E+18	6.767E+19	2.335E+18	4.629E+13	4.499E+12	5.262E+00	2.548E+01
42	113	332.9	-348.7	1.478E+18	7.468E+18	7.184E+18	6.577E+19	2.268E+18	4.521E+13	4.313E+12	5.157E+00	2.463E+01
42	110	332.9	-410.2	1.373E+18	6.887E+18	6.570E+18	6.220E+19	2.066E+18	4.231E+13	3.851E+12	4.811E+00	2.278E+01
42	108	332.9	-451.2	1.263E+18	6.235E+18	5.984E+18	5.947E+19	1.979E+18	3.975E+13	3.605E+12	4.525E+00	2.160E+01
42	105	332.9	-507.0	9.750E+17	5.041E+18	4.998E+18	5.547E+19	1.629E+18	3.442E+13	2.893E+12	3.757E+00	1.909E+01
42	101	332.9	-547.0	7.821E+17	4.060E+18	4.208E+18	5.247E+19	1.568E+18	3.073E+13	2.633E+12	3.297E+00	1.782E+01
42	96	332.9	-602.3	4.730E+17	2.742E+18	3.115E+18	4.814E+19	1.265E+18	2.500E+13	2.000E+12	2.490E+00	1.540E+01

See text in Appendix E for a more complete description of the parameters, the associated energy ranges, and any applicable caveats.

Table E.17. Partial axial trace corresponding to radial location for lower portion of HT-4.

IR	JZ	R	Z	FLUX-A s ⁻¹ m ⁻²	FLUX-B s ⁻¹ m ⁻²	FLUX-C s ⁻¹ m ⁻²	FLUX-D s ⁻¹ m ⁻²	GFLUX>2 s ⁻¹ m ⁻²	DOSE-N mrrem/h	DOSE-G mrrem/h	DPA/IY dpa/yr	HT RATE Watts/g
44	171	372.9	602.0	4.151E+17	2.186E+18	2.336E+18	3.484E+19	9.123E+17	1.893E+13	1.751E+12	1.958E+00	1.187E+01
44	166	372.9	547.0	7.304E+17	3.428E+18	3.292E+18	3.859E+19	1.175E+18	2.438E+13	2.367E+12	2.742E+00	1.412E+01
44	162	372.9	507.0	9.758E+17	4.453E+18	4.051E+18	4.140E+19	1.256E+18	2.664E+13	3.317E+00	1.544E+01	
44	159	372.9	451.3	1.343E+18	5.870E+18	5.117E+18	4.551E+19	1.592E+18	3.477E+13	3.399E+12	4.227E+00	1.603E+01
44	156	372.9	389.7	1.657E+18	7.249E+18	6.209E+18	5.013E+19	1.823E+18	4.060E+13	3.962E+12	5.019E+00	2.036E+01
44	154	372.9	348.7	1.830E+18	8.027E+18	6.843E+18	5.311E+19	1.940E+18	4.401E+13	4.280E+12	5.471E+00	2.175E+01
44	152	372.9	308.5	1.973E+18	8.674E+18	7.371E+18	5.584E+19	2.083E+18	4.690E+13	4.592E+12	5.846E+00	2.307E+01
44	149	372.9	248.5	2.163E+18	9.393E+18	7.940E+18	5.940E+19	2.283E+18	5.067E+13	4.958E+12	6.366E+00	2.472E+01
44	146	372.9	191.6	2.244E+18	9.703E+18	8.188E+18	6.219E+19	2.248E+18	5.270E+13	5.021E+12	6.601E+00	2.549E+01
44	144	372.9	155.7	2.237E+18	9.641E+18	8.176E+18	6.370E+19	2.275E+18	5.315E+13	5.059E+12	6.627E+00	2.592E+01
44	141	372.9	101.9	2.123E+18	9.096E+18	7.914E+18	6.575E+19	2.351E+18	5.255E+13	5.099E+12	6.500E+00	2.648E+01
44	138	372.9	50.0	1.755E+18	8.077E+18	7.432E+18	6.766E+19	1.997E+18	4.889E+13	4.514E+12	5.732E+00	2.557E+01
44	133	372.9	0.0	1.446E+18	6.865E+18	6.853E+18	6.947E+19	2.186E+18	4.600E+13	4.618E+12	5.262E+00	2.622E+01
44	128	372.9	-45.0	1.083E+18	5.849E+18	6.340E+18	7.087E+19	1.879E+18	4.220E+13	4.046E+12	4.496E+00	2.533E+01
44	126	372.9	-85.3	9.173E+17	5.164E+18	5.945E+18	7.172E+19	1.860E+18	4.051E+13	3.942E+12	4.214E+00	2.518E+01
44	125	372.9	-105.7	4.909E+17	4.909E+18	5.797E+18	7.197E+19	1.860E+18	3.973E+13	3.904E+12	4.075E+00	2.515E+01
44	123	372.9	-146.8	7.720E+17	4.574E+18	5.524E+18	7.212E+19	1.847E+18	3.879E+13	3.794E+12	3.921E+00	2.493E+01
44	120	372.9	-208.2	7.301E+17	4.378E+18	5.292E+18	7.143E+19	1.754E+18	3.792E+13	3.583E+12	3.800E+00	2.428E+01
44	118	372.9	-248.5	7.225E+17	4.343E+18	5.190E+18	7.044E+19	1.726E+18	3.745E+13	3.490E+12	3.759E+00	2.384E+01
44	115	372.9	-308.5	7.307E+17	4.283E+18	5.017E+18	6.822E+19	1.653E+18	3.656E+13	3.310E+12	3.702E+00	2.392E+01
44	113	372.9	-348.7	7.132E+17	4.174E+18	4.838E+18	6.626E+19	1.598E+18	3.552E+13	3.152E+12	3.595E+00	2.212E+01
44	110	372.9	-410.2	6.638E+17	3.832E+18	4.410E+18	6.260E+19	1.541E+18	3.334E+13	2.915E+12	3.378E+00	2.075E+01
44	108	372.9	-451.2	6.047E+17	3.469E+18	4.013E+18	5.979E+19	1.462E+18	3.139E+13	2.708E+12	3.168E+00	1.964E+01
44	105	372.9	-507.0	4.752E+17	2.232E+18	3.353E+18	5.561E+19	1.240E+18	2.797E+13	2.233E+12	2.744E+00	1.761E+01
44	101	372.9	-547.0	3.885E+17	2.300E+18	2.827E+18	5.243E+19	1.204E+18	2.550E+13	2.049E+12	2.473E+00	1.648E+01
44	96	372.9	-602.3	2.520E+17	1.595E+18	2.103E+18	4.787E+19	1.008E+18	2.182E+13	1.626E+12	2.026E+00	1.448E+01

See text in Appendix E for a more complete description of the parameters, the associated energy ranges, and any applicable caveats.

Table E.18. Full axial trace at radial location corresponding to HT-1 and HT-3.

IR	JZ	R mm	Z mm	FLUX-A s ⁻¹ m ⁻²	FLUX-B s ⁻¹ m ⁻²	FLUX-C s ⁻¹ m ⁻²	FLUX-D s ⁻¹ m ⁻²	GFLUX>2 s ⁻¹ m ⁻²	DOSE-N mrem/h	DOSE-G mrem/h	DPA/Y dpa/yr	HT RATE Watts/g
79	259	1071.3	2197.0	4.141E+11	3.201E+11	2.790E+11	4.174E+15	1.931E+16	1.544E+09	1.377E+10	1.278E-04	3.440E-02
79	245	1071.3	2057.0	2.064E+13	3.053E+13	4.270E+13	4.270E+17	4.780E+16	1.577E+11	3.170E+10	1.288E-02	1.711E-01
79	239	1071.3	1997.0	3.589E+13	6.077E+13	3.491E+13	6.655E+17	2.814E+16	2.130E+11	2.176E+10	5.052E-02	1.994E-01
79	229	1071.3	1796.6	2.491E+13	6.356E+13	4.902E+13	1.640E+18	6.051E+16	1.292E+11	1.176E+10	5.052E-02	3.911E-01
79	219	1071.3	1590.9	2.705E+13	6.777E+13	5.361E+13	2.827E+18	1.151E+16	1.043E+12	1.256E+10	8.707E-02	6.549E-01
79	210	1071.3	1405.7	3.529E+13	8.509E+13	6.861E+13	4.158E+18	1.720E+16	1.534E+12	1.671E+10	1.280E-01	9.588E-01
79	204	1071.3	1281.9	4.274E+13	1.042E+13	8.610E+13	2.233E+18	2.110E+16	1.931E+12	2.093E+10	1.611E-01	1.206E+00
79	200	1071.3	1199.4	5.004E+13	1.232E+14	1.020E+14	6.045E+18	2.482E+16	2.230E+12	2.542E+10	1.861E-01	1.396E+00
79	190	1071.3	993.1	7.231E+13	1.832E+14	1.667E+14	8.436E+18	3.527E+16	3.112E+12	3.798E+10	2.598E-01	1.955E-01
79	185	1071.3	889.9	8.687E+13	2.248E+14	2.237E+14	9.818E+18	3.958E+16	3.622E+12	4.474E+10	3.023E-01	2.277E+00
79	181	1071.3	807.4	9.925E+13	2.690E+14	2.912E+14	2.699E+19	4.099E+16	4.288E+12	5.011E+10	3.836E-01	2.551E+00
79	176	1071.3	704.2	1.259E+14	3.424E+14	4.046E+14	1.252E+19	5.302E+16	4.622E+12	6.333E+10	3.858E-01	2.921E+00
79	171	1071.3	602.0	1.511E+14	4.291E+14	5.492E+14	1.406E+19	5.943E+16	5.187E+12	7.331E+10	4.331E-01	3.285E+00
79	162	1071.3	507.0	1.739E+14	5.147E+14	6.985E+14	1.544E+19	6.549E+16	5.697E+12	8.249E+10	4.756E-01	3.613E+00
79	156	1071.3	389.7	2.032E+14	6.124E+14	8.690E+14	1.699E+19	7.375E+16	6.271E+12	9.444E+10	5.235E-01	3.985E+00
79	152	1071.3	308.5	2.186E+14	6.514E+14	9.533E+14	1.791E+19	7.912E+16	6.611E+12	1.022E+11	5.520E-01	4.208E+00
79	146	1071.3	191.6	2.265E+14	6.870E+14	1.013E+15	1.895E+19	7.764E+16	6.933E+12	1.032E+11	5.839E-01	4.404E+00
79	141	1071.3	101.9	2.334E+14	6.947E+14	1.005E+15	1.947E+19	8.356E+16	7.184E+12	1.087E+11	5.998E-01	4.568E+00
79	133	1071.3	0.0	2.384E+14	6.858E+14	6.503E+14	1.503E+19	8.712E+16	7.285E+12	1.112E+11	6.082E-01	4.634E+00
79	125	1071.3	-105.7	2.266E+14	6.459E+14	8.590E+14	1.966E+19	8.749E+16	7.254E+12	1.100E+11	6.057E-01	4.612E+00
79	120	1071.3	-208.2	2.066E+14	5.882E+14	7.657E+14	1.924E+19	7.712E+16	7.100E+12	9.854E+10	5.928E-01	4.492E+00
79	115	1071.3	-308.5	1.908E+14	5.350E+14	6.696E+14	1.853E+19	7.561E+16	6.839E+12	9.355E+10	5.710E-01	4.324E+00
79	112	1071.3	-369.3	1.816E+14	5.078E+14	6.078E+14	1.947E+19	8.356E+16	7.184E+12	1.087E+11	5.998E-01	4.568E+00
79	110	1071.3	-410.2	1.778E+14	4.852E+14	5.772E+14	1.755E+19	7.183E+16	6.478E+12	8.603E+10	5.408E-01	4.089E+00
79	105	1071.3	-507.0	1.653E+14	4.466E+14	5.073E+14	1.643E+19	6.943E+16	6.063E+12	8.014E+10	5.062E-01	3.826E+00
79	96	1071.3	-602.3	1.492E+14	3.906E+14	4.184E+14	1.519E+19	6.625E+16	5.603E+12	7.411E+10	4.678E-01	3.535E+00
79	91	1071.3	-705.2	1.292E+14	3.703E+14	3.369E+14	1.373E+19	5.767E+16	5.073E+12	6.339E+10	4.235E-01	3.191E+00
79	86	1071.3	-808.2	1.092E+14	2.762E+14	2.678E+14	1.227E+19	4.759E+16	4.530E+12	5.138E+10	3.781E-01	2.837E+00
79	82	1071.3	-890.5	9.614E+13	2.411E+14	2.245E+14	1.111E+19	4.470E+16	4.099E+12	4.664E-01	3.422E-01	2.567E+00
79	77	1071.3	-993.5	8.436E+13	2.083E+14	1.803E+14	9.702E+18	3.968E+16	3.579E+12	3.967E+10	2.988E-01	2.239E+00
79	67	1071.3	-1199.4	6.207E+13	1.491E+14	1.212E+14	7.154E+18	2.951E+16	2.639E+12	2.831E+10	2.203E-01	1.648E+00
79	57	1071.3	-1405.2	4.510E+13	1.080E+14	8.604E+13	5.035E+18	2.108E+16	1.857E+12	1.978E+10	1.550E-01	1.160E+00
79	48	1071.3	-1590.5	3.586E+13	8.650E+13	6.903E+13	3.473E+18	1.758E+16	1.281E+12	1.609E+10	1.069E-01	8.064E-01
79	38	1071.3	-1796.4	3.296E+13	8.304E+13	6.403E+13	2.036E+18	1.724E+16	7.515E+11	1.526E+10	6.275E-02	4.874E-01
79	28	1071.3	-1997.0	4.590E+13	7.882E+13	4.511E+13	8.313E+17	3.594E+16	3.071E+11	2.712E+10	2.562E-02	2.503E-01
79	22	1071.3	-2057.0	2.633E+13	4.481E+13	2.979E+13	5.336E+17	6.011E+16	1.971E+11	3.985E+10	1.610E-02	2.145E-01
79	8	1071.3	-2197.0	5.348E+11	4.146E+11	3.568E+11	5.163E+15	2.460E+16	1.910E+09	1.754E+10	1.579E-04	4.381E-02

See text in Appendix E for a more complete description of the parameters, the associated energy ranges, and any applicable caveats.

Table E.19. Axial trace up through VT-1,2,3,4.

IR	JZ	R	Z	FLUX-A s ⁻¹ m ⁻²	FLUX-B s ⁻¹ m ⁻²	FLUX-C s ⁻¹ m ⁻²	FLUX-D s ⁻¹ m ⁻²	GFLUX>2 s ⁻¹ m ⁻²	DOSE-N mrem/h	DOSE-G mrem/h	DPA/Y dpayr	HT RATE Watts/g
95	239	1390.7	1997.0	2.414E+13	4.246E+13	2.463E+13	4.068E+17	1.842E+16	1.503E+11	1.412E+10	1.254E-02	1.246E-01
95	229	1390.7	1796.6	1.861E+13	4.809E+13	3.721E+13	9.934E+17	9.958E+15	3.666E+11	8.975E+09	3.061E-02	2.416E-01
95	223	1390.7	1673.1	1.924E+13	4.913E+13	3.927E+13	1.394E+18	9.824E+15	5.144E+11	9.111E+09	4.295E-02	3.303E-02
95	222	1390.7	1652.6	1.974E+13	4.966E+13	4.018E+13	1.465E+18	1.062E+16	5.405E+11	9.687E+09	4.513E-02	3.473E-01
95	219	1390.7	1590.9	2.073E+13	5.248E+13	5.216E+13	1.685E+18	1.079E+16	6.217E+11	1.000E+10	5.191E-02	3.967E-01
95	210	1390.7	1405.7	2.646E+13	6.588E+13	5.278E+13	2.426E+18	1.399E+16	8.952E+11	1.290E+10	7.474E-02	5.674E-01
95	200	1390.7	1199.4	3.495E+13	8.695E+13	6.979E+13	3.415E+18	1.846E+16	1.260E+12	1.728E+10	1.052E-01	7.964E-01
95	190	1390.7	993.1	4.471E+13	1.114E+14	8.981E+13	4.580E+18	2.347E+16	1.689E+12	2.247E+10	1.410E-01	1.066E+00
95	185	1390.7	889.9	4.985E+13	1.253E+14	1.023E+14	5.215E+18	2.536E+16	1.924E+12	2.484E+10	1.606E-01	1.212E+00
95	181	1390.7	807.4	5.516E+13	1.389E+14	1.124E+14	5.739E+18	2.870E+16	2.117E+12	2.808E+10	1.767E-01	1.335E+00
95	176	1390.7	704.2	6.209E+13	1.560E+14	1.266E+14	6.397E+18	3.240E+16	2.360E+12	3.195E+10	1.970E-01	1.490E+00
95	171	1390.7	602.0	6.827E+13	1.723E+14	1.401E+14	7.036E+18	3.567E+16	2.595E+12	3.543E+10	2.167E-01	1.640E+00
95	162	1390.7	507.0	7.386E+13	1.854E+14	1.517E+14	7.597E+18	3.823E+16	2.802E+12	3.820E+10	2.340E-01	1.771E+00
95	156	1390.7	389.7	7.800E+13	1.963E+14	1.616E+14	8.217E+18	4.073E+16	3.031E+12	4.116E+10	2.530E-01	1.915E+00
95	152	1390.7	308.5	7.928E+13	2.021E+14	1.684E+14	8.583E+18	3.954E+16	3.166E+12	4.085E+10	2.643E-01	1.995E+00
95	146	1390.7	191.6	8.495E+13	2.135E+14	1.768E+14	8.993E+18	4.415E+16	3.317E+12	4.483E+10	2.769E-01	2.095E+00
95	141	1390.7	101.9	8.771E+13	2.212E+14	1.819E+14	9.201E+18	4.543E+16	3.394E+12	4.608E+10	2.833E-01	2.144E+00
95	133	1390.7	0.0	8.968E+13	2.264E+14	1.853E+14	9.315E+18	4.667E+16	3.426E+12	4.707E+10	2.869E-01	2.172E+00
95	125	1390.7	-105.7	8.986E+13	2.263E+14	1.840E+14	9.292E+18	4.685E+16	3.428E+12	4.696E+10	2.861E-01	2.166E+00
95	120	1390.7	-208.2	8.703E+13	2.179E+14	1.776E+14	9.135E+18	4.525E+16	3.370E+12	4.530E+10	2.813E-01	2.127E+00
95	115	1390.7	-308.5	8.136E+13	2.068E+14	1.711E+14	8.862E+18	4.026E+16	3.269E+12	4.088E+10	2.729E-01	2.057E+00
95	110	1390.7	-410.2	8.036E+13	1.997E+14	1.639E+14	8.477E+18	4.133E+16	3.127E+12	4.073E+10	2.610E-01	1.971E+00
95	106	1390.7	-490.3	7.757E+13	1.951E+14	1.586E+14	8.109E+18	3.993E+16	2.991E+12	3.910E+10	2.497E-01	1.886E+00
95	105	1390.7	-507.0	7.725E+13	1.911E+14	1.556E+14	8.026E+18	3.971E+16	2.961E+12	3.871E+10	2.472E-01	1.867E+00
95	96	1390.7	-602.3	7.317E+13	1.824E+14	1.473E+14	7.518E+18	3.731E+16	2.773E+12	3.613E+10	2.315E-01	1.748E+00

See text in Appendix E for a more complete description of the parameters, the associated energy ranges, and any applicable caveats.

Table E-20. Axial trace up through PT-1.

IR	I2	R	Z	FLUX-A s ⁻¹ m ⁻²	FLUX-B s ⁻¹ m ⁻²	FLUX-C s ⁻¹ m ⁻²	FLUX-D s ⁻¹ m ⁻²	GFLUX>2 s ⁻¹ m ⁻²	DOSE-N mrem/h	DOSE-G mrem/h	DPA1/Y dpa/yr	HT RATE Watts/g
108	239	1650.1	1997.0	1.599E+13	2.714E+13	1.500E+13	1.819E+17	1.235E+16	6.722E+10	9.609E-09	5.616E-03	6.379E-02
108	238	1650.1	1981.7	1.616E+13	2.970E+13	1.650E+13	2.004E+17	1.194E+16	7.40E+10	9.389E-09	6.189E-03	6.739E-02
108	237	1650.1	1961.1	1.688E+13	3.245E+13	1.858E+13	2.255E+17	1.161E+16	8.33E+10	9.273E+09	6.966E-03	7.268E-02
108	229	1650.1	1796.6	1.951E+13	4.319E+13	2.741E+13	4.342E+17	1.255E+16	1.60E+11	1.031E+10	1.339E-02	1.213E-01
108	219	1650.1	1590.9	2.657E+13	5.804E+13	3.680E+13	7.296E+17	1.731E+16	2.69E+11	1.410E+10	2.249E-02	1.958E-01
108	210	1650.1	1405.7	3.582E+13	7.720E+13	4.815E+13	1.040E+18	2.317E+16	3.81E+11	1.881E+11	3.208E-02	2.760E-01
108	200	1650.1	1199.4	4.794E+13	1.028E+14	6.381E+13	1.444E+18	3.118E+16	5.334E+11	2.523E+10	4.454E-02	3.811E-01
108	190	1650.1	993.1	6.177E+13	1.324E+14	8.201E+13	1.907E+18	4.043E+16	7.04E+11	3.274E+10	5.879E-02	5.017E-01
108	185	1650.1	889.9	6.923E+13	1.484E+14	9.173E+13	2.153E+18	4.522E+16	7.949E+11	3.669E+10	6.638E-02	5.657E-01
108	181	1650.1	807.4	7.543E+13	1.617E+14	9.988E+13	2.353E+18	4.936E+16	8.688E+11	4.007E+10	7.256E-02	6.182E-01
108	176	1650.1	704.2	8.284E+13	1.780E+14	1.099E+14	2.602E+18	5.427E+16	9.608E+11	4.411E+10	8.024E-02	6.832E-01
108	171	1650.1	602.0	8.992E+13	1.931E+14	1.191E+14	2.842E+18	5.903E+16	1.049E+12	4.797E+10	8.761E-02	7.455E-01
108	162	1650.1	507.0	9.562E+13	2.055E+14	1.270E+14	3.049E+18	6.246E+16	1.125E+12	5.089E+10	9.401E-02	7.985E-01
108	156	1650.1	389.7	1.015E+14	2.180E+14	1.346E+14	3.277E+18	6.619E+16	1.203E+12	5.401E+10	1.010E-01	8.565E-01
108	152	1650.1	308.5	1.051E+14	2.259E+14	1.396E+14	3.410E+18	6.867E+16	1.259E+12	5.602E+10	1.051E-01	8.909E-01
108	146	1650.1	191.6	1.093E+14	2.357E+14	1.456E+14	3.560E+18	7.173E+16	1.314E+12	5.851E+10	1.097E-01	9.301E-01
108	141	1650.1	101.9	1.126E+14	2.419E+14	1.492E+14	3.636E+18	7.382E+16	1.342E+12	6.014E+10	1.120E-01	9.508E-01
108	133	1650.1	0.0	1.141E+14	2.454E+14	1.514E+14	3.678E+18	7.482E+16	1.355E+12	6.093E+10	1.134E-01	9.621E-01
108	125	1650.1	-105.7	1.142E+14	2.451E+14	1.510E+14	3.671E+18	7.484E+16	1.355E+12	6.089E+10	1.131E-01	9.603E-01
108	120	1650.1	-208.2	1.122E+14	2.409E+14	1.486E+14	3.615E+18	7.346E+16	1.334E+12	5.972E+10	1.114E-01	9.452E-01
108	115	1650.1	-308.5	1.089E+14	2.332E+14	1.441E+14	3.517E+18	7.113E+16	1.298E+12	5.782E+10	1.084E-01	9.188E-01
108	110	1650.1	-410.2	1.047E+14	2.246E+14	1.390E+14	3.376E+18	6.809E+16	1.246E+12	5.531E+10	1.041E-01	8.817E-01
108	105	1650.1	-507.0	1.007E+14	2.149E+14	1.328E+14	3.211E+18	6.559E+16	1.185E+12	5.315E+10	9.901E-02	8.399E-01
108	96	1650.1	-602.3	9.545E+13	2.045E+14	1.262E+14	3.023E+18	6.231E+16	1.116E+12	5.041E+10	9.322E+02	7.917E-01

See text in Appendix E for a more complete description of the parameters, the associated energy ranges, and any applicable caveats.

Table E.21. Axial trace through side of reflector vessel (at mid-thickness).

IR	JZ	R	Z	FLUX-A s ⁻¹ m ⁻²	FLUX-B s ⁻¹ m ⁻²	FLUX-C s ⁻¹ m ⁻²	FLUX-D s ⁻¹ m ⁻²	GFLUX>2 s ⁻¹ m ⁻²	DOSE-N mrem/h	DOSE-G mrem/h	DPA/IY dpa/yr	HT RATE Watts/g
117	245	1762.5	2057.0	3.496E+12	6.542E+12	4.932E+12	7.006E+16	1.011E+16	2.588E+10	6.983E+09	2.122E-03	3.215E-02
117	239	1762.5	1997.0	6.492E+12	1.084E+13	7.434E+12	9.472E+16	1.361E+16	3.501E+10	9.496E+09	2.869E-03	4.384E-02
117	229	1762.5	1796.6	1.089E+13	1.947E+13	1.364E+13	2.117E+17	2.426E+16	7.820E+10	1.625E+10	6.408E-03	8.669E-02
117	219	1762.5	1590.9	1.608E+13	2.776E+13	1.894E+13	3.542E+17	3.867E+16	1.309E+11	2.543E+10	1.071E-02	1.398E-01
117	210	1762.5	1405.7	2.210E+13	3.734E+13	2.525E+13	5.039E+17	5.408E+16	1.861E+11	3.545E+10	1.524E-02	1.971E-01
117	200	1762.5	1199.4	2.987E+13	5.033E+13	3.368E+13	6.976E+17	7.419E+16	2.576E+11	4.847E+10	2.110E-02	2.714E-01
117	190	1762.5	993.1	3.888E+13	6.512E+13	4.339E+13	9.185E+17	9.726E+16	3.392E+11	6.348E+10	2.778E-02	3.566E-01
117	185	1762.5	889.9	4.361E+13	7.309E+13	4.864E+13	1.035E+18	1.096E+17	3.822E+11	7.155E+10	3.131E-02	4.018E-01
117	181	1762.5	807.4	4.753E+13	7.963E+13	5.288E+13	1.130E+18	1.196E+17	4.173E+11	7.809E+10	3.418E-02	4.386E-01
117	176	1762.5	704.2	5.228E+13	8.771E+13	5.824E+13	1.247E+18	1.319E+17	4.608E+11	8.610E+10	3.775E-02	4.841E-01
117	171	1762.5	602.0	5.668E+13	9.522E+13	6.287E+13	1.360E+18	1.437E+17	5.023E+11	9.375E+10	4.115E-02	5.274E-01
117	162	1762.5	507.0	6.054E+13	1.016E+14	6.715E+13	1.457E+18	1.537E+17	5.382E+11	1.002E+11	4.409E-02	5.647E-01
117	156	1762.5	389.7	6.456E+13	1.076E+14	7.149E+13	1.565E+18	1.645E+17	5.705E+11	1.072E+11	4.735E-02	6.054E-01
117	152	1762.5	308.5	6.698E+13	1.115E+14	7.387E+13	1.622E+18	1.711E+17	6.009E+11	1.115E+11	4.922E-02	6.295E-01
117	146	1762.5	191.6	7.004E+13	1.163E+14	7.701E+13	1.697E+18	1.786E+17	6.268E+11	1.163E+11	5.134E-02	6.566E-01
117	141	1762.5	101.9	7.158E+13	1.191E+14	7.875E+13	1.733E+18	1.826E+17	6.400E+11	1.190E+11	5.242E-02	6.710E-01
117	133	1762.5	0.0	7.235E+13	1.207E+14	7.987E+13	1.753E+18	1.846E+17	6.475E+11	1.203E+11	5.304E-02	6.787E-01
117	125	1762.5	-105.7	7.246E+13	1.208E+14	8.002E+13	1.750E+18	1.845E+17	6.463E+11	1.202E+11	5.294E-02	6.776E-01
117	120	1762.5	-208.2	7.136E+13	1.191E+14	7.882E+13	1.723E+18	1.816E+17	6.366E+11	1.183E+11	5.214E-02	6.673E-01
117	115	1762.5	-308.5	6.936E+13	1.152E+14	7.632E+13	1.677E+18	1.768E+17	6.195E+11	1.151E+11	5.074E-02	6.493E-01
117	110	1762.5	-410.2	6.567E+13	1.108E+14	7.373E+13	1.611E+18	1.693E+17	5.933E+11	1.102E+11	4.876E-02	6.231E-01
117	105	1762.5	-507.0	6.371E+13	1.061E+14	7.034E+13	1.534E+18	1.617E+17	5.667E+11	1.053E+11	4.642E-02	5.941E-01
117	96	1762.5	-602.3	6.024E+13	1.008E+14	6.706E+13	1.446E+18	1.546E+17	5.341E+11	9.942E+10	4.375E-02	5.603E-01
117	91	1762.5	-705.2	5.617E+13	9.393E+13	6.232E+13	1.341E+18	1.418E+17	4.955E+11	9.239E+10	4.057E-02	5.200E-01
117	86	1762.5	-808.2	5.169E+13	8.675E+13	5.773E+13	1.228E+18	1.301E+17	4.538E+11	8.484E+10	4.717E-02	5.493E-01
117	82	1762.5	-890.5	4.795E+13	8.059E+13	5.350E+13	1.136E+18	1.205E+17	4.197E+11	7.855E+10	3.438E-02	4.413E-01
117	77	1762.5	-993.5	4.318E+13	7.247E+13	4.821E+13	1.020E+18	1.080E+17	3.767E+11	7.040E+10	3.086E-02	3.953E-01
117	67	1762.5	-1199.4	3.398E+13	5.715E+13	3.821E+13	7.926E+17	8.437E+16	2.927E+11	5.509E+10	2.398E-02	3.085E-01
117	57	1762.5	-1405.2	2.567E+13	4.334E+13	2.947E+13	5.843E+17	6.262E+16	2.158E+11	4.099E+10	1.767E-02	2.233E-01
117	48	1762.5	-1590.5	1.885E+13	3.272E+13	2.243E+13	4.165E+17	4.537E+16	1.539E+11	2.986E+10	1.260E-02	1.643E-01
117	38	1762.5	-1796.4	1.307E+13	2.338E+13	1.629E+13	2.513E+17	2.890E+16	1.936E+10	7.610E-03	1.024E-01	
117	28	1762.5	-1997.0	7.96E+12	1.273E+13	8.693E+12	1.133E+17	1.631E+16	4.190E+10	1.136E+10	3.431E-03	5.248E-02
117	22	1762.5	-2057.0	4.056E+12	7.962E+12	6.060E+12	8.403E+16	1.208E+16	3.103E+10	8.332E+09	2.543E-03	3.847E-02

See text in Appendix E for a more complete description of the parameters, the associated energy ranges, and any applicable caveats.

Table E.22. Partial axial trace corresponding to radial location for lower portion of PF-1.

IR	JZ	R	Z	FLUX-A s ⁻¹ m ⁻²	FLUX-B s ⁻¹ m ⁻²	FLUX-C s ⁻¹ m ⁻²	FLUX-D s ⁻¹ m ⁻²	GFLUX>2 s ⁻¹ m ⁻²	DOSE-N nrem/h	DOSE-G nrem/h	DPA/Y dpa/yr	HT RATE Watts/g
123	171	1821.8	602.0	8.530E+12	1.004E+13	1.161E+13	2.401E+17	1.186E+17	8.866E+10	7.182E+10	7.330E-03	2.260E-01
123	162	1821.8	507.0	9.081E+12	1.085E+13	1.248E+13	2.573E+17	1.268E+17	9.502E+10	7.673E+10	7.855E-03	2.417E-01
123	156	1821.8	389.7	9.689E+12	1.148E+13	1.316E+13	2.764E+17	1.355E+17	1.020E+11	8.187E+10	8.435E-03	2.583E-01
123	152	1821.8	308.5	1.005E+13	1.193E+13	1.368E+13	2.875E+17	1.409E+17	1.061E+11	8.513E+10	8.774E-03	2.666E-01
123	152	1821.8	191.6	1.046E+13	1.250E+13	1.428E+13	3.000E+17	1.470E+17	1.107E+11	8.874E+10	9.156E-03	2.800E-01
123	146	1821.8	101.9	1.069E+13	1.282E+13	1.465E+13	3.063E+17	1.502E+17	1.130E+11	9.072E+10	9.349E-03	2.861E-01
123	141	1821.8	22.5	1.087E+13	1.305E+13	1.486E+13	3.090E+17	1.517E+17	1.141E+11	9.161E+10	9.436E-03	2.889E-01
123	136	1821.8	0.0	1.085E+13	1.292E+13	1.475E+13	3.097E+17	1.519E+17	1.143E+11	9.175E+10	9.451E-03	2.894E-01
123	133	1821.8	-105.7	1.083E+13	1.294E+13	1.481E+13	3.095E+17	1.517E+17	1.142E+11	9.163E+10	9.446E-03	2.890E-01
123	125	1821.8	-105.7	1.083E+13	1.294E+13	1.481E+13	3.095E+17	1.517E+17	1.142E+11	9.163E+10	9.446E-03	2.890E-01

See text in Appendix E for a more complete description of the parameters, the associated energy ranges, and any applicable caveats.

Table E.23. Partial axial trace corresponding to radial location for lower portion of PF-2.

IR	IZ	R	Z	FLUX-A s ⁻¹ m ⁻²	FLUX-B s ⁻¹ m ⁻²	FLUX-C s ⁻¹ m ⁻²	FLUX-D s ⁻¹ m ⁻²	GFLUX>2 s ⁻¹ m ⁻²	DOSE-N nrem/h	DOSE-G nrem/h	DPA/Y dpa/yr	HT RATE Watts/g
126	171	1853.0	602.0	3.633E+12	3.401E+12	3.425E+12	7.537E+16	8.641E+16	2.784E+10	5.595E+10	2.309E-03	1.517E-01
126	162	1853.0	507.0	3.923E+12	3.660E+12	3.679E+12	8.060E+16	9.226E+16	2.977E+10	5.968E+10	2.469E-03	1.619E-01
126	156	1853.0	389.7	4.182E+12	3.947E+12	3.951E+12	8.650E+16	9.829E+16	3.194E+10	6.354E+10	2.650E-03	1.723E-01
126	152	1853.0	308.5	4.345E+12	3.982E+12	4.047E+12	9.019E+16	1.022E+17	3.331E+10	6.603E+10	2.764E-03	1.794E-01
126	146	1853.0	191.6	4.538E+12	4.166E+12	4.198E+12	9.380E+16	1.064E+17	3.464E+10	6.876E+10	2.875E-03	1.8668E-01
126	141	1853.0	101.9	4.657E+12	4.232E+12	4.355E+12	9.586E+16	1.087E+17	3.540E+10	7.026E+10	2.937E-03	1.908E-01
126	133	1853.0	0.0	4.701E+12	4.329E+12	4.437E+12	9.684E+16	1.100E+17	3.577E+10	7.109E+10	2.967E-03	1.930E-01
126	130	1853.0	-22.5	4.756E+12	4.352E+12	4.482E+12	9.697E+16	1.102E+17	3.581E+10	7.121E+10	2.970E-03	1.933E-01
126	125	1853.0	-105.7	4.636E+12	4.324E+12	4.447E+12	9.698E+16	1.099E+17	3.581E+10	7.098E+10	2.972E-03	1.928E-01

See text in Appendix E for a more complete description of the parameters, the associated energy ranges, and any applicable caveats.

Table E.24. Trace along axis of the long slanted beam tube (LSBT).

IR	JZ	R	Z	FLUX-A s ⁻¹ m ⁻²	FLUX-B s ⁻¹ m ⁻²	FLUX-C s ⁻¹ m ⁻²	FLUX-D s ⁻¹ m ⁻²	GFLUX>2 s ⁻¹ m ⁻²	DOSE-N mrem/h	DOSE-G mrem/h	DPA/Y dp/yr	HT RATE Watts/g
92	254	1330.8	2147.0	1.034E+12	9.727E+11	1.024E+12	1.859E+16	2.190E+16	6.86E+09	1.436E+10	5.698E-04	3.894E-02
88	238	1251.0	1981.7	2.894E+13	5.363E+13	3.139E+13	5.820E+17	2.070E+16	2.149E+11	1.606E+10	1.794E-02	1.681E-01
84	229	1171.1	1796.6	2.255E+13	5.742E+13	4.410E+13	1.451E+18	1.168E+16	5.357E+11	1.059E+10	4.473E-02	3.467E-01
80	221	1091.3	1632.0	2.562E+13	6.253E+13	4.981E+13	2.510E+18	1.305E+16	9.260E+11	1.212E+10	7.731E-02	5.838E-01
77	213	1031.4	1467.4	2.175E+13	6.082E+13	6.534E+13	3.853E+18	1.722E+16	1.421E+12	1.647E+10	1.186E-01	8.910E-01
73	205	951.6	1302.5	5.016E+13	1.264E+14	1.058E+14	5.787E+18	2.290E+16	2.135E+12	2.407E+10	1.782E-01	1.336E+00
71	197	911.7	1137.5	8.032E+13	2.103E+14	2.067E+14	8.174E+18	3.704E+16	3.015E+12	4.07E+10	2.517E-01	1.904E+00
68	188	851.8	951.8	1.862E+14	5.578E+14	8.609E+14	1.212E+19	6.296E+16	4.474E+12	7.741E+10	3.736E-01	2.868E+00
68	184	851.8	869.3	2.446E+14	8.497E+14	1.527E+15	1.394E+19	7.222E+16	5.148E+12	9.298E+10	4.298E-01	3.310E+00
67	180	831.9	786.7	4.082E+14	1.596E+15	3.260E+15	1.639E+19	8.571E+16	6.053E+12	1.191E+11	5.056E-01	3.917E+00
66	176	811.9	704.2	7.332E+14	3.166E+15	7.140E+15	9.920E+19	1.057E+17	7.096E+12	1.577E+11	5.929E-01	4.636E+00
66	172	811.9	622.0	1.069E+15	4.863E+15	1.120E+16	2.167E+19	1.302E+17	8.011E+12	1.990E+11	6.695E-01	5.281E+00
65	164	792.0	534.5	1.896E+15	9.261E+15	2.199E+16	2.520E+19	1.626E+17	9.329E+12	2.601E+11	7.802E-01	6.215E+00
65	159	792.0	451.3	2.384E+15	1.229E+16	2.925E+16	2.779E+19	1.676E+17	1.029E+13	2.850E+11	8.611E-01	6.854E+00
65	155	792.0	369.3	2.949E+15	1.498E+16	3.577E+16	3.014E+19	2.034E+17	1.117E+13	3.380E+11	9.349E-01	7.502E+00

See text in Appendix E for a more complete description of the parameters, the associated energy ranges, and any applicable caveats. Note that the long slant beam tube is an off-vertical tube extending from (x1=593.85,y1=538.65,z1=365.24 mm), to (x2=-1559.95,y2=-2618.56,z2=51.56.80 mm). Starting with JZ=155 and extending up to JZ=254, these mesh intervals correspond to locations that are approximately 0, 100, 200, 300, 400, 500, 600, 700, 900, 1100, 1300, 1500, 1700, 1900 and 2100 mm up from the bottom of the tube, along its axis.

Table E.25. Trace along axis of PT-2 and PT-5.

IR	JZ	R	Z	FLUX-A s ⁻¹ m ⁻²	FLUX-B s ⁻¹ m ⁻²	FLUX-C s ⁻¹ m ⁻²	FLUX-D s ⁻¹ m ⁻²	GFLUX>2 s ⁻¹ m ⁻²	DOSE-N mrem/h	DOSE-G mrem/h	DPA/Y dp/yr	HT RATE Watts/g
111	242	1705.0	2027.0	1.126E+13	1.579E+13	9.085E+12	1.105E+17	1.208E+16	4.08E+10	9.043E+09	3.398E-03	4.645E-02
108	237	1650.1	1961.1	1.688E+13	3.245E+13	1.858E+13	2.255E+17	1.161E+16	8.335E+10	9.273E+09	6.966E-03	7.268E-02
104	233	1570.3	1878.9	1.852E+13	4.360E+13	4.295E+13	4.549E+17	1.055E+16	1.680E+11	9.021E+09	1.403E-02	1.228E-01
101	229	1510.4	1796.6	1.811E+13	4.645E+13	3.462E+13	7.339E+17	1.015E+16	2.709E+11	8.956E+09	2.262E-02	1.843E-01
98	226	1450.5	1734.9	1.836E+13	4.751E+13	3.722E+13	1.033E+18	9.857E+15	3.812E+11	8.923E+09	3.183E-02	2.502E-01
95	222	1390.7	1652.6	1.974E+13	4.966E+13	4.018E+13	1.465E+18	1.062E+16	5.405E+11	9.687E+09	4.513E-02	3.473E-01
91	218	1310.8	1570.3	2.212E+13	5.436E+13	4.408E+13	2.072E+18	1.163E+16	7.647E+11	1.068E+10	6.384E-02	4.838E-01
88	214	1251.0	1488.0	2.535E+13	6.187E+13	4.956E+13	2.731E+18	1.259E+16	1.007E+12	1.189E+10	8.411E-02	6.321E-01
85	211	1191.1	1426.3	2.918E+13	7.077E+13	5.671E+13	3.390E+18	1.416E+16	1.250E+12	1.366E+10	1.044E-01	7.817E-01

See text in Appendix E for a more complete description of the parameters, the associated energy ranges, and any applicable caveats. Note that PT-2 and PT-5 are geometrically similar off-vertical tubes in the upper/outermost corner of the ANS reflector. In the actual design, PT-2 extends from (x1=631.03,y1=1009.86,z1=1419.25 mm), to (x2=907.42,y2=1452.18,z2=2040.70 mm), while PT-5 extends from (x1=540.59,y1=1061.03,z1=419.26 mm), to (x2=-77.40,y2=1525.74,z2=2040.70 mm). Starting with JZ=211 and extending up to JZ=242, these mesh intervals correspond to locations that are approximately 0, 100, 200, 300, 400, 500, 600, 700 and 800 mm up from the bottom of each tube, along their respective axes.

Table E.26. Trace along axis of PT-3 and PT-4.

IR	JZ	R mm	Z mm	FLUX-A s ⁻¹ m ⁻²	FLUX-B s ⁻¹ m ⁻²	FLUX-C s ⁻¹ m ⁻²	FLUX-D s ⁻¹ m ⁻²	GFLUX>2 s ⁻¹ m ⁻²	DOSE-N mrem/h	DOSE-G mrem/h	DPAI/Y dpd/yr	HT RATE Watts/g
108	238	1650.1	1981.7	1.616E+13	2.970E+13	1.650E+13	2.004E+17	1.194E+16	7.40E+10	9.389E+09	6.189E-03	6.739E-02
105	234	1590.2	1899.4	1.820E+13	4.189E+13	2.725E+13	3.092E+17	1.437E+16	1.01E+11	9.101E+09	1.201E-02	1.085E-01
102	230	1530.4	1817.1	1.811E+13	4.597E+13	3.341E+13	6.470E+17	1.028E+16	2.389E+11	8.998E+09	1.994E-02	1.652E-01
99	226	1470.5	1734.9	1.854E+13	4.748E+13	3.734E+13	8.822E+17	1.012E+16	3.621E+11	9.119E+09	3.023E-02	2.392E-01
95	223	1390.7	1673.1	1.924E+13	4.913E+13	3.927E+13	1.394E+18	9.824E+15	5.144E+11	9.111E+09	4.295E-02	3.303E-01
92	219	1330.8	1590.9	2.140E+13	5.289E+13	4.290E+13	1.908E+18	1.134E+16	7.040E+11	1.038E+10	5.878E-02	4.68E-01
89	215	1270.9	1508.6	2.428E+13	5.954E+13	4.770E+13	2.512E+18	1.215E+16	9.34E+11	1.142E+10	7.800E-02	5.871E-01
86	212	1211.1	1446.9	2.777E+13	6.746E+13	5.403E+13	3.159E+18	1.350E+16	1.165E+12	1.295E+10	9.730E-02	7.291E-01
82	208	1131.2	1364.4	3.437E+13	8.333E+13	6.700E+13	4.155E+18	1.652E+16	1.533E+12	1.630E+10	1.279E-01	9.571E-01
79	204	1071.3	1281.9	4.274E+13	1.048E+14	8.610E+13	5.233E+18	2.110E+16	1.930E+12	2.093E+10	1.611E-01	1.206E+00
76	200	1011.5	1199.4	5.549E+13	1.387E+14	1.182E+14	6.532E+18	2.605E+16	2.409E+12	2.764E+10	2.011E-01	1.509E+00

See text in Appendix E for a more complete description of the parameters, the associated energy ranges, and any applicable caveats. Note that PT-3 and PT-4 are geometrically similar off-vertical tubes in the upper/outermost corner of the ANS reflector. In the actual design, PT-3 extends from ($x1=244.86, y1=982.05, z1=1206.33$ mm), to ($x2=414.26, y2=1661.52, z2=2040.70$ mm), while PT-4 extends from ($x1=158.33, y1=999.65, z1=1206.33$ mm), to ($x2=267.89, y2=169.22, z2=2040.70$ mm). Starting with JZ=200 and extending up to JZ=238, these mesh intervals correspond to locations that are approximately 0, 100, 200, 300, 400, 500, 600, 700, 800, 900 and 1000 mm up from bottom of each tube, along their respective axes.

APPENDIX F

A simple solid angle procedure for estimating fluxes and dose rates several meters down the horizontal beam tubes.



F. A SIMPLE SOLID ANGLE PROCEDURE FOR ESTIMATING FLUXES AND DOSE RATES SEVERAL METERS DOWN THE HORIZONTAL BEAM TUBES

The cross sectional area of an elliptical beam tube whose major and minor diameters are $a=200$ mm and $b=100$ mm is given by $A=\pi ab/4=\pi r^2$, where $r=0.5\sqrt{ab}=70.71$ mm is the effective radius of an equivalent cylindrical model.

Consider a point P located a distance X (several meters) down a horizontal beam tube whose hot end is located at (X_o, H) relative to the system centerline as shown in Fig. F.1. Assume that the beam tube is small enough that the fluxes at the end of the beam tube and around the idealized cylindrical body of the beam tube remain unperturbed and almost isotropic. To calculate the flux at point P , let us slice the beam tube into a number of small axial segments and consider the contribution due to neutrons streaming down toward point P from each segment, as well as from the end of the beam tube. The total uncollided flux at point P is then

$$\phi_P = \phi_o \left(\frac{\pi r^2}{4\pi X^2} \right) + \sum_i \phi_i f_i , \quad (\text{F-1})$$

where

- ϕ_o is the flux at the hot end of the beam tube (assumed isotropic),
- r is the effective radius of the beam tube as described above,
- X is the distance down the beam tube from the hot end to point P ,
- ϕ_i is the flux at any given axial segment along the beam tube (assumed isotropic),
- f_i is the fractional solid angle associated with that incremental length of the (cylindrical) wall of the beam tube as seen from point P .

Now consider the two circular discs in Fig. F.2. The fractional solid angle of the closer disk as seen from point P is $\pi r^2/(4\pi R_2^2)$, while the fractional solid angle of the more distant one as seen from point P is $\pi r^2/(4\pi R_1^2)$. The difference must therefore be the fractional solid angle associated with the cylindrical tube connecting the two disks as seen from point P . Noting that R_1 and R_2 in Fig. F.2 are essentially the same as X_b and $X_b - \Delta X$ in Fig. F.1, the equation for the flux at point P may then be written as

$$\phi_P = \phi_o \frac{\pi r^2}{4\pi X^2} + \sum_i^N \phi_i \left(\frac{\pi r^2}{4\pi X_i^2} - \frac{\pi r^2}{4\pi X_{i-1}^2} \right) , \quad (\text{F-2})$$

where $X_{i,1}$ and X_i are the distances down the beam tube from the beginning and end of each axial segment (i) to the point of interest (P), where $X_i > r$ for all i , and where the flux on the surface of the beam tube along any axial segment (ϕ_i) is assumed to be the unperturbed scalar flux at the corresponding location in the global 2-D DORT analysis.

This approximate procedure can and has been applied to each energy group separately to estimate the (nearly monodirectional) multigroup scalar flux at point P , several meters down the beam tube, after which the multigroup flux-to-dose-rate conversion factors may be applied to obtain the neutron and gamma dose rates at that point. Moreover, a small PC program called GETFLUX has been written to do exactly that.

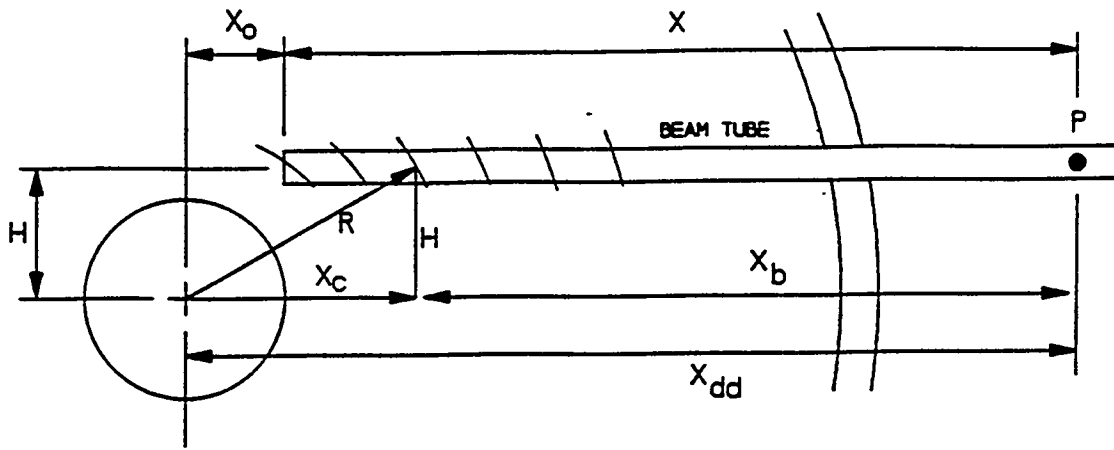


Fig. F.1. Location of a horizontal tangential beam tube relative to the system centerline and a point of interest, (P), several meters down the beam tube.

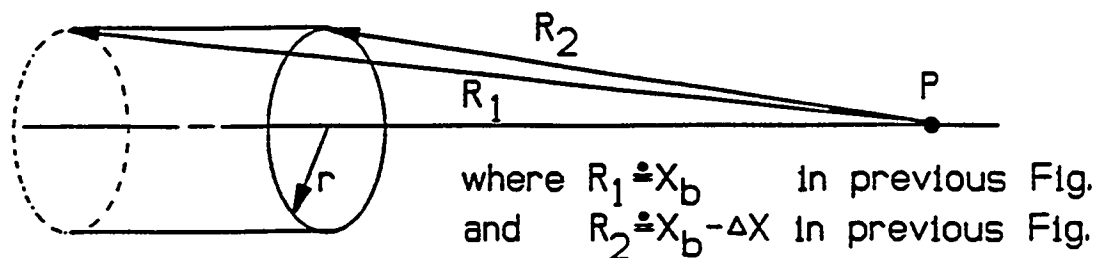


Fig. F.2. Sketch used to calculate the fractional solid angle subtended by an incremental length of the beam tube wall as seen from a point, (P), several meters down the beam tube.

After reading the multigroup DORT scalar fluxes for each of the 138 radial mesh intervals at the midplane of the ANS system (available as a small binary flux file stored on a floppy disk), it asks the user to input the positional parameters X_{dd} , X_o , and H (see Fig. F.1) describing the location of the beam tube and the point of interest (P). It also asks for the effective radius of the beam tube (r) shown in Fig. F.2. It then applies the above procedure to calculate the fluxes and dose rates at the point of interest (P) several meters down the beam tube.

Since rigorous DORT calculations for the horizontal beam tubes have not yet been performed for the current ANS design, it is impossible to say how accurate this approximation really is. There is, however, anecdotal evidence to suggest that it may be accurate to within about 20%. Based on an earlier 1988 design of the ANS reactor, Hayashi et al.^{F-1} reported rigorous results obtained for a horizontal tangential beam tube at the midplane. Their results are based on a rigorous DORT analysis of the horizontal beam tube using a boundary source applied to a buffer zone enveloping the entire beam tube. [This boundary source was obtained by using the VISTA and DTD codes^{F-2, F-3} transform the DORT angular flux field from an earlier global 2-D analysis of the entire system to the new (rotated) coordinate system used in their beam tube analysis.] At the point of interest, 5116 mm down the beam tube, they report fast and thermal neutron fluxes of 2.82E14 and 3.13E15 s⁻¹m⁻² and a total gamma (photon) flux of 2.15E15 s⁻¹m⁻². Using the simplistic GETFLUX routine described above, and the results from DORT Run 5 at the midplane, we obtain fast and thermal neutron fluxes of 3.20E14 and 3.73E15 s⁻¹m⁻² and a total gamma (photon) flux of 1.78E15 s⁻¹m⁻² at the point of interest -- i.e., results that are only 1.13 times higher, 1.19 times higher, and 1.21 times lower, respectively, when we use the parameters corresponding to Hayashi's original (now obsolete) beam tube design [$X_{dd}=5116$ mm, $X_o=266.77$ mm, $H=337.64$ mm, and $r=61.24$ mm]. This was considered most encouraging -- especially given the fact that one often needs quick approximate answers as the design parameters continue to evolve.

The simple algorithm embedded in the GETFLUX routine prints out the total multigroup scalar flux at point P as well as that portion of the flux at point P due only to the flux at the hot end of the beam tube, $\phi_p \approx \phi_o \pi r^2 / (4\pi X^2)$. From this it is clear that 80 to 95% of the uncollided (nearly monodirectional) flux at point P is due solely to the flux at the hot end of the beam tube -- i.e., the total at point P (several meters down the beam tube) is relatively unaffected by the flux along the sides of the beam tube deep in the reflector. Redefining r as the outside radius ($r=71.24$ mm) of the beam tube (rather than the inside radius previously used), keeping only the first term in the series [$\phi_p = \phi_o \pi r^2 / (4\pi X^2)$], and using the actual entrance fluxes at the hot end of the beam tube previously published by Hayashi [5.02E18 and 6.45E19 s⁻¹m⁻² for fast and thermal neutrons, and 4.29E19 s⁻¹m⁻² for the gamma (photon) flux], one can quickly estimate the fast and thermal neutron fluxes at the exit point as 2.43E14 and 3.13E15 s⁻¹m⁻², and the total gamma (photon) flux as 2.08E15 s⁻¹m⁻². These results are in even better agreement with his more rigorous exit values, with differences of 16%, 0%, and 3%, respectively. While one probably should use the effective inside radius of the beam tube and keep the whole series of terms described above and included in the GETFLUX routine, these comparisons between Hayashi's rigorous results and these very simplistic back-of-the-envelope calculations do tend to confirm that the fluxes and dose rates several meters down the beam tube will vary as $(r/X)^2$.

Using the current DORT Run 5 reference results at the midplane and the current design parameters for the horizontal tangential beam tubes [$X_o=275.77$ mm, $H=330.2$ mm, $r=70.711$ mm (based on $\alpha=200$ mm, $b=100$ mm)], the GETFLUX routine has been used to estimate the neutron and gamma dose rates impinging on the beam tube shield plug [at $X_{dd}=4170.32$ mm] to be $3.98E9$ and $3.33E8$ mrem/h, respectively, and the neutron and gamma dose rates downstream of the shield plug [at $X_{dd}=5486.4$ mm] with the shutter open to be $2.05E9$ and $1.79E8$ mrem/h, respectively. While these results must be regarded as very approximate until such time as more rigorous calculations are performed, they are still regarded as very useful and highly informative.

APPENDIX F. REFERENCES

- F-1. M. Hayashi et al., "Calculated Energy and Angular Dependence of Particle Fluxes at the Exit of the Advanced Neutron Source Radial and Tangential Beam Tubes," *Nuclear Science and Engineering* **109**, 391–400 (1991).
- F-2. W. A. Rhoades, "VITSA: A Vehicle Input Source Transformation and Assembly Code," distributed as part of ref. 1 (above); since renamed VISA and documented in Sect. II of *The TORSED Method for Construction of TORT Boundary Sources from External DORT Flux Files*, ORNL/TM-12359, Martin Marietta Energy Systems, Inc., Oak Ridge Natl. Lab., August 1993.
- F-3. R. A. Lillie, "DTD: A Coupling Code for Two-Dimensional R-Z Cylindrical Geometries," *Transactions of the American Nuclear Society* **61**, 381 (June 1990).



Internal Distribution

1. J. A. Bucholz
2. F. X. Gallmeier
3. D. T. Ingersoll
4. T. J. McManamy
5. J. V. Pace III
6. D. L. Selby
7. C. O. Slater
8. B. A. Worley
9. C. D. West
10. ORNL Patent Office
- 11-12. Central Research Library
Document Reference Section
13. Y-12 Technical Library
- 14-15. Laboratory Records Dept.
16. Laboratory Records (RC)

External Distribution

17. D. D. Carlson, U.S. Nuclear Regulatory Commission, T10G6, Washington, DC 20555.
18. U.S. Department of Energy, Oak Ridge Operations, FEDC, MS-8218, P.O. Box 2009, Oak Ridge, TN, 37831-8218.
19. Office of Scientific and Technical Information, P.O. Box 62, Oak Ridge, TN 37831.

